# NUMERICAL AND EXPERIMENTAL INVESTIGATION OF FORCED FILMWISE CONDENSATION OVER BUNDLE OF TUBES IN THE PRESENCE OF NONCONDENSABLE GASES

A THESIS SUBMITTED TO
THE GRADUATE SCHOOL OF NATURAL AND APPLIED SCIENCES
OF
MIDDLE EAST TECHNICAL UNIVERSITY

BY

ABDUL-GHANI M. RAMADAN

IN PARTIAL FULFILLMENT OF THE REQUIREMENTS
FOR THE DEGREE OF DOCTOR OF PHILOSOPHY
IN
MECHANICAL ENGINEERING

NOVEMBER 2006

Approval of the Graduate School of Natural and Applied Sciences

Prof. Dr. Canan ÖZGEN
Director

I certify that this thesis satisfies all the requirements as a thesis for the degree of Doctor of Philosophy.

Prof. Dr. Kemal İDER
Head of Department

This is to certify that we have read this thesis and that in our opinion it is fully adequate, in scope and quality, as a thesis for the degree of Doctor of Philosophy.

Assoc. Prof. Dr. Cemil YAMALI
Supervisor

Examining Committee Members

| | | |
|---|---|---|
| Prof. Dr. Orhan YEŞİN | (METU, ME) | ______________________ |
| Assoc. Prof. Dr. Cemil YAMALI | (METU, ME) | ______________________ |
| Prof. Dr. Kahraman ALBAYRAK | (METU, ME) | ______________________ |
| Prof. Dr. Nevzat ONUR | (GAZI UNIV., ME) | ______________________ |
| Prof. Dr. Mecit SİVRİOĞLU | (GAZI UNIV., ME) | ______________________ |

**I hereby declare that all information in this document has been obtained and presented in accordance with academic rules and ethical conduct. I also declare that, as required by these rules and conduct, I have fully cited and referenced all material and results that are not original to this work.**

Name, Last name: Abdul-ghani RAMADAN

Signature: ______________________

# ABSTRACT

NUMERICAL AND EXPERIMENTAL INVESTIGATION OF FORCED FILMWISE CONDENSATION OVER BUNDLE OF TUBES IN THE PRESENCE OF NONCONDENSABLE GASES

RAMADAN, Abdul-ghani

Ph.D., Department of Mechanical Engineering

Supervisor: Assoc. Prof. Dr. Cemil YAMALI

November 2006, 236 pages

The problem of the forced film condensation heat transfer of pure steam and steam-air mixture flowing downward a tier of horizontal cylinders is investigated numerically and experimentally. Liquid and vapor-air mixture boundary layers were solved by an implicit finite difference scheme. The effects of the free stream non-condensable gas (air) concentration, free stream velocity (Reynolds number), cylinder diameter, temperature difference and angle of inclination on the condensation heat transfer are analyzed. Inline and staggered tubes arrangements are considered. The mathematical model takes into account the effect of staggering of the cylinders and how condensation is affected at the lower cylinders when condensate does not fall on to the center line of the cylinders. An experimental setup was also manufactured and mounted at METU workshop. A set of experiments were conducted to observe the condensation heat transfer phenomenon and to verify the theoretical results.

Condensation heat transfer results are available in ranges from ($U_\infty = 1 - 30\ m/s$) for free stream velocity, ($m_{1,\infty} = 0.01 - 0.8$) for free stream air mass

fraction, ($d$ = $12.7$ -$50.8$ $mm$) for cylinder diameter and ($T_\infty$ -$T_w$ =$10$-$40$ $K$) for temperature difference. Results show that; a remarked reduction in the vapor side heat transfer coefficient is noticed when very small amounts of air mass fractions present in the vapor. In addition, it decreases by increasing in the cylinder diameter and the temperature difference. On the other hand, it increases by increasing the free stream velocity (Reynolds number). Average heat transfer coefficient at the middle and the bottom cylinders increases by increasing the angle of inclination, whereas, no significant change is observed for that of the upper cylinder. Although some discrepancies are noticed, the present study results are inline and in a reasonable agreement with the theory and experiment in the literature.

Down the bank, a rapid decrease in the vapor side heat transfer coefficient is noticed. It may be resulted from the combined effects of inundation, decrease in the vapor velocity and increase in the non-condensable gas (air) at the bottom cylinders in the bank.

Differences between the present study results and the theoretical and the experimental data may be resulted from the errors in the numerical schemes used. These errors include truncation and round off errors, approximations in the numerical differentiation for interfacial fluxes at the vapor-liquid interface, constant properties assumption and approximations in the initial profiles. Mixing and re-circulation in the steam-air mixture at the lower tubes may be the other reasons for these deviations.

Keywords: Forced Condensation, laminar flow, horizontal cylinder, inclination angle, non-condensable gas.

# ÖZ

## YOĞUŞMAYAN GAZLARIN MEVCUT OLDUĞU ORTAMDA TÜP KÜMELERİ ÜZERİNDEKİ ZORLANMIŞ FİLM YOĞUŞMANIN SAYISAL VE DENEYSEL OLARAK İNCELENMESİ

RAMADAN, Abdul-ghani

Doktora, Makina Mühendisliği Bölümü

Tez Yöneticisi: Doç. Dr. Cemil YAMALI

Kasım 2006, 236 Sayfa

Bu çalışmada, yatay borulardan oluşan bir düşey boru demetinin üstünde zorlanmış film yoğuşması problemi nümerik ve deneysel yöntemlerle incelenmiştir. Sıvı ve buhar-hava karışımı sınır tabakaları örtülü sonlu fark yaklaşımı kullanılarak çözdürülmüş. Serbest akış içerisindeki yoğuşmayan gaz (hava) konsantrasyonu, serbest akış hızı (Reynolds sayısı), silindir çapı, sıcaklık farkı ve eğim açısı gibi parametrelerin yoğuşma üzerindeki etkileri analiz edilmiştir. Sıralı ve şaşırtmalı boru düzenlemeleri dikkate alınmıştır. Matematik model şaşırtmalı silindir etkilerini ve yoğuşan suyun silindirlerin merkezine düşmediği durumda en alt silindirlerde yoğuşmanın nasıl etkilendigini içermektedir. Ayrıca deney düzeneğinin imalatı gerçekleştirilmiş ve deneysel çalışmaya hazırlanmıştır. Teorik sonuçları doğrulamak

ve yoğuşma sırasındaki ısı transferi olgusunu incelemek için bir takım deneysel çalışma yapılmıştır.

Sonuçlar serbest akış hızı ($U_\infty = 1 - 30\ m/s$), serbest akışdaki hava oranı ($m_{1,\infty} = 0.01 - 0.8$), silindir çapı ($d = 12.7 - 50.8\ mm$) ve sıcaklılık farkı ($T_\infty - T_w = 10 - 40\ ^oK$) aralıklarında mevcuttur. Elde edilen sonuçlara göre buhar içerisinde küçük miktarlarda havanın varlığı buhar tarafındaki ısı transferi katsayısında kayda değer azalmaya sebep olmuştur. Ayrıca buhar tarafındaki ısı transferi katsayısı artan silindir çapı ve sıcaklık farkı ile düşüşe geçiyor. Diğer taraftan bu değer artan serbest akış hızı (Reynolds sayısı) ile artıyor. Ortalama ısı transfer katsayısı orta ve alt silindirlerde artan eğim açısı ile artıyor. Bunun tam tersi üst silindir için ortalama ısı transfer katsayısında kayda değere herhangi bir değişim gözlemlenmemiştir. Bazı zıtlıklar gözlemlenmesine rağmen, bu çalışmadan elde edilen sonuçlar literatürdeki teorik ve deneysel sonuçlar ile uyum içerisindedir.

Alt silindirlere doğru buhar tarafındaki ısı transferi katsayısında hızlı bir düşüş gözlemlenmiştir. Bu duruma alt silindirlere doğru yoğuşan suyun birikmesi, buhar hızının azalması ve yoğuşmayan gaz miktarının (hava) artması gibi etkilerin toplamı neden olabilir.

Teorik ve deneysel sonuçlar arasındaki farka kullanılan numerik yaklaşımın içerdiği hatalar neden olabilir. Bu hatalar kesme ve yuvarlama hatalarını, sıvı-buhar ara yüzeyinde numerik türev almadan kaynaklanan hataları, özeliklerin sabit olduğu varsayımını ve başlangıç profillerinin tahminini içermektedir. Bu sapmaların diğer bir sebebide en alt taraftaki tüplerde buhar-hava karışımının sirkülasyonu ve karışımı olabilir.

Anahtar kelimeler: Zorlanmış yoğuşma, Düzgün akış, Yatay silindir, Eğim, Yoğuşmayan gaz

*To my parents, my wife and my children*

*who always support me in all aspects of my life*

## ACKNOWLEDGEMENTS

I would like to express my sincere appreciation and gratitude to my supervisor Assoc. Prof. Dr. Cemil YAMALI for his guidance, support and valuable contributions during all stages of preparing this research work. I gratefully acknowledge Mr. Mustafa YALÇIN, Mr. Servet ŞEHERLİ and METU workshop staff for their technical assistance in manufacturing and operating the experimental setup.

My thanks are extended to the academic staff members of mechanical engineering department, Libyan embassy staff and all friends whose help and moral support encouraged me to finilaize this research.

I express my gratitude and deepest thanks to my family for their support and encouragement throughout my education life.

## TABLE OF CONTENTS

ABSTRACT........................................................................................................ iv

ÖZ……………………………………………………………………………... vi

ACKNOWLEDGEMENTS............................................................................... ix

TABLE OF CONTENTS.................................................................................. x

LIST OF TABLES............................................................................................ xv

LIST OF FIGURES.......................................................................................... xvi

LIST OF SYMBOLS........................................................................................ xxviii

CHAPTER

1. INTRODUCTION........................................................................................ 1

 1.1 Condensation........................................................................................... 1

 1.2 Laminar and Turbulent flow.................................................................... 2

 1.3 Boundary layer theory.............................................................................. 3

 1.4 Separation................................................................................................ 3

 1.5 Non-condensable gases............................................................................ 4

2. REVIEW OF PREVIOUS WORK............................................................... 5

 2.1 Studies on pure vapors............................................................................. 5

 2.2 Studies on vapor-gas mixtures................................................................. 13

 2.3 Objectives of the present thesis work...................................................... 16

3. PHYSICAL AND MATHEMATICAL MODELLING................................ 18

3.1 Physical and mathematical model for pure vapor.................................. 18

3.1.1 Upper cylinder........................................................................... 19

3.1.2 Lower cylinders.......................................................................... 23

3.1.3 Liquid sheet falling between the cylinders……………………..... 25

3.1.4 Critical angle of inclination and condensate fall angle………..... 26

3.1.5 Method of solution for pure vapor model……..……………….... 28

3.2 Physical and mathematical model for vapor-air mixture....................... 29

3.2.1 Vapor-air mixture boundary layer…………………………….... 30

3.2.2 Liquid boundary layer…………………………………………... 31

3.2.3 Method of solution for vapor-air mixture model…..…………… 36

3.2.4 Starting the problem and the initial profiles…………………….. 36

3.2.5 Interface temperature and interface air fraction ……………….. 37

3.3 Heat transfer rate, heat transfer coefficient and Nusselt number……… 38

3.4 Thermodynamic and transport properties……………………………… 39

4. NUMERICAL ANALYSIS AND PROCEDURES.................................... 40

4.1 Numerical analysis for pure vapor model……………………….…….. 40

4.2 Numerical analysis for vapor-air mixture model…………………….... 44

4.2.1 Vapor- air mixture boundary layer……………………………..….. 45

4.2.2 Liquid boundary layer……………………………………..…. 50

4.3 Calculation of the main parameters………………………………….... 53

4.3.1 The film thickness……………………………………………… 53

4.3.2 The velocity component normal to the surface……………….... 55

4.3.3 The interfacial air fraction……………………………………..... 56

4.3.4 The interfacial velocity component parallel to the surface……... 56

4.3.5 The interfacial temperature…………………………………….... 57

4.4 The numerical procedure…………………………………………..... 58

4.4.1 Tri-diagonal matrix algorithm, TDMA……………………….…... 59

4.5 The Computer programs…………………………………….…..…… 61

4.5.1 The pure vapor program…………………………………..…….. 61

4.5.2 The vapor-air mixture program………………………………..... 64

5. EXPERIMENTAL STUDY........................................................................ 67

5.1 Cooling water tank……………………………………….………. 67

5.2 Boiler…………………………………………………………..………. 70

5.3 Test section…………………………………………………..……… 71

5.4 Water drainage unit………………………………………..……... 73

5.5 Air supply unit………………………………………………..……... 74

5.6 Temperature measurement system…………………………..……… 74

5.7 Experimental procedure……………………………………….……. 77

5.8 Calculation of the main parameters……………………………..….. 79

5.8.1 Test section tube wall temperature………………………….….... 79

5.8.2 Vapor mass flow rate at the test section…………………….…….. 80

5.8.3 Gas (air) mass flow rate…………………………………….…... 81

5.8.4 Gas (air) mass fraction…………………………………….………. 82

6. RESULTS AND DISCUSSIONS............................................................. 83

6.1 Numerical results for pure vapor on a tier of tubes……………..……... 83

6.1.1 The effect of the cylinder diameter............................................. 89

6.1.2 The effect of the temperature difference...................................... 92

6.2 Numerical results for vapor-air mixture on a single cylinder……..….. 96

6.2.1 Velocity, temperature and concentration profiles…….…….. 96

6.2.2 The effect of the free stream velocity…………….………… 101

6.2.3 The effect of the temperature difference……………………. 107

6.2.4 The effect of the non-condensable gas……………………… 110

6.2.5 The effect of the cylinder diameter………………….………. 113

6.2.6 The effect of the pressure gradient……………………..…….. 115

6.3 Numerical results for vapor-air mixture on a tier of tubes, inline arrangement………………………………………………..……… 118

6.3.1 The effect of the free stream velocity……………….………. 118

6.3.2 The effect of the temperature difference………….……… 122

6.3.3 The effect of the cylinder diameter……………….………. 126

6.4 Numerical results for vapor-air mixture on a tier of tubes, staggered arrangement……………………………………………… 129

6.4.1 The effect of the inclination angle…………………………..…... 130

6.4.2 The effect of the non-condensable gas……………………..…… 133

6.4.3 The effect of the Reynolds number……………………..……. 135

6.4.4 The effect of the temperature difference…………………..……. 139

6.4.5 The effect of the cylinder diameter……………………..……. 142

6.5 Experimental results for the present study…………………..……… 146

6.5.1 The effect of inclination angle……………………………..……. 146

6.5.2 The effect of the non-condensable gas……………..………… 152

6.5.3 The effect of the free stream velocity……………..………….. 154

6.6 Comparison of results………………………………..…………… 156

6.6.1 Comparison between the theoretical and experimental results

for the present study…………………..……………………..….. 156

6.6.2 Comparison between the present study results

and the literature for pure vapor………………………….……... 158

6.6.3 Comparison between the present study results

and the literature for vapor-air mixture……………………..……… 163

7. CONCLUSIONS AND RECOMMENDATIONS....................................... 173

7.1 Conclusions.......................................................................................... 173

7.2 Recommendations................................................................................ 176

REFERENCES............................................................................................... 177

APPENDICES

A. THERMODYNAMIC AND TRANSPORT PROPERTIES........................ 182

B. A SAMPLE OF THE EXPERIMENTAL DATA AND RESULTS............. 191

C. UNCERTAINTY ANALYSIS.................................................................... 196

D. COMPUTER CODES................................................................................. 202

CURRICULUM VITAE................................................................................. 236

## LIST OF TABLES

TABLE

3.1 The values of the critical inclination angle ($\varphi_{crit.}$) and the corresponding condensate fall angle ($\theta_0$) for different inclination angles and different cylinder diameters at (H=0.02 m)………………..... 27

5.1 Required thermocouples in the test section…………………………... 75

6.1 Comparison between experimental and numerical heat transfer rates at different inclination angles for ($\Delta$T=10 K, d=19mm and L= 65 mm)……………………………………………………….…..... 159

B.1 Experimental data and results for $0^o$ of inclination……………………... 191

B.2 Experimental data and results for $3^o$ of inclination……………………... 192

B.3 Experimental data and results for $6^o$ of inclination……………………... 193

B.4 Experimental data and results for $9^o$ of inclination……………………... 194

B.5 Experimental data and results for $12^o$ of inclination…………………… 195

C.1 Uncertainties in the independent variables used in Equation (5.1)……... 197

C.2 Uncertainties in the experimental results……………………………….. 200

## LIST OF FIGURES

FIGURE

3.1 Physical model of the problem………………………………………....... 19

3.2 Physical model and coordinate system for upper cylinder………………. 20

3.3 Physical model for the middle and bottom cylinders…………….......... 24

3.4 Schematic drawing shows the case of critical angle of inclination……… 26

3.5 Reference u and s surfaces at the liquid - vapor interface………......... 32

3.6 Physical model and the coordinate system for the upper cylinder………. 35

3.7 Physical model and the coordinate system for
the middle and bottom cylinders………………………………………… 35

4.1 Equivalent Cartesian coordinates……………………………………... 44

4.2 Finite difference mesh for the two dimensional boundary layer……...... 45

4.3 Flow chart of the pure vapor computer program……………………....... 63

4.4 Flow chart of the vapor-air mixture computer program…………………. 65

5.1 General view of the experimental setup…………………………………. 68

5.2 Cooling water tank……………………………………………………… 69

5.3 Cooling water division apparatus……………………………………..... 69

5.4 General view of the boiler……………………………………………….. 70

5.5a Schematic drawing of the test section…………………………………… 72

5.5b General view of the test section…………………………………………. 72

5.6 Layout of the condensation tubes………………………………………….. 75

5.7 Thermocouples layout……………………………………………………… 76

5.8 View of the datalogger………………………………………………....... 76

6.1a Variation of film thickness with angular position for upper, middle and bottom cylinders at (d=19 mm and $\Delta T=10\ ^{o}K$)………….. 84

6.1b Variation of film thickness with angular position for upper, middle and bottom cylinders at (d=19 mm and $\Delta T=10\ ^{o}K$)………….. 85

6.2a Variation of velocity with angular position for upper, middle and bottom cylinders at (d=19mm and $\Delta T=10\ ^{o}K$)……………………….. 86

6.2b Variation of velocity with angular position for upper, middle and bottom cylinders at (d=19mm and $\Delta T=10\ ^{o}K$)……………………….. 87

6.3a Variation of heat flux with angular position for upper, middle and bottom cylinders at (d=19mm and $\Delta T=10\ ^{o}K$), inline arrangement..... 88

6.3b Variation of heat flux with angular position for upper, middle and bottom cylinders at (d=19mm and $\Delta T=10\ ^{o}K$), staggered arrangement ………………………………………………... 88

6.4a Variation of film thickness with angular position for upper cylinder at different cylinder diameters…………………………………………… 90

6.4b Variation of film thickness with angular position for middle cylinder at different cylinder diameters………………………………… 90

6.4c Variation of film thickness with angular position for bottom cylinder at different cylinder diameters………………………………… 91

6.5 Variation of heat transfer coefficient with angular position for different cylinder diameters at different inclination angles…………… 92

6.6a Variation of film thickness with angular position for upper cylinder at different temperature differences…………………..... 93

6.6b Variation of film thickness with angular position for middle cylinder at different temperature differences…………………………... 93

6.6c Variation of film thickness with angular position for bottom cylinder at different temperature differences…………………………... 94

6.7 Variation of heat flux with temperature difference for upper, middle and bottom cylinders at different inclination angles……………….... 95

6.8 Variation of heat transfer coefficient with temperature difference for upper, middle and bottom cylinders at different inclination angles..... 95

6.9 Velocity distribution of liquid and vapor-mixture boundary layers at different locations on the periphery of the cylinder……………….. 97

6.10 Velocity distribution of liquid and vapor-mixture boundary layers at different locations on the periphery of the cylinder (x-axis in logarithmic scale)…………………………………………... 97

6.11 Velocity distribution of liquid boundary layer at different locations on the periphery of the cylinder……………………………………… 98

6.12 Temperature distribution of liquid and vapor-mixture boundary layers at different locations on the periphery of the cylinder……….... 99

6.13 Temperature distribution of vapor-mixture boundary layer at different locations on the periphery of the cylinder………………….. 99

6.14 Temperature distribution of liquid boundary layer at different locations on the periphery of the cylinder…………………………… 100

6.15 Air concentration distribution of vapor-mixture boundary layer at different locations on the periphery of the cylinder….................. 101
6.16 Velocity distribution of liquid and vapor-mixture boundary layers at the separation point…........................................ 102
6.17 Velocity distribution of liquid vapor-mixture boundary layer at separation point (x-axis in logarithmic scale)…........................ 102
6.18 Temperature distribution of liquid and vapor-mixture boundary layers at the separation point…........................................ 103
6.19 Air Concentration distribution of liquid and vapor-mixture boundary layers at the separation point…............................... 104
6.20 The effect of free stream velocity on dimensionless heat flux through the cylinder wall…................................................ 105
6.21 The effect of the free stream velocity on the film thickness…........ 105
6.22 The effect of free stream velocity on interfacial mass flow rate…..... 106
6.23 The effect of the free stream velocity on the local heat transfer Coefficient…........................................................ 106
6.24 The effect of the free stream velocity on the local Nusselt number..... 107
6.25 The effect of the temperature difference on the film thickness…...... 108
6.26 The effect of the temperature difference on the interfacial mass flow rate…......................................................... 108
6.27 The effect of temperature difference on the local heat transfer Coefficient…........................................................ 109
6.28 The effect of the temperature difference on the local Nusselt number…............................................................ 109

6.29 The effect of the noncondensable gas (Air) on the interfacial mass low rate………………………………………………………… 110
6.30 The effect of the noncondensable gas (air) on the dimensionless heat flux……………………………………………………….. 111
6.31 The effect of the noncondensable gas (air) on the local heat transfer Coefficient……………………………………………………….. 112
6.32 The effect of the noncondensable gas (air) on the local Nusselt number…………………………………………………………. 112
6.33 The effect of the cylinder diameter on the liquid film thickness………... 113
6.34 The effect of the cylinder diameter on the dimensionless heat flux…….. 114
6.35 The effect of the cylinder diameter on the local heat transfer coefficient……………………………………………………….. 114
6.36 The effect of the cylinder diameter on the local Nusselt number……….. 115
6.37 The effect of the pressure gradient on the liquid film thickness………… 116
6.38 The effect of the pressure gradient on the local heat transfer coefficient……………………………………………………….. 117
6.39 The effect of the pressure gradient on the local Nusselt number………... 117
6.40a The effect of the free stream velocity and the non-condensable gas concentrations on the average film thickness for the upper cylinder... 119
6.40b The effect of the free stream velocity and the non-condensable gas concentrations on the average film thickness for the middle cylinder…………………………………………………………. 119

6.40c The effect of the free stream velocity and the non-condensable gas concentrations on the average film thickness for the bottom cylinder…………………………………………………………….. 120
6.41a The effect of the free stream velocity and the non-condensable gas concentrations on the average heat transfer coefficient for the upper cylinder…………………………………………………………….. 121
6.41b The effect of the free stream velocity and the non-condensable gas concentrations on the average heat transfer coefficient for the middle cylinder………………………………………………………….. 121
6.41c The effect of the free stream velocity and the non-condensable gas concentrations on the average heat transfer coefficient for the bottom cylinder…………………………………………………………. 122
6.42a The effect of the temperature difference and the non-condensable gas concentrations on the average film thickness for the upper cylinder…………………………………………………………….. 123
6.42b The effect of the temperature difference and the non-condensable gas concentrations on the average film thickness for the middle cylinder…………………………………………………………….. 123
6.42c The effect of the temperature difference and the non-condensable gas concentrations on the average film thickness for the bottom cylinder…………………………………………………………….. 124
6.43a The effect of the temperature difference and the non-condensable gas concentrations on the average heat transfer coefficient for the upper cylinder…………………………………………………………. 124

6.43b The effect of the temperature difference and the non-condensable gas concentrations on the average heat transfer coefficient for the middle cylinder………………………………………………………… 125

6.43c The effect of the temperature difference and the non-condensable gas concentrations on the average heat transfer coefficient for the Bottom cylinder……………………………………………………….. 125

6.44a The effect of the cylinder diameter and the non-condensable gas concentrations on the average film thickness for the upper cylinder... 126

6.44b The effect of the cylinder diameter and the non-condensable gas concentrations on the average film thickness for the middle cylinder……………………………………………………………… 127

6.44c The effect of the cylinder diameter and the non-condensable gas concentrations on the average film thickness for the bottom cylinder……………………………………………………………… 127

6.45a The effect of the cylinder diameter and the non-condensable gas concentrations on the average heat transfer coefficient for the upper cylinder……………………………………………………………… 128

6.45b The effect of the cylinder diameter and the non-condensable gas concentrations on the average heat transfer coefficient for the middle cylinder………………………………………………………… 128

6.45c The effect of the cylinder diameter and the non-condensable gas concentrations on the average heat transfer coefficient for the bottom cylinder……………………………………………………... 129

6.46a The effect of the angle of inclination on the local film thickness for upper, middle and bottom cylinders at ($\varphi=3^o$, $\theta_o=13^o$)………………….. 130

6.46b The effect of the angle of inclination on the local film thickness for upper, middle and bottom cylinders at ($\varphi=6^o$, $\theta_o=26^o$)………………….. 131

6.46c The effect of the angle of inclination on the local film thickness for upper, middle and bottom cylinders at ($\varphi=9^o$, $\theta_o=39^o$)………………….. 131

6.47a The effect of the angle of inclination on the local heat transfer coefficient for upper, middle and bottom cylinders at ($\varphi=3^o$, $\theta_o=13^o$)….. 132

6.47b The effect of the angle of inclination on the local heat transfer coefficient for upper, middle and bottom cylinders at ($\varphi=6^o$, $\theta_o=26^o$)….. 132

6.47c The effect of the angle of inclination on the local heat transfer coefficient for upper, middle and bottom cylinders at ($\varphi=9^o$, $\theta_o=39^o$)….. 133

6.48a The effect of the non-condensable gas concentrations on the local heat transfer coefficient for the upper cylinder……………………………….. 134

6.48b The effect of the non-condensable gas concentrations on the local heat transfer coefficient for the middle Cylinder……………………………. 134

6.48c The effect of the non-condensable gas concentrations on the local heat transfer coefficient for the bottom cylinder…………………………….. 135

6.49a The effect of Reynolds number on the local film thickness for the upper cylinder……………………………………………………………... 136

6.49b The effect of Reynolds number on the local film thickness for the middle cylinder………………………………………………………… 136

6.49c The effect of Reynolds number on the local film thickness for the bottom cylinder………………………………………………………… 137

6.50a The effect of Reynolds number on the local heat transfer coefficient for the upper cylinder………………………………………………………... 137

6.50b The effect of Reynolds number on the local heat transfer coefficient for the middle cylinder……………………………………………………..... 138

6.50c The effect of Reynolds number on the local heat transfer coefficient for the bottom cylinder……………………………………………………..... 138

6.51a The effect of the temperature difference on the local film thickness for the upper cylinder………………………………………………………... 139

6.51b The effect of the temperature difference on the local film thickness for the middle cylinder……………………………………………………..... 140

6.51c The effect of the temperature difference on the local film thickness for the bottom cylinder………………………………………………………. 140

6.52a The effect of the temperature difference on the local heat transfer coefficient for the upper cylinder……………………………………... 141

6.52b The effect of the temperature difference on the local heat transfer coefficient for the middle cylinder……………………………………. 141

6.52c The effect of the temperature difference on the local heat transfer coefficient for the bottom cylinder…………………………………..... 142

6.53a The effect of the cylinder diameter on the local film thickness for upper cylinder………………………………………………………………. 143

6.53b The effect of the cylinder diameter on the local film thickness for middle cylinder…………………………………………………………..…. 143

6.53c The effect of the cylinder diameter on the local film thickness for bottom cylinder……………………………………………………………. 144

6.54a The effect of the cylinder diameter on the local heat transfer coefficient for upper cylinder………………………………………………………... 144

6.54b The effect of the cylinder diameter on the local heat transfer coefficient for middle cylinder…………………………………………………..... 145

6.54c The effect of the cylinder diameter on the local heat transfer coefficient for bottom cylinder…………………………………………………..... 145

6.55a Variation of heat transfer rates with temperature difference for $0^o$ of inclination………………………………………………………………... 147

6.55b Variation of heat transfer coefficients with temperature difference for $0^o$ of inclination…………………………………………………………….. 147

6.56a Variation of heat transfer rates with temperature difference for $3^o$ of inclination………………………………………………………………... 148

6.56b Variation of heat transfer coefficients with temperature difference for $3^o$ of inclination…………………………………………………………….. 148

6.57a Variation of heat transfer rates with temperature difference for $6^o$ of inclination………………………………………………………………... 149

6.57b Variation of heat transfer coefficients with temperature difference for $6^o$ of inclination…………………………………………………………….. 149

6.58a Variation of heat transfer rates with temperature difference for $9^o$ of inclination………………………………………………………………... 150

6.58b Variation of heat transfer coefficients with temperature difference for $9^o$ of inclination…………………………………………………………….. 150

6.59a Variation of heat transfer rates with temperature difference for $12^o$ of inclination………………………………………………………………... 151

6.59b Variation of heat transfer coefficients with temperature difference for $12^o$ of inclination…………………………………………………….... 151

6.60a Variation of heat transfer coefficient with temperature difference at two values of air fractions for upper cylinder…………………………… 152

6.60b Variation of heat transfer coefficient with temperature difference at two values of air fractions for middle cylinder………………………..… 153

6.60c Variation of heat transfer coefficient with temperature difference at two values of air fractions for bottom cylinder………………………..… 153

6.61a Variation of heat transfer coefficient with temperature difference at two values of free stream velocities for upper cylinder……………….... 154

6.61b Variation of heat transfer coefficient with temperature difference at two values of free stream velocities for middle cylinder………………... 155

6.61c Variation of heat transfer coefficient with temperature difference at two values of free stream velocities for bottom cylinder………………... 155

6.62 Comparison between heat transfer coefficients for the theoretical and experimental results of the present study at two values of air fractions... 157

6.63 Comparison between heat transfer coefficients for the theoretical and experimental results of the present study at two values of free stream velocities………………………………………………………………... 158

6.64 Comparison between heat transfer coefficients of the present study and those obtained from the literature…………………………………… 160

6.65 Comparison between the present study results with the theoretical and the experimental data in the literature………………………………….. 162

6.66 Effects of $T_\infty - T_w$ and $m_{1,\infty}$ on condensation heat transfer for steam-air; ($P_\infty = 100\,kPa, U_\infty = 0.305\,m/s\ and\ R = 0.01905m$)…………………..... 164

6.67 Effects of $T_\infty - T_w$ and $m_{1,\infty}$ on condensation heat transfer for steam-air;($P_\infty = 100\,kPa, U_\infty = 3.05\,m/s\ and\ R = 0.01905m$)………………….. 164

6.68a Comparison of theory and experiment for steam-air mixture ($U_c$=*1.8 m/s*)……………………………………………………... 166

6.68b Comparison of theory and experiment for steam-air mixture ($U_c$=*3.3 m/s*)……………………………………………………... 167

6.69 Comparison of steam-air mixture data with Equation (6.5)……………... 168

6.70a Effect of free stream air concentrations on condensation from steam-air mixtures-comparison with theory and experiment……………………..... 169

6.70b Effect of free stream vapor velocity on condensation from steam-air mixtures-comparison with theory and experiment……………………..... 170

6.71a Effect of air fractions and free stream vapor velocity on condensation from steam-air mixtures, comparison with theory and experiment ($U_\infty$= *4.4 m/s*)……………………………………………………. 171

6.71b Effect of air fractions and free stream vapor velocity on condensation from steam-air mixtures, comparison with theory and experiment ($U_\infty$= *7.0 m/s*)……………………………………………………. 171

C.1 Variation of heat transfer coefficients with temperature difference for $0^o$ of inclination (with error bars)……………………………………... 201

C.2 Experimental heat transfer coefficients for different rows of the present study at two values of air fractions (with error bars)……………. 201

## LIST OF SYMBOLS

| | |
|---|---|
| $C_p$ | specific heat at constant pressure, J/(kg.K) |
| $G$ | gravity, (m/s$^2$) |
| $D$ | diameter of the cylinder, (m) |
| $D_{12}$ | binary diffusion coefficient, (m$^2$/s) |
| $F$ | dimensionless parameter, ($\mu g d h_{fg}/kU_v^2\Delta T$) |
| $Fr$ | Froude Number = $gR/4U^2_\infty$ |
| $H$ | heat transfer coefficient, W/(m$^2$.K) |
| $h_{fg}$ | latent heat of evaporation, (J/kg) |
| $H$ | distance between cylinders (m) |
| $j$ | mass diffusion flux |
| $k$ | thermal conductivity, W/(m.K) |
| $m$ | mass fraction |
| $\dot{m}$ | interfacial mass flux = $\rho v\vert_s$, (kg/m$^2$.s) |
| $Nu$ | Nusselt number |
| $p$ | partial pressure, (Pa) |
| $P$ | total pressure, (Pa) |
| $Pr$ | Prandtl number = $\mu C_p/k$ |
| $q$ | heat flux, (W/m$^2$) |
| $q_{Nu}$ | Nusselt heat flux, (W/m$^2$) |
| $Q$ | heat transfer rate, (W) |

| | |
|---|---|
| $R$ | radius of the cylinder, (m) |
| $Re$ | Reynolds number |
| $Sc$ | Schmidt number $= \nu / D_{12}$ |
| $T$ | absolute temperature, (°$K$) |
| $T_1, \ldots, T_{25}$ | thermocouples |
| $U$ | downward velocity, (m/s) |
| $U_H$ | liquid free fall velocity, Equation (3.24), (m/s) |
| $U_\delta$ | Vapor-liquid interface velocity, (m/s) |
| $\overline{U}$ | average velocity (m/s) |
| $u$ | x-component of velocity, (m/s) |
| v | y-component of velocity, (m/s) |
| $x,y$ | boundary layer Coordinates |

Greek Letters

| | |
|---|---|
| $\delta$ | liquid film thickness, (m) |
| $2\delta_H$ | width of the falling liquid film, Equation (3.25), (m) |
| $\eta$ | dimensionless film thickness |
| $\theta$ | angular position of the tube, (degree) |
| $\mu$ | dynamic viscosity, (Pa.s) |
| $\gamma$ | kinematic viscosity, (m$^2$/s) |
| $\rho$ | density, (kg/m$^3$) |
| $\tau$ | shear stress, (N/m$^2$) |
| $\Delta$ | Condensate fall thickness, (m) |
| $\Delta_v$ | Vapor-air mixture boundary layer thickness, (m) |
| $\Gamma$ | Mass flow rate per unit length, (kg/m.s) |

Subscripts

| | |
|---|---|
| $c$ | coolant water |
| $e$ | at the vapor –air mixture boundary layer edge |
| $i$ | at the vapor-liquid interface |
| $in$ | inlet cooling water |
| $l$ | in the liquid phase |
| $out$ | outlet cooling water |
| $s$ | at the s-surface, Figure 3.5 |
| $sat$ | saturation |
| $u$ | at the u-surface, Figure 3.5 |
| $v$ | in the vapor phase |
| $w$ | at the tube wall |
| $1$ | air |
| $2$ | vapor |
| $\infty$ | at free stream |
| $g$ | gas |
| $crit.$ | critical |

# CHAPTER 1

# INTRODUCTION

## 1.1 Condensation

Condensation occurs when the temperature of a vapor is reduced below its saturation temperature. In industrial equipment, the process commonly results from contact between the vapor and a cool surface. The latent energy of the vapor is released, heat is transferred to the surface and the condensate is formed. Other common modes are homogenous condensation where vapor condenses out as droplets suspended in a gas phase to form a fog, and the direct contact condensation, which occurs when vapor is brought into contact with a cold fluid.

Condensation may occur in two ways depending on the condition of the surface namely, film condensation and drop-wise condensation. Film condensation is generally characteristic of clean, in-contaminated surfaces, in which a liquid film covers the entire condensing surface, and under the action of gravity the film flows continuously from the surface [52].

If the surface is coated with a substance that inhibits wetting, it is possible to maintain drop-wise condensation. The drops form in cracks, pits and cavities on the surface and may grow and coalesce through condensation. The condensate provides a resistance to heat transfer between the vapor and the surface. This resistance increases as condensate thickness increases. In terms of maintaining high condensation and heat transfer rates, droplet formation is superior to film condensation. The heat transfer rates in drop-wise condensation are more than an order of magnitude larger than those associated with film condensation. In industrial applications, it is desirable to achieve drop-wise condensation [52].

## 1.2 Laminar and Turbulent flow

For any fluid flow problem, it is very important to distinguish between the two flow regimes, laminar or turbulent. Since the solution techniques and procedures strongly depend on which of these conditions are exist.

In laminar flow, the fluid motion is highly ordered and it is possible to identify streamlines along which particles move. The flow structure is characterized by a motion in layers.

In Turbulent flow, fluid motion is highly irregular and is characterized by velocity fluctuations. These fluctuations enhance the transfer of momentum and energy. Turbulent flow is characterized by random, three dimensional motions of fluid particles superimposed on the mean motion [58].

Whether a flow is laminar or turbulent depends on the properties of the particular flow. Laminar or turbulent is determined by the value of a dimensionless parameter, the Reynolds number,

$$Re = \frac{\rho \overline{U} d}{\mu} \quad \text{..........................................................................} (1.1)$$

In reality, there is no single value of Reynolds number at which flow changes from laminar to turbulent. There is a range of Reynolds number. Thus, it is more meaningful to talk of a lower value of Reynolds number below which the flow is always laminar and a higher value above which the flow is always turbulent [58].

For a flat plate, the boundary layer is initially laminar, but at some distance from the leading edge, small disturbances are amplified and transition to turbulent flow begins to occur. Fluid fluctuations begin to develop in the transition region, and the boundary layer eventually becomes completely turbulent [52].

## 1.3 Boundary layer theory

In 1904, Ludwig Prandtl presented the theory of the boundary layer. It played a major role in a series of investigations and further developments which have been among the most important contributions in all of fluid mechanics.

In this theory, he proposed that all the viscous effects are concentrated in a thin layer near the boundary and that outside this layer the fluid behaves as though it is inviscid. This inviscid external flow is closely approximated by the potential flow a round the body.

Since there is no obvious division between the inviscid flow and the viscous layer, an arbitrary definition is employed; the edge of the boundary layer, with thickness designated by $\delta$, is the locus of the points at which the velocity is 99 percent of the potential flow wall velocity.

The boundary layer usually begins as laminar flow, with sufficient development length it undergoes transition to turbulent flow [59]

## 1.4 Separation

Separation occurs when the main stream flow leaves the body and forms a free stream surface, a dividing stream surface, in the interior of the fluid. This stream surface may exhibit considerable unsteadiness. The location of the separation point is strongly dependent upon the geometry of the body. An abrupt change in the geometry, such as a backward facing step or a corner of a building, will cause the flow to separate. The main stream may separate from a body because of an adverse (positive) pressure gradient. Separation is also influenced by a number of characteristics of the flow. The Reynolds number is a primary parameter influencing separation; of secondary importance are the free stream fluctuation amplitude, wall roughness and wall temperature [59]. Generally, the point on the boundary layer where normal velocity gradient is equal to zero is called the point of separation.

During laminar film condensation, a build up of gas concentration near the film surface creates a buoyant force that acts against the flow direction. The magnitude of the buoyant force is maximum at the liquid-vapor mixture interface and decreases toward the free stream flow where it becomes equal to zero. The result of the buoyant force is to change the mixture velocity profile so that at some location along the plate where mixture velocity gradient becomes zero at the interface, separation occurs [42].

### 1.5 Non-condensable gases

In many engineering applications, like in steam power plants, condensers generally work below atmospheric pressure. This increases the possibility of air leakage into the condenser. Observations and experimentation show that even for very small amounts of air content, a remarked reduction in the heat transfer coefficient was noticed. This is attributed to the increase in the air concentration at the liquid-vapor mixture interface. This can be explained as follows;

During the condensation process at the interface, the condensate velocity increases towards the condensate surface, as if there is suction at the interface. Since the vapor condensates at the interface, only non-condensable gas remains at the vicinity of the interface. As a result, the gas concentration increases at the interface.

At equilibrium, the rate of removal of the gas by diffusion and convection away from the condensing surface equals the rate at which it is brought to the interface. The resulting increased gas concentration at the interface reduces the partial pressure of the vapor, and hence the vapor saturation temperature [60]. Consequently, the heat transfer rate is reduced.

Another reason for the heat reduction is the fact that the non-condensable gas acts as a barrier between the vapor and the wall. The vapor has to diffuse through the gas layer in order to reach to the condensate surface.

# CHAPTER 2

# REVIEW OF PREVIOUS WORK

An extensive amount of work on the film condensation phenomenon is available in the literature. Many researchers conducted both experimental and numerical studies on laminar film condensation of vapor on a single tube and bundle of tubes. In general, they investigated the effects of different parameters known to affect the condensation heat transfer for different geometries under different working conditions. Different pure vapors, binary vapors and vapor-gas mixtures were tested and analyzed.

This review covers also many theoretical correlations and empirical relations on both pure vapors and vapor-gas mixtures applications. The main findings and the important conclusions are summarized.

## 2.1 Studies on pure vapors

Nusselt [1] was the first who studied the problem of laminar film condensation. He proposed a simple model to calculate film thickness and heat transfer coefficient for different geometrical configurations. The effects of both energy convection and fluid accelerations and the shear stress at the liquid-vapor interface were neglected. Nusselt assumed that flow throughout the film is laminar and only gravity forces are acting on the condensate layer. A uniform temperature of pure vapor was assumed. In addition, he assumed that heat transfer from vapor to liquid is only carried out by conduction and constant fluid properties.

Sparrow and Gregg [2] studied the problem of laminar film condensation on a vertical plate using the mathematical techniques of boundary layer theory. A similarity solution is applied. Energy convection and fluid acceleration were fully taken into consideration. It was found that the inclusion of the acceleration terms had a little effect on the heat transfer for Prandtl numbers greater than 1.0. For lower Prandtl numbers, the acceleration terms played a more important rule.

Sparrow and Gregg [3] investigated the laminar film condensation on a horizontal cylinder using the principles of the boundary layer theory. They included both the inertia forces and energy convection terms. A similarity transformation is applied to reduce the partial differential equations to ordinary differential equations. They found that the effects of both energy convection and inertia forces are very small for small condensate films. For high Prandtl numbers, the effects of energy convection are dominant over inertia forces effects. However, for low Prandtl numbers, the effects of inertia forces are dominant.

Duckler [4] developed new equations for velocity and temperature distribution in thin vertical films based on equation of Deissler for eddy viscosity near a solid boundary. Graphical relationships were presented to determine the velocity distribution, the film thickness, the local heat transfer coefficient, and the average coefficient over the entire condenser. Theoretical results showed a good agreement with the experimental data. The results confirmed the usefulness of the equation of Deisseler.

Koh et al. [5] studied the two-phase flow problem in laminar film condensation. Shear forces at the liquid-vapor interface were taken into account. He showed that the problem can be formulated as an exact boundary layer solution. He found that the effects of the interfacial shear on the heat transfer are negligible for Prandtl numbers of ten or greater and are quite small even for Prandtl number of one. For liquid metals, he found that the interfacial shear causes substantial reductions in heat transfer.

Chen [6] solved the boundary layer equations for laminar film condensation for both single cylinder and a vertical bank of horizontal tubes. He included the inertia effects and assumed stationary vapor outside the vapor boundary layer for the case of single horizontal cylinder. Velocity and temperature distributions were found by similarity approach. For the bank of tubes, he included the effect of condensation between tubes, which partly responsible for high heat transfer rate. He neglected the inertia effects. He compared heat transfer coefficients with the experiments. He attributed the higher heat transfer coefficients rates than the theory for some of the data to splashing, intermittent and local dripping. He also presented approximate formulas for ease of application.

Koh [7] analyzed the problem of laminar film condensation of a saturated vapor in forced flow over a flat plate. He followed the exact boundary layer solution principles. Numerical results revealed that for low Prandtl number liquids (liquid metals), the effect of energy convection is negligibly small and it is quite important for high Prandtl number liquids.

Shekriladze and Gomelauri [8] studied the problem of laminar film condensation of a vapor flow along a flat plate and vertically on a cylinder. They found that momentum transfer is dominant in fluid dynamics of the condensation process. They compared their results with the available experimental data.

Denny and Mills [9] developed a general computer program that solves the finite difference scheme based on boundary layer theory for laminar film condensation on a vertical surface. In addition, closed form analytical solution was presented based on the Nusselt assumptions that have been extended to include the effect of non-isothermal condenser wall. They defined the local variable fluid properties in terms of reference temperature, $T_r = T_w + \alpha(T_s - T_w)$. In both solutions, vapor shear was accounted for by means of asymptotic solution of the vapor boundary layer under strong suction. They evaluated the validity of the extended Nusselt result in terms of forced vapor flow, variable wall temperature and variable fluid properties. Ten fluids was studied including water, all having Prandtl numbers greater than unity. They found that except for severe wall temperature variations that the value of $\alpha$ depends on the fluid specie led to less than 2 percent deviation between the analytical and numerical results.

Denny and Mills [10] studied the problem of laminar film condensation of a flowing vapor on a horizontal cylinder at normal gravity. They applied the same solution technique introduced for vertical surface [9]. It was found that, for angles up to 140 degrees, there was less than a 2 percent discrepancy between the analytical solution and the numerical results. As 180 degrees is approached, a big deviation is noticed. This results from the gross violation of the Nusselt assumptions. The values of the reference parameter $\alpha$ that derived for the vertical surface [9] were found to be adequate for the horizontal cylinder too.

Fujii and Uehara [11] solved two-phase boundary layer equations of laminar filmwise condensation with an approximate method due to Jacobs under the conditions that saturated vapor is flowing over the surface, uniform wall temperature and both body force and forced convection are considered. They developed an approximate expression that approximates the average heat transfer coefficient. There was a fairly good agreement between the approximate expression and the experimental data for the cases where temperature differences were restricted within some limitations for $Nu_m$ smaller than $2\times10^4$. When the value of $Nu_m$ was larger than $2\times10^4$, the experimental value of is $Nu_m$ is about 1.3 to 1.9 times larger than the expected value for the cases of small heat flux.

Fujii et al [12] solved two-phase boundary layer equations of filmwise condensation on a horizontal cylinder with an approximate method due to Jacobs. An approximate expression was developed. When heat transfer coefficients predicted by the approximate expression were compared with the experimental data, a good agreement was achieved. Temperature distribution on the cylinder is usually affected by oncoming vapor velocity and surface heat flux. They concluded that about 80 percent of total condensation takes place in the upper half of the cylinder.

Fujii et al [13] conducted an experimental work on condensation in horizontal cross flow of low pressure saturated steam through both in-line and staggered arranged tube banks. Simple expressions for heat transfer coefficients of steam side and pressure drops through tube banks were proposed. A comparison was made between the results of in-line and staggered tube arrangement. Some observations about the peripheral temperature distribution, leaked air and breathing flow of steam were also reported.

Lee and Marschall [14] used the linear stability theory to study stability characteristics of laminar gravity-induced condensate film flow down an arbitrarily inclined wall. Results showed that laminar condensate films are unstable in all practical situations there are some stabilizing effects that acting on the film flow; namely, the angle of inclination, the surface tension, the condensation rate at small Reynolds numbers and Prandtl number to a certain extent.

Gaddis [15] solved the two phase boundary layer equations for the condensation of a flowing vapor on a horizontal cylinder. The governing partial differential equations were transformed into ordinary differential equations.

The numerical solutions presented the local values of the Nusselt number on the periphery of the cylinder as a function of the different governing parameters.

Rose [16] studied the effect of pressure gradient in forced convection film condensation on a horizontal tube. He found that pressure gradient led to higher heat transfer coefficient over the forward half of the tube. He showed also that under certain circumstances the solution of film thickness around the tube is not possible for the lower part of the cylinder. He analyzed the causes for the increase in the heat transfer coefficient when pressure gradient is considered. A conservative equation for estimating the mean heat transfer coefficient for the whole tube is also given and compared with available experimental data.

Lee et al [17] reported heat transfer measurements for condensation of refrigerant-113 and ethanediol (ethylene glycol) on a single horizontal tube with vertical downflow. Vapor velocities up to 6 m/s were obtained for refrigerant-113, while for ethanediol, velocities in excess of 100 m/s were reached. A comparison between the study results and literature was done. Deviations in results between the theory and experiment for R-113 were noticed. At higher vapor velocities the observed heat transfer coefficients significantly exceed the predicted values due to turbulence in the condensate film. For ethanediol, at higher velocities, the variation of vapor pressure around the tube has a significant effect. The lower mean heat transfer coefficients may be due to relatively strong temperature variation a round the tube.

Kutateladze and Gogonin [18] conducted an experimental work on heat transfer in condensation of moving vapor on a single horizontal cylinder. Experimental data were presented for a wide range of determining parameters. When compared to the predicted relations confirm the validity of the basic assumptions made for the solution of condensation heat transfer problems in the works of Cherny, Cess and other authors. It was found that the friction on the vapor-liquid interface depends on the magnitude of the substance cross flow.

Kutateladze and Gogonin [19] studied experimentally heat transfer in film condensation of flowing vapor on horizontal tube banks. They concluded that for quiescent vapor, heat transfer in condensation on tube banks depends only on the condensate flow rate. When the vapor velocity was higher than its critical value, fragmentation of condensate droplets and streamlets occurred. At vapor velocities range between quiescent and critical one, heat transfer depends on both the condensate flow rate and the friction on the vapor-liquid interface.

Kutateladze et al [20] extended their experimental work to study the problem of film condensation of practically quiescent vapor on the banks of horizontal smooth tubes of different diameters. They concluded that when $\mathrm{Re}\rangle 50$, vapor condensation on super-cooled drops and discrete liquid streamlets contributes substantially to heat transfer. In addition, the starting length of the thermal boundary layer depends on both the film Reynolds number and the diameter of the cylinder. Finally, the experimental results agree satisfactorily with their study results.

Marzo and Casarella [21] studied the problem of laminar film condensation over a horizontal cylinder for combined gravity and forced flow. They formulate the governing equations for the problem over a two-dimensional horizontal cylinder. A wide range of Froude number was used to allow a distinction between gravity dominant flow and forced flow. Heat transfer coefficient at the surface of the cylinder was computed over a wide range of Froude, Jakob and Prandtl numbers and interfacial ratios. The average value of heat transfer coefficient over the cylinder was also evaluated. Comparison with literature was also done for a range of different parameters.

Churchill [22] presented solutions in closed form for the effects of the heat capacity of the condensate, the inertia, the drag of the vapor and the curvature of the surface on the rate of laminar, non-rippling condensation of a saturated vapor on a vertical, isothermal surface. He presented algebraic equations that can be solved by iteration since some of these closed form solutions do not allow direct specification of the usual independent variables. These solutions are very accurate for large Prandtl numbers. However, they are restricted for small Prandtl numbers. Both inertia and vapor drag are found to be appreciable for $\mathrm{Pr}\langle 5$.

Honda et al [23] studied experimentally the problem of film condensation of R-113 on staggered bundles of horizontal finned tubes. Two tubes with flat-sided annular fins and four tubes with three- dimensional fins were tested. A comparison was made between these results and the previous results for in-line bundles of the same test tubes and a staggered bundle of smooth tubes. Decrease in the heat transfer due to inundation was the most significant for the in-line bundles of the three-dimensional fin tubes, whereas the decrease was very slow for both the staggered and in-line bundles of the flat-sided fin tubes. At low vapor velocity, a fairly well agreement between the previous theoretical results for bundle of flat-sided fin tubes model and the measured data. The highest heat transfer performance was provided by the staggered bundle of flat-sided fin tubes.

Michael et al [24] conducted an experimental work to study the problem of forced convection condensation of steam on a small bank of staggered horizontal tubes. The tube bundle has 10 rows with 4 and 3 tubes per row. They concluded that the vapor-side heat transfer coefficient was found to decrease down the bank. They attributed that to the drop-off of the vapor shear effect and increases condensation inundation. A row-to-row saw-tooth variation of the vapor-side heat transfer coefficient was observed. They attributed that to the fact the dummy half-tubes deflect the steam toward the inner tubes and do not contribute to the reduction in vapor velocity as vapor crosses the row. A comparison with the previous studies was also done.

Memory et al [25] studies the problem of forced convection film condensation on a horizontal tube, effect of surface temperature variation. They found that higher mean heat transfer coefficients were obtained when a simple surface shear approximation was adopted with variable wall temperature. A comparison with the previous studies was also done.

Memory and Rose [26] investigated the effect of variable viscosity in the presence of variable wall temperature on condensation on a horizontal tube. They developed variable viscosity solutions that obtained taking into account both radial and tangential temperature variation. Solutions have been obtained for ethylene glycol. They concluded that circumferential viscosity variation has a stronger effect on heat transfer in condensation on a horizontal tube than does previously considered radial variation. In addition, heat fluxes and so heat transfer coefficients when circumferential viscosity is considered were higher than those evaluated at uniform viscosity. Moreover, the effect of circumferential viscosity variation becomes more important as the surface temperature becomes more non-uniform. Finally, the theoretical results were compared with heat transfer measurements for condensation of ethylene glycol.

Memory et al [27] studied the problem of free and forced convection laminar film condensation on a horizontal elliptical tube. Pure saturated vapor flow vertically downward the tube. Free and forced convection were studied. For free convection, they found that mean heat transfer coefficient for elliptical tube is 11 percent higher than that for the circular tube of equivalent surface area. For forced convection, a small decrease about 2 percent in the mean heat transfer coefficient resulted. However, for the same pressure drop, heat transfer performance for an elliptical tube is increased by up to 16 percent.

Kumar et al [28] investigated the augmentation of outside tube heat transfer coefficient during condensation of steam over horizontal copper tubes experimentally. They tested the condensation of steam over a plain tube, a circular integral-fin tube (CIFT) and a spine integral-fin tube (SIFT). They found that the CIFT and SIFT have enhanced the heat transfer coefficient by a factor of 2.5 and 3.2 respectively. A comparison between the heat transfer coefficient for CIFT and that predicted by previous studies reveals that the Honda and Nozu model under-predicted the values of heat transfer coefficient in a range of 10 to 20 percent when

Browne and Bansal [29] presented an overview of the heat transfer characteristics of shell and tube condensing heat exchangers for the case of downward flowing vapor on the tube bundles. They reviewed 70 papers in the literature. They found that accurate models are available for predicting heat transfer coefficients for single tubes (smooth and integral-finned) under both stationary vapor and vapor shear conditions. However, more studies and investigations should be conducted in order to develop theoretical models for enhanced tube surfaces operating under both single and tube bank conditions. In addition, effect of vapor shear down tube bundles (both smooth and finned tubes) is still opened for investigation since the prediction of velocity distribution through the tube bank is not easy task.

Asbik et al [30] studied numerically the laminar condensation of downward flowing vapor on a single horizontal cylinder or a bank of tubes. An implicit finite difference method is used. The results show that the vapor boundary layer separation depends on the Froude number. Good agreement between the results of heat transfer in inter-tube space with the experimental data was obtained.

Mosaad [31] analyzed the problem of laminar film condensation on an inclined circular tube under the condition of combined free and forced convection. The vapor shear at the condensate surface was modeled by assuming potential vapor flow outside the vapor boundary layer, together with employing the infinite condensation rate approximation of Shekriladze and Gomeluri [8]. A numerically obtained solution reveals the effects of vapor velocity and gravity forces on local and mean Nusselt numbers. Based on numerical results, an explicit expression has been obtained for the case of an inclined tube with infinite length.

Kumar et al [32] conducted an experimental work to augment the heat transfer rate by enhancing the heat transfer coefficient during the condensation of pure vapors and R-134a over horizontal finned tubes. Different types of tubes were tested, namely, plain tubes, circular integral-fin tubes (CIFT), spine integral-fin tubes (SIFT) and partially spined circular integral-fin tubes (PCIFT). Results showed that SIFT out performed the CIFT for the condensation of R-134a by about 16 percent. However, the spines were found most effective in the bottom side of the CIFT. The PCIFT with the spines only in the bottom side of the tube augmented the heat transfer coefficient by 20 percent and 11 percent for the condensation of steam and R-134a, respectively, in comparison to CIFT.

Cavallini et al [33] reviewed the most recent results appeared in the open literature and pertinent to thermal design of condensers for the air conditioning and refrigeration industry; both inside and outside horizontal tubes. They concluded that the well-known semi-empirical correlations for predicting the heat transfer during condensation may be quite inaccurate in some new applications. As a result, more investigations and analysis should be carried out to study the effect of various parameters on the condensation heat transfer.

## 2.2 Studies on vapor-gas mixtures

The effect of non-condensable gas on the film condensation phenomena was also investigated. Minkowycz [34], Minkowycz and Sparrow [35], and Sparrow et al [36] had studied laminar film condensation of water vapor on an isothermal vertical surface. He considered the effect of non-condensable gases on the film condensation process. Results showed that; heat transfer rate decreases monotonically as the concentration of air in the vapor mixture increases. They also studied the effect of superheating, interfacial resistance, thermal diffusion and diffusion thermo. They found that; superheating causes a significant percentage-wise increase in the surface heat transfer relative to the corresponding case with no superheating. Practically, interfacial resistance has a negligible effect on the condensation heat transfer for a mixture of steam and air in either a saturated or a superheated state. Thermal diffusion and diffusion thermo have no significant effect on altering the condensation heat transfer for a mixture of steam and air.

In their studies, Denny et al [37] and Jusionis [38] investigated the effect of non-condensable gas on laminar film condensation of vapor undergoing forced flow along a vertical surface. Heat transfer results showed that the influence of non-condensable gas is most marked for low vapor velocities and large gas concentrations.

Denny and South III [39] studied the effects of forced flow, non-condensable gas, and variable thermo-physical properties on laminar film condensation of pure and binary vapors at the forward stagnation point of a horizontal cylinder. They found that, the effects of non-condensable gas on $q/q_{Nu}$ under quiescent conditions are markedly less severe with forced flow. For steam-air mixture, with $0.01 \le m_{1,\infty} \le 0.15$ , $q/q_{Nu}$ approximately doubles as $u_\infty$ increases from 1 to 10 ft/s. For binary film condensation of steam-methanol mixtures, the effect is similar to that for non-condensable gas.

Al-diwany and Rose [40] conducted experimental work for film condensation of steam on a vertical plane surface in the presence of air, argon and helium, under free convection conditions. Results indicate greater reductions in heat transfer, for given non-condensing gas concentrations, than suggested by earlier reports.

Saddy and Del Pozo [41] proposed a simple model based on forced convection condensation boundary layer flow to study the mechanisms by which heat is transferred to a solid wall, in the presence of non-condensable and superheating, plus viscous dissipation in the gas-vapor. They found that; through an increase in the temperature at the condensate gas vapor interface, the effect of viscous dissipation is to decrease the thickness of the thermal boundary layer set up on the vapor side on top of the condensate, in a similar manner as the effect caused by superheating. Both effects cause an increase in the heat flux to the wall.

V.Srzic [42] and V. Srzic et al [43] studied laminar film condensation from mixtures of a vapor and a lighter non-condensable gas flowing downward along inclined isothermal plates. It was found that the reduction of gas concentration caused an increase in the separation distance for steam-hydrogen and Freon 12 – air mixtures but a decrease in mercury-air case. It is also shown that the heat transfer values experience significant reduction due to the presence of the gas. This reduction in heat transfer is more pronounced for lighter gases than heavier gases.

Approximate theoretically-based equations are obtained by Rose [44] for forced convection condensation in the presence of a non-condensing gas on a flat plate and horizontal cylinder. They are relating the mass flux of vapor to the condensing surface (condensation rate) to the free-stream and condensate surface conditions. They may be used with suitable equations to calculate the heat flux for a given free-stream velocity, composition and temperature and condenser surface temperature. He found a good agreement with experimental data for steam-air mixture data.

Lee and Rose [45] obtained accurate and repeatable heat transfer data for filmwise condensation from pure vapors (steam and R113) and four vapor-gas mixtures flowing vertically downwards over a single horizontal tube. For pure vapors at low to moderate velocities, the mean vapor-side heat transfer coefficients were in satisfactory agreement with earlier measurements and with theory, whereas at higher velocities, the coefficients are somewhat smaller than those predicted by theory. For all four vapor-gas mixtures, excellent agreement between the approximate equation of Rose [44] and experimental data is achieved.

Abdullah et al. [46] conducted an experimental work. Data are presented for condensation from steam-air and R113-air mixtures on a bank of tubes. The test bank consisted of 10 staggered rows of four and five tubes per row. Good agreement with theory at top rows of the bank, whereas, differences appear between theory and experiment at the bottom rows. The cause of these discrepancies is thought to be due to buoyancy effects influencing the build up of air on the lower tubes.

Briggs and Sabaratnam [47] studied experimentally the condensation of steam in the presence of air on a single tube and a tube bank. The tube bank consisted of ten staggered rows of two and one tubes per row. For pure steam, a good agreement between the theory and experiment for both the single tube and tube bank is noticed. For the steam-air mixtures, the single tube data gave good agreement with theory. For the bank of tubes, the data were significantly under predicted by single tube theory.

Briggs and Sabaratnam [48] presented experimental data for condensation from pure steam and steam-air mixtures on integral-fin tubes in a bank. Data are reported for condensation of steam with and without the presence of air on three rows of integral-fin tubes situated in a bank of plain tubes. He compared to plain tubes, the heat transfer to the finned tubes was much more susceptible to the presence of non-condensing gas in the vapor.

## 2.3 Objectives of the present thesis work

According to literature, several theoretical and experimental studies on the problem of forced film condensation of vapors or vapor-gas mixtures flowing downward on a single horizontal tube or a flat plate have been undertaken. The approaches have been used with different assumptions and approximations. For condensation on the bank of tubes, the flow pattern is generally involves complex interactions between vapor and condensate. In practice, the situation may be further complicated by the presence of noncondensable gases, which build up in the bank as vapor is removed by condensation. Few studies are available in literature on the combined effect of noncondensing gas and vapor velocity for condensation on tube banks.

In the present thesis work, Numerical and experimental approaches have to be investigated so as to study the effect of noncondensables and forced flow on heat transfer during film condensation over bundle of tubes. In additon to the other known parameters that effect the process such as; tube diameter, vapor to tube wall temperature difference.

The methodology of this study is mainly based on the theoretical and experimental studies. In the theoretical study, mathematical modelling, setting suitable boundary conditions, programming and data processing with the help of a computer alogritms should be taken in consideration. Moreover, the experimental investigation will help in verification and validation of the theoretical results. An experimental setup has to be designed and erected in order to match the research needs.

Condensation phenomenon on Tier of tubes may be also investigated by inclining the set up at different inclination angles. The reason of inclining the setup to predetermined angles is to investigate the effect of staggering of cylinders on the heat transfer rates and to see how condensation is affected at the lower tubes when condensate does not fall onto the center line of the tubes. According to the factors mentioned above, there is a necessity for conducting an original scientific research work based on a suitable research methodology to come up with the desired results.

In this respect, this thesis work will aim to;

- Mathematical modeling of the film condensation problem over bundle of tubes by 2-D, non-linear partial differential equations (continuity, momentum, energy and species).
- Setting up the suitable boundary conditions and initial profiles.
- Numerical analysis and computer programming.
- Studying the effect of vapor velocity and non-condensable gases beside the other parameters on the film condensation heat transfer.
- Designing and mounting an experimental setup and conducting experimental work.
- Verification of the numerical results, comparison and discussing the differences.

# CHAPTER 3

# PHYSICAL AND MATHEMATICAL MODELING

The problem of forced film condensation heat transfer of vapor and vapor-air mixture flowing downward a tier of horizontal cylinders is investigated numerically and experimentally. Both inline and staggered arrangements are considered.

Two mathematical models are proposed for the solution of the problem based on the state of the vapor used whether pure vapor or vapor-air mixture and on the physical situation of the problem and the related assumptions and approximations used. For pure vapor, the physical situation of the problem is not complicated when compared with that of vapor-air mixture. Integral approach is implemented. Two systems of nonlinear differential equations is reduced to nonlinear system of algebraic equations solved by Newton Raphson method. For vapor-air mixture, a differential approach based on the boundary layer theory for two phase flow is considered. The system of nonlinear partial differential equations for both liquid and vapor –air mixture boundary layers are transformed to an implicit finite difference scheme solved numerically by tri-diagonal matrix algorithm.

## 3.1 Physical and mathematical model for pure vapor

A mathematical model has been developed with the help of the lecture notes of Arpacı [54] and Makas [61]. Two systems of nonlinear ordinary differential equations, which are obtained by applying the principles of conservation of mass and conservation of momentum on the condensate layer, are transformed into the finite difference forms. Thus, the problem is turned to a state that can be solved numerically by the computer. A computer program, which uses the Newton-Raphson method, has been implemented in order to analyze the problem. The program gives the film thickness and the velocity distribution of the condensate for each condensation tube. Figure 3.1 shows the physical model of the problem.

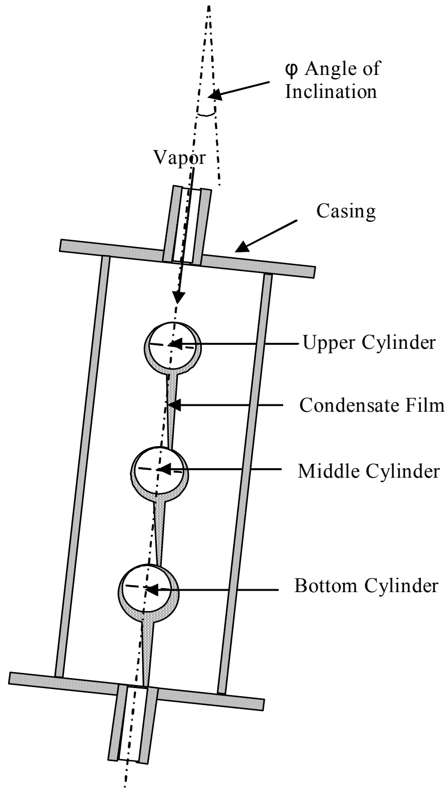


Figure 3.1 Physical model of the problem

### 3.1.1 Upper cylinder

The theoretical approach to laminar film condensation is developed from conservation of mass and conservation of momentum principles which are applied to the condensate. Some assumptions should be made before starting the analysis;

- laminar flow and constant properties are assumed for the liquid film;
- the vapor is at uniform temperature and quiescent;
- heat transfer from vapor to liquid is only carried out by condensation;

the shear stress at the liquid-vapor interface is assumed to be negligible in which case $\left.\frac{\partial u}{\partial y}\right|_{y=\delta} = 0$;

- heat transfer through the condensate film occurs only by conduction. Therefore, temperature distribution in the film is linear;
- The condensate falling down to the lower cylinders can be thought as a second layer above the film thickness, δ. The velocity profile of the second layer is uniform. As condensate flows downward around the cylinder, the thickness of the second layer (Δ) goes to zero as seen in Figure 3.3. The analysis is normally carried out after this merge point of two condensate layers [61].

The definition of the problem on the sketch is given in Figure 3.2. The condensate film begins to form at the top of the condensation tube. Film thickness increases while the condensate flows down on the tube as the steam condenses over them.

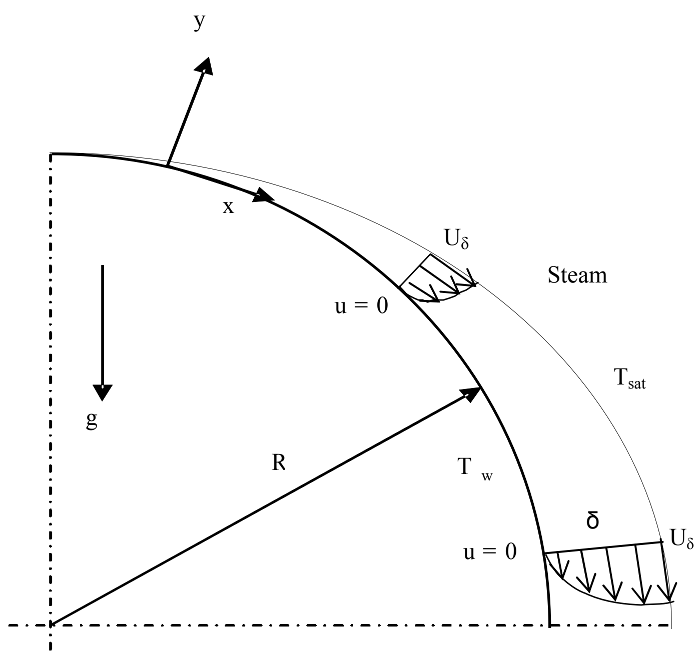


Figure 3.2 Physical model and coordinate system for upper cylinder.

The approximate velocity profile is expressed in terms of free stream velocity, condensate film thickness and the distance from the wall as outlined in [54].

In order to get an approximate formula for velocity profile, the approximate analysis of the laminar boundary layer can be used. The boundary conditions that proposed velocity profile should satisfy;

$$\begin{aligned} &at \quad y=0, \quad x\geq 0: \qquad u=0, \qquad \frac{\partial^2 u}{\partial y^2}=0 \\ &at \quad y=\delta, \quad x\geq 0: \qquad u=U_\delta, \qquad \frac{\partial u}{\partial y}=0 \end{aligned} \tag{3.1}$$

A cubic polynomial will satisfy the boundary conditions above; let us assume that;

$$\frac{u}{U_\delta}=A+By+Cy^2+Dy^3 \tag{3.2}$$

where, A, B, C, and D can be functions of x. Using the above boundary conditions we see that;

$$A=0, \qquad B=\frac{3}{2\delta}, \qquad C=0, \qquad D=-\frac{1}{2\delta^3} \tag{3.3}$$

Therefore, a good approximation for the velocity profile in a laminar flow, [54] is;

$$u=U_\delta\left[\frac{3}{2}\left(\frac{y}{\delta}\right)-\frac{1}{2}\left(\frac{y}{\delta}\right)^3\right] \tag{3.4}$$

The analysis is started by taking an integral control volume within the condensate film. If the conservation of mass principle is applied on the control volume, we get;

$$\int_0^\delta \rho_l u dy+\frac{k_l}{h_{fg}}\frac{\Delta T}{\delta}dx=\int_0^\delta \rho_l u dy+\frac{\partial}{\partial x}\left(\int_0^\delta \rho_l u dy\right)dx \tag{3.5}$$

$$\frac{d}{dx}\left(\int_0^\delta \rho_l u dy\right) = \frac{k_l}{h_{fg}}\frac{\Delta T}{\delta} \tag{3.6}$$

Since only conduction type heat transfer mechanism and unit depth are assumed at the beginning of the analysis, heat transfer rate through the area ($dx \times 1$);

$$dQ = -k_l \left.\frac{\partial T}{\partial y}\right|_{y=0} dx = k_l \frac{T_{sat} - T_w}{\delta} dx \tag{3.7}$$

Heat transfer rate can be expressed in terms of the mass flow of the condensate through any *x*- position of the film and the latent heat of condensation of steam. Thus

$$dQ = d\dot{m}\, h_{fg} \tag{3.8}$$

The second term in Equation (3.5) can be readily obtained by equalizing Equation (3.7) and Equation (3.8);

$$d\dot{m} = \frac{k_l}{h_{fg}}\frac{\Delta T}{\delta} dx \tag{3.9}$$

Recalling Equation (3.4) and substituting it into Equation (3.6);

$$\frac{d}{dx}\left(\int_0^\delta U_\delta \left[\frac{3}{2}\left(\frac{y}{\delta}\right) - \frac{1}{2}\left(\frac{y}{\delta}\right)^3\right] dy\right) = \frac{k_l}{\rho_l h_{fg}}\frac{\Delta T}{\delta} \tag{3.10}$$

Solving the integral for y we get;

$$\frac{5}{8}\frac{d}{dx}\left(\delta U_\delta\right) - \frac{k_l}{\rho_l h_{fg}}\frac{\Delta T}{\delta} = 0 \tag{3.11}$$

There are two unknowns in this equation and one more equation is needed to solve the problem. The required equation can be obtained from the conservation of momentum principle. Therefore;

$$\frac{d}{dx}\left(\int_0^\delta \rho_l u^2 dy\right) - \rho_l \delta f_x + \tau_s\big|_{y=0} = 0 \tag{3.12}$$

$f_x$ is body force and it is defined in terms of gravity force in this problem. For the condensate around a cylinder;

$$f_x = g\sin\theta \tag{3.13}$$

As gravity force drags the condensate downward, shear force of the condensate layer retards the motion of the condensate. The shear stress in Equation (3.12) may be expressed with Newton's law of viscosity;

$$\tau_s = \mu \left.\frac{du}{dy}\right|_{y=0} \tag{3.14}$$

Substituting by $u$ from Equation (3.4) and taking the derivative, one can obtain;

$$\tau_s = \frac{3}{2}\mu\frac{U_\delta}{\delta} \tag{3.15}$$

As it is done in the conservation of mass principle, similarly recalling Equation (3.4) and integrating Equation (3.12);

$$\frac{17}{35}\rho_l\frac{d}{dx}\left(\delta U_\delta^{\,2}\right) - \delta\rho_l g\sin\theta + \frac{3}{2}\mu\frac{U_\delta}{\delta} = 0 \tag{3.16}$$

### 3.1.2 Lower cylinders

Using the same procedure, as for the case of upper cylinder above, an integral control volume within the condensate film for the lower cylinders is considered as shown in Figure 3.3. The conservation of mass principle is applied on the control volume as;

$$\int_0^{\delta} \rho_l u dy + \int_{\delta}^{\Delta} \rho_l U_{\delta} dy + \frac{k_l}{h_{fg}} \frac{\Delta T}{\delta} dx = \int_0^{\delta} \rho_l u dy + \int_{\delta}^{\Delta} \rho_l U_{\delta} dy + \frac{\partial}{\partial x}\left( \int_0^{\delta} \rho_l u dy \right) dx + \frac{\partial}{\partial x}\left( \int_{\delta}^{\Delta} \rho_l U_{\delta} dy \right) dx \tag{3.17}$$

$$\frac{d}{dx}\left( \int_0^{\delta} \rho_l u dy \right) + \frac{d}{dx}\left( \int_{\delta}^{\Delta} \rho_l U_{\delta} dy \right) = \frac{k_l}{h_{fg}} \frac{\Delta T}{\delta} \tag{3.18}$$

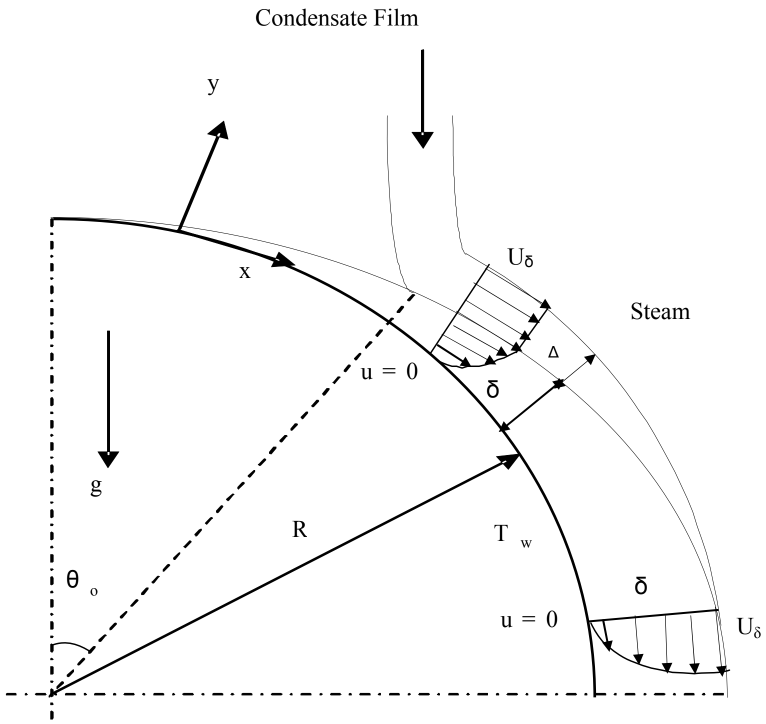


Figure 3.3 Physical model for the middle and bottom cylinders.

Recalling Equation (3.4) and substituting it into Equation (3.18) we get;

$$\frac{d}{dx}\left(\int_0^{\delta} U_{\delta}\left[\frac{3}{2}\left(\frac{y}{\delta}\right)-\frac{1}{2}\left(\frac{y}{\delta}\right)^3\right]dy\right)+\frac{d}{dx}(U_{\delta}\Delta)=\frac{k_l}{\rho_l h_{fg}}\frac{\Delta T}{\delta} \tag{3.19}$$

Solving the integral for y;

$$\frac{5}{8}\frac{d}{dx}\left(\delta U_{\delta}\right)+\frac{d}{dx}(U_{\delta}\Delta)-\frac{k_l}{\rho_l h_{fg}}\frac{\Delta T}{\delta}=0 \tag{3.20}$$

There are three unknowns in this equation, namely, the condensate film thickness δ, the vapor-liquid interface velocity $U_\delta$ and the second layer thickness **Δ**. Referring to the last assumption, the second term of the above equation diminishes at the merge point which is the point where the analysis is assumed to start from. As a result, the number of unknowns is reduced to two unknowns, δ and $U_\delta$. One more equation is needed to solve the problem. The required equation can be obtained from the conservation of momentum principle. Therefore;

$$\frac{d}{dx}\left(\int_0^{\delta}\rho_l u^2 dy\right)+\frac{d}{dx}\left(\int_{\delta}^{\Delta}\rho_l U_{\delta}^2 dy\right)-\rho_l\delta f_x+\tau_s\big|_{y=0}=0 \tag{3.21}$$

$f_x$ in this case is defined in terms of gravity force and angle of inclination, φ, for the condensate around the lower cylinder;

$$f_x = g\sin\theta\cos\varphi \tag{3.22}$$

Shear force of the condensate layer is defined according to equation (3.15). As it is done in the conservation of mass principle, similarly recalling Equation (3.4) and integrating Equation (3.21) we get;

$$\frac{17}{35}\rho_l\frac{d}{dx}\left(\delta U_{\delta}^{\,2}\right)+\rho_l\frac{d}{dx}(\Delta U_{\delta}^2)-\delta\rho_l g\sin\theta\cos\varphi+\frac{3}{2}\mu\frac{U_{\delta}}{\delta}=0 \tag{3.23}$$

### 3.1.3 Liquid sheet falling between the cylinders

The governing equations between the upper and lower cylinders are treated as presented by Asbik et al [30]. The liquid velocity between the upper and lower cylinders was given as;

$$U_H = \sqrt{2gH} \tag{3.24}$$

The liquid descends vertically as a continuous sheet with mass flow rate ($2\Gamma$), and its local width ($2\delta_H$) can be expressed as;

$$2\delta_H = \frac{2\Gamma}{\rho_l U_H} \tag{3.25}$$

### 3.1.4 Critical angle of inclination and condensate fall angle

Critical Angle of Inclination, $\varphi_{crit,}$ is defined as the angle which ensures that the condensate spilling from the upper cylinder fall tangentially to the periphery of

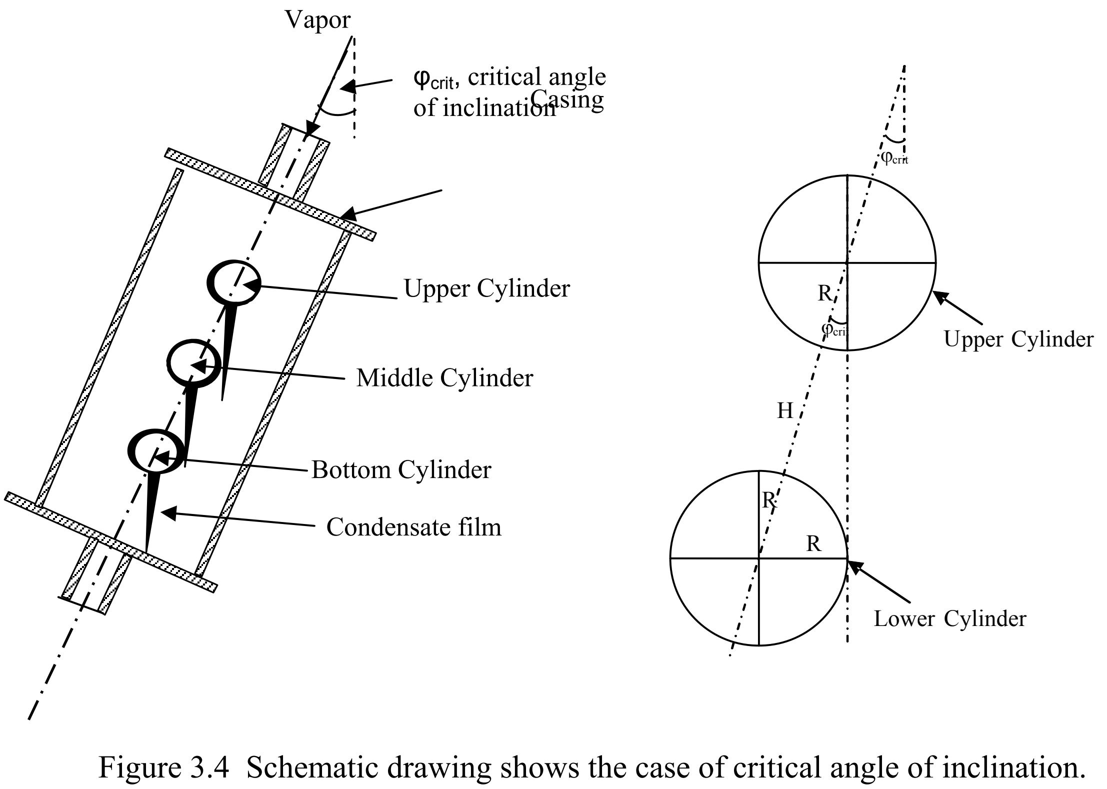


Figure 3.4 Schematic drawing shows the case of critical angle of inclination.

the lower cylinder. It corresponds to a condensate fall angle ($\theta_o$) of 90°. This is depicted in Figure 3.4. This angle can be calculated by simple trigonometric relations. It depends mainly on the radius of the cylinder, R, and the height between the cylinders, h;

$$\sin(\varphi_{crit.}) = \frac{R}{2R + H} \tag{3.26}$$

Results show that; the critical angle of inclination is 21° for H= 20 mm and R= 25.4 mm, see Table 3.1. By a similar procedure, condensate fall angle on the lower cylinders, $\theta_0$, can be calculated for different angles of inclination.

For example, for $R$ =25.4 mm, $\theta_0$ = 12.84° at $\varphi$ = 3° , $\theta_0$ = 25.67° at $\varphi$ = 6° and $\theta_0$ = 38.5° at $\varphi$ = 9°. For the special case of a vertical tier of horizontal cylinders when $\varphi$ = 0°, $\theta_0$ =0°.

Table (3.1): The values of the critical inclination angle ($\varphi_{crit.}$) and the corresponding condensate fall angle ($\theta_0$) for different inclination angles and different cylinder diameters at (H=0.02 m).

| R (m) | H(m) | φ(degrees) | $\varphi_{crit}$ (degrees) | θo (degrees) |
|---|---|---|---|---|
| **0.0254** | **0.02** | **3** | **21.03454618** | **12.83602687** |
| | **0.02** | **6** | **21.03454618** | **25.67205374** |
| | **0.02** | **9** | **21.03454618** | **38.50808061** |
| | **0.02** | **12** | **21.03454618** | **51.34410748** |
| | **0.02** | **15** | **21.03454618** | **64.18013435** |
| | **0.02** | **18** | **21.03454618** | **77.01616122** |
| | **0.02** | **21** | **21.03454618** | **89.85218809** |
| **0.01905** | **0.02** | **3** | **19.15003833** | **14.09918849** |
| | **0.02** | **6** | **19.15003833** | **28.19837698** |
| | **0.02** | **9** | **19.15003833** | **42.29756547** |
| | **0.02** | **12** | **19.15003833** | **56.39675396** |
| | **0.02** | **15** | **19.15003833** | **70.49594245** |
| | **0.02** | **18** | **19.15003833** | **84.59513094** |
| | **0.02** | **21** | **19.15003833** | **98.69431943** |
| **0.0127** | **0.02** | **3** | **16.25266948** | **16.61265556** |
| | **0.02** | **6** | **16.25266948** | **33.22531111** |
| | **0.02** | **9** | **16.25266948** | **49.83796667** |
| | **0.02** | **12** | **16.25266948** | **66.45062223** |
| | **0.02** | **15** | **16.25266948** | **83.06327779** |
| | **0.02** | **18** | **16.25266948** | **99.67593334** |
| **0.00635** | **0.02** | **3** | **11.2030658** | **24.10054577** |
| | **0.02** | **6** | **11.2030658** | **48.20109155** |
| | **0.02** | **9** | **11.2030658** | **72.30163732** |
| | **0.02** | **12** | **11.2030658** | **96.40218309** |

### 3.1.5 Method of solution for pure vapor model

Initial profiles for condensate film thickness and velocity distribution are needed to start the iteration. These initial profiles can be derived from Nusselt's original theory. Film thickness for a vertical flat plate is given by Nusselt's theory as;

$$\delta(x) = \left[ \frac{4k_l \mu_l (T_{sat} - T_w) x}{g\rho_l (\rho_l - \rho_v) h_{fg}} \right]^{1/4} \tag{3.27}$$

Neglecting the density of vapor since it is very small when compared to the density of the fluid and taking the curvature of the cylinder into consideration, the following expression is obtained for the film thickness;

$$\delta(x) = \left[ \frac{3\nu k_l (T_{sat} - T_w) x}{g\rho_l h_{fg} \sin\left(\frac{x}{R}\right)} \right]^{1/4} \tag{3.28}$$

The velocity profile in the film is [1];

$$u = \frac{g\rho_l \delta^2 \sin(\frac{x}{R})}{\mu_l} \left[ \frac{y}{\delta} - \frac{1}{2}\left(\frac{y}{\delta}\right)^2 \right] \tag{3.29}$$

Initial velocity profile along the liquid-vapor interface can be obtained substituting δ into Equation (3.29);

$$U_\delta = \frac{g\rho_l \delta^2}{2\mu_l} \sin(\frac{x}{R}) \tag{3.30}$$

It is necessary to transform the ordinary differential equations into finite difference equations in order to solve Equations (3.11) and (3.16) simultaneously, and the same method is applied to Equations (3.20) and (3.23) for the lower cylinders. Hence, Equation (3.11) yields;

$$\frac{5}{8}\frac{\left(\delta_i U_{\delta i}-\delta_{i-1}U_{\delta i-1}\right)}{\Delta x}-\frac{k_l}{\rho_l h_{fg}}\frac{\Delta T}{\delta_i}=0 \tag{3.31}$$

Equation (3.16) yields;

$$\frac{17}{35}\rho_l\left(\frac{\delta_i\left(U_{\delta i}\right)^2-\delta_{i-1}\left(U_{\delta i-1}\right)^2}{\Delta x}\right)-\delta_i\rho_l g\sin\theta+\frac{3}{2}\mu\frac{U_{\delta i}}{\delta_i}=0 \tag{3.32}$$

Similarly, Equation (3.20) yields;

$$\frac{5}{8}\frac{\left(\delta_i U_{\delta i}-\delta_{i-1}U_{\delta i-1}\right)}{\Delta x}+\frac{\left(\Delta_i U_{\delta i}-\Delta_{i-1}U_{\delta i-1}\right)}{\Delta x}-\frac{k_l}{\rho_l h_{fg}}\frac{\Delta T}{\delta_i}=0 \tag{3.33}$$

Equation (3.23) yields;

$$\frac{17}{35}\rho_l\left(\frac{\delta_i\left(U_{\delta i}\right)^2-\delta_{i-1}\left(U_{\delta i-1}\right)^2}{\Delta x}\right)+\rho_l\left(\frac{\Delta_i\left(U_{\delta i}\right)^2-\Delta_{i-1}\left(U_{\delta i-1}\right)^2}{\Delta x}\right)-$$
$$\delta_i\rho_l g\sin\theta\cos\varphi+\frac{3}{2}\mu\frac{U_{\delta i}}{\delta_i}=0 \tag{3.34}$$

Newton-Raphson method is used to solve the above system of nonlinear algebraic equations. A detailed description for the numerical analysis and procedures is mentioned in chapter 4.

### 3.2 Physical and Mathematical model for vapor-air mixture

Based on the boundary layer theory for two phase flow and on the mathematical models described everywhere in references [34], [37] and [38] for forced film condensation on a flat plate in the presence of non-condensable gases and on the mathematical model proposed by Denny and South III [39] for forced film condensation on a cylinder in the presence of non-condensable gases, the governing partial differential equations (continuity, momentum, species and energy) for both liquid and vapor-mixture boundary layers. A slight modification for the term of body force effects takes into account the effect of angle of inclination, $\varphi$ (staggered arrangement), where (inline arrangement) is treated as a special case corresponds to ($\varphi=0$ ). In order to start the analysis, some assumptions are made as follows;

- the flow is two-dimensional, laminar and steady; constant properties are assumed then the term $\dfrac{\partial \ln C_{p,v}}{\partial y}$ in Equation (3.38) below will be equal to zero under this assumption;
- no chemical reaction;
- heat transfer from vapor to liquid is only carried out by condensation;
- heat transfer through the condensate film occurs only by conduction. Therefore, temperature distribution in the liquid film is linear;
- the vapor properties are evaluated at its saturation state.
- the effects of thermal diffusion, diffusion thermo, superheating and interfacial resistance are neglected;
- outside the vapor-air mixture boundary layer, the flow is potential.
- The condensate falling down to the lower cylinders can be thought as a second layer above the film thickness, $\delta$. The velocity profile of the second layer is uniform. As condensate flows downward around the cylinder, the thickness of the second layer ($\Delta$) goes to zero as seen in Figure 3.7. The analysis is normally carried out after this merge point of two condensate layers.

### 3.2.1 Vapor-air mixture boundary layer

Referring to the model proposed by Denny and South [39], and the other mentioned references that are mentioned above, the governing differential equations and the boundary conditions can be written as seen below. It should be noted that a modification to the term of body force that take into account the effect of angle of inclination ($\varphi$), i.e the staggering effect.

$$\frac{\partial}{\partial x}(\rho_v u_v) + \frac{\partial}{\partial y}(\rho_v v_v) = 0 \tag{3.35}$$

$$\rho_v u_v \frac{\partial u_v}{\partial x} + \rho_v v_v \frac{\partial u_v}{\partial y} = \frac{\partial}{\partial y}(\mu_v \frac{\partial u_v}{\partial y}) + \rho_v g \sin(\frac{x}{R})\cos(\varphi) - \frac{dP}{dx} \tag{3.36}$$

$$\rho_v u_v \frac{\partial m_1}{\partial x} + \rho_v v_v \frac{\partial m_1}{\partial y} = \frac{\partial}{\partial y}(\frac{\mu_v}{Sc}\frac{\partial m_1}{\partial y}) \tag{3.37}$$

$$\rho_v u_v \frac{\partial T_v}{\partial x} + \rho_v v_v \frac{\partial T_v}{\partial y} = \frac{\partial}{\partial y}(\frac{\mu_v}{\Pr}\frac{\partial T_v}{\partial y}) + \frac{\mu_v}{\Pr}\frac{\partial T_v}{\partial y}\left[\frac{\partial \ln C_{p,v}}{\partial y} + \frac{\Pr}{Sc}\frac{C_{p,1} - C_{p,2}}{C_{p,v}}\frac{\partial m_1}{\partial y}\right] \tag{3.38}$$

### 3.2.2 Liquid boundary layer

$$\frac{\partial^2 u_l}{\partial y^2} = -\left[\rho_l g \sin(\frac{x}{R})\cos(\varphi) - \frac{dP}{dx}\right] \Big/ \mu_l \tag{3.39}$$

$$\frac{d^2 m_1}{dy^2} = \frac{d^2 T_l}{dy^2} = 0 \qquad \text{(3.40) and (3.41)}$$

It should be noted that the usage of the extended Nusselt-type analysis for solving the liquid boundary layer, as formulated above by Equation (3.39), Equation (3.40) and Equation (3.41), whereby Nusselt assumptions were taken into consideration, results in negligible error when compared with the results of the fully numerical solution for both the film and the vapor boundary layer [38].

Based on potential flow theory, the static pressure gradient ($\frac{dP}{dx}$) appears in Equation (3.36) and Equation (3.39) is taken as;

$$-\frac{dP}{dx} = \left[(\frac{4\rho_\infty U_\infty^2}{R})\cos(\frac{x}{R}) - \rho_\infty g\right]\sin(\frac{x}{R}) \tag{3.42}$$

Equations (3.35) - (3.41) are subjected to the boundary conditions;

$$u_v \rightarrow U_e \equiv 2U_\infty \sin\left(\frac{x}{R}\right), \qquad \mathrm{m}_1 \rightarrow m_{1,\infty}, \qquad \text{and } \mathrm{T_v} \rightarrow \mathrm{T_\infty} \tag{3.43}$$

at the edge of the boundary layer;

$$u_l = 0, \qquad \frac{dm_1}{dy} = 0, \qquad \text{and } \mathrm{T_l} = \mathrm{T}_w \tag{3.44}$$

at the surface of the cylinder.

At the liquid-vapor interface, according to Jusionis [38], interfacial boundary conditions were written in terms of reference u and s surfaces at liquid-vapor interface as shown in Figure 3.5 below.

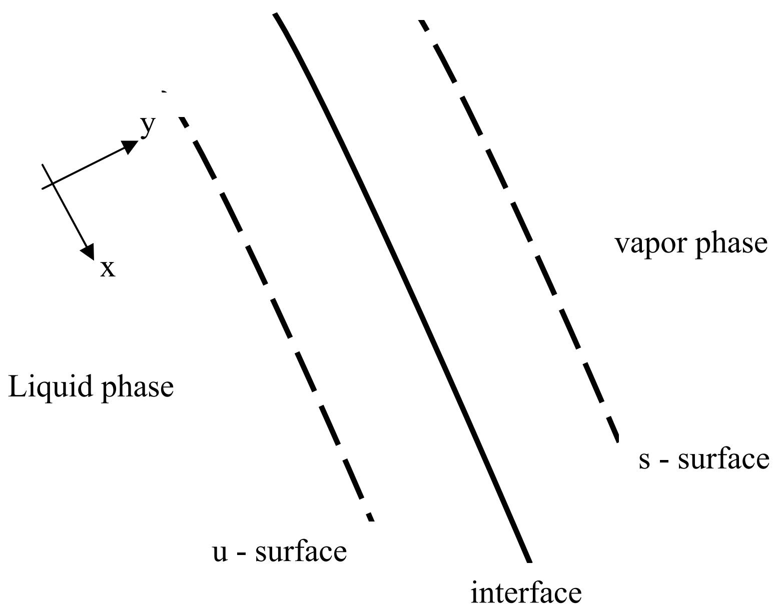


Figure 3.5 Reference u and s surfaces at the liquid - vapor interface.

Then, the interfacial boundary conditions can be written as;

$$u_l\big|_u = u_v\big|_s = u_i \tag{3.45}$$

$$u_l \frac{\partial u_l}{\partial y}\bigg|_u = u_v \frac{\partial u_v}{\partial y}\bigg|_s = \tau_i \tag{3.46}$$

$$\dot{m}m_1\big|_u = \dot{m}m_1\big|_s + j_{1,y}\big|_s = \dot{m}m_1\big|_s - \rho_v D_{12} \frac{\partial m_1}{\partial y}\bigg|_s \tag{3.47}$$

$$m_{1,u} = m_{1,u}(m_{1,s}, P_\infty) \tag{3.48}$$

$$T_l\big|_u = T_v\big|_s = T_i(m_{1,s}, P_\infty) \tag{3.49}$$

$$k_l \frac{\partial T_l}{\partial y}\bigg|_u = -\dot{m}\, h_{fg} + k_v \frac{\partial T_v}{\partial y}\bigg|_s \tag{3.50}$$

In equation (3.47), a logical physical fact that the net mass flow of non-condensable gas vanish at the liquid-vapor interface, $\dot{m}_{g,i} = 0$ since the interface is impermeable to the non-condensable gas (air) as stated in reference [34]. Equation (3.47) can be reformulated as;

$$\dot{m} = \frac{\rho_v D_{12}}{m_{1,s}} \frac{\partial m_1}{\partial y}\bigg|_s \tag{3.51}$$

where

$$m_1\big|_s = m_1\big|_u = m_1\big|_i$$

In Equation (3.48) and Equation (3.49), thermodynamic equilibrium is assumed to apply. The interfacial mass flux is given by;

$$\rho_v v\big|_s \equiv \dot{m} = -\frac{d}{dx}\int_0^{\delta} \rho u_l \, dy\Big|_l \tag{3.52}$$

The local film thickness $\delta(x)$ is calculated based on the following heat balance;

$$k_l \frac{\partial T_l}{\partial y}\bigg|_u = k_v \frac{\partial T_v}{\partial y}\bigg|_s + \frac{d}{dx}\int_0^{\delta(x)} \rho_l u_l \left[h_{fg} + C_{p,l}(T_i - T_l)\right] dy \tag{3.53}$$

In addition, there is the equation of state of an ideal gas mixture, $P = \rho_v RT$, and the thermodynamic constraint that the interface condition is a saturation state for the condensing vapor. From thermodynamic tables;

$$T_i = T_i(m_{1,i}, P) \tag{3.54}$$

where it is assumed that the interface exhibits negligible departure from thermodynamic equilibrium.

Interface temperature, $T_i$, and interface mass fraction, $m_{1,i}$, are calculated based on the procedures mentioned by Minkowycz [34], Minkowycz and Sparrow [35] and Jusionis [38], see section 3.2.5.

Figure 3.6 and Figure 3.7 show the physical situation and coordinate system for the problem. An orthogonal curvilinear coordinates system is presented. Physical parameters and thermo-physical properties are presented in Appendix A.

It should be noted that; the governing equations for liquid sheet falling between the cylinders, critical angle of inclination and condensate fall angle are treated as in described in section 3.1 above.

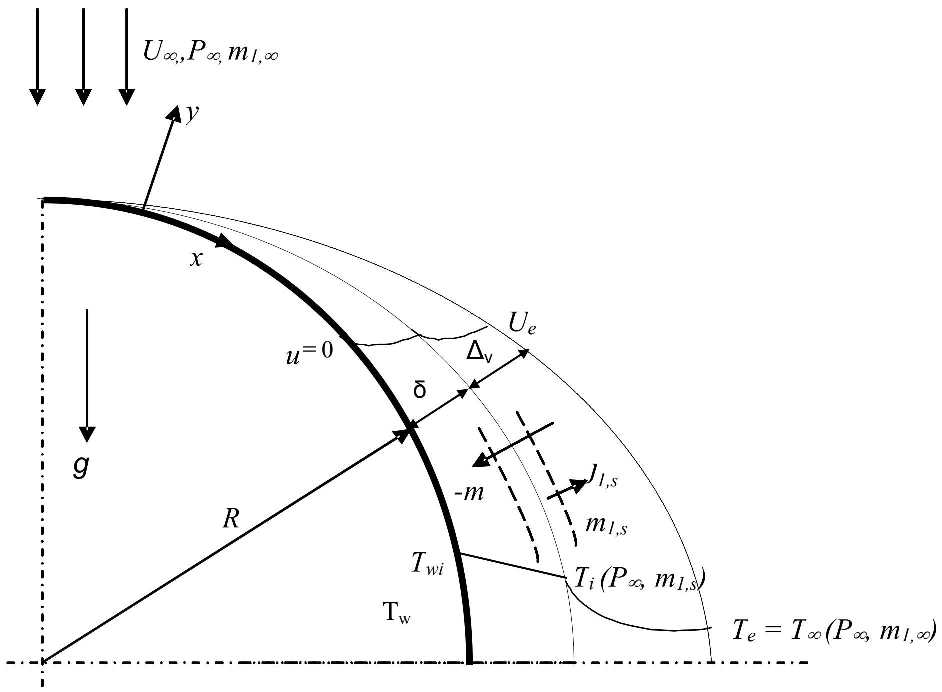


Figure 3.6 Physical model and the coordinate system for the upper cylinder.

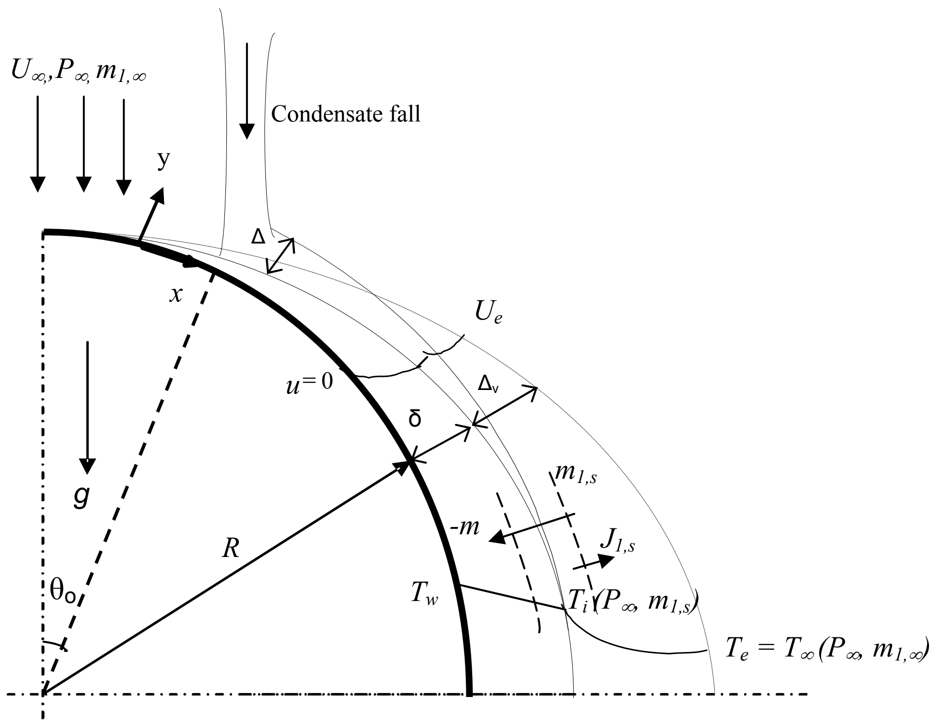


Figure 3.7 Physical model and the coordinate system for the middle and bottom cylinders.

### 3.2.3 Method of solution for vapor-air mixture model

An implicit finite difference scheme is used for numerical approximations of system of boundary layer equations for vapor and liquid sides. The resulted tri-diagonal matrices are solved by so called the Tri-Diagonal Matrix Algorithm (TDMA) mentioned in reference [49]. A two dimensional finite difference mesh with suitable number of nodes, codes and step sizes is formed. Then a computer program is written in Fortran77. Runs and outputs are recorded and plotted with the help of Excel software. In the computer program, 180 equally spaced layers in x-direction (each 1 degree on the cylinder periphery), 250 equally spaced layers for the liquid boundary layer and 250 equally spaced layers for the vapor-mixture boundary layer were taken.

A detailed description for the numerical analysis and procedures is mentioned in chapter 4.

### 3.2.4 Starting the problem and the initial profiles

Initial profiles for film thickness, velocity and temperature distributions based on Nusselt theory are needed to initiate the complete numerical solutions using finite difference scheme for the boundary layer equations. Initial profiles proposed by Srzic [42] are followed in this study.

The liquid film thickness and velocity profile at the liquid boundary layer are evaluated based on Equation (3.28) and Equation (3.29) respectively.

In addition, the temperature profile at the liquid boundary layer is calculated according to the following equation;

$$T_l(y) = (T_i - T_w)\eta(y) + T_w \tag{3.55}$$

where, $\eta = \dfrac{y}{\delta}$ is introduced in a dimensionless form for normalization.

Within the vapor-air mixture boundary layer, velocity, concentration and temperature are initiated as;

$$u_v(y) = U_\infty \tag{3.56}$$

$$m_1(y) = m_{1,\infty} \tag{3.57}$$

$$T_v(y) = T_\infty \tag{3.58}$$

### 3.2.5 Interface temperature and interface air fraction

In order to evaluate the interface temperature, interface air concentration, there is a procedure that can be implemented and incorporated. The procedure that mentioned by Minkowycz [34] and Minkowycz and Sparrow [35] can be summarized as follows;

- Under the assumption that the vapor is at its saturation state, it is possible to evaluate the free stream total system pressure from Gibbs-Dalton law as;

$$P_\infty = P_{sat}(T_\infty)\left[\frac{M_g + m_{1,\infty}(M_v - M_g)}{M_g - m_{1,\infty}M_g}\right] \tag{3.59}$$

where

$P_{sat}(T_\infty)$ can be taken from vapor (steam) tables or from the correlation mentioned in reference [42 ];

$$P_{sat}(T_\infty) = \exp\left(\frac{B}{T_{sat} - A} - C\right) \tag{3.60}$$

where

A, B and C are given for two pressure or temperature ranges;

| | |
|---|---|
| $0.611\,kPa \le P_{sat} \langle 12.33\times10^3\ kPa$ | $12.33\times10^3\ kPa \le P_{sat} \le 22.1\times10^3 kPa$ |
| $273.15K \le T_{sat} \langle 600.0\text{K}$ | $600.0K \le T_{sat} \langle 647.3\text{K}$ |
| $A = 0.426776\times10^2$ | $A = -0.387592\times10^3$ |
| $B = -0.38927\times10^4$ | $B = -0.125875\times10^5$ |
| $C = -0.948654\times10^1$ | $C = -0.152578\times10^2$ |

- interface temperature, $T_i$, can be evaluated from the energy balance at the liquid-vapor interface, Equation (3.50) above;
- evaluate the corresponding partial pressure of the vapor at the interface, $P_{v,i}(T_i)$, and the density from the tabulated properties of the vapor (steam tables) or by the help of the Equation (3.60). where $P_{sat}(T_\infty)$ and $T_{sat}$ in Equation (3.60) are changed to $P_{v,i}(T_i)$ and $T_i$ respectively;
- evaluate the partial pressure of the non-condensable gas (air), $P_{g,i}$, at the liquid-vapor interface according to this relation;

$$P_{g,i} = P_\infty - P_{v,i} \tag{3.61}$$

  where $P_\infty$ and $P_{v,i}$ are the free stream total system pressure and partial pressure of the vapor at the liquid – vapor interface respectively.
- from the knowledge of interface temperature, $T_i$, and the partial air pressure at the interface, $P_{g,i}$, the density of the air at the interface can be calculated from perfect gas law.
- finally, the corresponding non-condensable gas (air) fraction at the liquid – vapor interface is evaluated as;

$$m_{1,i} = \frac{\rho_{g,i}}{\rho_{g,i} + \rho_{v,i}} \tag{3.62}$$

$$\rho_i = \rho_{g,i} + \rho_{v,i} \tag{3.63}$$

## 3.3 Heat transfer rate, heat transfer coefficient and Nusselt number

After knowing the value of interface temperature, $T_i$ local heat flux can be calculated directly from the basic formula as;

$$q(x) = k_l \left( \frac{\partial T_l}{\partial y} \right)_{y=0} = k_l \frac{\left( T_i(x) - T_w \right)}{\delta(x)} \tag{3.64}$$

It should be noted the value of $T_i(x)$ represents the uniform saturation vapor temperature at the vapor boundary layer, $T_{sat}$ in the case of pure vapor boundary layer model. However, it represents the interfacial temperature, $T_i$ in the case of vapor-air mixture boundary layer model.

$$q(x) = -\dot{m}(x)\, h_{fg} \tag{3.65}$$

local heat transfer coefficient can be also evaluated from the relation;

$$h(x) = \frac{q(x)}{T_{sat} - T_w} \tag{3.66}$$

local Nusselt number is finally calculated as follows;

$$Nu(x) = \frac{h(x)d}{k_l} \tag{3.67}$$

### 3.4 Thermodynamic and transport properties

In order to solve the system of the governing equations and to conduct the analysis procedures, it is very important to know the thermo-physical and transport properties for liquid water, steam and air in addition to steam-air mixture.

It should be noted that all liquid water properties $\rho_l$, $\mu_l$, $k_l$ and $C_{p,l}$ except $h_{fg}$ are evaluated at the reference temperature, $T_r$ [34]. Latent heat of vaporization, $h_{fg}$ is evaluated at the interface temperature, $T_i$.

$$T_r = T_w + 0.33\,(T_i - T_w) \tag{3.68}$$

For liquid water, steam and air properties, the correlations used by Srzic [42] are implemented in this study. For steam-air mixture properties, the correlations

proposed by Hirschfelder et al [50] are also followed. Detailed information about these properties is available in Appendix A.

# CHAPTER 4

# NUMERICAL ANALYSIS AND PROCEDURES

In this chapter, a detailed description of the numerical methods that are used for solving the problem of forced film condensation heat transfer of vapor or vapor-air mixture flowing downward horizontal cylinders is presented. For pure vapor, a system of non-linear ordinary differential equations is reduced to a system of non-linear algebraic equations that can be solved by Newton Raphson method. For vapor-air mixture, an implicit finite difference scheme is used to approximate the boundary layer equations that can be solved by a procedure called Tri-Diagonal Matrix Algorithm (TDMA) which is described by White [49].

Computer algorithms are also developed to solve the above problems. Like the other computer programs, the program includes; a main program, subroutines, functions and data blocks.

Finally, numerical approximations for the initial profiles and the interfacial fluxes are also illustrated.

## 4.1 Numerical analysis for pure vapor model

The system of non-linear algebraic equations, derived in chapter 3, Equations (3.31) to Equation (3.34), can be solved numerically by Newton Raphson method. In general, the derivation of the method and the solution procedure is mainly based on Taylor series approximation. The solution procedure can be summarized as follows; Let;

$$f_1(x, y) = 0 \tag{4.1}$$

$$f_2(x, y) = 0 \tag{4.2}$$

be a system of nonlinear equations;

Taylor series expansion;

$$f_1(x_{i+1,} y_{i+1}) = f_1(x_i, y_i) + \frac{\partial f_1}{\partial x}(x_{i+1} - x_i) + \frac{\partial f_1}{\partial y}(y_{i+1} - y_i) + \ldots\ldots\ldots\ldots \quad (4.3)$$

$$f_2(x_{i+1,} y_{i+1}) = f_2(x_i, y_i) + \frac{\partial f_2}{\partial x}(x_{i+1} - x_i) + \frac{\partial f_2}{\partial y}(y_{i+1} - y_i) + \ldots\ldots\ldots\ldots \quad (4.4)$$

Suppose $(x_{i+1}, y_{i+1})$ are both very close to the actual root $(\bar{x}, \bar{y})$, so that the left hand side of above Equation (4.3) and Equation (4.4) are almost zero.

$$0 = f_1(x_i, y_i) + \frac{\partial f_1}{\partial x}(x_{i+1} - x_i) + \frac{\partial f_1}{\partial y}(y_{i+1} - y_i) + \ldots\ldots\ldots\ldots \quad (4.5)$$

$$0 = f_2(x_i, y_i) + \frac{\partial f_2}{\partial x}(x_{i+1} - x_i) + \frac{\partial f_2}{\partial y}(y_{i+1} - y_i) + \ldots\ldots\ldots\ldots \quad (4.6)$$

let;

$$x_{i+1} - x_i = h \quad (4.7)$$

$$y_{i+1} - y_i = k \quad (4.8)$$

then;

$$0 = f_1(x_i, y_i) + \frac{\partial f_1}{\partial x} h + \frac{\partial f_1}{\partial y} k + \ldots\ldots\ldots\ldots \quad (4.9)$$

$$0 = f_2(x_i, y_i) + \frac{\partial f_2}{\partial x} h + \frac{\partial f_2}{\partial y} k + \ldots\ldots\ldots\ldots \quad (4.10)$$

Re-arranging we get;

$$\frac{\partial f_1}{\partial x} h + \frac{\partial f_1}{\partial y} k = -f_1(x_i, y_i) \quad (4.11)$$

$$\frac{\partial f_2}{\partial x} h + \frac{\partial f_2}{\partial y} k = -f_2(x_i, y_i) \quad (4.12)$$

The resulting system of equations can be solved by using Cramer's rule; Determinant of coefficients (J);

$$J = \begin{vmatrix} \dfrac{\partial f_1}{\partial x} & \dfrac{\partial f_1}{\partial y} \\ \dfrac{\partial f_2}{\partial x} & \dfrac{\partial f_2}{\partial y} \end{vmatrix} \neq 0\,; \tag{4.13}$$

$$h = \frac{\begin{vmatrix} -f_1(x_i, y_i) & \dfrac{\partial f_1}{\partial y} \\ -f_2(x_i, y_i) & \dfrac{\partial f_2}{\partial y} \end{vmatrix}}{J}\,; \tag{4.14}$$

$$k = \frac{\begin{vmatrix} \dfrac{\partial f_1}{\partial x} & -f_1(x_i, y_i) \\ \dfrac{\partial f_2}{\partial x} & -f_2(x_i, y_i) \end{vmatrix}}{J} \tag{4.15}$$

$$x_{i+1} = x_i + h \tag{4.16}$$

$$y_{i+1} = y_i + k \tag{4.17}$$

Equation (4.16) and equation (4.17) are the two-equation version of the Newton Raphson method.

By invoking the above procedure to our problem, the corresponding system of equations for the Upper Cylinder can be written as follows;

For the case of the Upper Cylinder;

$\delta_i \rightarrow x_i$

$U_{\delta,i} \rightarrow y_i$

$$f_1(x_i, y_i) = f_1(\delta_i, U_{\delta,i}) = \frac{5}{8}\frac{(\delta_i U_{\delta,i} - \delta_{i-1}U_{\delta,i-1})}{\Delta x} - \frac{k_l}{\rho_l h_{fg}}\frac{\Delta T}{\delta_i} = 0 \tag{4.18}$$

$$f_2(x_i, y_i) = f_2(\delta_i, U_{\delta,i}) = \frac{17}{35}\rho_l \frac{(\delta_i U_{\delta,i}^2 - \delta_{i-1}U_{\delta,i-1}^2)}{\Delta x} - \delta_i \rho_l g \sin\theta \cos\varphi + \frac{3}{2}\mu_l \frac{U_{\delta,i}}{\delta_i} = 0 \tag{4.19}$$

then;

$$\frac{\partial f_1}{\partial \delta} = \frac{\left[\frac{5}{8}\frac{(\delta_i + \delta_{inc})U_{\delta,i} - \delta_{i-1}U_{\delta,i-1}}{\Delta x} - \frac{k\Delta T}{\rho_l h_{fg}(\delta_i + \delta_{inc})}\right] - \left[\frac{5}{8}\frac{\delta_i U_{\delta,i} - \delta_{i-1}U_{\delta,i-1}}{\Delta x} - \frac{k_l \Delta T}{\rho_l h_{fg}\delta_i}\right]}{\delta_{inc}} \tag{4.20}$$

$$\frac{\partial f_1}{\partial U_\delta} = \frac{\left[\frac{5}{8}\frac{\delta_i(U_{\delta,i} + U_{inc}) - \delta_{i-1}U_{\delta,i-1}}{\Delta x}\right] - \left[\frac{5}{8}\frac{\delta_i U_{\delta,i} - \delta_{i-1}U_{\delta,i-1}}{\Delta x}\right]}{U_{inc}} \tag{4.21}$$

$$\frac{\partial f_2}{\partial \delta} = \frac{\left[\frac{17}{35}\rho_l \frac{(\delta_i + \delta_{inc})U_{\delta,i}^2 - \delta_{i-1}U_{\delta,i-1}^2}{\Delta x} - (\delta_i + \delta_{inc})\rho_l g \sin\theta\cos\varphi + \frac{3}{2}\mu_l \frac{U_{\delta,i}}{(\delta_i + \delta_{inc})}\right] - \left[\frac{17}{35}\rho_l \frac{(\delta_i U_{\delta,i}^2 - \delta_{i-1}U_{\delta,i-1}^2)}{\Delta x} - \delta_i \rho_l g \sin\theta\cos\varphi + \frac{3}{2}\mu_l \frac{U_{\delta,i}}{\delta_i}\right]}{\delta_{inc}} \tag{4.22}$$

$$\frac{\partial f_2}{\partial U_\delta} = \frac{\left[\frac{17}{35}\rho_l \frac{\delta_i(U_{\delta,i} + U_{inc})^2 - \delta_{i-1}U_{\delta,i-1}^2}{\Delta x} - \delta_i \rho_l g \sin\theta\cos\varphi + \frac{3}{2}\mu_l \frac{(U_{\delta,i} + U_{inc})}{\delta_i}\right] - \left[\frac{17}{35}\rho_l \frac{(\delta_i U_{\delta,i}^2 - \delta_{i-1}U_{\delta,i-1}^2)}{\Delta x} - \delta_i \rho_l g \sin\theta\cos\varphi + \frac{3}{2}\mu_l \frac{U_{\delta,i}}{\delta_i}\right]}{U_{inc}} \tag{4.23}$$

It should be noted that the partial derivative elements of the square matrix, Equation (4.13), are approximated above by numerical differentiation instead of analytical differentiation. The parameters $\delta_i$ and $U_{\delta i}$ are increased by increments $\delta_{inc}$ and $U_{inc}$, subtracted from the original values and divided by the suitable increment. For the lower cylinders, the same procedure can be used as mentioned above.

The details of the computer program and the program flow chart are illustrated in section 4.5.

## 4.2 Numerical analysis for vapor-air mixture model

The physical model is shown in orthogonal curvilinear coordinates. The arc length x is measured along the surface of the cylinder and has an initial value of zero at the upper stagnation point. The normal distance y is measured from the surface of the cylinder. For the system under consideration, the equivalent model in Cartesian coordinates is shown in Figure 4.1.

For the boundary layer model considered, the finite difference mesh for two-dimensional boundary layer is shown in Figure 4.2.

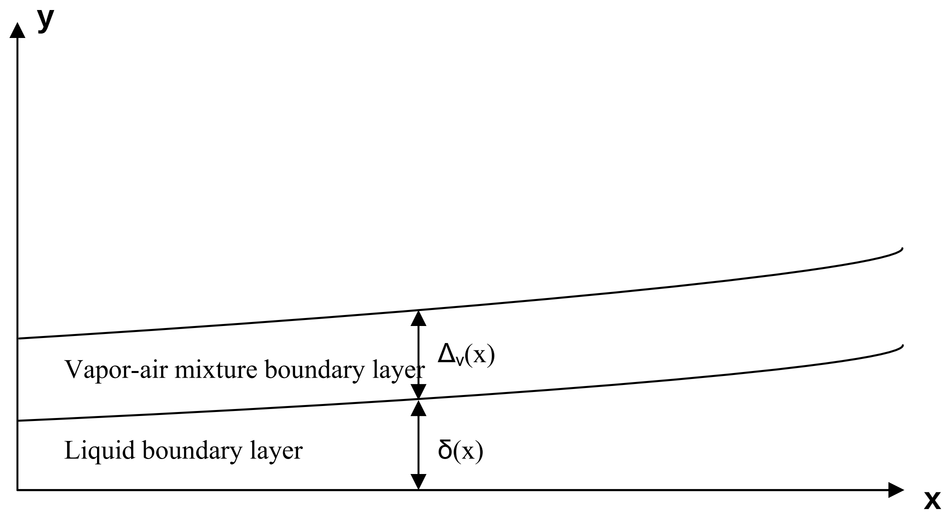


Figure 4.1 Equivalent Cartesian coordinates.

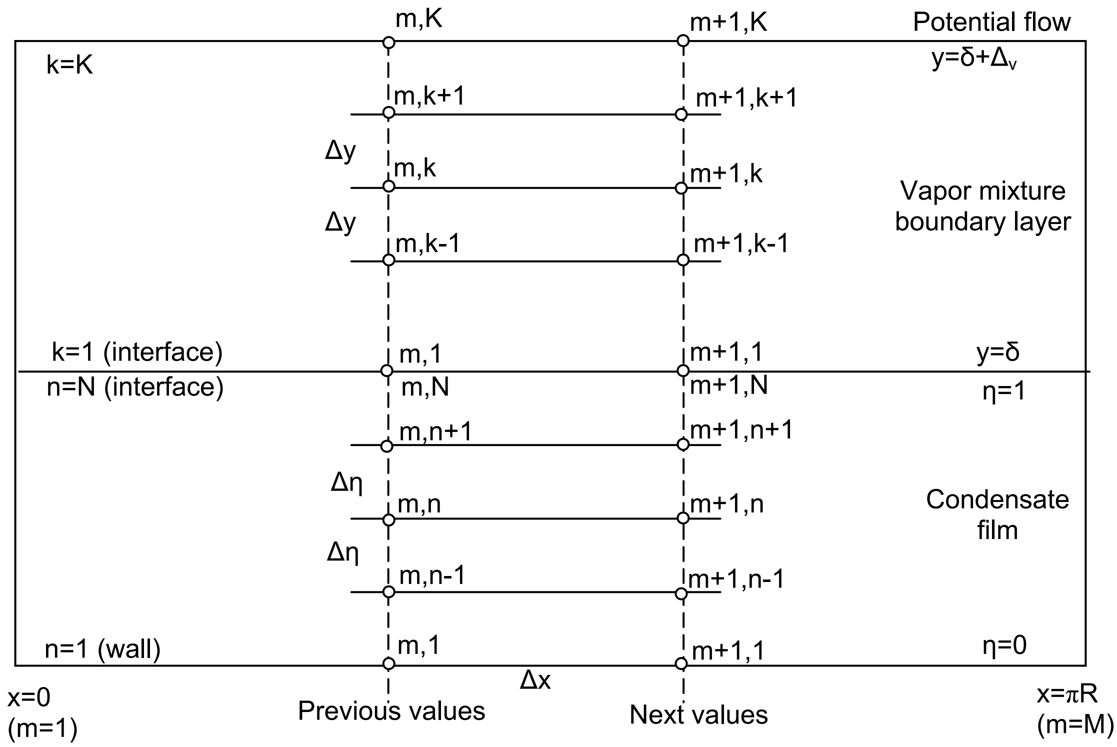


Figure 4.2 Finite difference mesh for the two dimensional boundary layer.

### 4.2.1 Vapor- air mixture boundary layer

Following, White [49], the finite difference approximations for the continuity, momentum, species and energy equations beside the other parameters such as; initial, interfacial and boundary conditions can be written as follows;

***Continuity equation***

$$\frac{\partial u_v}{\partial x} + \frac{\partial v_v}{\partial y} = 0 \tag{4.24}$$

$$\frac{\partial u_v}{\partial x} = \frac{u_v(m+1,k) - u_v(m,k)}{\Delta x} \quad \text{(forward difference)} \tag{4.25}$$

$$\frac{\partial v_v}{\partial y} = \frac{v_v(m+1,k) - v_v(m+1,k-1)}{\Delta y} \quad \text{(backward difference)} \tag{4.26}$$

Substituting by Equations (4.25) and (4.26) into Equation (4.24) we get;

$$\frac{u_v(m+1,k) - u_v(m,k)}{\Delta x} + \frac{v_v(m+1,k) - v_v(m+1,k-1)}{\Delta y} = 0 \tag{4.27}$$

$$v_v(m+1,k) = v_v(m+1,k-1) - \frac{\Delta y}{\Delta x}\left[u_v(m+1,k) - u_v(m,k)\right] \tag{4.28}$$

The numerical accuracy of Equation (4.28) is poor, White [49]. It was suggested to use what so called an average value;

$$\left.\frac{\partial u_v}{\partial x}\right|_{avg} \approx \frac{1}{2}\left[\frac{u_v(m+1,k) - u_v(m,k)}{\Delta x} + \frac{u_v(m+1,k-1) - u_v(m,k-1)}{\Delta x}\right] \tag{4.29}$$

$$v_v(m+1,k) \approx v_v(m+1,k-1) - \frac{\Delta y}{2\Delta x}\left[u_v(m+1,k) - u_v(m,k) + u_v(m+1,k-1) - u_v(m,k-1)\right] \tag{4.30}$$

***Momentum equation***

$$u_v \frac{\partial u_v}{\partial x} + v_v \frac{\partial u_v}{\partial y} = \gamma_v \frac{\partial^2 u_v}{\partial y^2} + g\sin(\frac{x}{R})\cos(\varphi) - \frac{1}{\rho_v}\frac{dP}{dx} \tag{4.31}$$

$$\frac{\partial u_v}{\partial x} = \frac{u_v(m+1,k) - u_v(m,k)}{\Delta x} \quad \text{(forward difference)} \tag{4.32}$$

$$\frac{\partial u_v}{\partial y} = \frac{u_v(m,k+1) - u_v(m,k-1)}{2\Delta y} \quad \text{(central difference)} \tag{4.33}$$

$$\frac{\partial^2 u_v}{\partial y^2} = \frac{u_v(m+1,k+1) - 2u_v(m+1,k) + u_v(m+1,k-1)}{\Delta y^2} \quad \text{(central difference)} \tag{4.34}$$

Referring to White [49], the pressure gradient term is defined according to the following formula;

$$\frac{dp}{dx} = -\rho_v U_v \frac{dU_v}{dx} \tag{4.35}$$

using the form $U_v \dfrac{dU_v}{dx} = \dfrac{d(U_v{}^2/2)}{dx}$, and writing the forward finite difference approximation, we can approximate the pressure gradient term as shown in Equation (4.35). Substituting by Equations (4.32), (4.33), (4.34) and (4.35) into Equation (4.31) we get;

$$\begin{aligned} &u_v(m,k)\left[\frac{u_v(m+1,k)-u_v(m,k)}{\Delta x}\right]+v_v(m,k)\left[\frac{u_v(m,k+1)-u_v(m,k-1)}{2\Delta y}\right]= \\ &\gamma_v\left[\frac{u_v(m+1,k+1)-2u_v(m+1,k)+u_v(m+1,k-1)}{\Delta y^2}\right]+g\sin(\frac{x}{R})\cos(\varphi)+\frac{U_{e,m+1}^2-U_{e,m}^2}{2\Delta x} \end{aligned} \tag{4.36}$$

Equation (4.36) can be re-written as;

$$(1+2\alpha_k)u_v(m+1,k) = \alpha_k\, u_v(m+1,k+1)+\alpha_k\, u_v(m+1,k-1)+C_k \tag{4.37}$$

where;

$$\alpha_k = \frac{\gamma\ \ \Delta x}{u_v(m,k)\Delta y^2} \tag{4.38}$$

$$C_k = u_v(m,k) - \frac{v_v(m,k)\,\Delta x}{2u_v(m,k)\,\Delta y}\left[u_v(m,k+1)-u_v(m,k-1)\right]+\frac{U_{e,m+1}^2-U_{e,m}^2}{2u(m,k)}+g\sin(\frac{x}{R})\cos(\varphi)\frac{\Delta x}{u_v(m,k)} \tag{4.39}$$

***Species equation***

$$u_v\frac{\partial m_1}{\partial x}+v_v\frac{\partial m_1}{\partial y}=\frac{\gamma_v}{Sc}\frac{\partial^2 m_1}{\partial y^2} \tag{4.40}$$

$$\frac{\partial m_1}{\partial x} = \frac{m_1(m+1,k) - m_1(m,k)}{\Delta x} \qquad \text{(forward difference)} \tag{4.41}$$

$$\frac{\partial m_1}{\partial y} = \frac{m_1(m,k+1) - m_1(m,k-1)}{2\Delta y} \qquad \text{(central difference)} \tag{4.42}$$

$$\frac{\partial^2 m_1}{\partial y^2} = \frac{m_1(m+1,k+1) - 2m_1(m+1,k) + m_1(m+1,k-1)}{\Delta y^2} \qquad \text{(central difference)} \tag{4.43}$$

Substituting by Equations (4.41), (4.42) and (4.43) into Equation (4.40) we get;

$$u_v(m,k)\left[\frac{m_1(m+1,k) - m_1(m,k)}{\Delta x}\right] + v_v(m,k)\left[\frac{m_1(m,k+1) - m_1(m,k-1)}{2\Delta y}\right] = \frac{\gamma_v}{Sc}\left[\frac{m_1(m+1,k+1) - 2m_1(m+1,k) + m_1(m+1,k-1)}{\Delta y^2}\right] \tag{4.44}$$

$$\left(1 + 2\beta_k\right) m_1(m+1,k) = \beta_k \; m_1(m+1,k+1) + \beta_k \; m_1(m+1,k-1) + F_k \tag{4.45}$$

where;

$$\beta_k = \frac{\gamma_v \; \Delta x}{Sc \, u_v(m,k) \Delta y^2} \tag{4.46}$$

$$F_k = m_1(m,k) - \frac{v_v(m,k)\,\Delta x}{2u_v(m,k)\,\Delta y}\left[m_1(m,k+1) - m_1(m,k-1)\right] \tag{4.47}$$

***Energy equation***

$$u_v \frac{\partial T_v}{\partial x} + v_v \frac{\partial T_v}{\partial y} = \frac{\gamma_v}{\Pr}\frac{\partial^2 T_v}{\partial y^2} + \frac{\gamma_v}{\Pr}\frac{\partial T_v}{\partial y}\left[\frac{\partial \ln C_{p,v}}{\partial y} + \frac{\Pr}{Sc}\frac{C_{p,1} - C_{p,2}}{C_{p,v}}\frac{\partial m_1}{\partial y}\right] \tag{4.48}$$

$\dfrac{\partial \ln C_{p,v}}{\partial y} = 0$ (constant properties assumption) then;

$$u_v \frac{\partial T_v}{\partial x} + v_v \frac{\partial T_v}{\partial y} = \frac{\gamma_v}{\Pr} \frac{\partial^2 T_v}{\partial y^2} + \frac{\gamma_v}{\Pr} \frac{\partial T_v}{\partial y} \left[ \frac{\Pr}{Sc} \frac{C_{p,1} - C_{p,2}}{C_{p,v}} \frac{\partial m_1}{\partial y} \right] \tag{4.49}$$

$$\frac{\partial T_v}{\partial x} = \frac{T_v(m+1,k) - T_v(m,k)}{\Delta x} \quad \text{(forward difference)} \tag{4.50}$$

$$\frac{\partial T_v}{\partial y} = \frac{T_v(m,k+1) - T_v(m,k-1)}{2\Delta y} \quad \text{(central difference)} \tag{4.51}$$

$$\frac{\partial^2 T_v}{\partial y^2} = \frac{T_v(m+1,k+1) - 2T_v(m+1,k) + T_v(m+1,k-1)}{\Delta y^2} \quad \text{(central difference)} \tag{4.52}$$

Substituting by Equations (4.50), (4.51) and (4.52) into Equation (4.49) we get;

$$\begin{gathered} u_v(m,k)\left[\frac{T_v(m+1,k) - T_v(m,k)}{\Delta x}\right] + v_v(m,k)\left[\frac{T_v(m,k+1) - T_v(m,k-1)}{2\Delta y}\right] = \\ \frac{\gamma_v}{\Pr}\left[\frac{T_v(m+1,k+1) - 2T_v(m+1,k) + T_v(m+1,k-1)}{\Delta y^2}\right] + \frac{\gamma_v}{\Pr}\left[\frac{T_v(m,k+1) + T_v(m,k-1)}{2\Delta y}\right] \\ \left\{\frac{\Pr}{Sc}\left(\frac{C_{p,1} - C_{p,2}}{C_{p,v}}\right)\left(\frac{m_1(m,k+1) + m_1(m,k-1)}{2\Delta y}\right)\right\} \end{gathered} \tag{4.53}$$

$$\left(1 + 2\phi_k\right) T_v(m+1,k) = \phi_k \, T_v(m+1,k+1) + \phi_k \, T_v(m+1,k-1) + G_k \tag{4.54}$$

where

$$\phi_k = \frac{\gamma_v \, \Delta x}{\Pr u_v(m,k) \Delta y^2} \tag{4.55}$$

$$\begin{gathered} G_k = T_v(m,k) - \frac{v_v(m,k)\Delta x}{2u_v(m,k)\Delta y}\left[T_v(m,k+1) - T_v(m,k-1)\right] + \frac{\gamma_v \, \Delta x(\frac{C_{p,1} - C_{p,2}}{C_{p,v}})}{4Scu_v(m,k)\Delta y^2}\left[T_v(m,k+1) - T_v(m,k-1)\right] \\ \left[m_1(m,k+1) - m_1(m,k-1)\right] \end{gathered} \tag{4.56}$$

### 4.2.2 Liquid boundary layer

***Continuity equation***

The same procedure as for vapor-mixture boundary layer is followed.

The only difference is that the variable ($\eta = \frac{y}{\delta}$) is introduced for normalization.

$$\frac{\partial u_l}{\partial x} + \frac{\partial v_l}{\partial y} = 0 \tag{4.57}$$

$$\frac{\partial u_l}{\partial x} = \frac{u_l(m+1,n) - u_l(m,n)}{\Delta x} \qquad \text{(forward difference)} \tag{4.58}$$

$$\frac{\partial v_l}{\partial y} = \frac{v_l(m+1,n) - v_l(m+1,n-1)}{\Delta y} \qquad \text{(backward difference)} \tag{4.59}$$

$$\frac{u_l(m+1,n) - u_l(m,n)}{\Delta x} + \frac{v_l(m+1,n) - v_l(m+1,n-1)}{\Delta y} = 0 \tag{4.60}$$

$$v_l(m+1,n) \approx v_l(m+1,n-1) - \frac{\delta_{m+1}\,\Delta\eta}{2\Delta x}\left[u_l(m+1,n) - u_l(m,n) + u_l(m+1,n-1) - u_l(m,n-1)\right] \tag{4.61}$$

***Momentum equation***

$$\frac{\partial^2 u_l}{\partial y^2} = -\frac{1}{\mu_l}\left[\rho_l g \sin(\frac{x}{R})\cos(\varphi) - \frac{dP}{dx}\right] \tag{4.62}$$

Recalling Equation (3.42), pressure distribution can be written as;

$$-\frac{dP}{dx} = \left[\left(\frac{4\rho_\infty U_\infty^2}{R}\right)\cos(\frac{x}{R}) - \rho_\infty g\right]\sin(\frac{x}{R}) \tag{4.63}$$

By introducing the variable; $\eta = \dfrac{y}{\delta}$ for normalization;

$$\frac{\partial^2 u_l}{\partial \eta^2} = -\frac{\delta^2}{\mu_l}\left[\rho_l g \sin(\frac{x}{R})\cos(\varphi) - \frac{dP}{dx}\right] \tag{4.64}$$

The boundary conditions are;

at $\eta = 0$ $\quad u_l = 0;$ (4.65)

at $\eta = 1$ $\quad \left.\frac{\mu_l}{\delta}\frac{du_l}{d\eta}\right|_u = \left.\mu_v \frac{du_v}{dy}\right|_s = \tau_i;$ (4.66)

Following, Rose [16], the velocity distribution at the liquid boundary layer can be determined by the Integration of Equation (4.64) twice with respect to ($\eta$) and invoking the boundary conditions, yields;

$$u_l(\eta) = -\frac{\delta^2}{\mu_l} g \sin(\frac{x}{R})\left[(\rho_l - \rho_\infty)\cos(\varphi) + \frac{\rho_\infty}{Fr}\cos(\frac{x}{R})\right](\frac{\eta^2}{2} - \eta) + \frac{\tau_i \delta}{\mu_l}\eta \tag{4.67}$$

***Species equation***

$$\frac{d^2 m_1}{d\eta^2} = 0 \tag{4.68}$$

The boundary conditions are;

$\eta = 0$ $\quad \dfrac{dm_1}{d\eta} = 0$ (4.69)

$\eta = 1$ $\quad m_1\big|_u = \mathrm{m}_{1,u}(m_{1,s}, P_\infty)$ (4.70)

Integration of Equation (4.68) twice with respect to ($\eta$), yields;

$$\frac{dm_1}{d\eta} = C_3 \tag{4.71}$$

$$m_1 = C_3\eta + C_4 \tag{4.72}$$

The constants, $C_3$ and $C_4$, can be evaluated after invoking the boundary conditions as;

$$C_3 = 0 \tag{4.73}$$

$$C_4 = m_1\big|_u (m_{1,s}, P_\infty) \tag{4.74}$$

Substitute by the constants, $C_3$ and $C_4$, into equation (4.72), we get;

$$m_1(\eta) = m_1\big|_u (m_{1,s}, P_\infty) \tag{4.75}$$

It should be noted that; the net mass flow of non-condensable gas vanish at the liquid-vapor interface, $\dot{m}_{g,i} = 0$ since the interface is impermeable to the non-condensable gas (air) as stated in reference [34]. As a result, for vapor-air systems, Equation (4.75) can be written as; $m_1(\eta) = 0$.

***Energy equation***

$$\frac{d^2T_l}{d\eta^2} = 0 \tag{4.76}$$

The boundary conditions are;

$$\eta = 0 \qquad T_l = T_w \tag{4.77}$$

$$\eta = 1 \qquad T_l = T_i \tag{4.78}$$

Integration of Equation (4.76) twice with respect to ($\eta$), yields;

$$\frac{dT_l}{d\eta} = C_5 \tag{4.79}$$

$$T_l(\eta) = C_5\eta + C_6 \tag{4.80}$$

The constants, $C_5$ and $C_6$, can be evaluated after invoking the boundary conditions;

$$C_5 = T_i - T_w \tag{4.81}$$

$$C_6 = T_w \tag{4.82}$$

$$T_l(\eta) = (T_i - T_w)\eta + T_w \tag{4.83}$$

## 4.3 Calculation of the main parameters

### 4.3.1 The film thickness

$$k_l \left.\frac{\partial T_l}{\partial y}\right|_{y=0} = k_v \left.\frac{\partial T_v}{\partial y}\right|_s + \frac{d}{dx}\int_0^{\delta(x)} \rho_l u_l \left[h_{fg} + C_{p,l}(T_i - T_l\ )\right] dy \tag{4.84}$$

Applying the variable; $\eta = \dfrac{y}{\delta}$ for normalization;

$$\frac{k_l}{\delta}\left.\frac{\partial T_l}{\partial \eta}\right|_{\eta=0} = k_v \left.\frac{\partial T_v}{\partial y}\right|_s + \frac{d}{dx}\int_0^1 \rho_l \delta\, u_l \left[h_{fg} + C_{p,l}(T_i - T_l)\right] d\eta \tag{4.85}$$

Substitute by the velocity distribution, $u_l$, Equation (4.67) into Equation (4.85);

$$u_l(\eta) = -\frac{\delta^2}{\mu_l} g \sin(\frac{x}{R})\left[(\rho_l - \rho_\infty)\cos(\varphi) + \frac{\rho_\infty}{Fr}\cos(\frac{x}{R})\right](\frac{\eta^2}{2} - \eta) + \frac{\tau_i \delta}{\mu_l}\eta \tag{4.86}$$

The value of $(T_i - T_l)$ can be evaluated from re-writing Equation (4.83) as;

$$(T_i - T_l) = \Delta T(1-\eta) \tag{4.87}$$

where

$$\Delta T = T_i - T_w \tag{4.88}$$

Substituting by the value of velocity, Equation (4.86) and the value of $(T_i - T_l)$, Equation (4.87) into Equation (4.85) and take the integration with respect to ($\eta$) we get;

$$\frac{k_l}{\delta}\frac{\partial T_l}{\partial \eta}\bigg|_{\eta=0} = k_v \frac{\partial T_v}{\partial y}\bigg|_s + \left[\rho_l h_{fg} B\delta - \rho_l h_{fg} A\delta^2 + \frac{\rho_l}{3} Cp_l \Delta T B\delta - \frac{3}{8}\rho_l Cp_l \Delta T A \delta^2\right]\frac{d\delta}{dx} \tag{4.89}$$

where

$$A = -\frac{g}{\mu_l}\sin(\frac{x}{R})\left[(\rho_l - \rho_\infty) + \frac{\rho_\infty}{Fr}\cos(\frac{x}{R})\right] \tag{4.90}$$

$$B = \frac{\tau_{i,m}}{\mu_l} \tag{4.91}$$

By applying finite difference approach to Equation (4.89) using forward finite difference we get;

$$\begin{aligned}\frac{k_l}{\delta_m}\frac{T_l(m+1,2) - T_l(m+1,1)}{\Delta\eta} &= k_v \frac{T_v(m+1,2) - T_v(m+1,1)}{\Delta y} + \\ &\left[\rho_l h_{fg} B\delta_m - \rho_l h_{fg} A\delta_m^2 + \frac{\rho_l}{3} Cp_l \Delta T B\delta_m - \frac{3}{8}\rho_l Cp_l \Delta T A\delta_m^2\right]\frac{\delta_{m+1} - \delta_m}{\Delta x}\end{aligned} \tag{4.92}$$

$$\delta_{m+1} = \frac{\frac{k_l \, \Delta x}{\delta_m} \frac{T_l(m+1,2) - T_l(m+1,1)}{\Delta \eta} - k_v \, \Delta x \frac{T_v(m+1,2) - T_v(m+1,1)}{\Delta y} + C\delta_m}{C} \tag{4.93}$$

where

$$C = \left[ \rho_l h_{fg} B \delta_m - \rho_l h_{fg} A \delta_m^2 + \frac{\rho_l}{3} \Delta T C p_l B \delta_m - \frac{3}{8} \rho_l C p_l \Delta T A \delta_m^2 \right] \tag{4.94}$$

### 4.3.2 The velocity component normal to the surface

Referring to reference [62], the interfacial mass conservation at the interface requires the following condition;

$$\rho_v \left( u_v \frac{d\delta}{dx} - V_v \right) = \frac{k_l}{h_{fg}} \left( \frac{dT_l}{dy} \right)_{y=0} \tag{4.95}$$

Recalling the interfacial condition for the shear stress, Equation (3.46) and refer to Equation (4.95) beside introducing the dimensionless film thickness parameter ($\eta$), the interfacial velocity component normal to the surface can be written as;

$$V_v = -\frac{k_l}{h_{fg} \rho_v \delta} \left( \frac{\partial T}{\partial \eta} \right)_{\eta=0} + u_v \frac{d\delta}{dx} \tag{4.96}$$

The finite difference form for Equation (4.96) can be written as;

$$V_v(m+1,n) = -\frac{k_l}{h_{fg} \rho_v \delta} \frac{T_l(m+1,2) - T_l(m+1,1)}{\Delta \eta} + u_v(m+1,n) \frac{\delta_{m+1} - \delta_m}{\Delta x} \tag{4.97}$$

In addition, these conditions are also present at the vapor-liquid interface;

$$u_v(1,k) = u_l(1,n) \tag{4.98}$$

$$V_v(1,k) = V_l(1,n) \tag{4.99}$$

### 4.3.3 The interfacial air fraction

$$\dot{m} = \frac{\rho D_{12}}{m_1(I,1)} \left. \frac{dm_1}{dy} \right|_s \tag{4.100}$$

$$\left. \frac{dm_1}{dy} \right|_s = \frac{-m_1(I,3) + 4m_1(I,2) - 3m_1(I,1)}{2\Delta y} \tag{4.101}$$

Substituting by Equation (4.101) into Equation (4.100), yields;

$$\dot{m} = \frac{\rho D_{12}}{m_1(I,1)} \left[ \frac{-m_1(I,3) + 4m_1(I,2) - 3m_1(I,1)}{2\Delta y} \right] \tag{4.102}$$

Then, the interfacial air mass fraction can be evaluated as follows;

$$m_1(I,1) = a\, m_1(I,3) + b\, m_1(I,2) \tag{4.103}$$

where

$$a = \frac{-1}{2\Delta y\, c} \tag{4.104}$$

$$b = \frac{2}{\Delta y\, c} \tag{4.105}$$

$$c = \left[ \frac{\dot{m}}{\rho D_{12}} + \frac{3}{2\Delta y} \right] \tag{4.106}$$

### 4.3.4 The interfacial velocity component parallel to the surface

$$\tau_i = \mu_v \left. \frac{du_v}{dy} \right|_s \tag{4.107}$$

$$\left.\frac{du_v}{dy}\right|_s = \frac{-u_v(I,3)+4u_v(I,2)-3u_v(I,1)}{2\Delta y} \tag{4.108}$$

$$\tau_i = \mu_v\left[\frac{-u_v(I,3)+4u_v(I,2)-3u_v(I,1)}{2\Delta y}\right] \tag{4.109}$$

$$u_v(I,1) = \bar{a}\,u_v(I,3)+\bar{b}\,u_v(I,2)-\bar{c}\,\tau_i \tag{4.110}$$

where

$$\bar{a} = \frac{-\mu_v}{2\Delta y\bar{d}} \tag{4.111}$$

$$\bar{b} = \frac{2\mu_v}{\Delta y\,\bar{d}} \tag{4.112}$$

$$\bar{c} = \frac{-1}{\bar{d}} \tag{4.113}$$

$$\bar{d} = \frac{3\mu_v}{2\Delta y} \tag{4.114}$$

### 4.3.5 The interfacial temperature

$$q_s = k_v\left.\frac{dT_v}{dy}\right|_s \tag{4.115}$$

$$\left.\frac{dT_v}{dy}\right|_s = \frac{-T_v(I,3)+4T_v(I,2)-3T_v(I,1)}{2\Delta y} \tag{4.116}$$

$$q_s = k_v\left[\frac{-T_v(I,3)+4T_v(I,2)-3T_v(I,1)}{2\Delta y}\right] \tag{4.117}$$

$$T_v(I,1) = \hat{a}\,T_v(I,3)+\hat{b}\,T_v(I,2)-\hat{c}q_s \tag{4.118}$$

$$\hat{a} = \frac{-k_v}{2\Delta y \hat{d}} \tag{4.119}$$

$$\hat{b} = \frac{2k_v}{\Delta y\, \hat{d}} \tag{4.120}$$

$$\hat{c} = \frac{-1}{\hat{d}} \tag{4.121}$$

$$\hat{d} = \frac{3k_v}{2\Delta y} \tag{4.122}$$

**4.4 The numerical procedure**

The governing differential equations presented in section 3.2 were solved by an implicit finite difference scheme. The solution procedure for steam-air problem was advanced from previous station, $x_o$ to present station, $x_1$ as follows;

Given the initial profiles, the boundary conditions and the physical and thermal properties, the liquid film thickness, $\delta$ , interfacial velocity, $u_i$ , interfacial temperature, $T_i$ and the condensation rate, $\dot{m}$ at previous station, $x_o$ were calculated based on Nusselt theory. For the next station, $x_1$ based on the previous data that calculated at $x_o$, velocity and temperature distributions at liquid boundary layer were calculated. Then, liquid film thickness, $\delta$ interfacial velocity, $u_i$ and interfacial temperature, $T_i$ were also determined. For steam-air mixture boundary layer, velocity, temperature and species distributions were calculated based on a procedure called tri-diagonal matrix algorithm, TDMA. More details about this algorithm are illustrated in section 4.4.1. In addition, numerical differentiation can be used to evaluate the interfacial shear, $\tau_i$ , heat flux, $q_y\big|_s$ and interfacial air mass fraction, $m_{1,i}$ . By knowing the value of interfacial mass fraction, $m_{1,i}$, improved values of interfacial temperature, $T_i$ were evaluated from equilibrium relations. Moreover, the calculated value of the interfacial air mass fraction can be also used to evaluate the condensation rate, $\dot{m}$. For the next stations, the same procedure was followed. The solution is advanced until it reached a specified criterion where the condition of separation is satisfied. Then, the values of film thickness and velocity at this point plus the data from the solution of the liquid sheet equations, Equation (3.24) and Equation (3.25), and the initial profiles for temperature and species are updated and considered as initial values for the second tube. The solution is advanced also by the same way. For the third tube, the same procedure is followed.

### 4.4.1 Tri-diagonal matrix algorithm,TDMA

When the system of governing differential equations mentioned in section 4.2 are treated numerically. The resulting matrices are tri-diagonal matrices. The tri-diagonal matrices can be solved by a procedure called the tri-diagonal matrix algorithm (TDMA), which originally proposed by Patankar [64] and mentioned later by White [49]. Referring to Figure 4.2, consider $k=1$ as the liquid-vapor interface and $k=K$ as the free stream. If the momentum equation, Equation (4.37) is considered as an example, the TDMA procedure according to White [49] can be summarized as follows;

It works because there are only two unknowns at the bottom at level $k=2$ where the value of velocity $u_v$ at previous level $k=1$ is a known value of $u_i$ and only two at the top, at level $k=K$ where the value of velocity $u_v$ is also known, $U_e$

Thus, start by elimination of one variable at the bottom at a time until reaching to the top, where the value of velocity, $u_v$ at level $k=K-1$ is immediately found. Then, by back substitution, the value of velocity at level $k$, $u_v(k)$ can be found in terms of the value of velocity at level $k+1$, $u_v(k+1)$ until we secure the final value of velocity at level $k=2$, $u_v(k=2)$.

In order to illustrate the TDMA procedure, eliminate the notation $(m+1)$ as superfluous, Equation (4.37) can be written at any level $k$ as follows;

$$\left(1+2\alpha_k\right)u_v(k)=\alpha_k\,u_v(k+1)+\alpha_k\,u_v(k-1)+C_k \tag{4.123}$$

where $\alpha_k$ and $C_k$ are defined by Equation (4.38) and Equation (4.39) respectively.

The back substitution recurrence relation is;

$$u_v(k)=P_k u_v(k+1)+Q_k \tag{4.124}$$

First calculate $P_k$ and $Q_k$. Begin at the bottom, $u_v(k=1)=u_i$, by computing

$$P_2=\frac{\alpha_2}{1+2\alpha_2} \qquad Q_2=\frac{\alpha_2 u_i+C_2}{1+2\alpha_2} \tag{4.125}$$

The remaining $P$'$s$ and $Q$'$s$ are calculated by the recurrence relation;

$$P_k=\frac{\alpha_k}{1+2\alpha_k-\alpha_k P_{k-1}} \qquad Q_k=\frac{C_k+\alpha_k Q_{k-1}}{1+2\alpha_k-\alpha_k P_{k-1}} \tag{4.126}$$

At the top, $u_v(K)=U_e$, the value of velocity just follows at level $k=K-1$ is;

$$u_v(K-1)=\frac{\alpha_{K-1}U_\infty+\alpha_{K-1}Q_{K-1}+C_{K-1}}{1+2\alpha_{K-1}-\alpha_{K-1}P_{K-1}} \tag{4.127}$$

With $u_v(K-1)$ known, plus all the $P$'$s$ and $Q$'$s$, we work our way downward using Equation (4.128) until we reach the final unknown value of velocity, $u_v(2)$.

Species and energy equations, Equation (4.45) and Equation (4.54), could be worked out by the same algorithm.

### 4.5 The Computer programs

In this section, computer programs were developed to solve the system of nonlinear algebraic equations that resulted from the derivation of the problem of pure vapor presented in section 3.1 in addition to the highly coupled system of nonlinear finite difference equations that represent the problem of vapor-air mixture model, section 3.2. Since the two models were derived by different approaches, two computer programs were developed to match the different solution procedures and methods implemented.

The computer programs like any computer program consist of main program, subroutines, functions and input and output data blocks. Details of these programs and their flow charts are presented in the following sections.

#### 4.5.1 The pure vapor program

Based on the Newton Raphson method, an iterative computer algorithm was developed and executed. This algorithm takes into account all the necessary calculations and mathematical manipulations. In addition to the geometrical dimensions and trigonometry relations that consider the tube bank arrangements, inline and staggered. Invoking Initial and boundary conditions and initial profiles was also considered.

Referring to the flowchart presented in Figure 4.3, the program starts by reading the input data concerning the liquid and vapor properties, physical and thermal properties, in addition to other geometrical dimensions data of the cylinder.

Then, the initial profiles for film thickness, $\delta$ and velocity $U_\infty$ were calculated based on the basic Nusselt theory and assumptions. At the first point of the complete numerical solution, improved values of the film thickness and velocity were calculated based on the calculated values of the initial profiles. Then, the complete numerical solution was advanced for the upper cylinder until we reach the final point of the solution domain. At each point, maximum of twenty iterations were executed to approach as possible as to the exact values. After obtaining the value of change in the variables $\delta$ and $U_\infty$, variables are updated by adding the value of change to the previous iteration. It should be noted that local heat flux, $q(x)$, local heat transfer coefficient, $h(x)$ and local Nusselt number, $Nu(x)$ values at each step were calculated according to section 3.2.6. Then, Output data were stored after each iterate. Once iterations are completed for the upper cylinder, the data from the solution of the liquid sheet equations, Equation (3.24) and Equation (3.25), are updated together with the final data points for the upper cylinder and treated as initial values for the starting of the numerical solution for the second cylinder. The same procedure as illustrated above in the case of upper cylinder was followed. Again, for the condensate fall film between the middle and bottom cylinders, the same calculation procedure was followed. Together with the final data from the middle cylinder, the data were considered as initial values for the full numerical solution of the bottom cylinder. Finally, the main parameters results were stored in output files. Different values of input parameters and working conditions were tried. The computer code D.1, is shown in Appendix D.

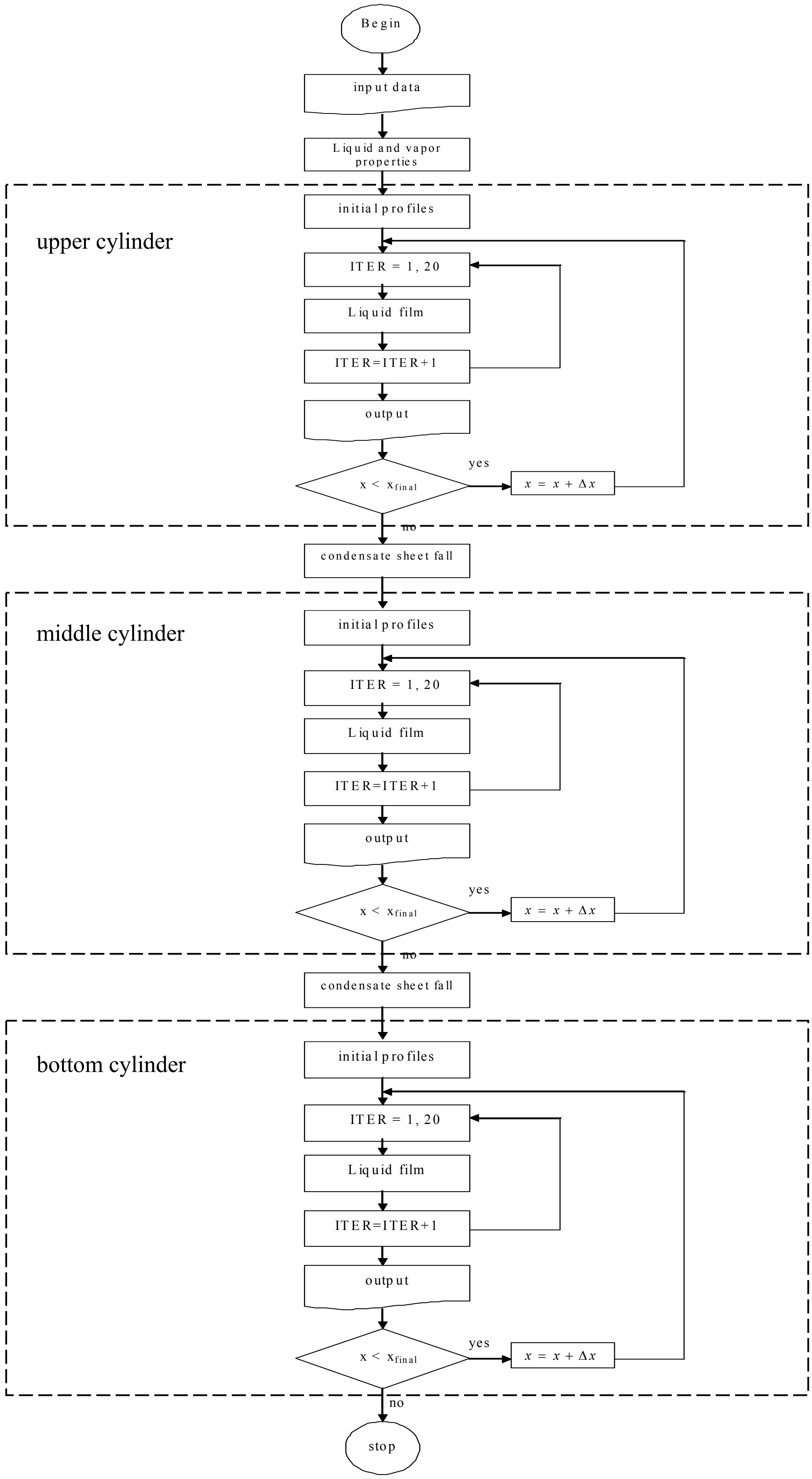


Figure 4.3 Flow chart of the pure vapor computer program.

### 4.5.2 The vapor-air mixture program

Based on the implicit finite difference scheme approximations and the tri-diagonal matrix algorithm for solving the vapor-air mixture boundary layer model, a computer program was developed to solve the problem. Flow chart of this program is presented in Figure 4.4. Initially, as in the case of pure vapor program, the solution procedure was started by reading the input data of the main parameters, liquid, vapor and vapor-air mixture thermo-physical and thermal properties. In addition to the geometrical data and dimensions for the cylinder. The program then starts to calculate the initial profiles and interfacial parameters such as Interfacial velocity, $u_i$, condensate rate, $\dot{m}$ and interfacial shear, $\tau_i$ in addition to liquid film thickness, $\delta$ according to Nusselt theory and its assumptions.

The resulted initial profiles data were considered as initial data to start the complete numerical solution. The program was started by solving for velocity and temperature distributions at the liquid boundary layer. Interfacial velocity, $u_i$, the condensation rate, $\dot{m}$ and the interfacial shear, $\tau_i$ in addition to the liquid film thickness, $\delta$ were also obtained.

Then, the solution procedure was started at the vapor-air mixture boundary layer using the tri-diagonal matrix algorithm that illustrated in section 4.4.1. As a result, velocity, species and temperature distributions at the vapor-air mixture boundary layer were evaluated. Interfacial fluxes such as interfacial shear, $\tau_i$ and interfacial vapor side heat flux, $q|_s$ were also obtained. Interfacial temperature, $T_i$ and interfacial air fraction, $m_{1,i}$ were calculated based on the procedure that illustrated by Minkowycz [34] and Minkowycz and Sparrow [35], section 3.2.5 or by finite difference approximations for the interfacial fluxes section 4.3. The calculation procedure and mathematical manipulations were included also in the computer program.

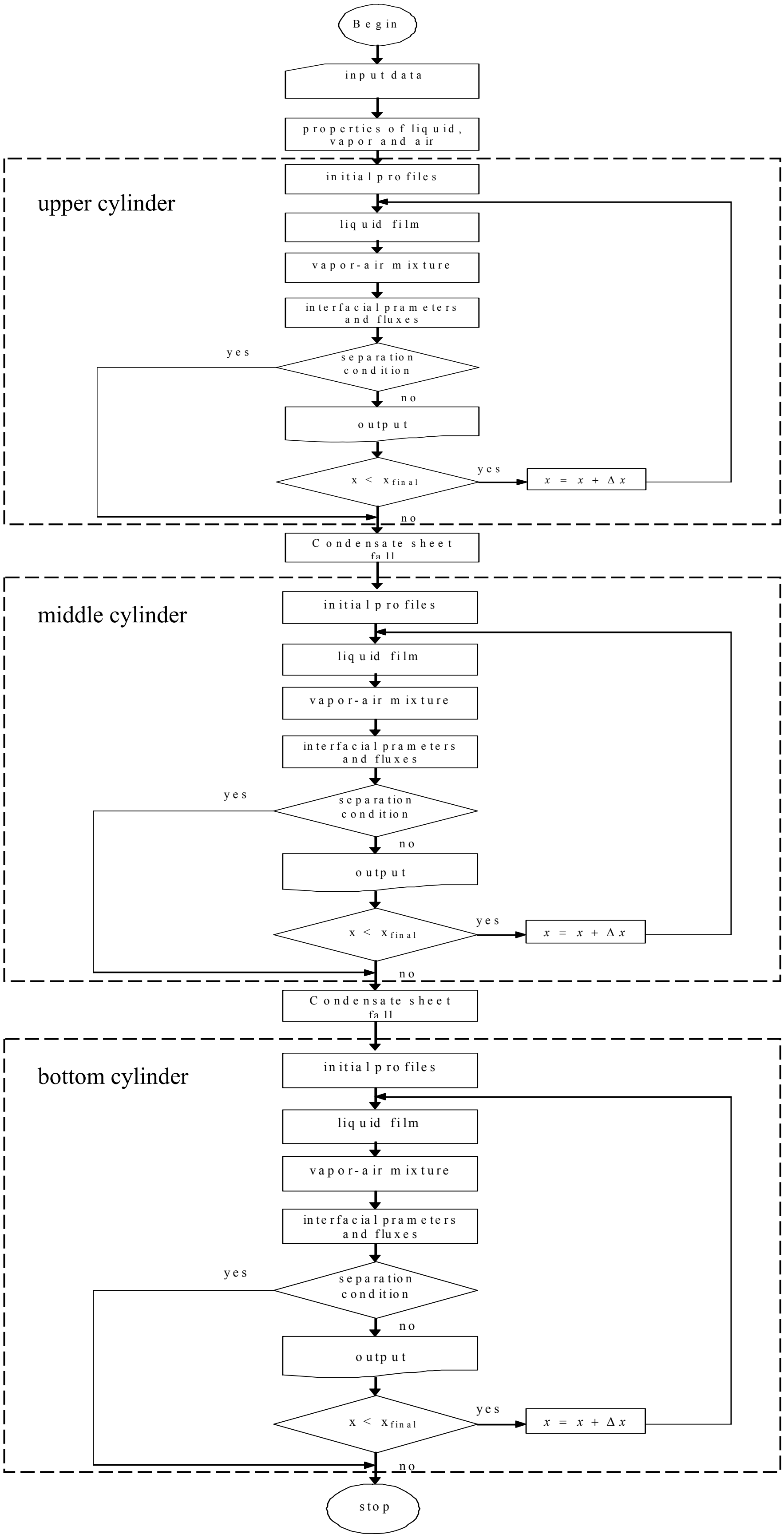


Figure 4.4 Flow chart of the vapor-air mixture computer program.

Then, the condition of boundary layer separation is checked. If the separation occurs, the program should be stopped for the upper cylinder and start to solve for the initial profiles for the middle cylinder. On the other hand, if the condition of separation was not satisfied, the solution procedure was advanced to the next step until the final step where the condition of separation is satisfied.

When separation occurs, the program start the solution for the middle cylinder by considering the data from the upper cylinder at the final step, at the separation point, and the data obtained from the solution of the condensate fall sheet equations, section 3.1.3, as initial conditions for the complete numerical solution of the middle cylinder.

The same procedure was followed for the middle cylinder as for the upper cylinder, starting from calculating the initial profiles and ending by the condition of separation. Again the final data of the middle cylinder at the separation point together with the solution of the condensate fall sheet between the cylinders were updated and treated as initial conditions for the full numerical solution of the bottom cylinder.

Finally, the necessary calculated parameters such as heat flux, $q\big|_s$ , heat transfer coefficient, $h$ and Nusselt number, $Nu$ were stored in the output files. Different design and working conditions were considered. The computer code D.2, is shown in Appendix D.

# CHAPTER 5

# EXPERIMENTAL STUDY

The verification of the theoretical results could be done by experimentation. The approximations in the assumptions and in the initial profiles could be analyzed and discussed. For this purpose, an experimental setup was designed, manufactured and mounted on an existing apparatus frame at the heat transfer laboratory at the mechanical engineering department of METU.

The main components of the setup are shown in Figure 5.1 as follows;

- Cooling water tank;
- Boiler;
- Test section;
- Temperature measurement system;
- Drainage unit;
- Air supply unit.

## 5.1 Cooling water tank

During the condensation process, vapor condenses on the tubes' surface when its temperature falls down its saturation temperature. As result, heat is transferred from the steam to the cooling water that pass through the condensation tubes. An increase of the cooling water temperature is occurred. In order to keep the temperature of condensation tubes constant, continuously constant temperature cooling water is supplied through the horizontal tubes in the test section. For this purpose, cooling water tank, Figure 5.2, is placed above the test section to allow the cooling water to flow downward to the test section by the effect of gravity.

The body of the water tank is made of stainless steel. The dimensions of the tank are 600mm of height, 240mm of diameter. The city water from the upper side inlet port fills it. A float valve is used in order to keep a constant water level at the tank. The water is allowed to flow downward to the test section through an outlet port located at the upper half of the water tank below and next to the inlet port. The reason behind this is to give enough time for the water temperature to distribute homogenously and to enter the test section at steady values.

Figure 5.1 General view of the experimental setup.

Four electric heaters, 2 kW capacity each, are used to heat the water to the desired temperatures. Then water is allowed to flow to the test section.

An overflow pipe is mounted to avoid extra water flow and to prevent water flooding. Control valves are also provided at inlet, outlet and overflow pipes for purpose of cleaning and maintenance. Climaflex insulates the tank in order to prevent heat loss.


Figure 5.2 Cooling water tank.

Figure 5.3 Cooling water division apparatus.

## 5.2 Boiler

The boiler, Figure 5.4, is used to generate the steam that flows from the top of the boiler to the test section through a high heat resistant hose. The boiler used is originally manufactured at the workshop of METU by earlier researchers. It is made of stainless steel. The dimensions are 40 cm of length, 30 cm of width and 37 cm of height with 45 liters of capacity. The boiler is provided by three electric heaters 1.5, 1.5 and 2 kW in capacity. The usage of the three heating elements ensures the variation of vapor flow rates from low to high rates. This can be done by switching between the heaters. In addition, a short time is needed for water to reach to its vapor phase.

Climaflex insulates boiler in order to prevent heat losses. The boiler is filled by cold water from the top. It is equipped by a pressure gauge and a thermometer to measure the pressure and temperature of the steam. The boiler supplies steam to the test section at temperature of 100 $^{o}$C at the atmospheric pressure. Mass flow rates of the vapor and its free stream velocity, $U_{\infty}$ can be determined according to procedures mentioned in Section 5.8.2. For the purpose of cleaning, it is provided with a drainage pipe and a valve at the bottom side.

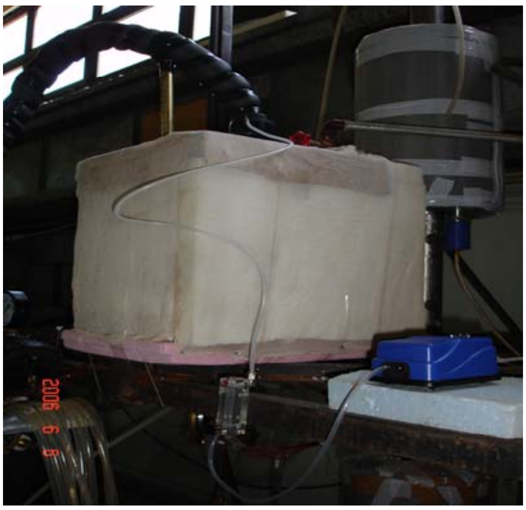


Figure 5.4 General view of the boiler.

The boiler is located just above and close to the test section. This assures the quick supply of the vapor directly to the test section and to minimize the heat loss through the hose.

## 5.3 Test section

The test section is manufactured at the METU workshop. It is completely made of stainless steel. The reason for using stainless steel is to avoid undesirable effects of water corrosion. The test section, as shown in Figure 5.5, is rectangular shaped condenser with dimensions of 150 mm ×300 mm×250 mm. It contains a bank of tubes of 3 rows, each of three stainless tubes with outside diameter of 21.3 mm and inside diameter of 18.3 mm.

The tubes are inline arrangement with horizontal pitch of 30 mm and vertical pitch of 30 mm. The effective length of the tubes which exposed to the steam is 300 mm. Test section can be inclined at different positions $3^o$, $6^o$, $9^o$ and $12^o$ by the help of using adjustable screws mounted on a steel frame. The reason for inclining the test section is to study the condensation at the lower tubes when condensate does not fall on to the centerline of the tubes. This resembles the staggered arrangement.

A three-way steam distributor is installed at the top cap of the test section and equipped with three control valves to ensure uniform distribution of vapor at the entrance of the test section. It is connected to the heat resistant hose from one end while it delivers the vapor or vapor mixture through three ports to the test section.

At the top part of the test section in front of the three inlet ports, a curved shaped stainless plate was located to divert and diffuse the forced steam which was passed through two perforated plates before it flows downward over the condensate tubes. This arrangement eliminates the vapor shear and the possibility of non-uniform distribution of vapor or vapor-air mixture over the tube bank.

At the bottom of the test section, a v-shaped condensate collector with 70 mm of height and inclination of $25^o$. It was used to collect the condensate, which in turn flows downward through a copper tube out of the test section.

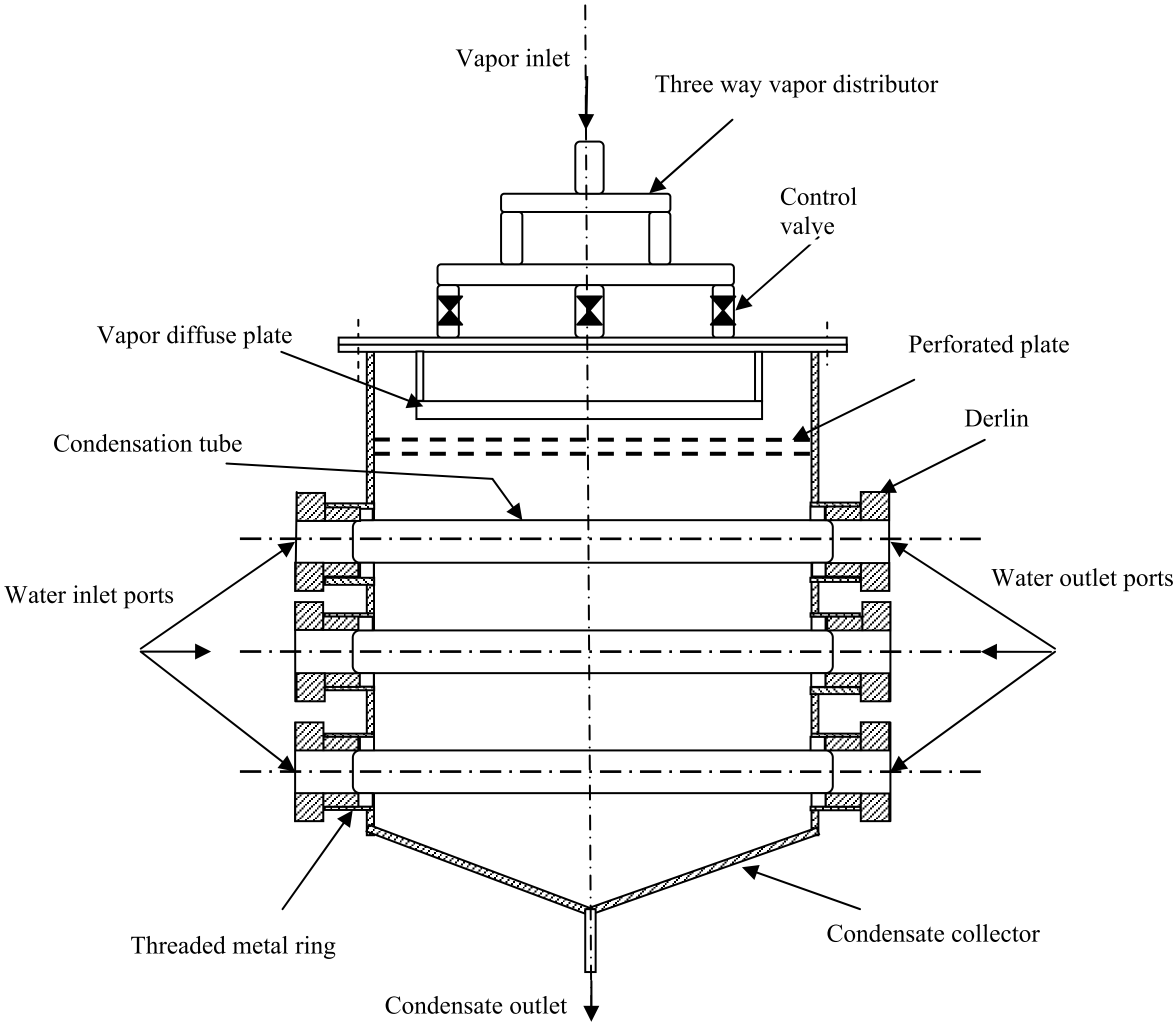


Figure 5.5a Schematic drawing of the test section.

Figure 5.5b General view of the test section.

Glass window was fitted at the front side of the test section to allow observation of the tubes. The window size is 300 mm×170 mm. It is made of heat resistant glass.

In addition, the test section is equipped with a relief valve to extract the excess vapor and a pressure gauge installed at the top. The condensation tubes should be securely fitted against leakage from the both ends by special non-metallic fitting made from Derlin.

Derlin is a nonmetallic material that works at high temperatures applications. A special seals and gaskets were used. For the purpose of cleaning and reaching inside the test section, a top cap was mounted and fixed to the test section by a set of fastening bolts and a heat resistant rubber seal. The test section is completely insulated in order to prevent heat losses and to eliminate undesirable condensation effects resulted from the walls of the test section.

## 5.4 Water drainage unit

A big amount of Cooling water of total flow rate of 745 (kg/hr) was circulated through the test section condensation tubes so as to execute the condensation process. At the outlet of each condensate tube, a water hose was fitted to discharge the water to the drainage unit. In order to prevent water flooding, a water drainage unit was assembled and mounted near to the test section.

Water drainage unit consists of collecting water tank, automatic float type switch and a drainage pump.

After it discharged at the outlet of the condensate tubes, the cooling water passed to the collecting plastic water tank through the water hoses. When the water level at the collecting water tank reached its maximum limit, a float type switch was activated. Automatically, the drainage pump was operated to discharge the water that accumulated in the water tank to the main drain pipe at the laboratory. As soon as the water level at the collecting water tank reached its minimum limit, the float type switch cuts the power from the drainage pump and so on.

## 5.5 Air supply unit

In order to study the effect of a non-condensable gas (air) on the film condensation heat transfer, air should be injected at uniform flow rates to the vapor at the top of the boiler. Then air that mixed with the vapor as a vapor- air mixture was passed through the hose to the test section.

For this purpose, air supply unit was installed as shown in Figure 5.4. It consists of a small air compressor, air flowmeter and air tube with fittings. The air compressor supplies air at different air mass fractions, minimum air mass fraction of ($m_{1,\infty}$ = 0.001) and high air mass fraction of ($m_{1,\infty}$ = 0.021), to the vapor by using adjustable switch. After air compressor, air passed through the air flowmeter and then to the top of the boiler through the air tube.

## 5.6 Temperature measurement system

Different temperature measuring points were located at different positions in the test section condensation tubes, Figure 5.6, so as to measure the temperature variations at each point and to help in analysis of the related parameters. Total of 15 measuring points were located at the tubes' walls in the test section to measure the tubes' wall temperature. In addition to 10 points were located at the inlet and outlet of the condensation tubes to measure the temperature of the inlet and outlet cooling water temperatures. Figure 5.7 shows the positions of the measuring points and the layout of the thermocouples. Table 5.1 shows the required thermocouples in the test section. T–type copper-constantan thermocouples were used. The installation of the thermocouples has been carried out at the METU workshop.

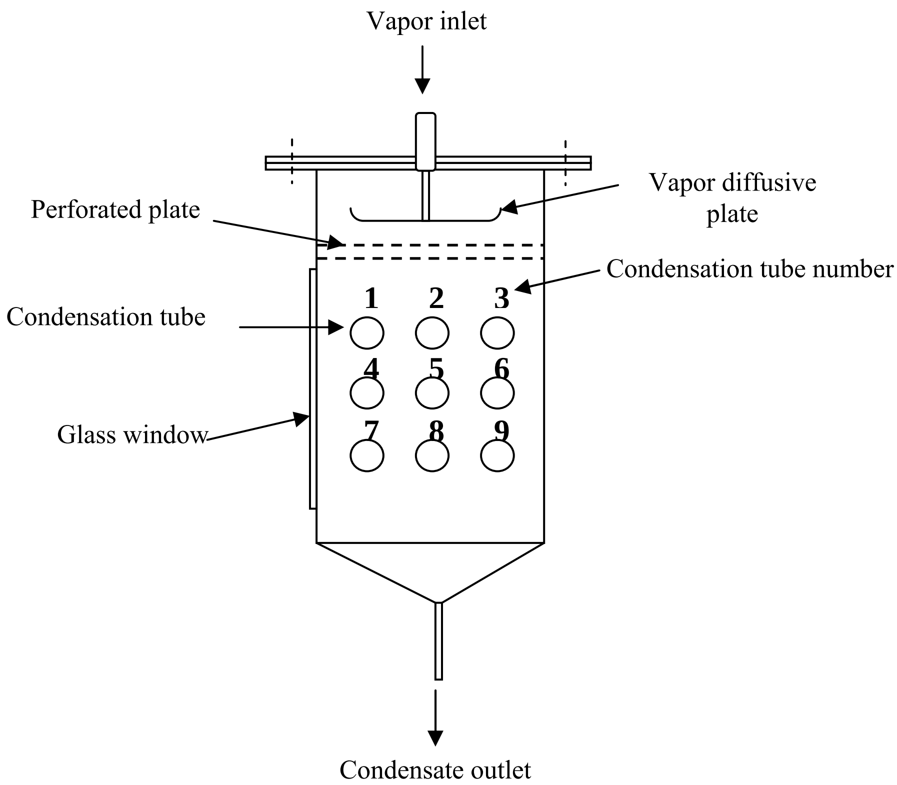


Figure 5.6  Layout of the condensation tubes.

Table 5.1 Required thermocouples in the test section.

| Code | Tube type | Thermo-couples required | Code | Tube type | Thermo-couples required |
|---|---|---|---|---|---|
| $T_1$ | Condensation tube, No.1 | 1 | $T_{16}$ | outlet cooling water tube | 1 |
| $T_2$,$T_3$ | Condensation tube, No.2 | 2 | $T_{17}$ | outlet cooling water tube | 1 |
| $T_4$ | Condensation tube, No.3 | 1 | $T_{18}$ | outlet cooling water tube | 1 |
| $T_5$,$T_6$ | Condensation tube, No.4 | 2 | $T_{19}$ | outlet cooling water tube | 1 |
| $T_7$,$T_8$,$T_9$ | Condensation tube, No.5 | 3 | $T_{25}$, $T_{20}$ | inlet and outlet cooling water tube | 2 |
| $T_{10}$,$T_{11}$ | Condensation tube, No.6 | 2 | $T_{21}$ | outlet cooling water tube | 1 |
| $T_{12}$ | Condensation tube, No.7 | 1 | $T_{22}$ | outlet cooling water tube | 1 |
| $T_{13}$,$T_{14}$ | Condensation tube, No.8 | 2 | $T_{23}$ | outlet cooling water tube | 1 |
| $T_{15}$ | Condensation tube, No.9 | 1 | $T_{24}$ | outlet cooling water tube | 1 |
| Total number of thermocouples | | 15 | Total number of thermocouples | | 10 |

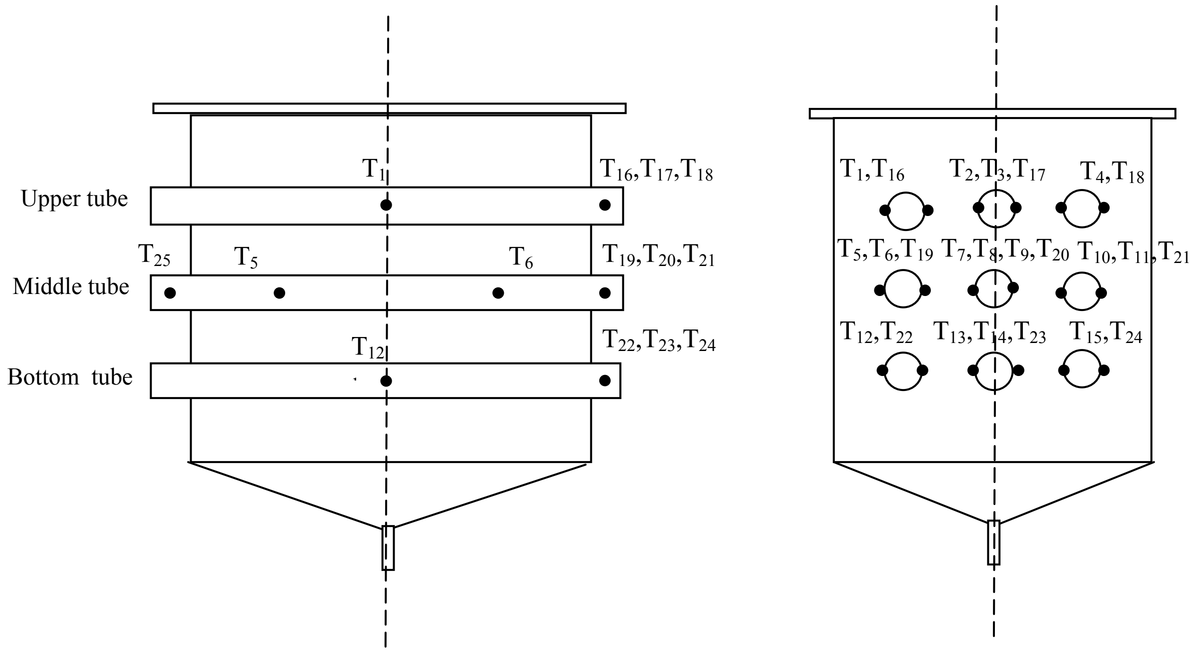


Figure 5.7 Thermocouples layout.

For the condensation tubes, a rectangular hole of (0.5cm×0.5cm) was cut at the surface of the tube at the specified location. One end of the thermocouple was welded by silver welding while the other end was connected to the datalogger. The datalogger, Figure 5.8, can measure a maximum of 32 measuring points. It was manufactured by Elimko Company with a reading accuracy of 0.1$^{o}$C.


Figure 5.8 View of the datalogger

In addition, it was provided with special software that deals with the measured data automatically. It stored and saved the data on specified files at the PC and help in processing and analyzing these data.

It should be noted that in some condensation tubes where two or three measuring points were suggested, the thermocouples were located at $90^o$ and $270^o$ angles on the periphery of the tube wall so that the average measured temperature of these points was considered in the analysis. Along the condensation tube length, the thermocouples were located at the midpoint of the condensate tube for the tubes number 1,3,7 and 9 whereas they were located at one fourth of the tube length from both ends for tubes number 2,4,5,6 and 8, see Figure 5.7.

On the other hand, for the cooling water inlet and outlet temperature measurement, the thermocouples were placed by drilling a hole at the non metallic fitting at the inlet and outlet ports of the cooling water. Then, one end of the thermocouple was put to the center of the fitting through the hole to ensure the direct contact with cooling water. The other end was connected to the datalogger. To prevent leakage of cooling water, a strong adhesive agent, Sun-Fix, was used to fill the hole.

### 5.7 Experimental procedure

Experiments were carried out to investigate the effect of various parameters such as vapor velocity, non-condensable gas fractions and vapor to tube wall temperature difference on the condensation heat transfer phenomenon. The main aim of the experimentation is to find out the amount of heat transfer rates from vapor and vapor-air mixture to cold water and the heat transfer coefficient. In addition, it was aimed to verify the theoretical results that obtained from the numerical analysis of the problem and to compare them with the experimental data.

During the condensation process, energy in the form of latent heat is released; this heat is transferred through the condensate layer to the tube wall and then to the cold water. For steady state condition, heat given by the steam is equal to the heat gained by the cold water. The equality below is used to calculate the heat transfer rate and the heat transfer coefficient;

$$Q = \dot{m} C_p (T_{out} - T_{in}) = h\ A (T_{sat} - T_w) \tag{5.1}$$

The film condensation heat transfer over bundle of tubes was investigated not only for inline arrangement but also for staggered arrangement. This has been carried out by inclining the test section to predefined inclination angles of $0^o$, $3^o$, $6^o$, $9^o$ and $12^o$. The idea behind inclining the test section is to see how condensation is affected when the condensate does not fall on the centerline of the tubes. This simulates the staggered arrangement for a bank of tubes.

The effect of steam to tube wall temperature difference or simply the effect of sub-cooling was achieved by varying the inlet cooling water temperatures which in turn affects the value of the tube wall temperature and hence the condensation rate along the tube surface. Different inlet cooling water temperatures were proposed ($15^oC$, 25 $^oC$, 35 $^oC$, 45 $^oC$ and 55 $^oC$ ). A sample of the experimental results is shown in Appendix B.

The effect of the non-condensable gas (air) could be investigated by adjusting air flow rates via the air compressor flow control switch. This air was passed through the air flowmeter and then to the top of the boiler to mix with vapor. Different non-condensable gas fractions could be studied.

By switching between the three electric heaters that were mounted in the boiler body, vapor or vapor-mixture velocity could be obtained at different rates. For example, maximum vapor velocity could be achieved when the three electric heaters were switched on.

Prior to experimentation, the whole set up fittings, connections, tubes, hoses….etc, should be checked against leakage. In addition, special attention should be taken into account for electric wiring, connections, grounding, and all safety measures to avoid undesirable electricity source accidents.

The experiments started by switching on the power to the electric heaters at the boiler. The heater of the cooling water tank could be switched on when needed. It took 30 minutes for the boiler to produce the vapor and became ready to send it to the test section when the three heaters were turned on. Meanwhile, the temperature of the cooling water tank reached to the desired value by using a thermostat. The cooling water could be supplied to the test section at a uniform flow rate by adjusting the control valve that was mounted on the inlet port of the cooling water division apparatus.

Before supplying cooling water, enough time should be allowed for vapor or vapor-mixture to fill the test section. Then, cooling water could be supplied to the test section at a uniform flow rate. Cooling water mass flow rate for each tube could be determined by measuring the time for filling a predefined vessel.

After a period of time when steady state conditions were reached, data reading and processing could be done by the help of the datalogger and the computer.

Finally, the data are analyzed and interpreted by the help of some equations and formulas presented everywhere in the literature. In addition, the uncertainty in the experimental measurements is studied and checked by the help of a procedure that proposed by Kline and Mc Clintock [55]. The uncertainty analysis shown in Appendix C, reveals that; the uncertainties in the experimental heat transfer rates and heat transfer coefficients for the upper, middle and bottom cylinders are about 5%. Some other sources of uncertainties in the experimental measurements may result from the human measuring and reading mistakes, poor calibration of some devices and electricity power oscillations, impurities and contaminations in the cooling water, …etc.

## 5.8 Calculation of the main parameters

Following the procedures mentioned by Lee [65] and Lee and Rose [45] in their experimental studies concerning forced convection film condensation on a horizontal tube with and without non-condensing gases, the main parameters calculation procedure could be summarized as follows;

### 5.8.1 Test section tube wall temperature

In the test section tubes where two or three junctions of the thermocouples are located, the arithmetic mean of the wall temperature values is considered. The thermocouples are oriented at $90^o$ and $270^o$ to the vertical on either side of the forward stagnation point.

### 5.8.2 Vapor mass flow rate at the test section

Vapor mass flow rate at the test section can be evaluated according to a steady flow energy balance between the boiler inlets (condensate return and gas) and the test section (vapor, gas, condensate on walls resulting from losses, $q_2$). Lee [65] and Lee and Rose [45] proposed the following equation to calculate the vapor mass flow rate;

$$\dot{m}_v = \left[\frac{1}{h_{fg} + C_{pl}(T_\infty - T_2)}\right]\left[q_H - q_1 - \dot{m}_g C_{pg}(T_\infty - T_1) - q_2(1 + \frac{C_{pl}(T_\infty - T_2)}{h_{fg}})\right] \quad (5.2)$$

where;

$q_1$**:** is the heat transfer rate to the environment (heat losses) from the boilers, the vertical vapor supply duct above the boilers and the horizontal upper duct which sloped slightly towards the boilers.

It is calculated according to the following equation;

$$q_1 = q_H - (\dot{m}_1 + \dot{m}_2)h_{fg} \quad (5.3)$$

$q_2$**:** is the heat transfer rate to the environment (heat loss) from the vertical supply duct above the test condenser tube.

It is calculated according to the following equation;

$$q_2 = \dot{m}_2 h_{fg} \quad (5.4)$$

$q_H$**:** is the power input to the boilers.

$\dot{m}_1$**:** is the condensate flow rate measured at the exit from auxiliary condenser.

$\dot{m}_2$: is the condensation rate on the walls of the vertical supply duct above the test section tube.

$T_1$: is the temperature of gas at entry to the boiler.

$T_2$: is the temperature of the condensate return at entry to the boiler.

For the present study, Equation 5.2 can be used with some modifications for the thermal losses terms $q_1$ and $q_2$. In the present study, a short flexible heat resistant hose properly insulated is used to carry pure vapor or vapor-air mixture from the outlet of the boiler to the inlet of the test section, see Figure 5.1.

As a result, heat loss from the hose to the environment is very small and it can be neglected. Then, $q_1$ and $q_2$ could be eliminated from Equation (5.2). The modified form of Equation (5.2) can be written as follows;

$$\dot{m}_v = \left[\frac{1}{h_{fg} + C_{p_l}(T_\infty - T_2)}\right]\left[q_H - \dot{m}_g C_{p_g}(T_\infty - T_1)\right] \tag{5.5}$$

The free stream velocity of pure vapor or vapor-air mixture ($U_\infty$) can be calculated by evaluating the mean vapor velocity over the exposed length of the test section tubes from the mass flow rate using a seventh power velocity profile for turbulent flow. For more details, refer to the above mentioned references, [45] and [65].

### 5.8.3 Gas (air) mass flow rate

Gas (air) mass flow rate could be calculated according to the following equation;

$$\dot{m}_g = \dot{V}_{ind}\sqrt{\rho\rho_o} \tag{5.6}$$

where;

$\dot{V}_{ind}$ : is the indicated volume flow rate of gas at the inlet of the gas flow meter.

$\rho$ : is the density of gas at temperature $T$ and pressure $P$.

$\rho_o$ : is the density of gas evaluated at standard temperature ($T_o$*=288.15 K*) and pressure ($P_o$*=100 kPa*).

By treating the gas (air) as an ideal gas, Equation 5.6 can be written as;

$$\dot{m}_g = \frac{\dot{V}_{ind}}{R_g}\left[\frac{P\,P_o}{T\,T_o}\right]^{1/2} \tag{5.7}$$

where;

$R_g$ : is the specific ideal gas constant of gas (air).

### 5.8.4 Gas (air) mass fraction

Air mass fraction can be calculated by two methods;

i) From the mass flow rates of air and vapor as;

$$m_{1,\infty} = \frac{\dot{m}_g}{\dot{m}_g + \dot{m}_v} \tag{5.8}$$

ii) From the pressure and temperature measurements in the test section assuming saturation conditions and the Gibbs-Dalton ideal gas mixture equations, thus;

$$m_{1,\infty} = \frac{P_\infty - P_s(T_\infty)}{P_\infty - \left[(1 - \frac{M_v}{M_g})\right] P_s(T_\infty)} \tag{5.9}$$

where;

$P_s(T_\infty)$ : is the saturation pressure of the vapor corresponding to $T_\infty$.

$M_v, M_g$ : are the relative molecular masses of the vapor and gas respectively.

# CHAPTER 6

# RESULTS AND DISCUSSION

The results of the numerical and experimental investigation are presented to show the effect of different parameters on the film condensation heat transfer phenomenon over bundle of tubes. These parameters include; free stream velocity, free stream non-condensable gas (air) mass fractions, free stream temperature to wall temperature difference, tube diameter and the angle of inclination. Heat transfer rates and heat transfer coefficients are evaluated at different working conditions for both inline and staggered arrangements.

The results are analyzed and interpreted in three categories; numerical results, experimental results and comparison of the experimental results with the literature and of the present study theoretical results.

## 6.1 Numerical results for pure vapor on a tier of tubes

A computer code in Fortran77 has been implemented and executed for the analysis of film condensation of steam flowing downward on a tier of horizontal cylinders. It is based on the theoretical model which is developed to calculate various parameters known to affect the condensation heat transfer phenomena numerically by Newton-Raphson method. Thermo-physical properties and geometric dimensions are defined at the beginning of the program. The fundamental geometric parameter is the diameter of the tubes. The effect of the tube diameter on the film thickness, velocity of the condensate, heat flux and heat transfer coefficient will be discussed.

The results which are obtained at different tube diameters will be used to study the effect of tube diameter on the condensation heat transfer. Another parameter that significantly affects the condensation rate is the difference between the saturation temperature of steam and the wall temperature of the tube. The results which are obtained for different values of $\Delta T$ will be used to study the effect of steam to wall temperature difference on condensation heat transfer. Numerical results are presented for the same tubes dimension and test working conditions for the experimental setup that was used by earlier researcher [61], at METU laboratory, (d=19 mm and $\Delta T$=10 K), under different angles of inclination $0^o$, $3^o$, $6^o$ and $10^o$. Figure 6.1 shows the variation of film thickness with respect to angular position ($\theta$) at the upper, middle and the bottom tubes for both inline and staggered arrangements at different inclination angles.

The condensate fall angle ($\theta_o$) and the angular position ($\theta$) are measured from the top of the tube. Results show that the film thickness increases as the condensate flows downward on the tube. The reason of this increase is the additional condensation of steam as the condensate flows downward. The upper tube has a comparatively faster increase in the film thickness as compared to the lower tubes in the column. However, the smallest film thickness is observed on the upper tube.

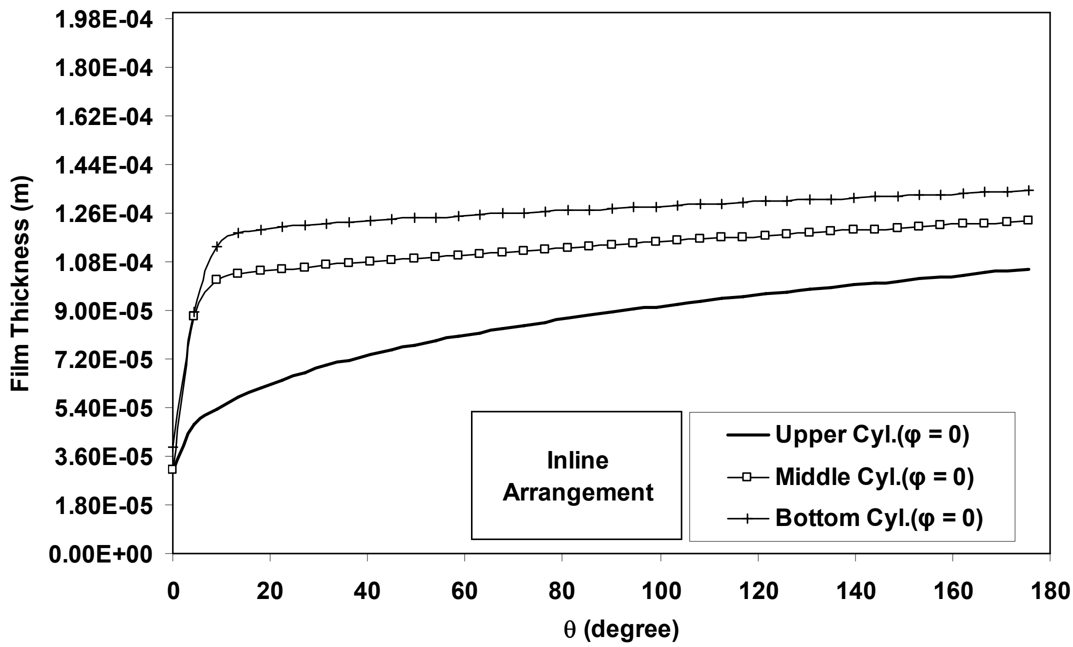


Figure 6.1a Variation of film thickness with angular position for upper, middle and bottom cylinders at (d=19 mm and $\Delta T$=10 $^oK$).

The lower the tube is, the larger the condensate film thickness becomes. The effect of angle of inclination on the film thickness is also investigated as seen in Figure 6.1b. For the upper cylinder, the data are similar to those presented in Figure 6.1a. For the middle and the bottom cylinders, film thickness gradually increases as for the upper cylinder until the point where the condensate falls from the upper cylinder on the middle cylinder which corresponds to ($\theta_o$). In this case, the film thickness remarkably increases and then increases with the same trend as angular position increases. This is attributed to the amount of condensate that enters the control volume per unit time and the effect of transfer of momentum. As angle of inclination increases, condensate fall angle ($\theta_o$) increases too, resulting in retarding the sudden increase of the film thickness that caused by the condensate falling. In addition, film thickness for the bottom cylinder is much higher than that of the middle cylinder. The reason of this increase in the condensate thickness is obviously the condensate dripping from the upper tubes.

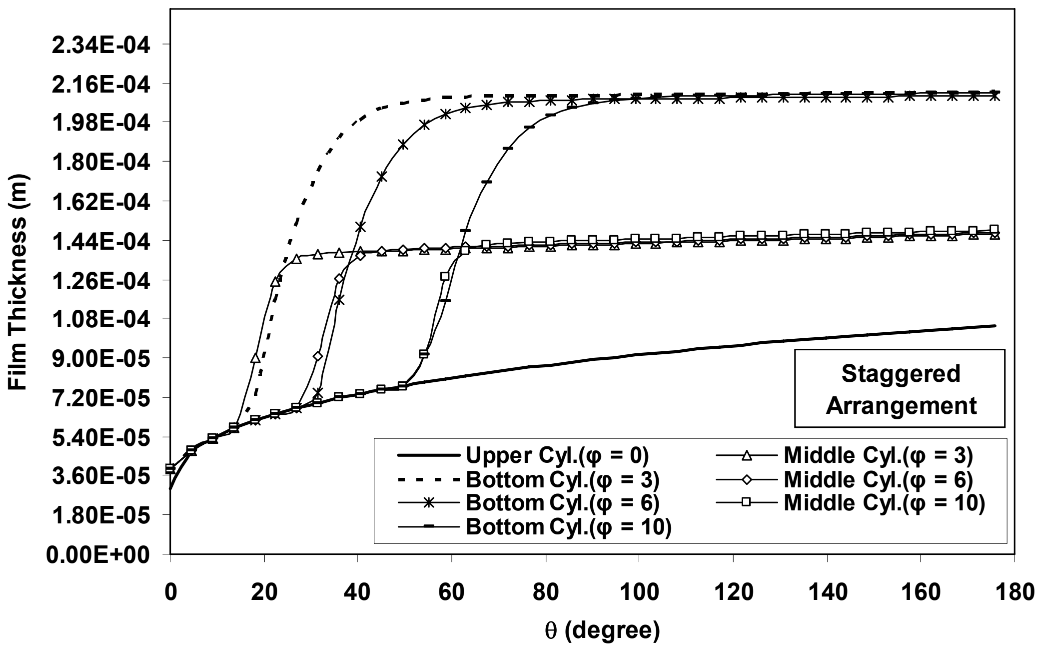


Figure 6.1b Variation of film thickness with angular position for upper, middle and bottom cylinders at (d=19 mm and $\Delta T$=10 $^oK$).

The behavior of the variation of the velocity as a function of the angular position with different angles of inclination $0^o$, $3^o$, $6^o$ and $10^o$ is similar to that of the film thickness variation as depicted in Figure 6.2.

The velocities on the upper tube are less than those on the lower tubes. Since the thickness of the condensate is much smaller at smaller angular positions on the upper tube, condensation rate is higher there which results in a rapid increase in the velocity. However, on the lower tubes velocities reached considerably high values and consequently shear stresses are large and balance the gravitational forces.

A fluctuation in the velocities is observed at the angular positions smaller than 20° at the middle and the bottom tubes. This fluctuation is due to the numerical instability taking place at the very small angular position values. Calculations stabilize after a few steps later. Again there is a remarkable increase in the velocities corresponding to the different angles of inclination. This results from the condensate fall from the upper cylinder. The bottom cylinder has larger values of velocities than the others for the same reasons mentioned above

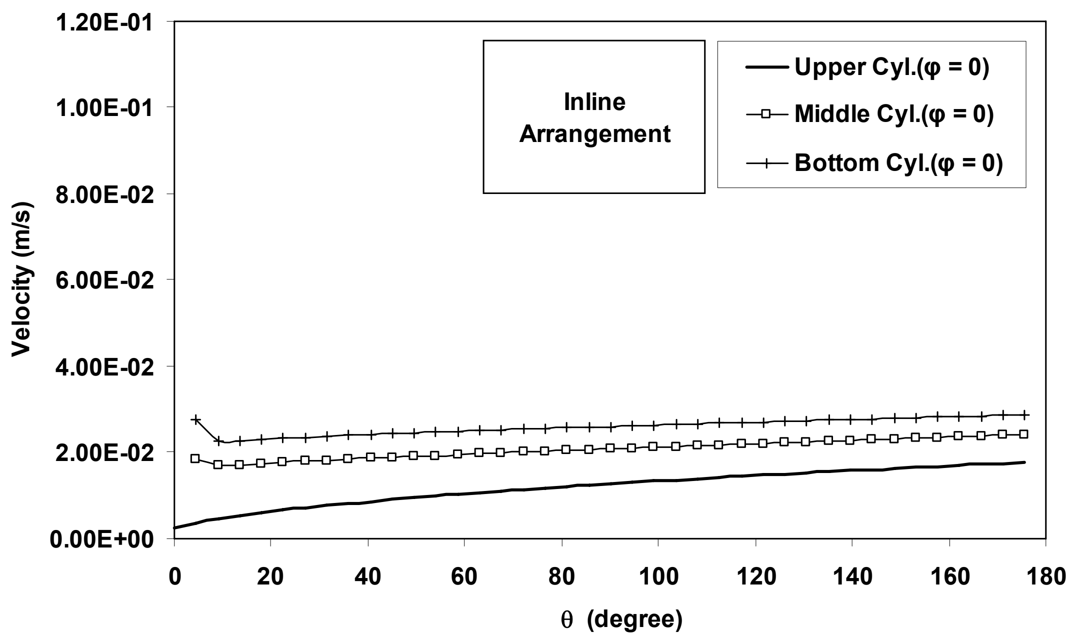


Figure 6.2a Variation of velocity with angular position for upper, middle and bottom cylinders at (d=19mm and $\Delta T=10\ ^oK$).

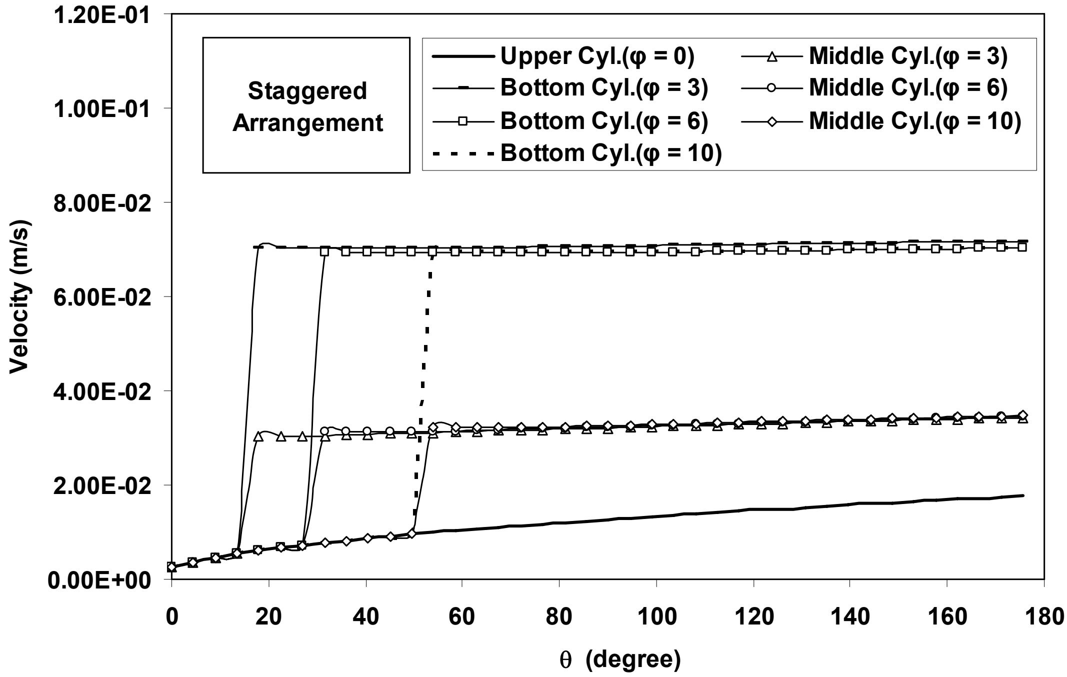


Figure 6.2b Variation of velocity with angular position for upper, middle and bottom cylinders at (d=19mm and $\Delta T=10\ ^{o}K$).

Since linear temperature distribution and only conduction type heat transfer through the condensate is assumed at the beginning of the analysis, heat fluxes can be calculated by Fourier's law of conduction:

$$q = k\frac{(T_{sat} - T_w)}{\delta} \tag{6.1}$$

Heat fluxes are calculated as a function of the angular position by Equation 6.1 are shown in Figure 6.3 for both inline and staggered arrangements.

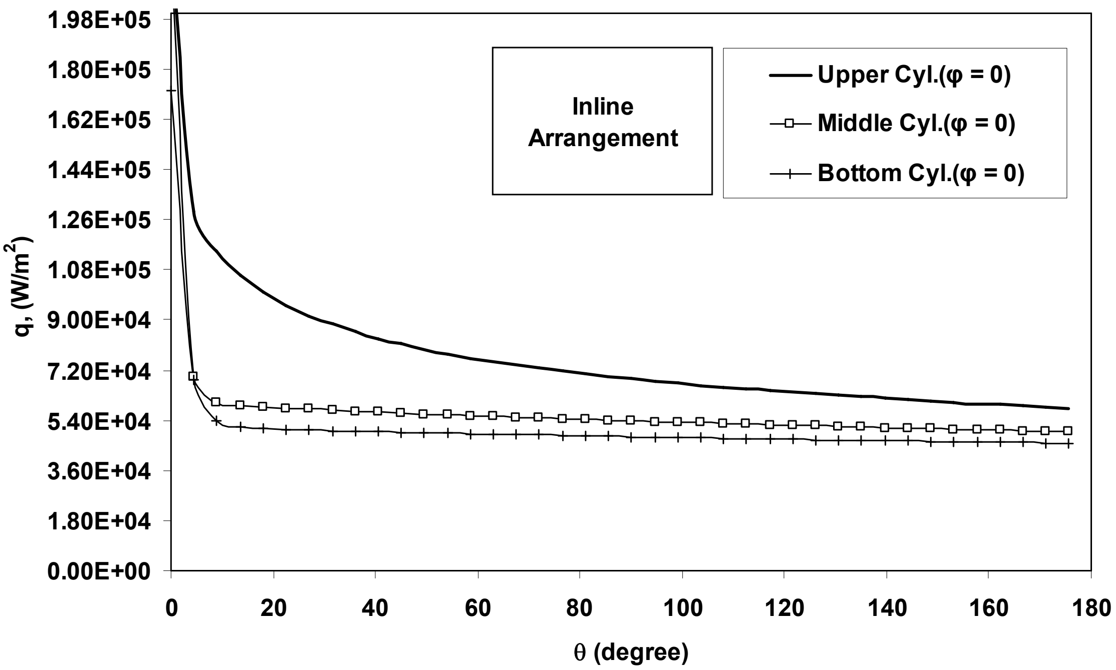


Figure 6.3a Variation of heat flux with angular position for upper, middle and bottom cylinders at (d=19mm and $\Delta T=10\ ^oK$), inline arrangement.

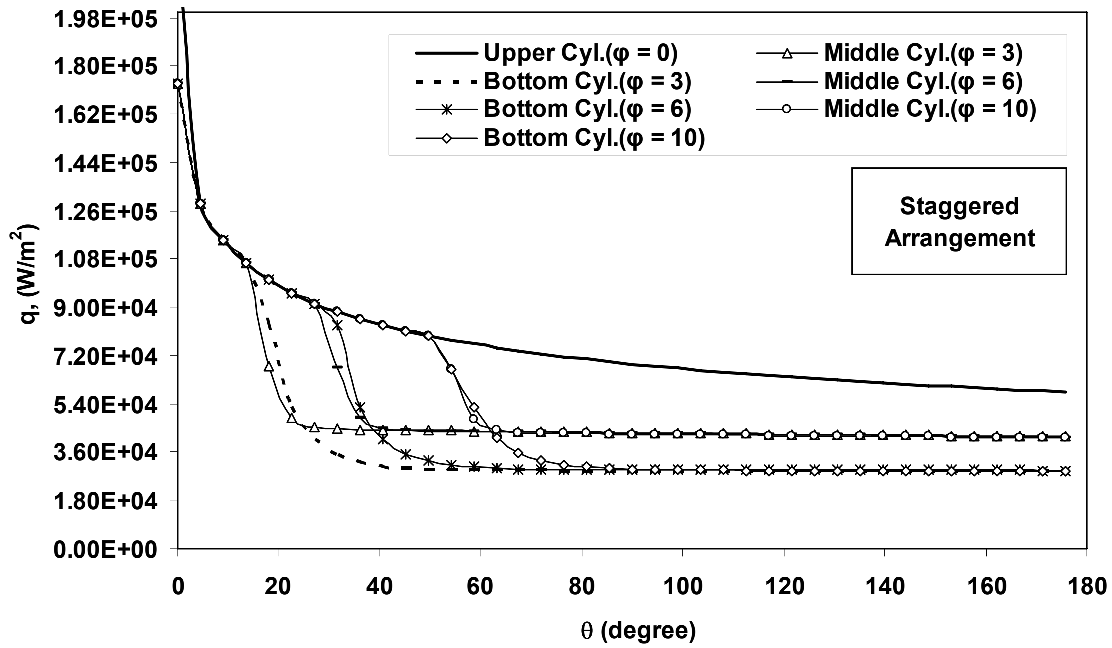


Figure 6.3b Variation of heat flux with angular position for upper, middle and bottom cylinders at (d=19mm and $\Delta T=10\ ^oK$), staggered arrangement.

If the heat flux curve for the upper tube is observed, it is seen that the heat flux values gradually decrease while the condensate gets thicker as it flows downward on the tube. The lower tubes have less heat flux values because of the condensate inundation. Since the condensate resists to heat transfer, the lower tubes can hardly conduct the heat as compared to the upper tube. A noticeable decrease in the heat fluxes at different inclination angles is also attributed to the increase of the resistance of the condensate film to heat transfer as its thickness increases at these locations. Heat transfer coefficients for the condensate can be calculated by the convection heat transfer formula:

$$h = \frac{q}{\left(T_{sat} - T_w\right)} = \frac{k}{\delta} \tag{6.2}$$

Since the heat transfer coefficient is directly proportional to the heat flux, a similar effect is expected for the heat transfer coefficient curves. As a consequence, the larger the condensate film thickness gets, the lower the heat transfer coefficient becomes.

### 6.1.1 The effect of the cylinder diameter

Variations of the film thickness of the condensate with angular position for upper, middle and bottom cylinders at various tube diameters and different angles of inclination are presented in Figure 6.4. It is aimed in these figures to find out how tube diameter affects the condensation heat transfer. The present results study numerical results are obtained based on the cylinder diameter and working conditions for an earlier experimental study conducted by Makas [61] at METU laboratory. Diameter of the cylinders used in the experiments is 19mm. According to Figure 6.4, film thickness increases as the diameter of the tubes increases for the same angular position and angle of inclination. This is attributed to the increase in the condensation heat transfer surface area which results in increasing the vapor condensation rates. In addition, as the diameter of the tube increases, the critical inclination angle increases and the condensate fall angle decreases, see Table 3.1.

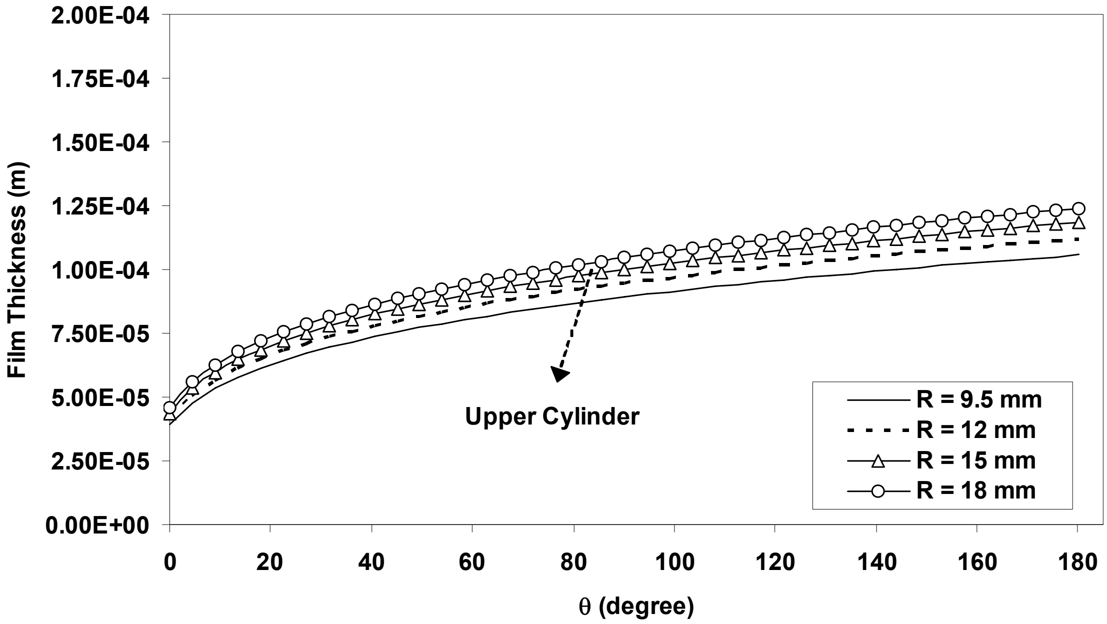


Figure 6.4a Variation of film thickness with angular position for upper cylinder at different cylinder diameters.

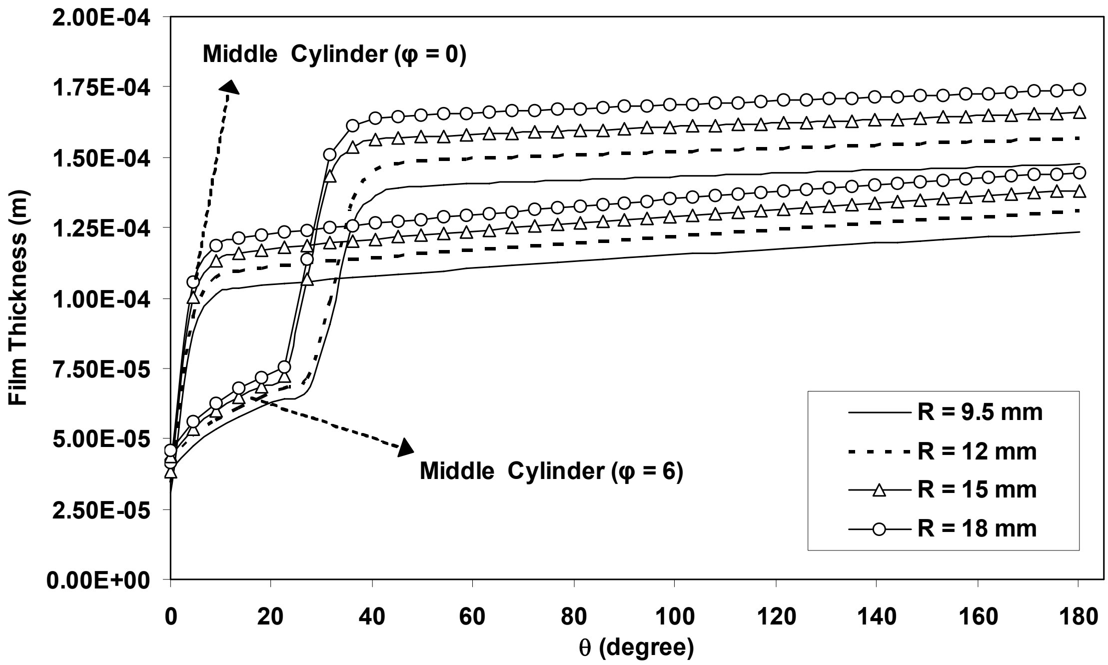


Figure 6.4b Variation of film thickness with angular position for middle cylinder at different cylinder diameters.

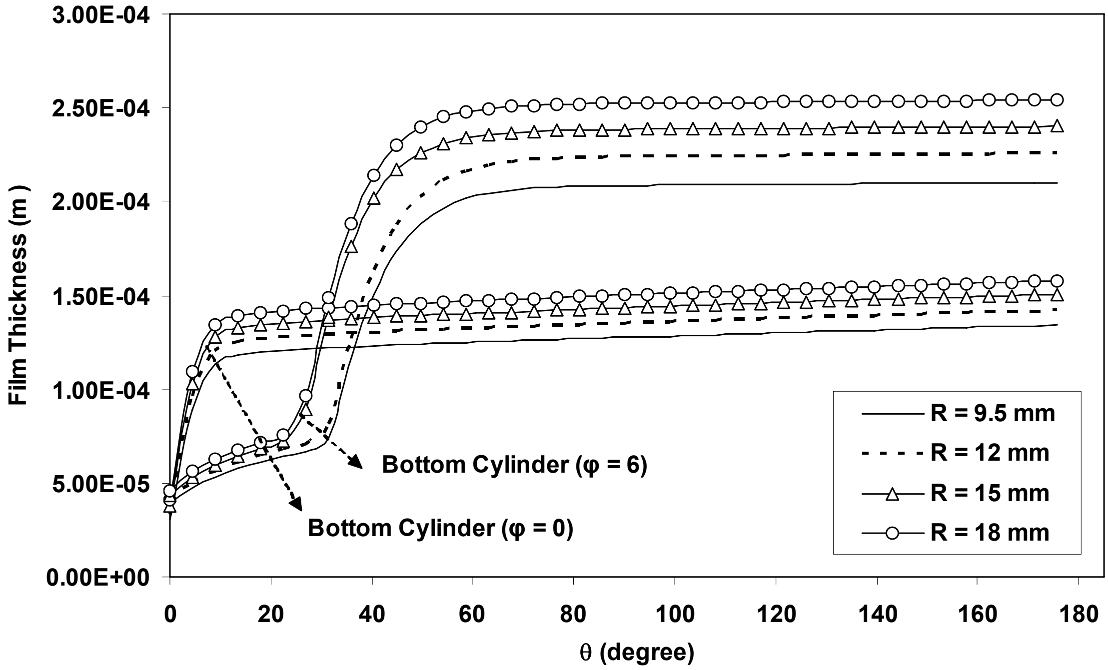


Figure 6.4c Variation of film thickness with angular position for bottom cylinder at different cylinder diameters.

The values of heat transfer coefficient are also calculated for a given tube diameter. The results are shown in Figure 6.5. In this figure, a decrease in the average heat transfer coefficient is observed as the tube diameter is increased. The effect of inclination angle on the heat transfer coefficient is also investigated.

The higher the inclination angle is, the higher the mean heat transfer coefficient becomes. This is attributed to the fact that there is a condensate from the upper tube falls on the lower tube at larger condensate fall angle. This will retard the sharp increase in the film thickness resulted from the condensate fall of the upper cylinder on the lower cylinder. As a result, the values of the average heat transfer coefficient will be higher than the others when the inclination angle is lower. Larger film thickness causes a larger thermal resistance and, as a result, heat transfer coefficient decreases as the tube diameter increases.

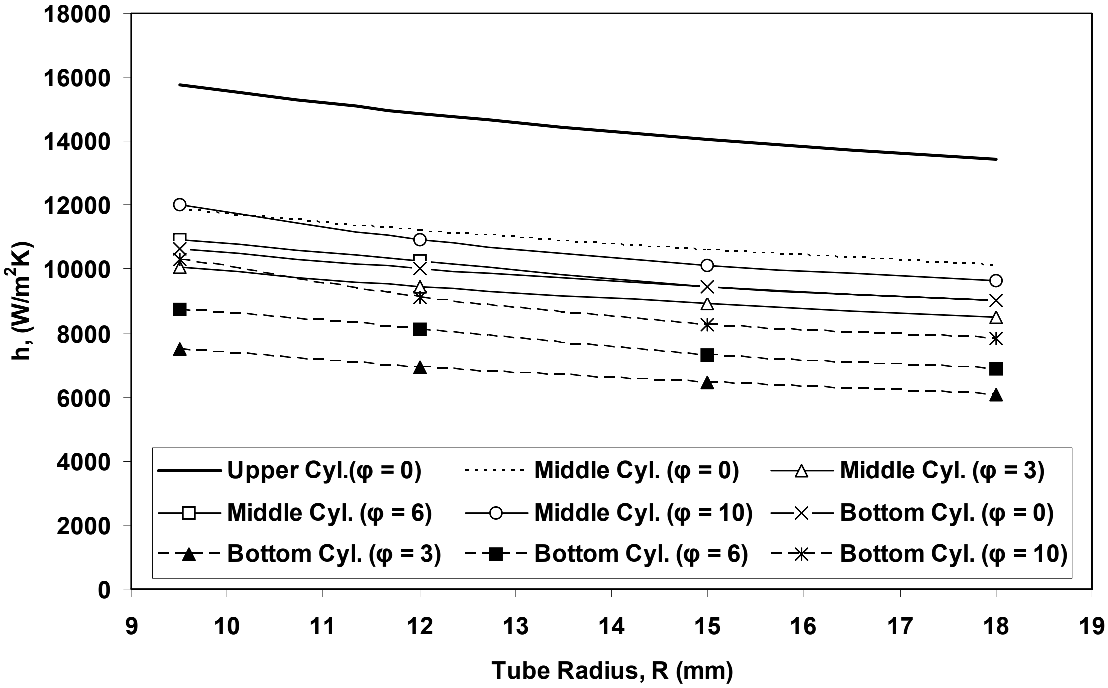


Figure 6.5 Variation of heat transfer coefficient with angular position for different cylinder diameters at different inclination angles.

### 6.1.2 The effect of the temperature difference

The theoretical analysis has been extended to investigate the condensation phenomenon at different $\Delta T$ values. Variations of the film thickness of the condensate with angular position for different steam to wall temperature differences at different inclination angles are presented in Figure 6.6. It is seen from the figure that; a small temperature difference has a considerable effect on the film thickness of the condensate. Film thickness increases as the temperature difference increase. This is expected from the fundamentals of heat transfer, since any increase in the temperature difference will lead to a corresponding increase in the condensation rates.

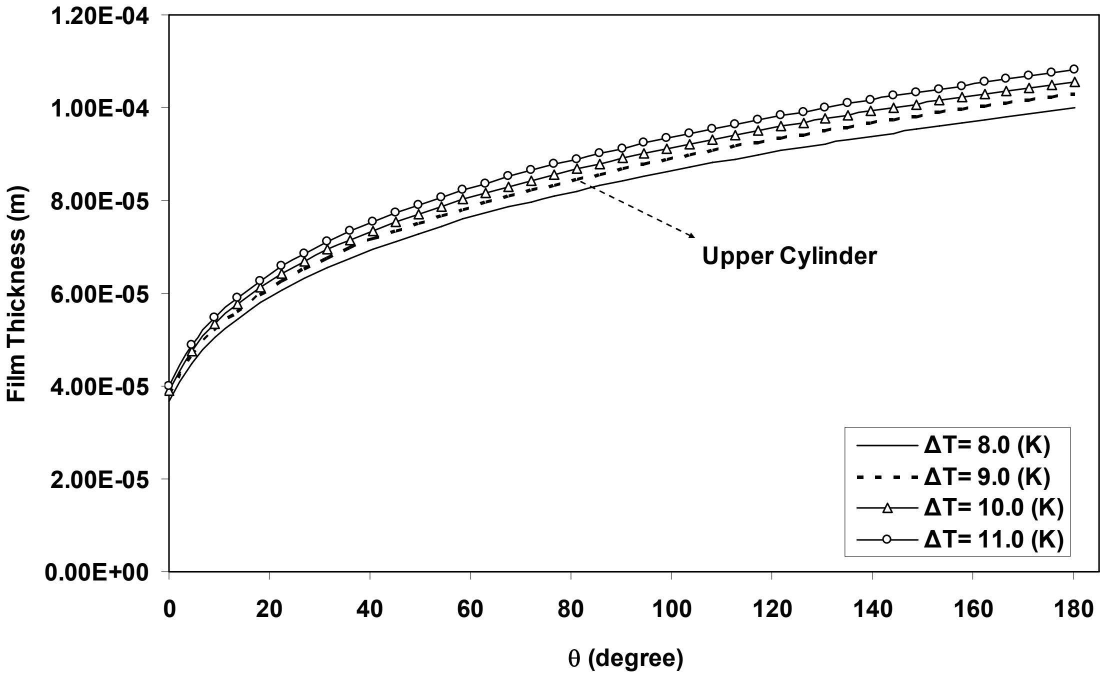


Figure 6.6a Variation of film thickness with angular position for upper cylinder at different temperature differences.

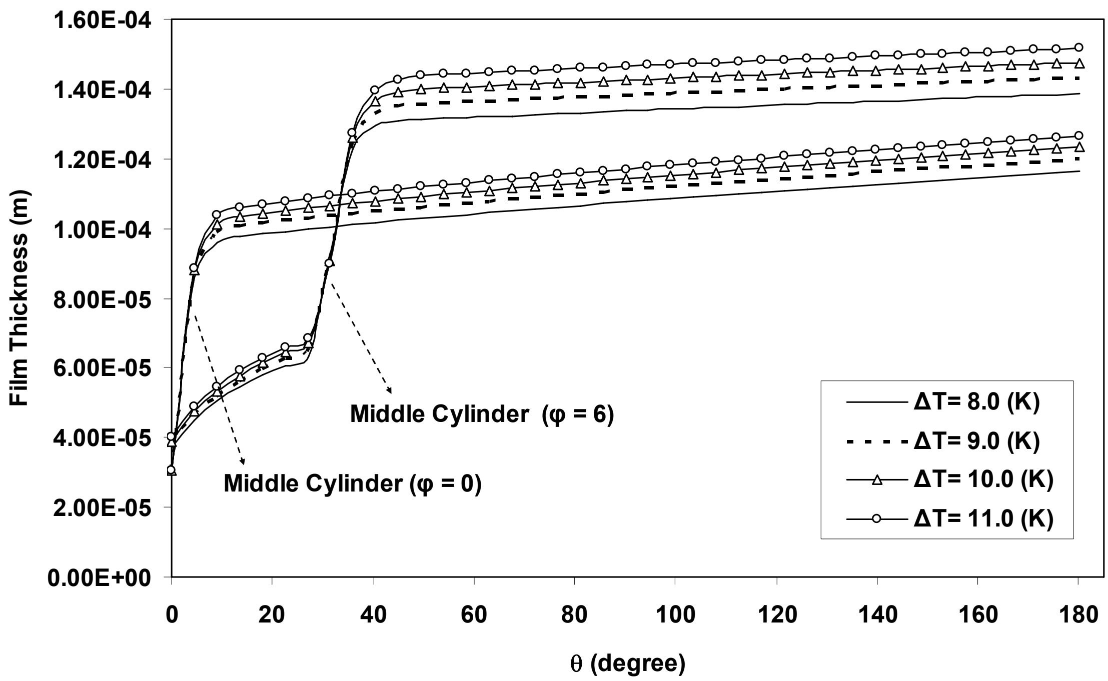


Figure 6.6b Variation of film thickness with angular position for middle cylinder at different temperature differences.

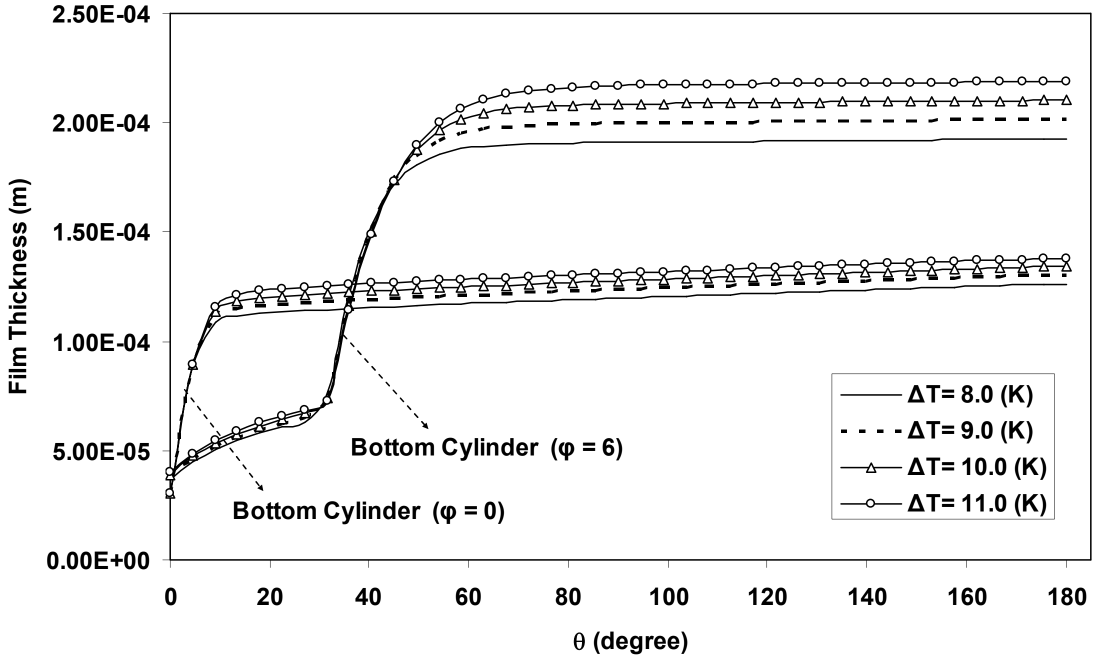


Figure 6.6c Variation of film thickness with angular position for bottom cylinder at different temperature differences.

Figures 6.7 and Figure 6.8 are constructed to show the variations of heat fluxes and heat transfer coefficients with temperature difference for upper, middle and bottom cylinders at different inclination angles.

It is deduced from Figure 6.7 and Figure 6.8 that; while the heat fluxes increase, the heat transfer coefficients decrease with increasing temperature differences. At higher heat fluxes, the rate of condensation is higher and thus the condensate layer becomes thicker, which in turn reduces the value of heat transfer coefficient. Heat fluxes and heat transfer coefficients increase as the angle of inclination increases, for the same value of temperature difference.

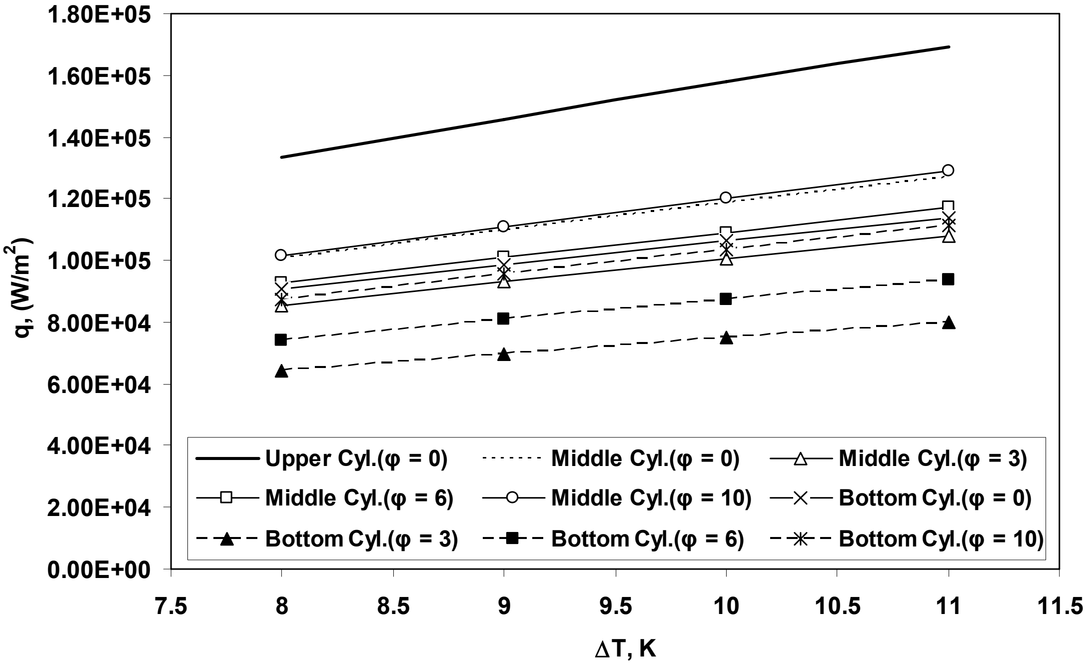


Figure 6.7 Variation of heat flux with temperature difference for upper, middle and bottom cylinders at different inclination angles.

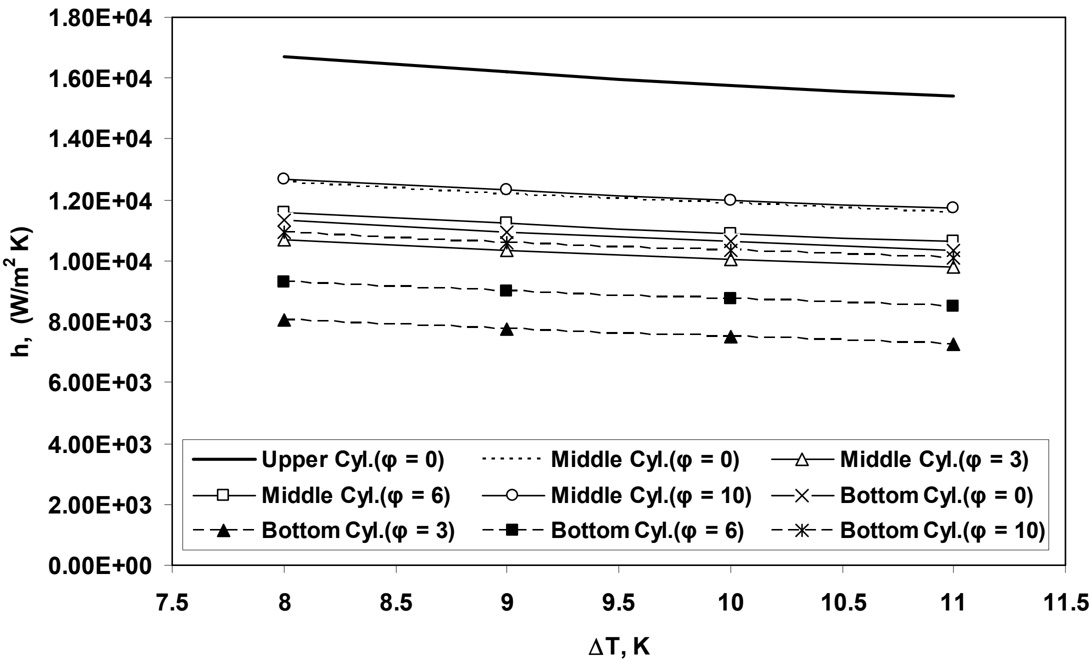


Figure 6.8 Variation of heat transfer coefficient with temperature difference for upper, middle and bottom cylinders at different inclination angles.

## 6.2 Numerical results for vapor-air mixture on a single cylinder

Numerical results for forced flow film condensation of the steam flowing downward a horizontal cylinder in the presence of air as a noncondensable gas is presented. The effect of various parameters known to influence the laminar film condensation phenomena is analyzed and investigated. These parameters include free stream velocity ($U_\infty$), overall temperature difference ($T_\infty - T_w$), free stream noncondensable mass fraction ($m_{1,\infty}$), cylinder diameter ($d$) and pressure gradient ($\frac{dP}{dx}$). Different ranges are selected to cover most of the working conditions.

### 6.2.1 Velocity, Temperature and Concentration Profiles

Figures 6.9, 6.10, 6.11, 6.12 and 6.13 illustrate velocity, temperature and air concentration profiles respectively at free stream velocity of 20 m/s, free stream air concentration of 0.05 and at different locations on periphery of the cylinder. It can be seen from Figure 6.9 and Figure 6.10 that velocity increases as vapor mixture moves downward on the periphery of the cylinder according to potential flow theory. It increases gradually from locations where $\theta = 20^{\circ}$ until $\theta = 80^{\circ}$. Then velocity starts to decrease at $\theta = 100^{\circ}$. This is attributed to the effect pressure gradient and the assumptions of potential flow theory.

Figure 6.11 shows the velocity distribution of the liquid boundary layer at $U_\infty = 20\ m/s$ and $m_{1,\infty} = 0.05$. The velocity starts to increase gradually from $\theta = 20^{\circ}$ to $\theta = 60^{\circ}$. Then, liquid velocity starts to decrease at location where $\theta = 80^{\circ}$. The values of velocities for liquid boundary layer are small when compared to that of vapor mixture boundary layer. This is due to higher viscous effects and shear forces at the liquid boundary layer which resist the flow when compared to that of the vapor-mixture boundary layer.

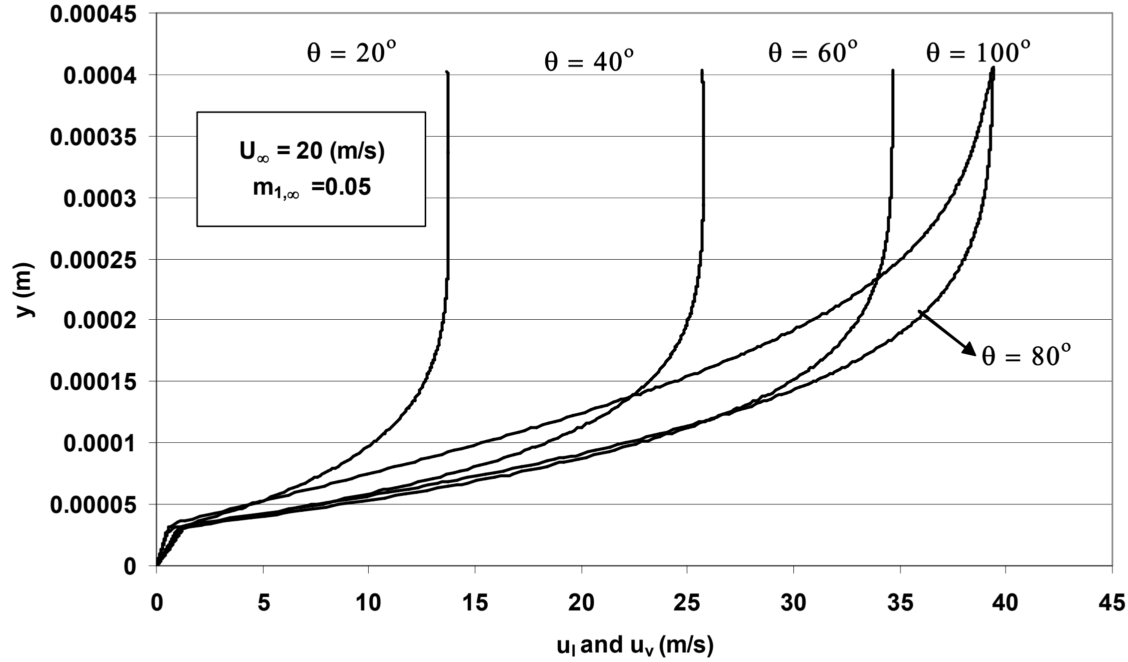


Figure 6.9 Velocity distribution of liquid and vapor-mixture boundary layers at different locations on the periphery of the cylinder.

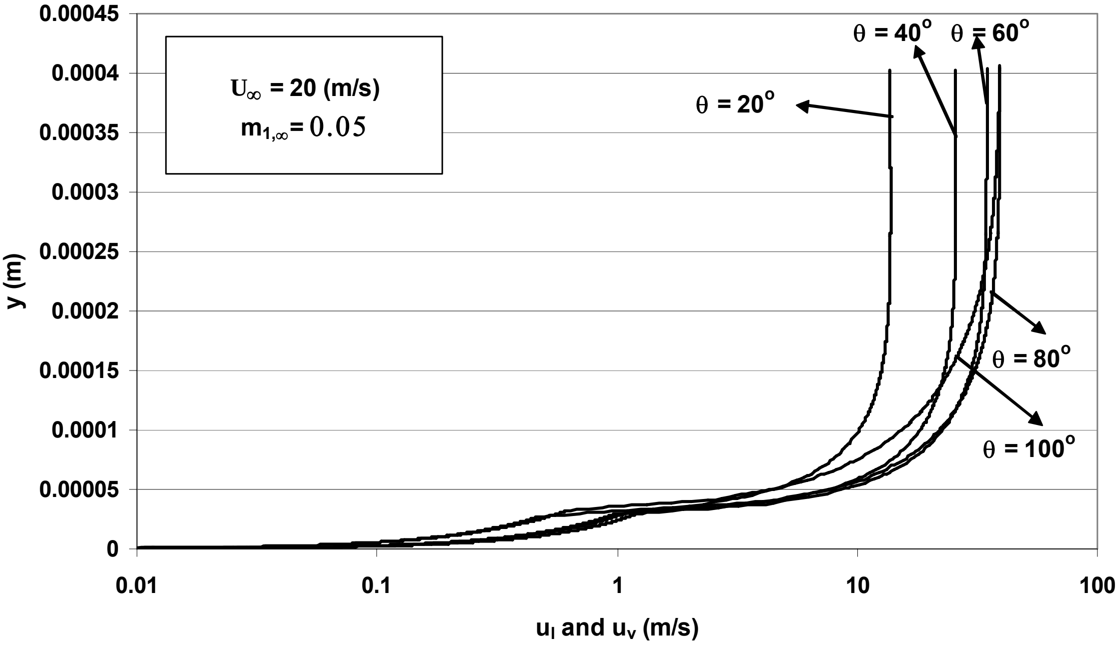


Figure 6.10 Velocity distribution of liquid and vapor-mixture boundary layers at different locations on the periphery of the cylinder (x-axis in logarithmic scale)

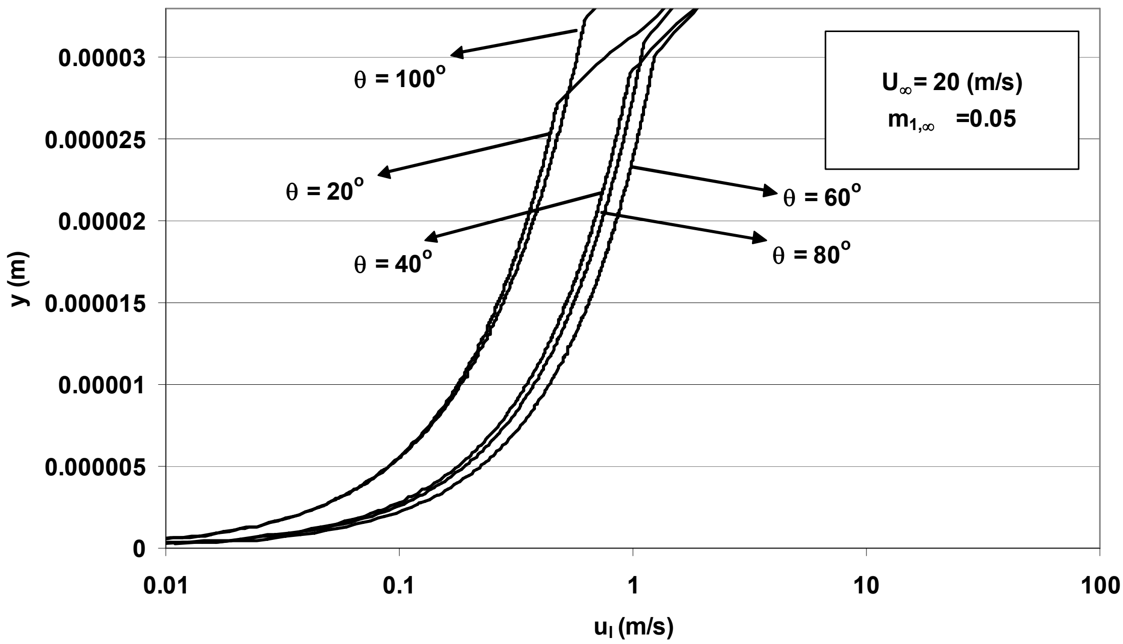


Figure 6.11 Velocity distribution of liquid boundary layer at different locations on the periphery of the cylinder.

Figures 6.12, 6.13 and 6.14 show the temperature distribution of the liquid and vapor-mixture boundary layers at different locations on the cylinder periphery at ( $U_{\infty} = 20\ m/s$ and $\mathrm{m}_{1,\infty} = 0.05$ and $\Delta\mathrm{T} = 10\ ^{\circ}\mathrm{K}$ ). Figure 6.13 illustrates the temperature distribution of vapor-mixture boundary layer. It can be seen that temperature decreases as long as angle ($\theta$) increases. This is attributed to the effect of the air and its distribution across the vapor-mixture boundary layer. As air mass fraction increases near the vapor-liquid interface, partial pressure of the vapor decreases. As a result, the corresponding saturation temperature decreases too, since thermodynamic equilibrium at interface is assumed and the vapor at its saturation state.

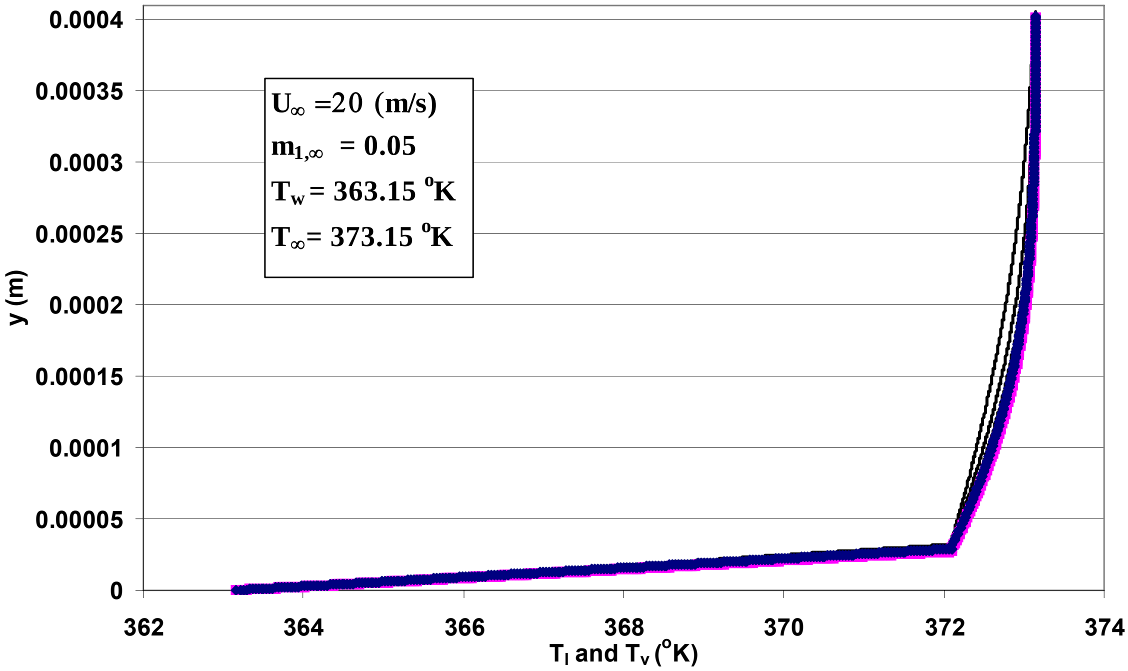


Figure 6.12 Temperature distribution of liquid and vapor-mixture boundary layers at different locations on the periphery of the cylinder.

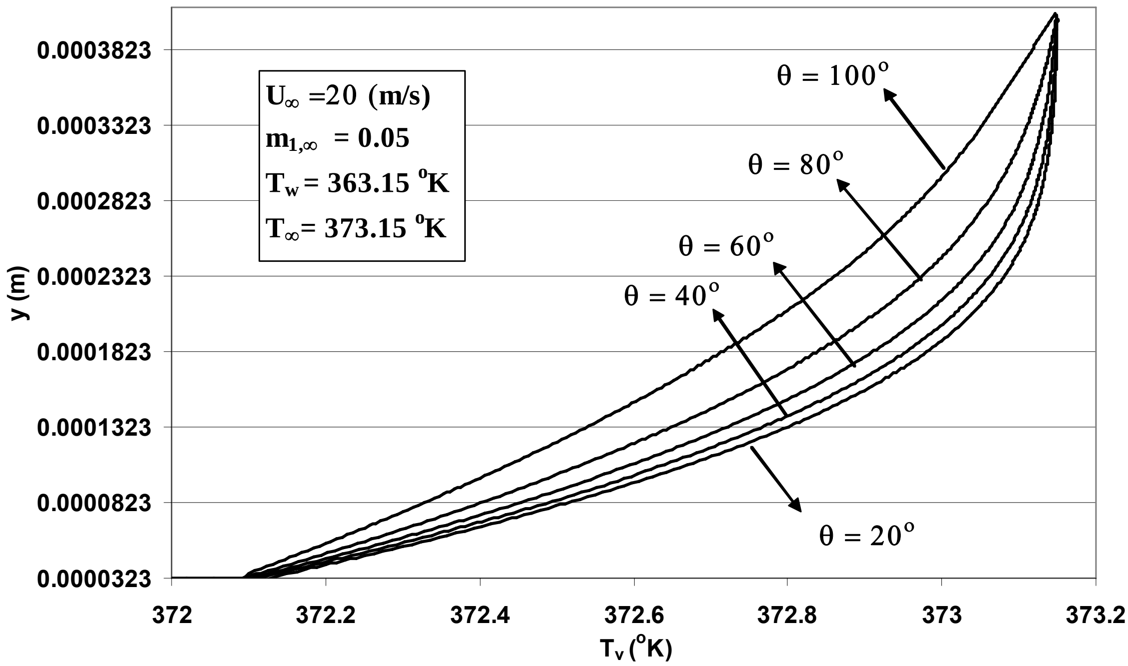


Figure 6.13 Temperature distribution of vapor-mixture boundary layer at different locations on the periphery of the cylinder.

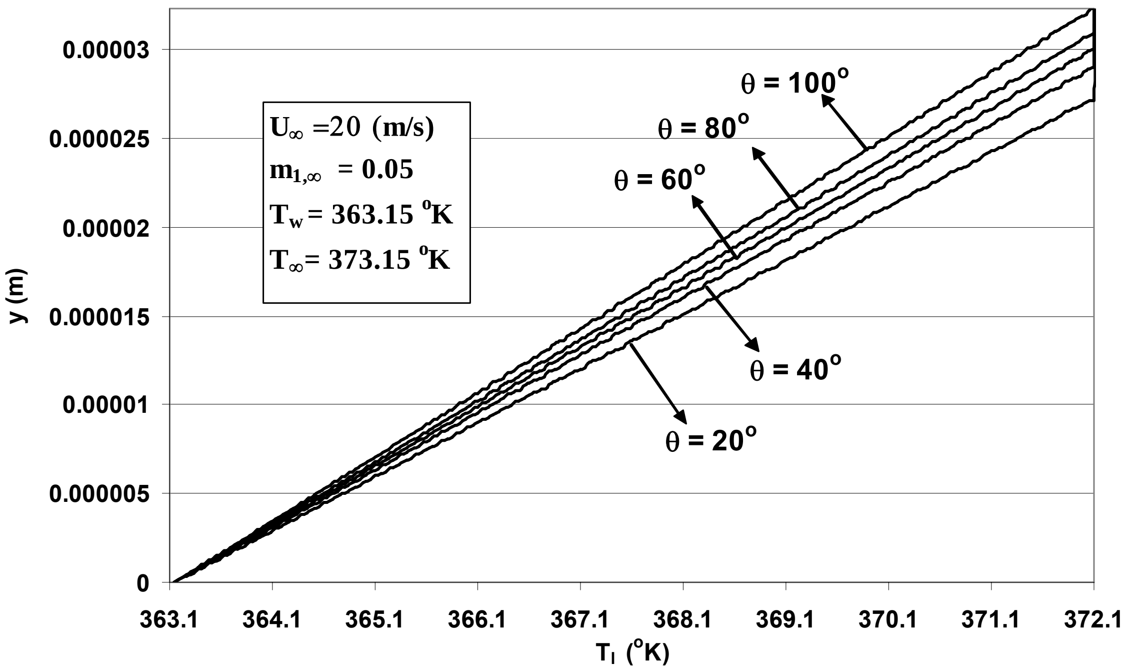


Figure 6.14 Temperature distribution of liquid boundary layer at different locations on the periphery of the cylinder.

Figure 6.14 shows the temperature distribution at the liquid boundary layer. It can be seen that the temperature decreases as long as angle ( $\theta$ ) increases. This is attributed to the effect of non-condensable gas (air) accumulation at the liquid-vapor interface which in turn affects the interface temperature by reducing it. This leads to a decrease in the temperature difference at liquid boundary layer.

Figure 6.15 shows the non-condensable gas (air) concentration distribution at vapor-mixture boundary layer at different locations on the periphery of the cylinder for ( $U_\infty = 20\ m/s$ and $m_{1,\infty} = 0.05$ and $\Delta T = 10\ ^oK$ ). As expected, air concentration increases towards the liquid –vapor interface due to diffusion of air and convective inflow of free stream air to the liquid-vapor interface. At equilibrium, the interface air concentration is high enough so that the resulting diffusion away from the interface into the ambient just balances the rate at which its concentration increases due to condensation process. In addition, air concentration increases as $\theta$ increases.

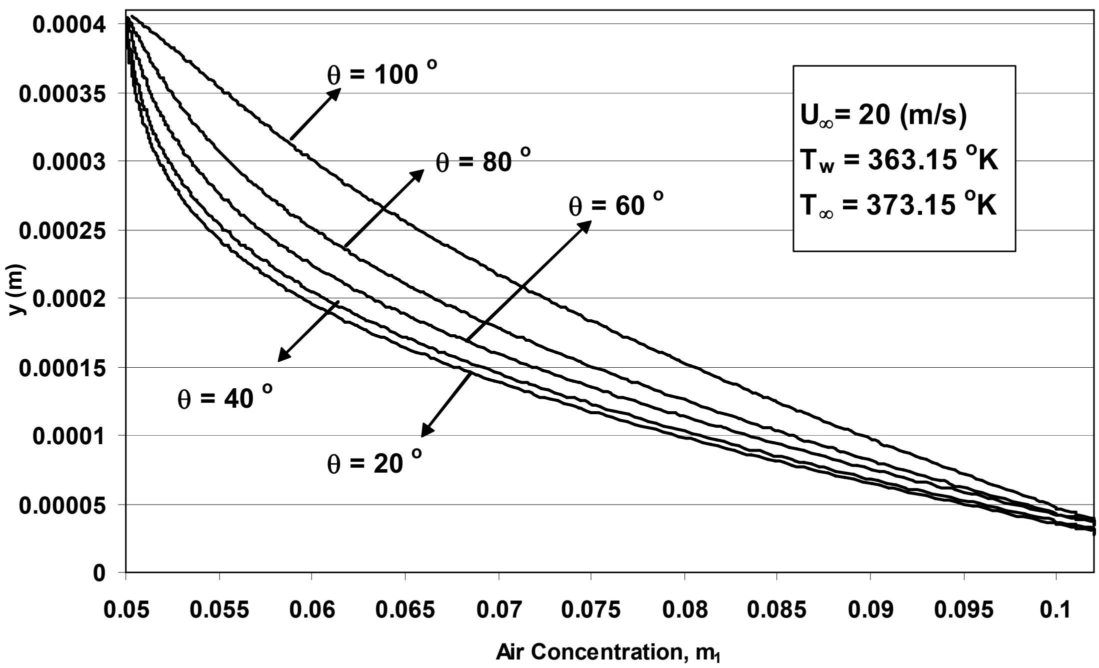


Figure 6.15 Air concentration distribution of vapor-mixture boundary layer at different locations on the periphery of the cylinder.

### 6.2.2 The effect of the free stream velocity

The effect of free stream velocity, $U_\infty$ on the velocity, temperature and air concentration profiles for liquid and vapor-mixture boundary layers and on the separation angle is presented in Figures 6.16, 6.17, 6.18 and 6.19. These figures show those distributions located at the separation point. In Figure 6.16 and Figure 6.17, as the free stream velocity increases from (10 m/s to 30 m/s), a remarked reduction in the vapor-mixture boundary layer thickness, $y$, and in the liquid film thickness, $\delta$, is noticed. The vapor-air mixture thickness, $y$, changes from about 0.00072 m at $U_\infty$ = 10 m/s to 0.0003 m at 30 m/s, which in turn affects the amount of heat transferred through the cylinder wall. Velocity profiles tend to be flattened as velocity increases. This effect is attributed to the increase of shear drag as velocity increases. In other words, the effects of forced convection are more pronounced and dominant on free convection. Separation point location also decreases slightly as velocity effects increase (separation occurs at $\theta = 132$ ° when $U_\infty$ =10 m/s and it occurs at $\theta = 129°$ when $U_\infty$ =30 m/s.

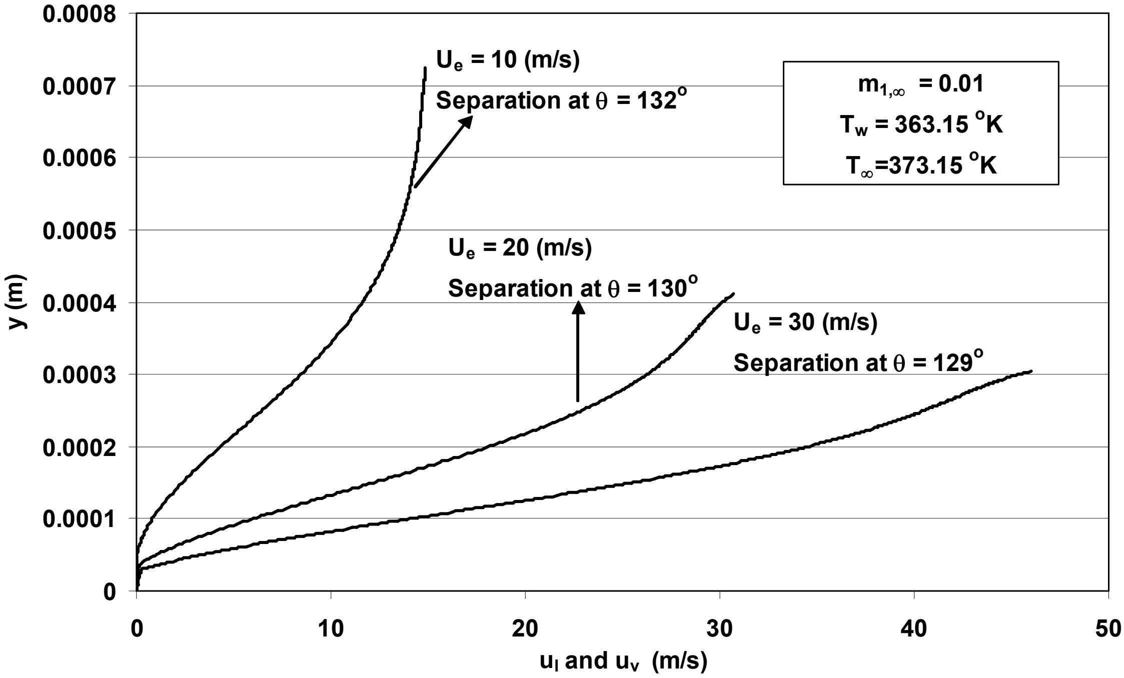


Figure 6.16 Velocity distribution of liquid and vapor-mixture boundary layers at the separation point.

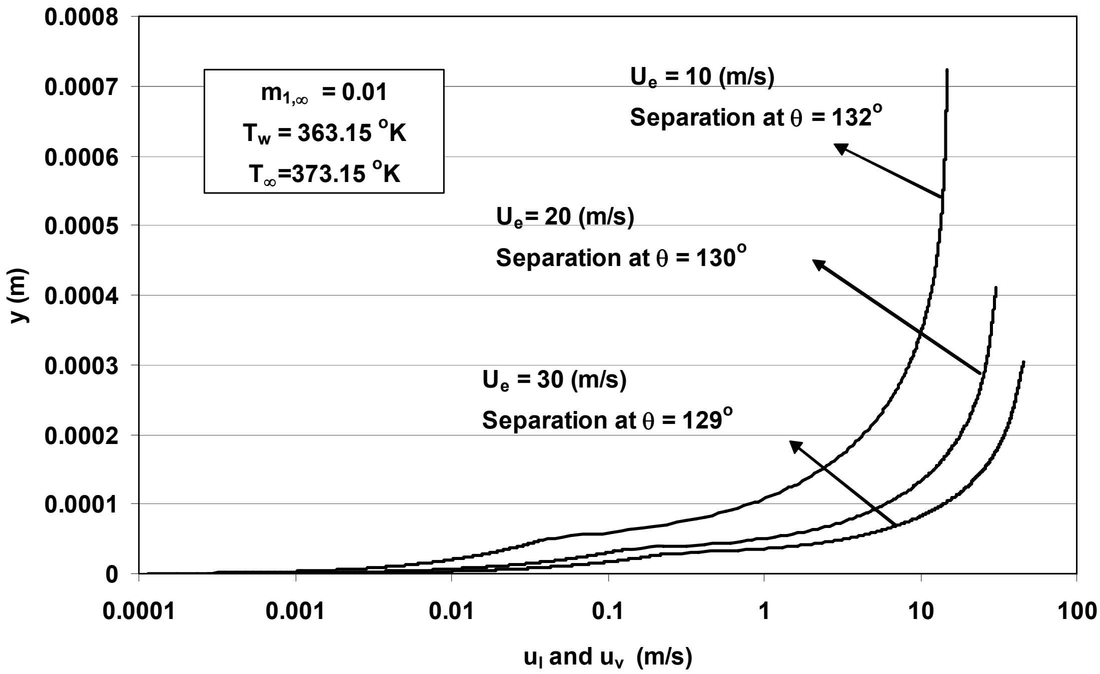


Figure 6.17 Velocity distribution of liquid vapor-mixture boundary layer at separation point (x-axis in logarithmic scale).

Figure 6.18 shows the temperature distribution of liquid and vapor-mixture boundary layers at separation point ( $m_{1,\infty} = 0.01$ and $\Delta T = 10\ ^{o}K$ ). In the same manner, as in the case of velocity distribution profiles above, the vapor-mixture boundary layer thickness, $y$, and liquid film thickness, $\delta$, decrease as free stream velocity increases, which in turn affects the amount of heat transferred through the cylinder wall.

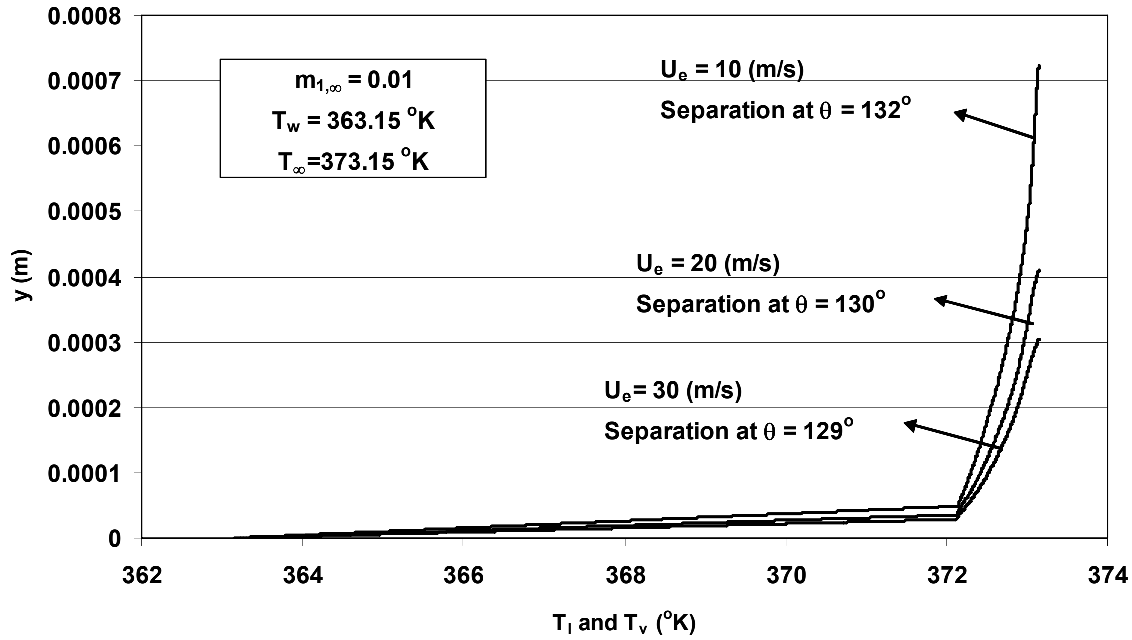


Figure 6.18 Temperature distribution of liquid and vapor-mixture boundary layers at the separation point.

Figure 6.19 shows the noncondensable gas concentration distribution for vapor-mixture boundary layers at the separation point ( $\Delta T = 10\ ^{o}K$ ). Again, a reduction in the liquid and vapor-mixture boundary layer thicknesses is remarked.

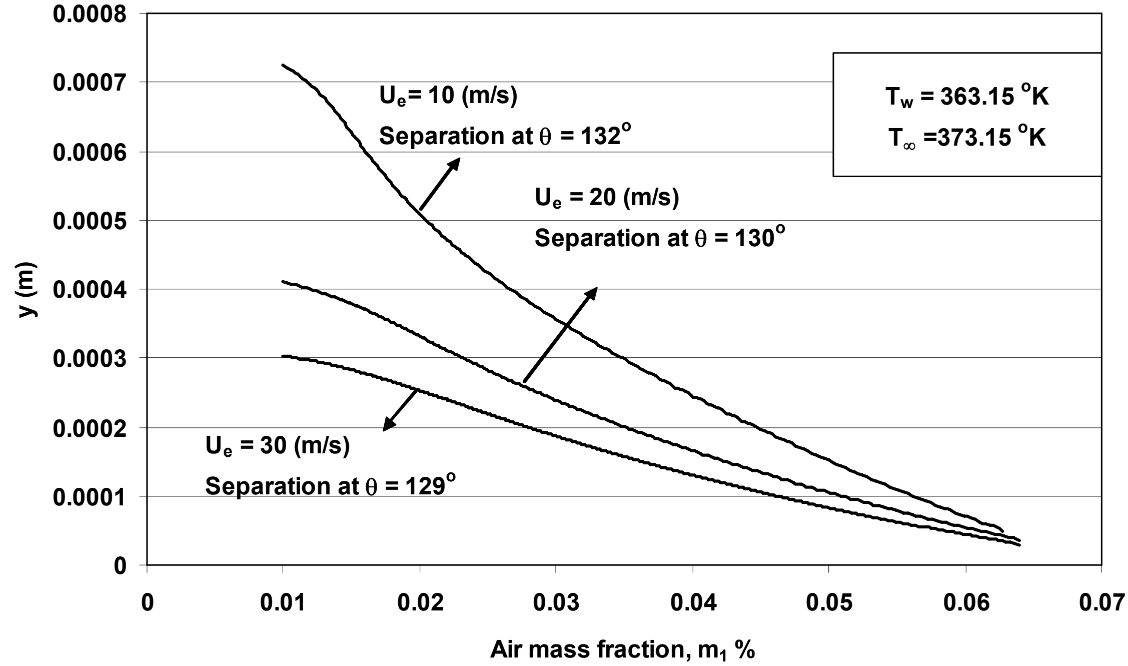


Figure 6.19 Air Concentration distribution of liquid and vapor-mixture boundary layers at the separation point.

Figure 6.20 presents the effect of the free stream velocity on dimensionless heat flux through the cylinder wall. It is clearly shown that; dimensionless heat flux through the cylinder wall increases with the increase of free stream velocity due to the effect of shear drag. Shear drag tends to decrease the thickness of liquid boundary layer results in a corresponding increase in the amount of heat flux transferred.

Figure 6.21 shows the effect of free stream velocity on liquid film thickness. As the free stream velocity increases, liquid film thickness decreases. This is because of shear drag and forced convection effects.

The interfacial mass flow rate, the local heat transfer coefficient and the local Nusselt number increase as free stream velocity increases. This is true since these parameters are proportionally related to the amount of heat flux transferred. These effects are shown in Figures 6.22, 6.23 and 6.24 respectively.

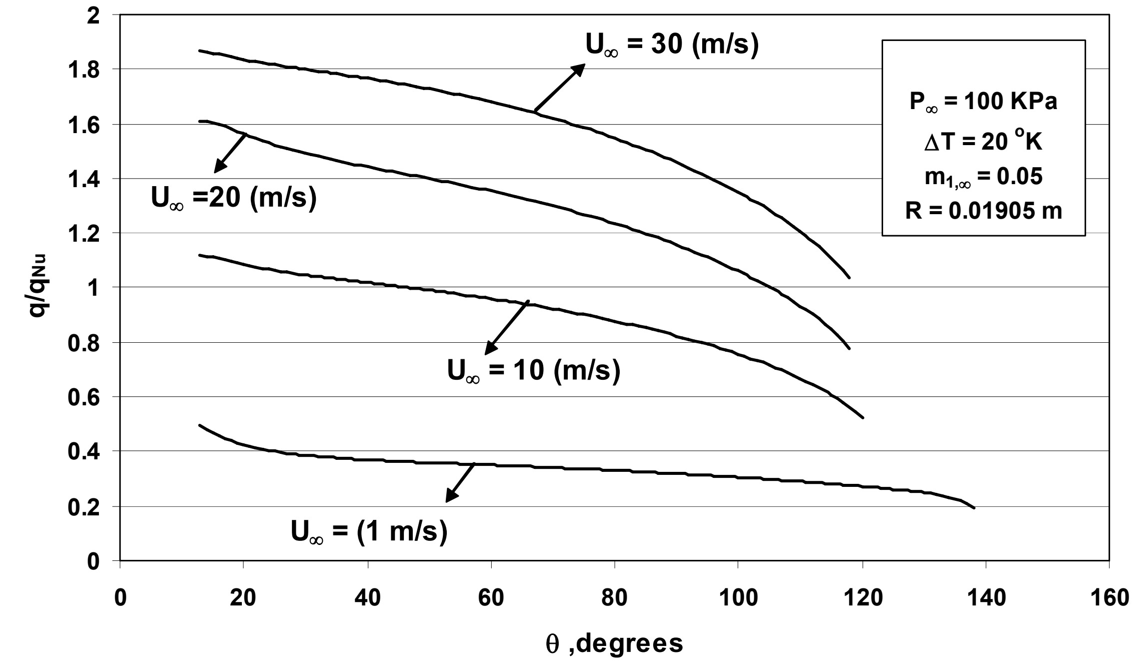


Figure 6.20 The effect of free stream velocity on dimensionless heat flux through the cylinder wall.

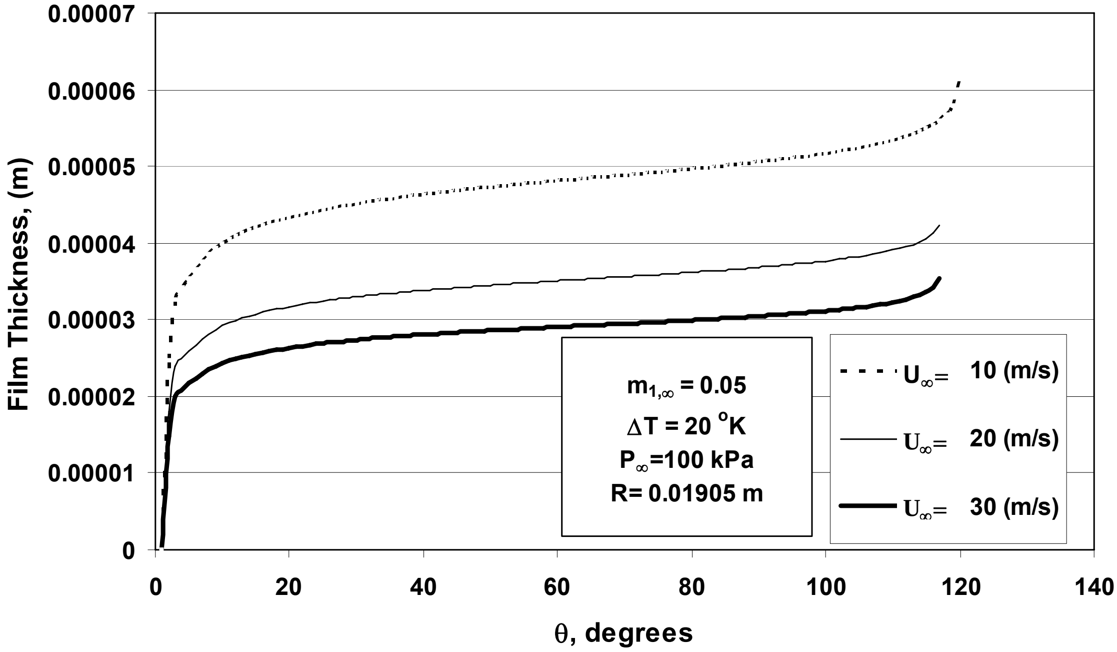


Figure 6.21 The effect of the free stream velocity on the film thickness.

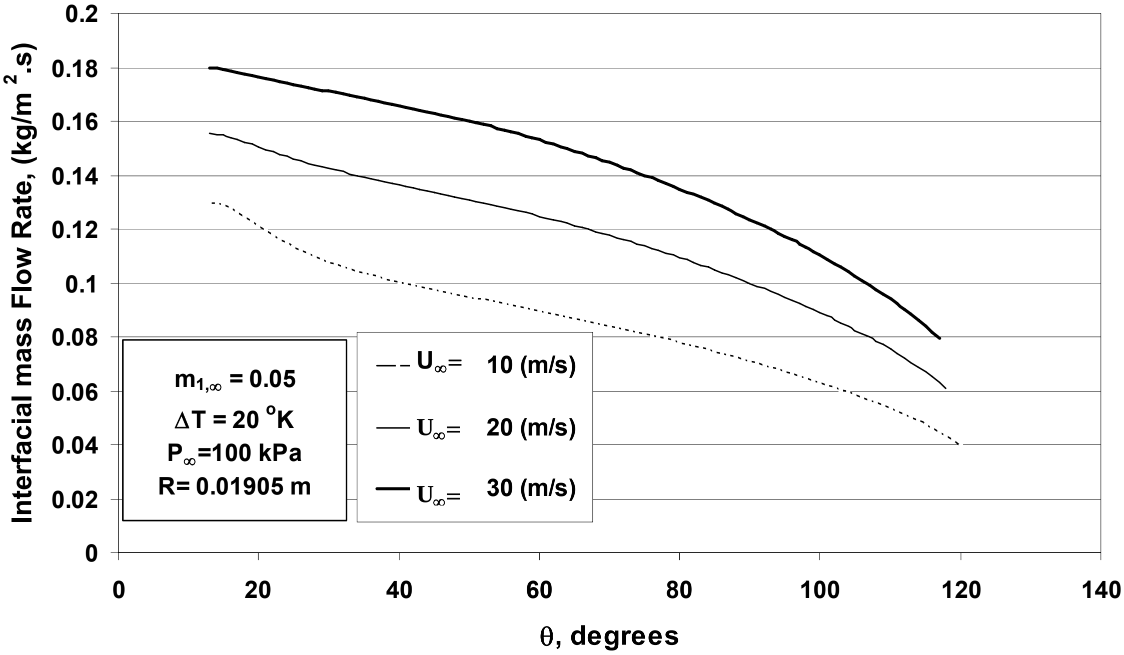


Figure 6.22 The effect of free stream velocity on interfacial mass flow rate.

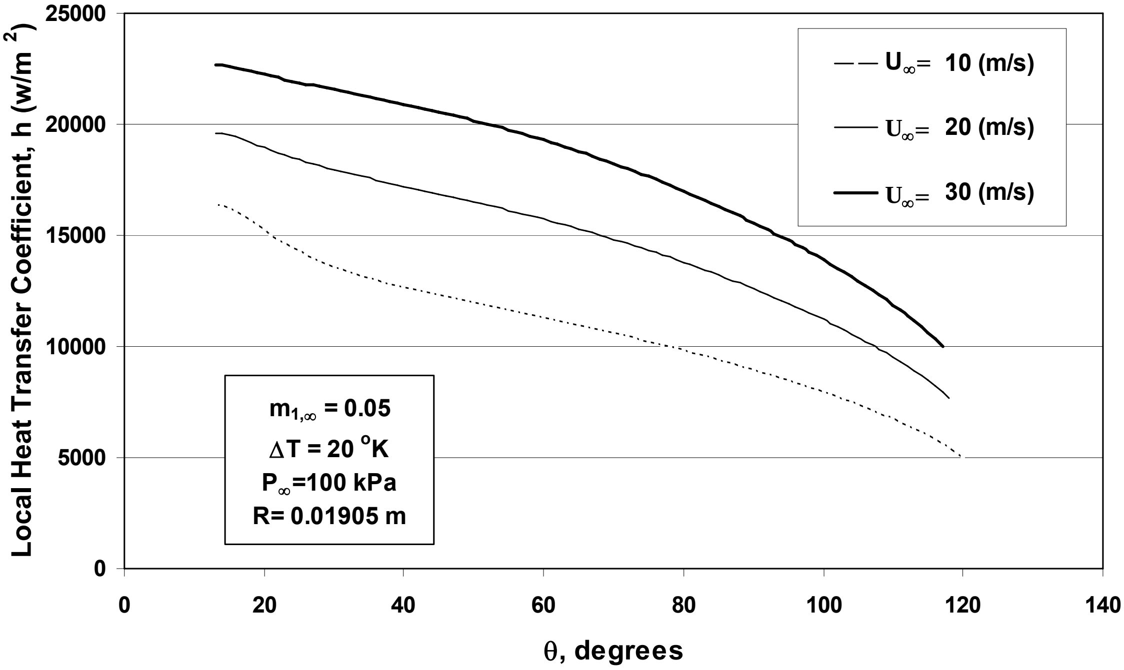


Figure 6.23 The effect of the free stream velocity on the local heat transfer coefficient.

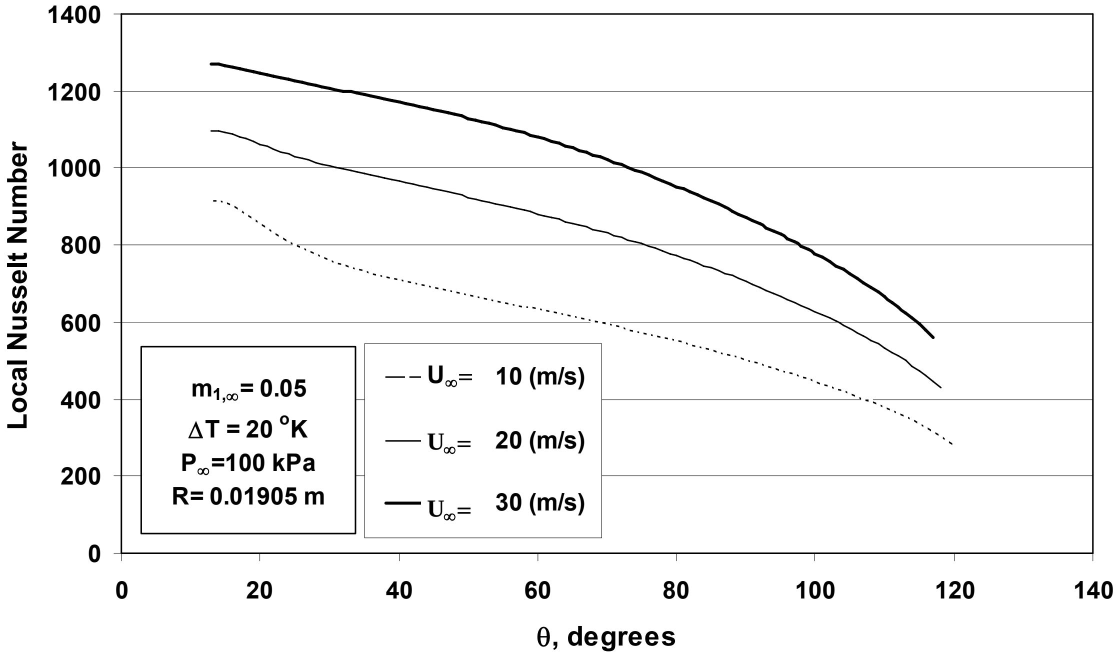


Figure 6.24 The effect of the free stream velocity on the local Nusselt number.

### 6.2.3 The effect of the temperature difference

Figures 6.25, 6.26, 6.27 and 6.28 are constructed to investigate the effect of the temperature difference on the different parameters that influence the film condensation heat transfer. These parameters include; film thickness, interfacial mass flow rate, local heat transfer coefficient and local Nusselt number. Figure 6.25 and Figure 6.26 shows the effect of temperature difference on the film thickness and on the interfacial mass flow rate. The condensate flow rate and the liquid film thickness tend to increase as temperature difference increases. This is physically the case since the increase in the temperature difference leads vapor to liberate more latent heat of energy which in turn increases the condensate flow rate and the liquid film thickness as well.

Figures 6.27 and 6.28 illustrate the effect of the temperature difference on the local heat transfer coefficient and the local Nusselt number respectively for $m_{1,\infty} = 0.01$, $P_\infty = 100\ kPa\ and\ U_\infty = 10\ m/s, R = 0.01905m$ . Local heat transfer coefficient and local Nusselt number decrease as temperature difference increases.

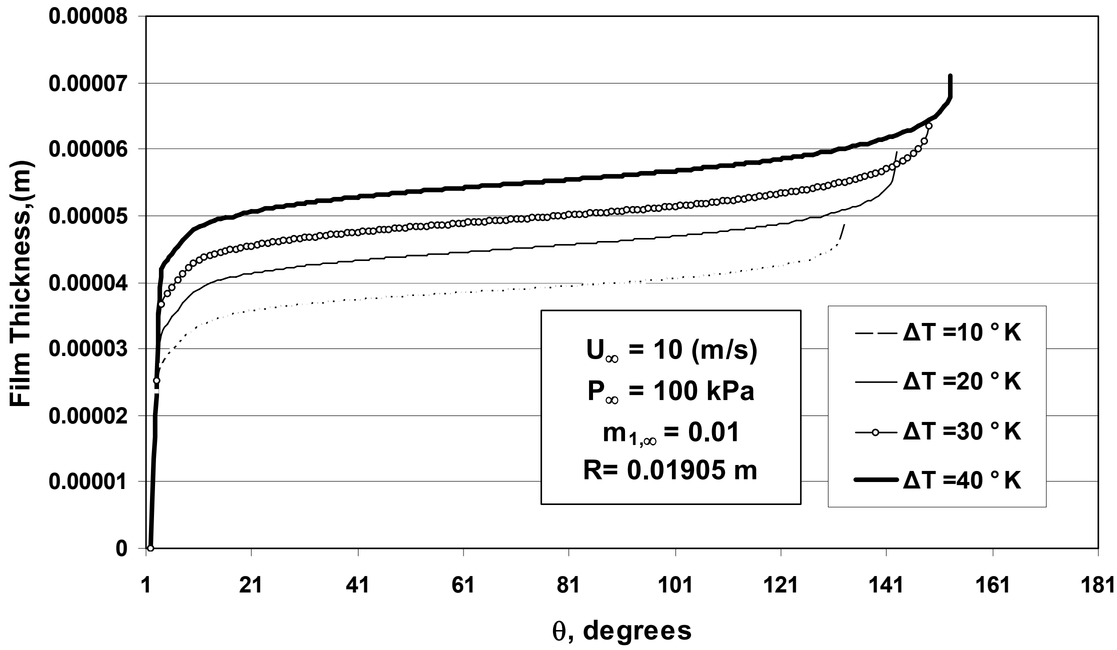


Figure 6.25 The effect of the temperature difference on the film thickness.

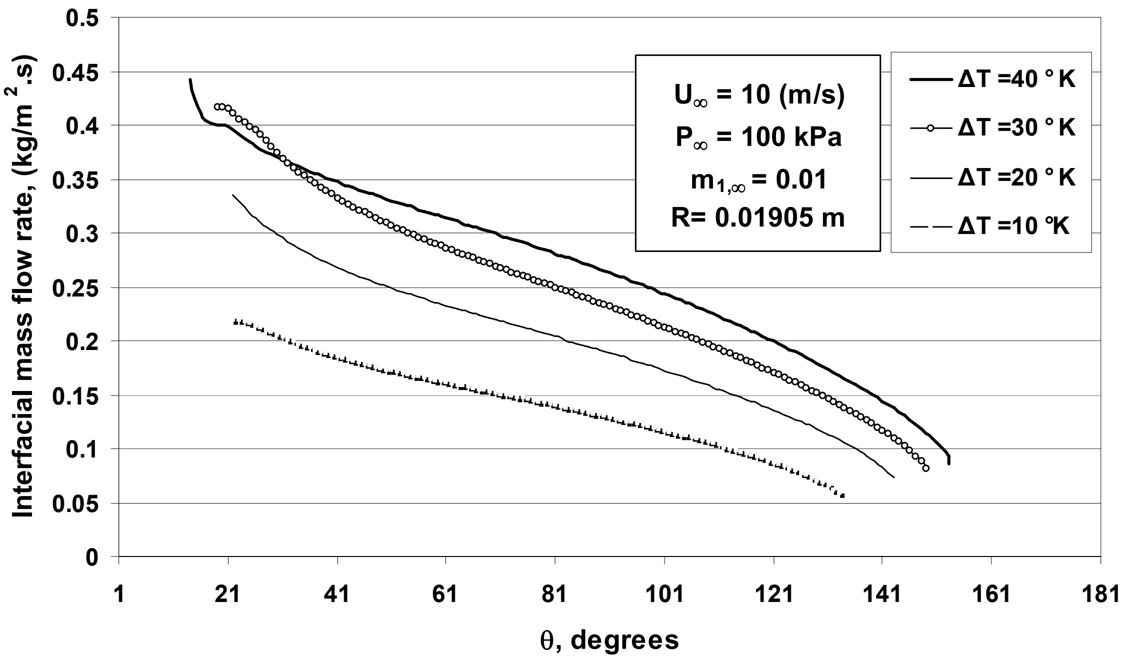


Figure 6.26 The effect of the temperature difference on the interfacial mass flow rate.

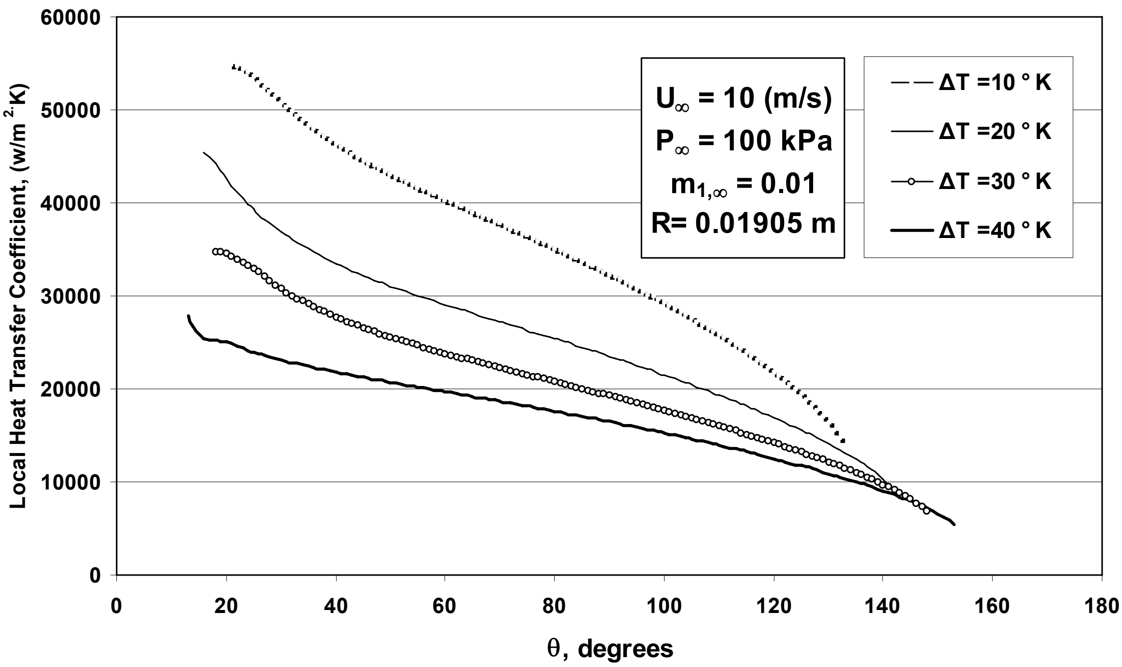


Figure 6.27 The effect of temperature difference on the local heat transfer coefficient.

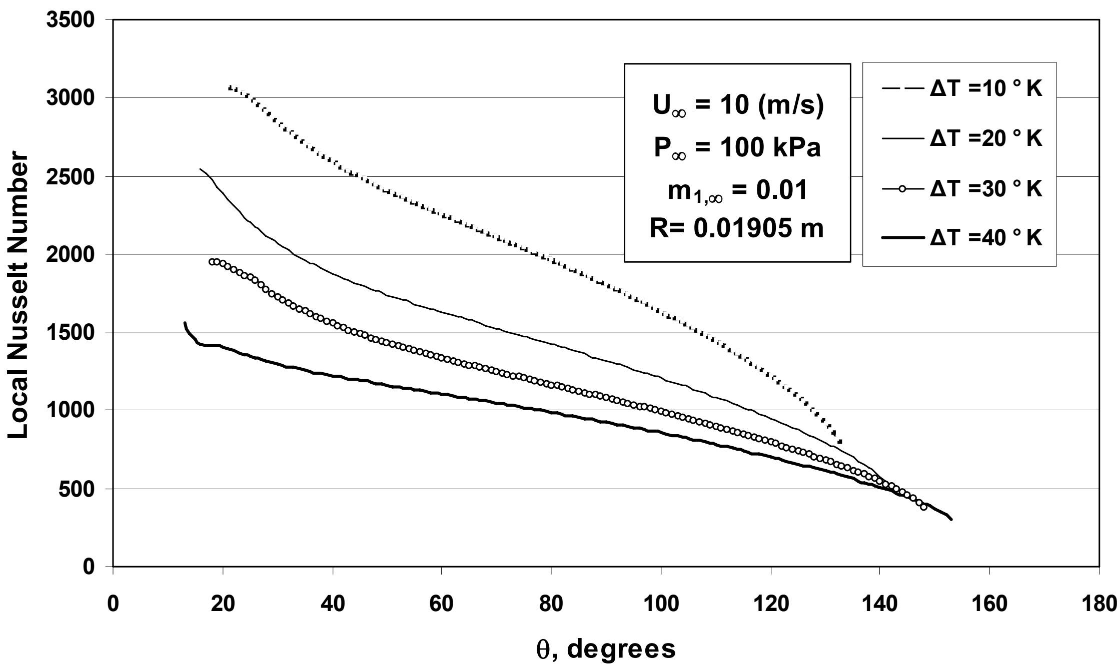


Figure 6.28 The effect of the temperature difference on the local Nusselt number.

### 6.2.4 The effect of the non-condensable gas

Figures 6.29, 6.30, 6.31 and 6.32 indicate the effect of the non-condensable gas (air) on the film condensation heat transfer. Its effect on the interfacial mass flow rate, the dimensionless heat transfer, the local heat transfer coefficient and the local Nusselt number is analyzed and investigated.

Figure 6.29 presents the effect of the non-condensable gas on the interfacial mass flow rate at different free stream air concentrations. Interfacial mass flow rate decreases as non-condensable gas (air) concentration increases. This is attributed to the non-condensable gas diffusion and accumulation of air near the liquid –vapor interface. Air concentration increases towards the liquid – vapor interface. At equilibrium, the interface concentration of air is high enough so that the resulting diffusion of this component away from the interface into the ambient just balances the rate at which its concentration increases due to condensation. This negatively affects vapor condensation at the liquid –vapor mixture interface. As a result, interfacial mass flow rate is reduced.

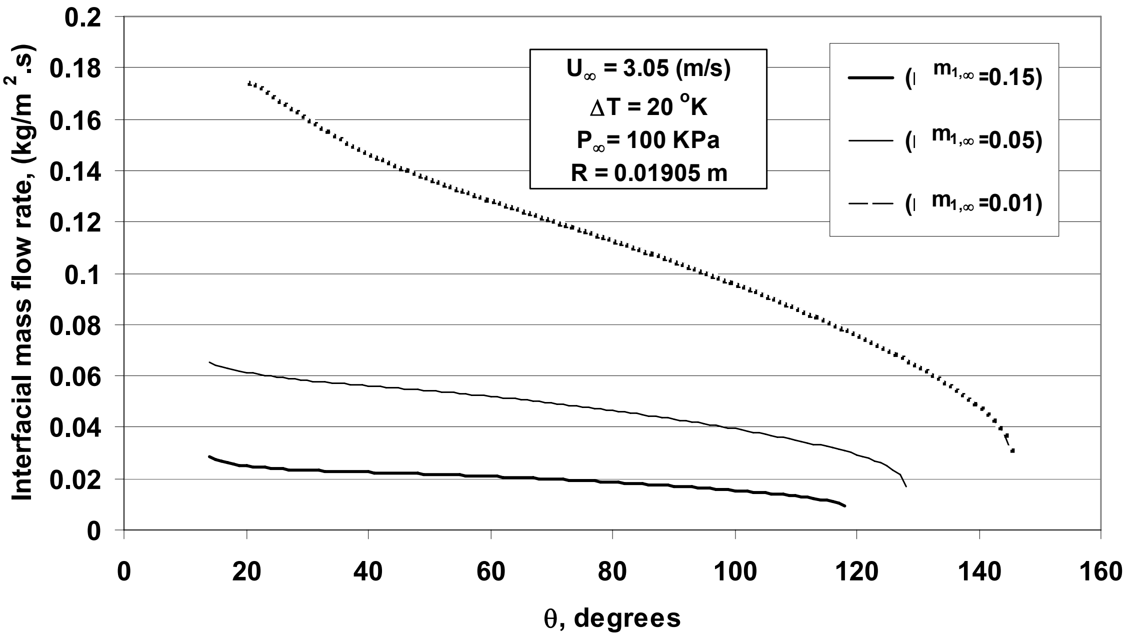


Figure 6.29 The effect of the non-condensable gas (air) on the interfacial mass low rate.

In addition, the separation angle is also affected by the non-condensable gas concentration. As air concentration increases, separation angle decreases. It reduced from $\theta = 145^o$ at $m_{1,\infty} = 0.01$ to $\theta = 118^o$ at $m_{1,\infty} = 0.15$ .This agrees with the results and findings of Srzic [42].

Figures 6.30, 6.31 and 6.32 represent the effect of the non-condensable gas on the dimensionless heat flux, the local heat transfer coefficient and the local Nusselt number. Generally, the dimensionless heat flux, the local heat transfer coefficient and the local Nusselt number are decreased as non-condensable gas concentration increases. As explained above, air accumulates at the liquid-vapor mixture interface reducing vapor condensation process. This is agrees with the results mentioned everywhere in the literature [34], [35], [36], [37], [38], [39] and [42].

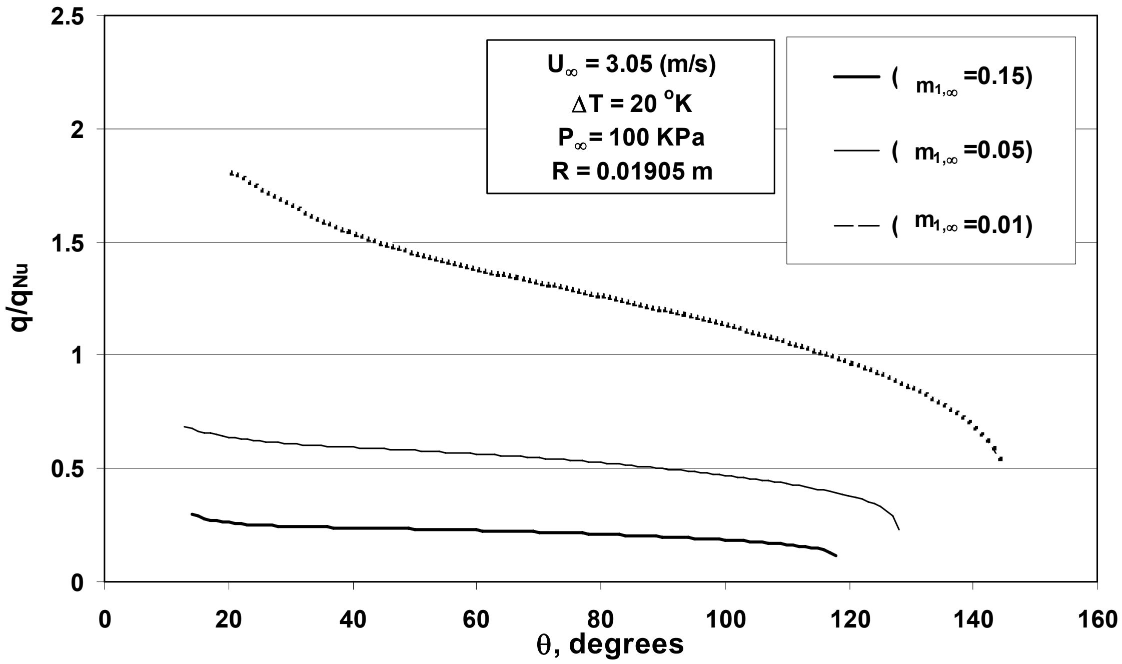


Figure 6.30 The effect of the non-condensable gas (air) on the dimensionless heat flux.

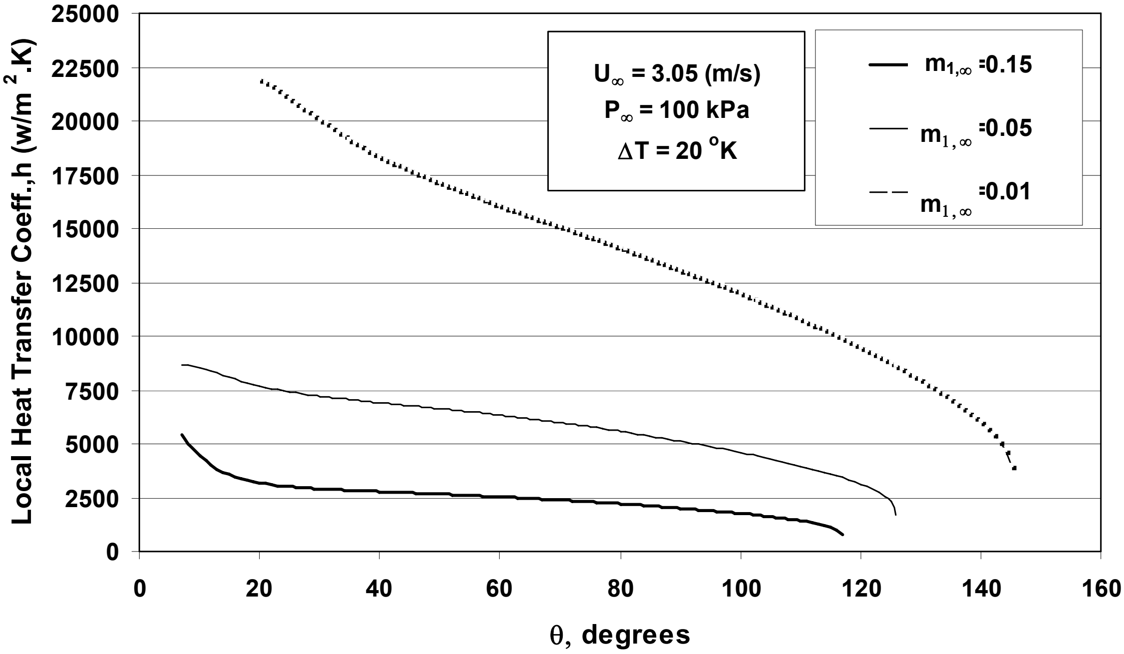


Figure 6.31 The effect of the non-condensable gas (air) on the local heat transfer coefficient.

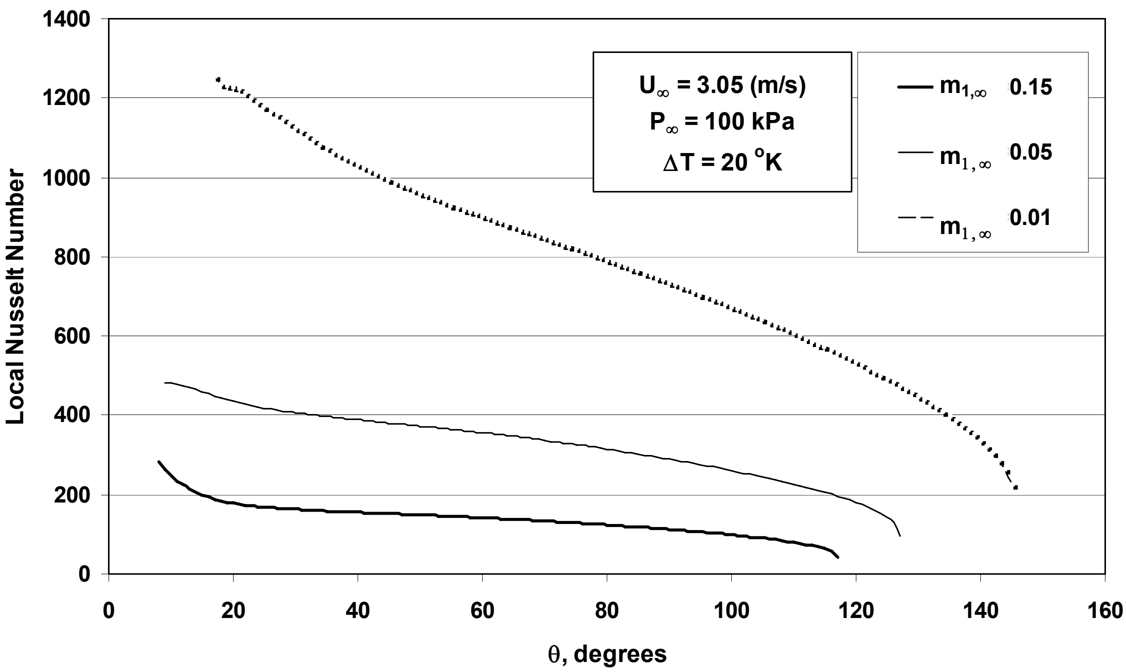


Figure 6.32 The effect of the non-condensable gas (air) on the local Nusselt number.

### 6.2.5 The effect of the cylinder diameter

Figures 6.33, 6.34, 6.35 and 6.36 show the effect of the cylinder diameter on the parameters related to film condensation heat transfer process, namely; (the liquid film thickness, the dimensionless heat flux, the local heat transfer coefficient and the local Nusselt number). Figure 6.33 illustrates the effect of the cylinder diameter on the film thickness. It is clearly shown that the liquid film thickness increases as the diameter of the cylinder increases. This attributed to the increase in the heat transfer surface area as the diameter of the cylinder increases. As a result, more chance for the vapor to condensate on the cylinder wall.

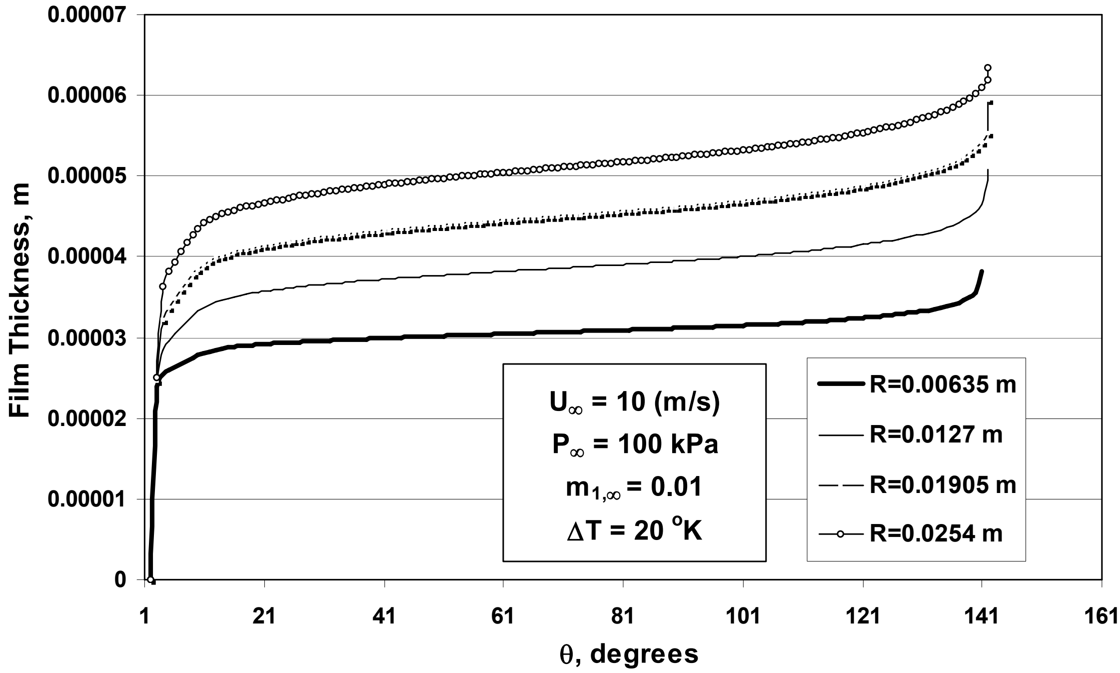


Figure 6.33 The effect of the cylinder diameter on the liquid film thickness

The dimensionless heat flux, the local heat transfer coefficient and the local Nusselt number are evaluated for a given cylinder diameter so as to investigate the effect of the cylinder diameter on the film condensation heat transfer. Results are shown in Figures 6.34, 6.35 and 6.36. In figure 6.34, a reduction in the dimensionless heat flux is noticed as the cylinder diameter is

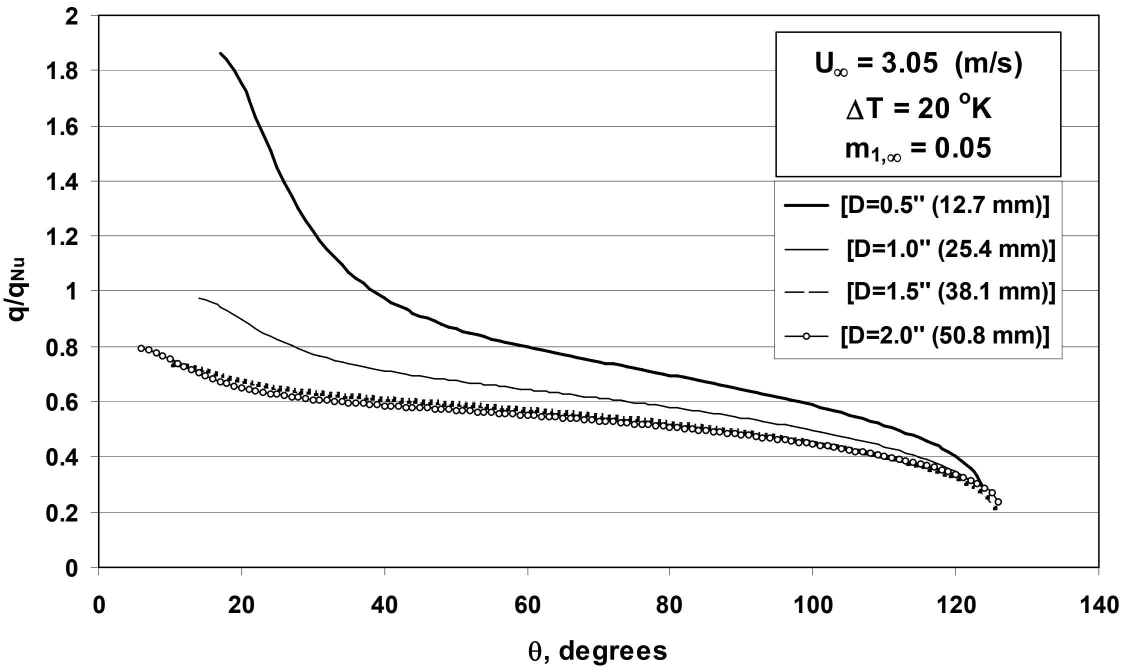


Figure 6.34 The effect of the cylinder diameter on the dimensionless heat flux.

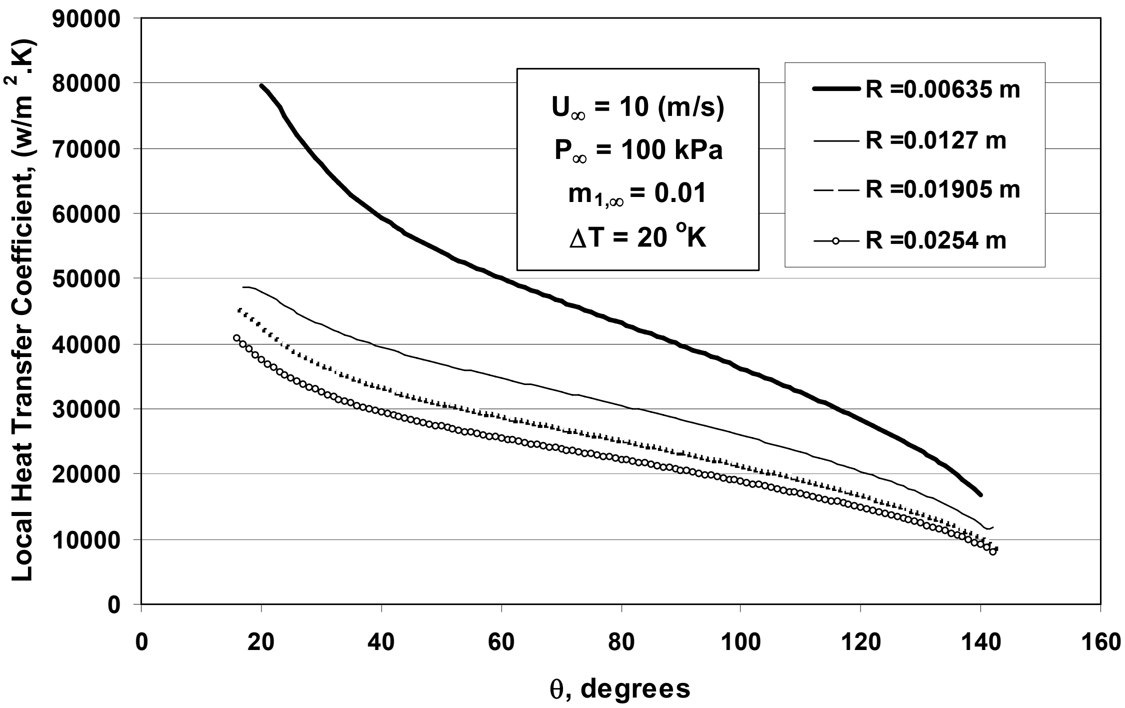


6.35 The effect of the cylinder diameter on the local heat transfer coefficient.

increased. Increase in the film thickness leads to a large thermal resistance and as a result, it decreases the dimensionless heat flux. A similar effect is observed in the local heat transfer coefficient, Figure 6.35.

The effect of the cylinder diameter on the local Nusselt number is investigated. As diameter of the cylinder increases, the local Nusselt number increases. This is true since Nusselt number is directly proportional to the cylinder diameter.

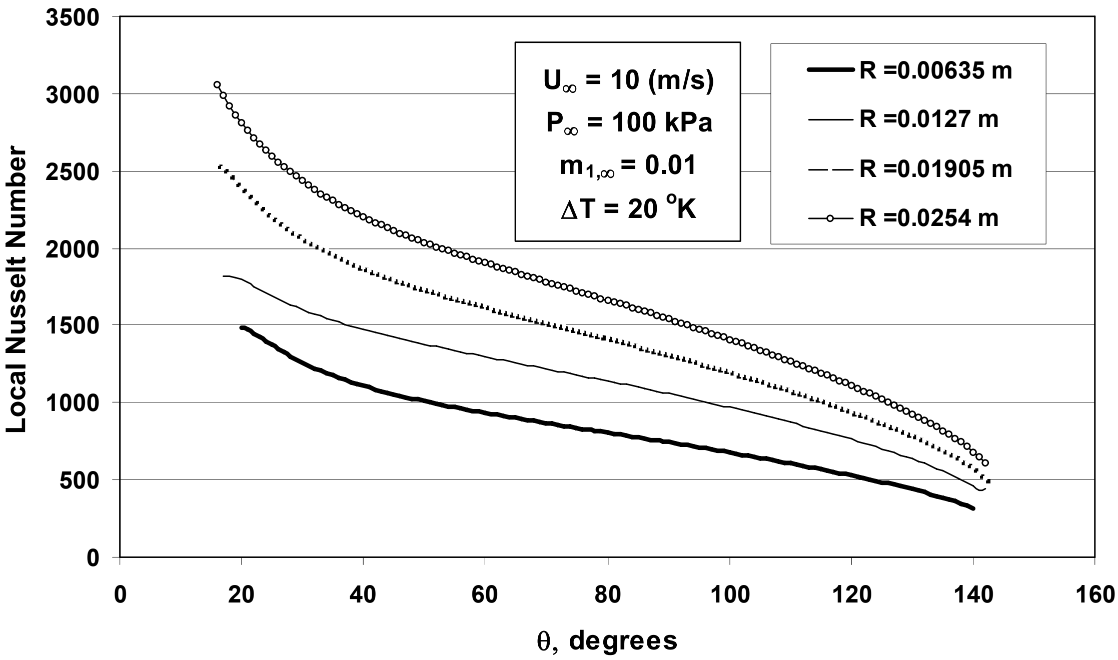


Figure 6.36 The effect of the cylinder diameter on the local Nusselt number.

### 6.2.6 The effect of the pressure gradient

The effect of the pressure gradient on the liquid film thickness, the local heat transfer coefficient and the local Nusselt number is presented in Figures 6.37, 6.38 and 6.39. Figure 6.37 shows the effect of the pressure gradient on the liquid film thickness at two values of air concentrations, $m_{1,\infty} = 0.01$ *and* $m_{1,\infty} = 0.05$. Liquid film thickness increases to about two times in the case with zero pressure gradients when compared with that when pressure gradient is considered. This is may be the result of the effect of the shear drag and the velocity gradient at the vapor boundary layer edge. Since pressure gradient is a function of free stream velocity according to Equation (3.42).

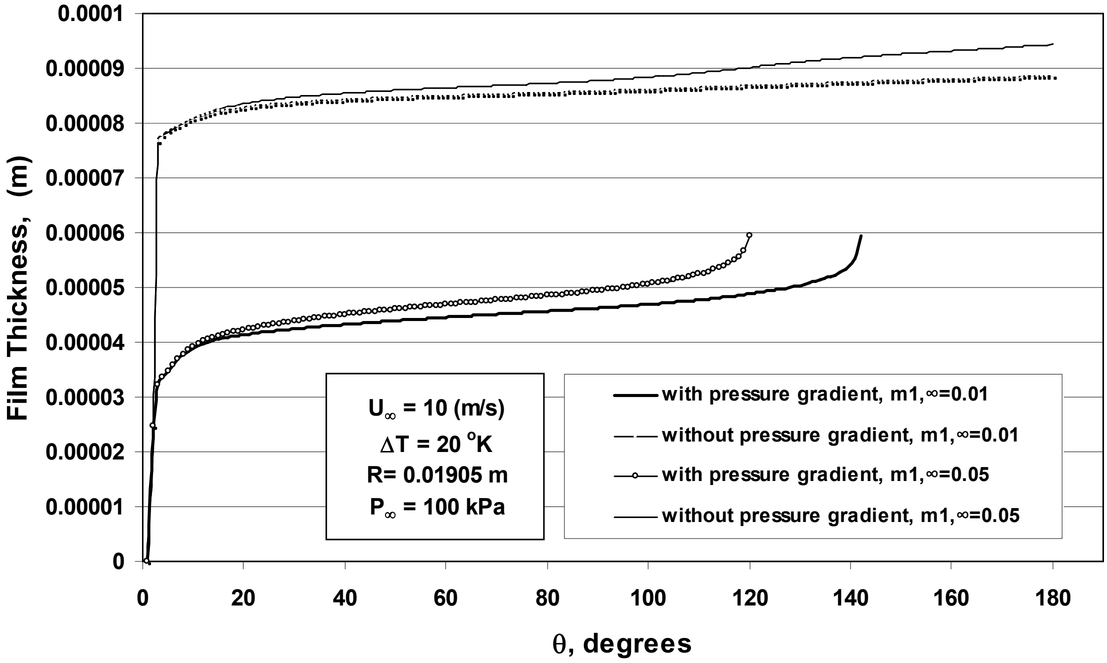


Figure 6.37 The effect of the pressure gradient on the liquid film thickness.

Figure 6.38 and Figure 6.39 represent the effect of the pressure gradient on the local heat transfer coefficient and the local Nusselt number respectively. The local heat transfer coefficient increases with the pressure gradient when compared to that with no pressure gradients especially near stagnation region of the cylinder. The results of local heat transfer coefficient for zero pressure gradients are similar to that of the flat plate case. In the same manner, the effect of pressure gradient on the local Nusselt number is interpreted.

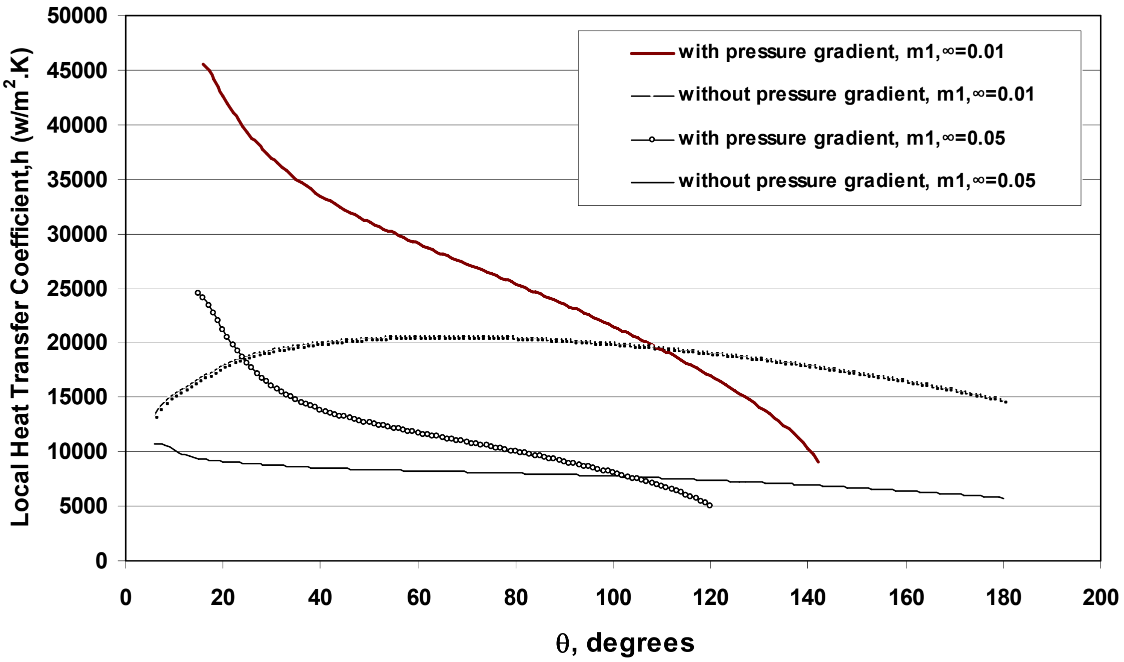


Figure 6.38 The effect of the pressure gradient on the local heat transfer coefficient.

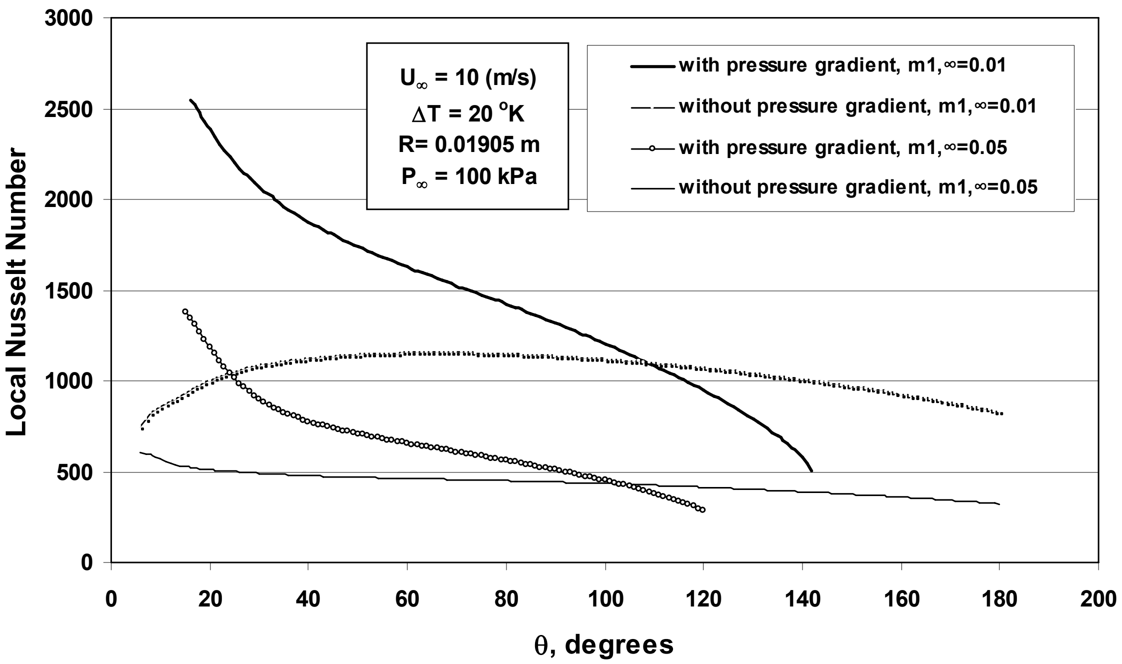


Figure 6.39 The effect of the pressure gradient on the local Nusselt number.

## 6.3 Numerical results for vapor-air mixture on a tier of tubes, inline arrangement

Numerical results for forced film condensation of steam flowing downward a tier of horizontal (inline arrangement) and inclined cylinders (staggered arrangement) at different inclination angles $0^o$, $3^o$ and $9^o$ in the presence of non-condensable gas (air) are presented. Figures 6.40 to 6.58 are constructed to study the effect of different parameters on condensation heat transfer phenomenon. These parameters include; free stream velocity ($U_\infty$), Reynolds number ($Re$), free stream non-condensable gas fraction ($m_{1,\infty}$), cylinder diameter (d) and free stream temperature to wall temperature difference ($\Delta T$). The condensate fall angle ($\theta_o$) and the angular position ($\theta$) are measured from the top of the cylinder. Different ranges of the studied parameters are selected to cover most of the working conditions.

### 6.3.1 The effect of the free stream velocity

Figure 6.40 and Figure 6.41 show the effect of the free stream velocity and the non-condensable gas fractions on the average film thickness and on the average heat transfer coefficient for the upper, middle and bottom cylinders. Results show that; film thickness increases as the condensate flows downward on the cylinder. This increase is attributed to the additional condensation of steam as the condensate flows downward. The upper cylinder has a comparatively faster increase in the film thickness as compared to the lower cylinders in the column. However, the smallest film thickness is observed on the upper cylinder. The lower the cylinder is, the larger the condensate film thickness becomes. As free stream velocity increases, film thickness decrease. In addition, film thickness tends to decrease as non-condensable gas fractions increase.

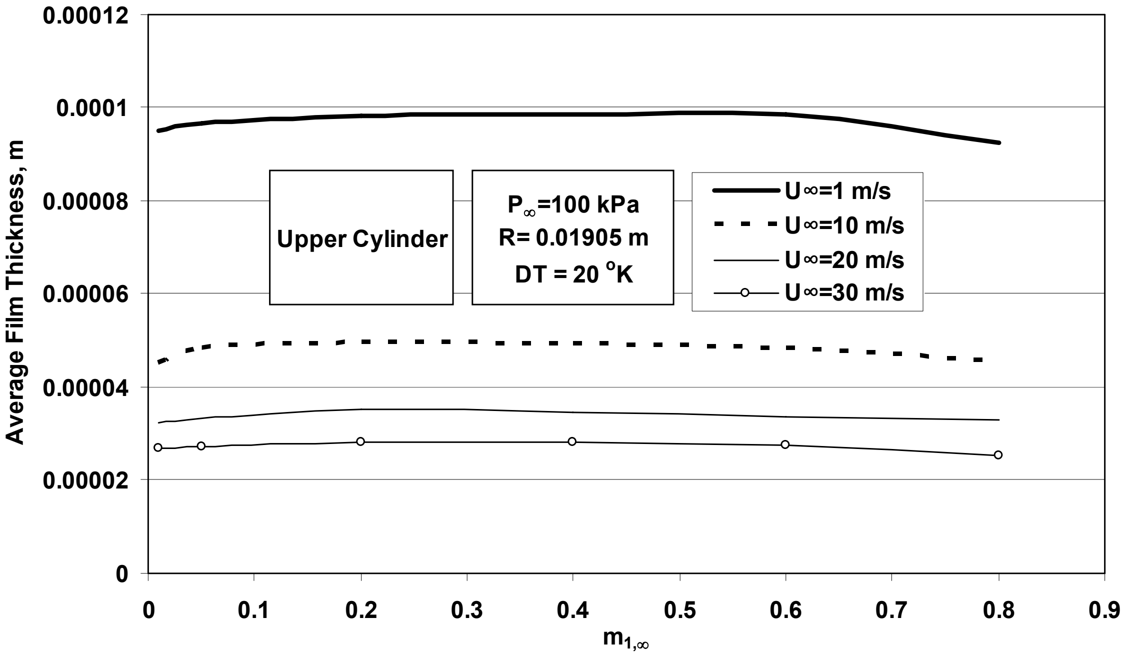


Figure 6.40a The effect of the free stream velocity and the non-condensable gas concentrations on the average film thickness for the upper cylinder.

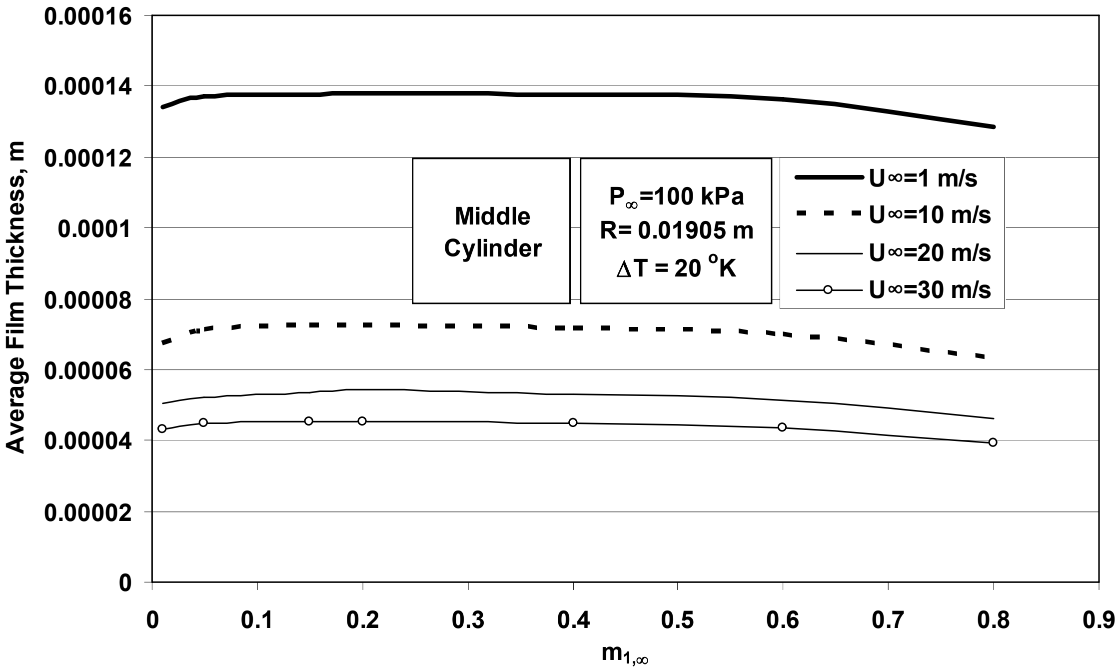


Figure 6.40b The effect of the free stream velocity and the non-condensable gas concentrations on the average film thickness for the middle cylinder.

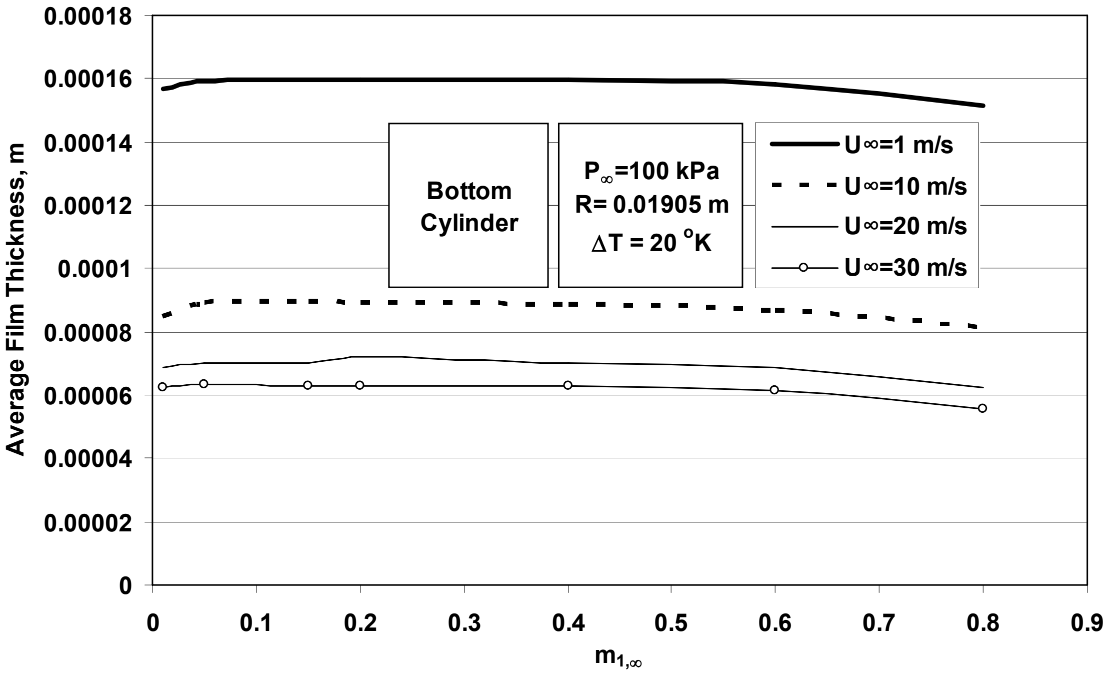


Figure 6.40c The effect of the free stream velocity and the non-condensable gas concentrations on the average film thickness for the bottom cylinder.

Figure 6.41 illustrates the effect of the above parameters on the average heat transfer coefficient. As expected, average heat transfer coefficient increases as the free stream velocity increases. However, it decreases as the non-condensable gas fractions increase. In addition, it decreases at lower cylinders in the column when compared with the upper cylinder. This is true since condensation heat transfer resistance increases at the middle and bottom cylinders.

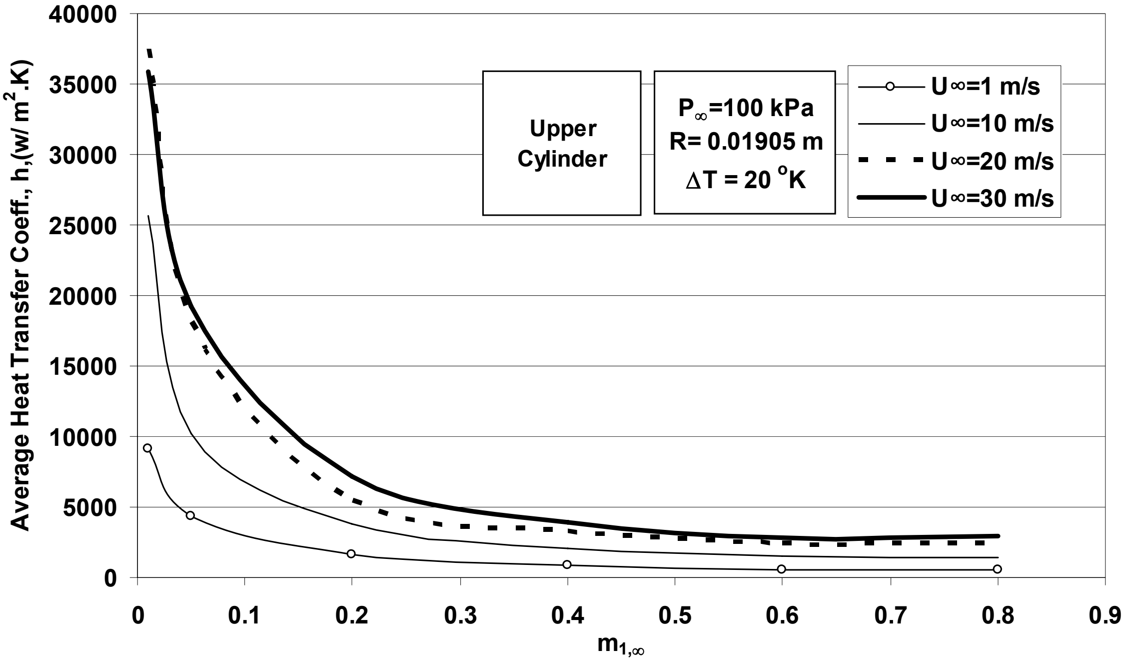


Figure 6.41a The effect of the free stream velocity and the non-condensable gas concentrations on the average heat transfer coefficient for the upper cylinder.

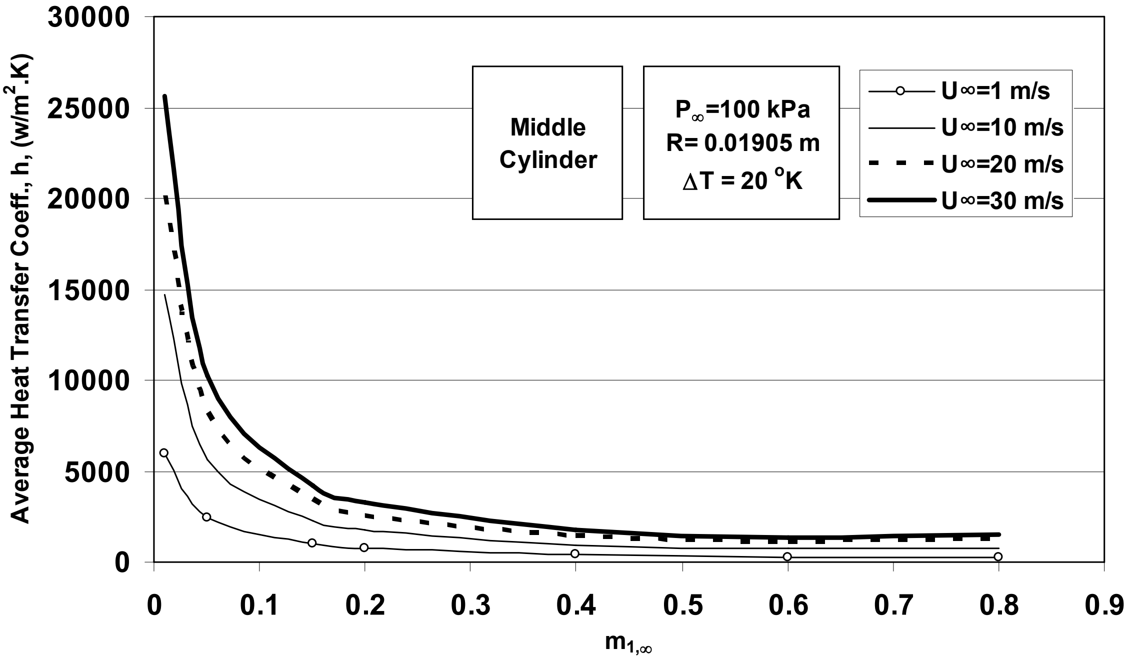


Figure 6.41b The effect of the free stream velocity and the non-condensable gas concentrations on the average heat transfer coefficient for the middle cylinder.

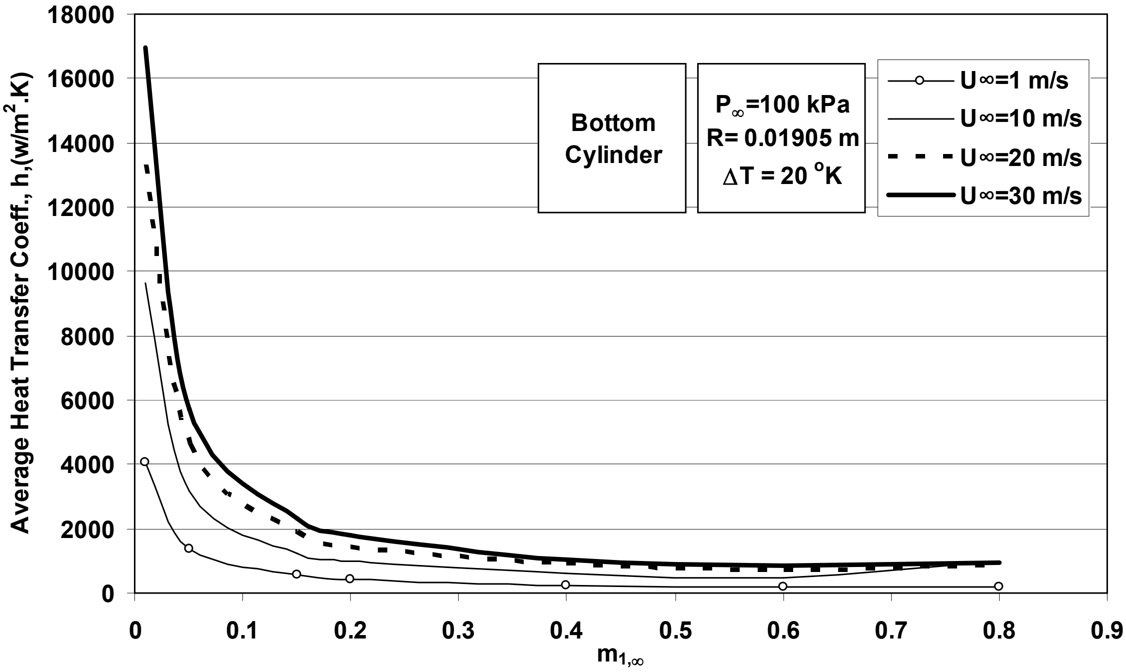


Figure 6.41c The effect of the free stream velocity and the non-condensable gas concentrations on the average heat transfer coefficient for the bottom cylinder.

### 6.3.2 The effect of the temperature difference

Figures 6.42 and Figure 6.43 are constructed to show the effect of the temperature difference and the non-condensable gas fractions on the average film thickness and on the average heat transfer coefficient. The temperature difference range is (10 to 30 $^{o}$K) under atmospheric pressure conditions and specified working conditions. Again, average film thickness increases as temperature difference increases. It increases for the lower cylinders due to inundation and spilling from upper cylinders. It tends to decrease as non-condensable gas fractions increases. This is attributed to the non-condensable gas diffusion and accumulation near the liquid-vapor interface. This leads to an increase in the non-condensable gas concentration at the vapor-liquid interface.

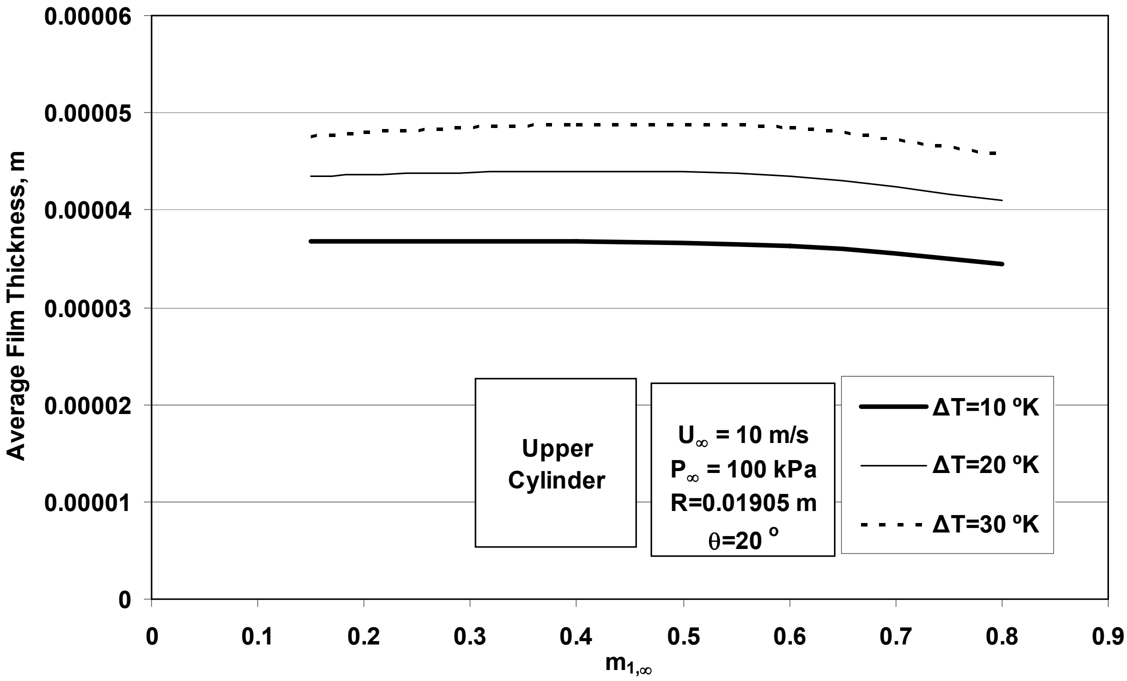


Figure 6.42a The effect of the temperature difference and the non-condensable gas concentrations on the average film thickness for the upper cylinder.

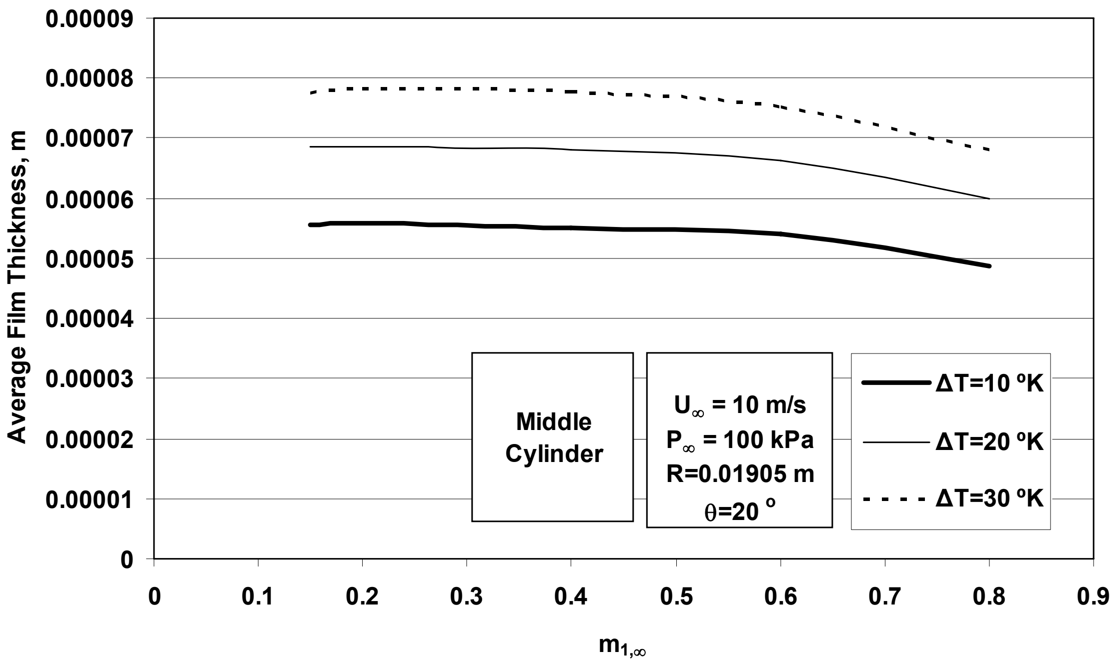


Figure 6.42b The effect of the temperature difference and the non-condensable gas concentrations on the average film thickness for the middle cylinder.

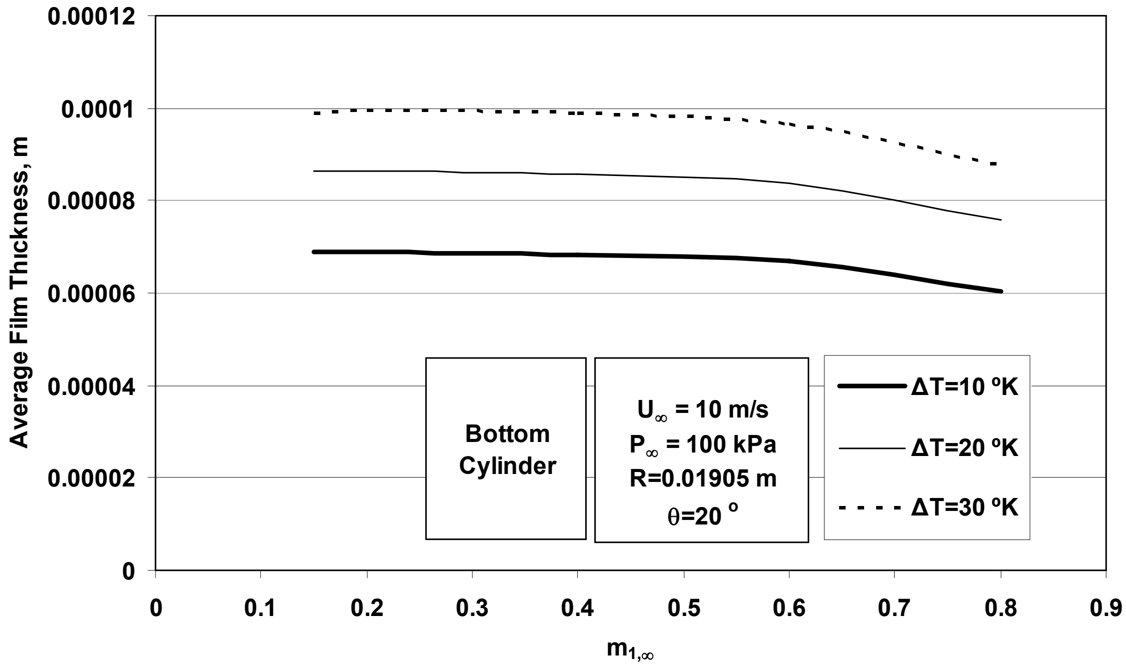


Figure 6.42c The effect of the temperature difference and the non-condensable gas concentrations on the average film thickness for the bottom cylinder.

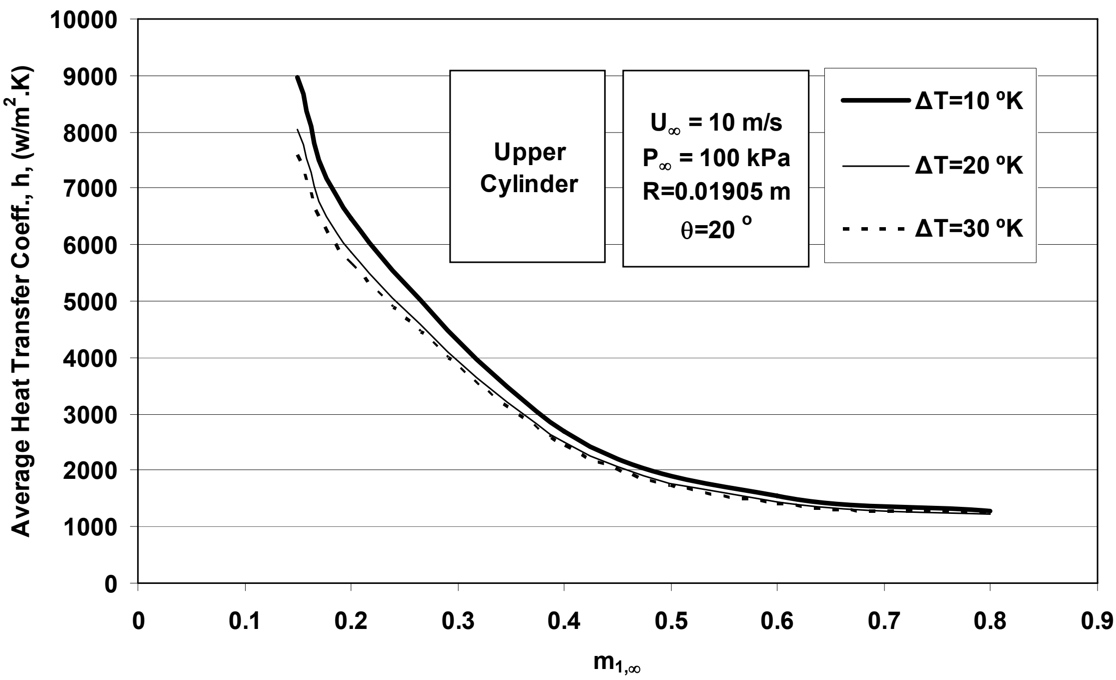


Figure 6.43a The effect of the temperature difference and the non-condensable gas concentrations on the average heat transfer coefficient for the upper cylinder.

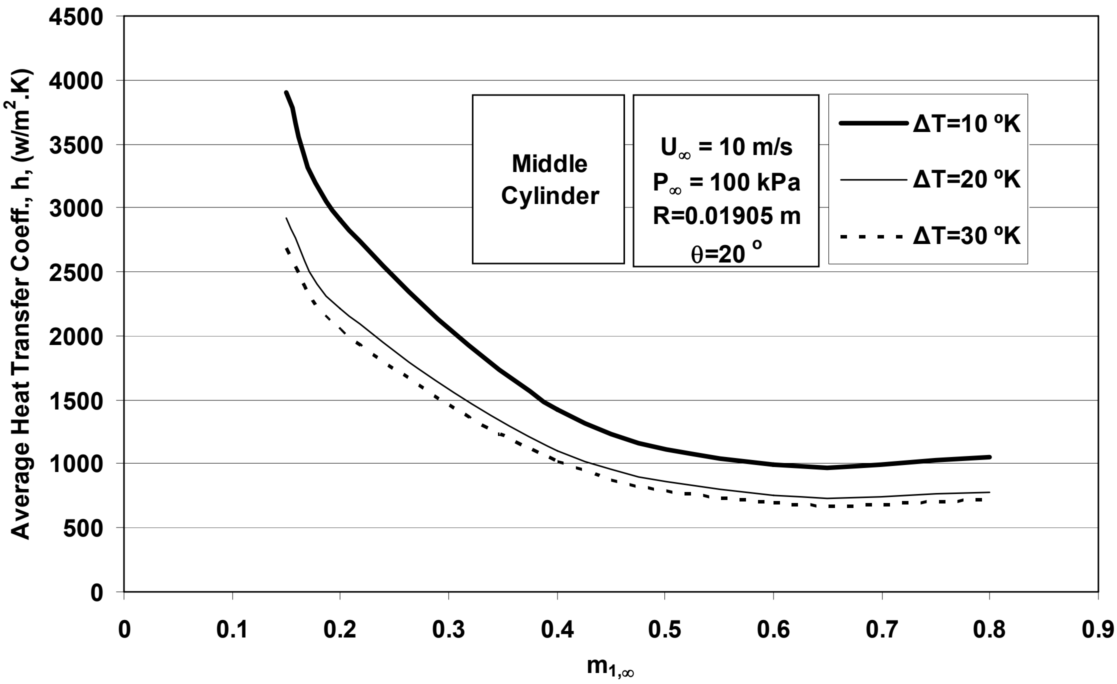


Figure 6.43b The effect of the temperature difference and the non-condensable gas concentrations on the average heat transfer coefficient for the middle cylinder.

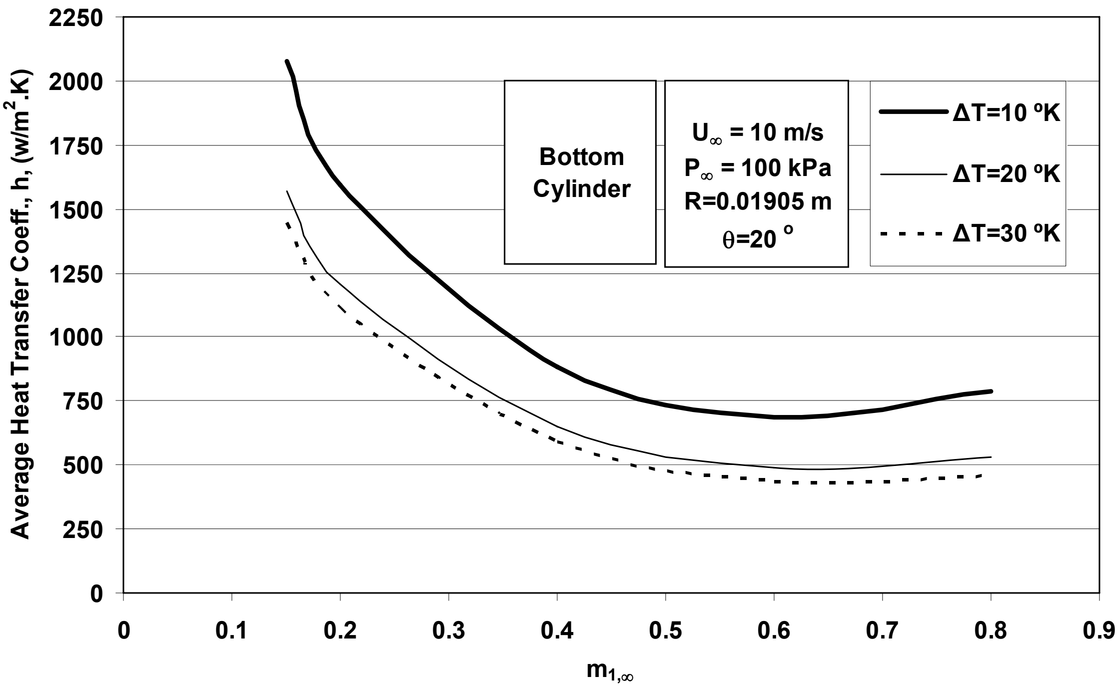


Figure 6.43c The effect of the temperature difference and the non-condensable gas concentrations on the average heat transfer coefficient for the bottom cylinder.

At equilibrium, the interface concentration of air is high enough so that the resulting diffusion of this component away from the interface into the ambient just balances the rate at which its concentration increases due to condensation. This reduces the rate of condensation at the liquid-vapor interface resulting in decreasing the film thickness.

Average heat transfer coefficient decreases as temperature difference increases. In comparison with the upper cylinder, it decreases to about its half values for middle cylinder and to about quarter values for bottom cylinder.

### 6.3.3 The effect of the cylinder diameter

Theoretical results are extended to illustrate the effect of the cylinder diameter on the average film thickness and the average heat transfer coefficient. This is clearly shown in Figure 6.44 and Figure 6.45. Generally, average film thickness increases as cylinder diameter increases while average heat transfer coefficient decreases as cylinder diameter increases.

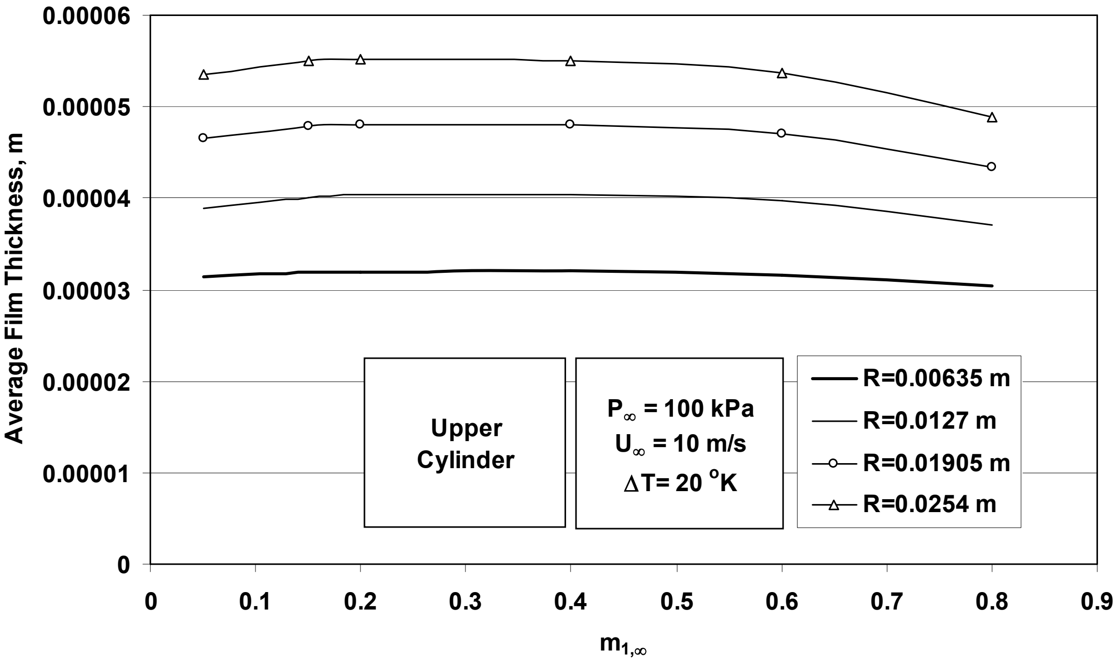


Figure 6.44a The effect of the cylinder diameter and the non-condensable gas concentrations on the average film thickness for the upper cylinder.

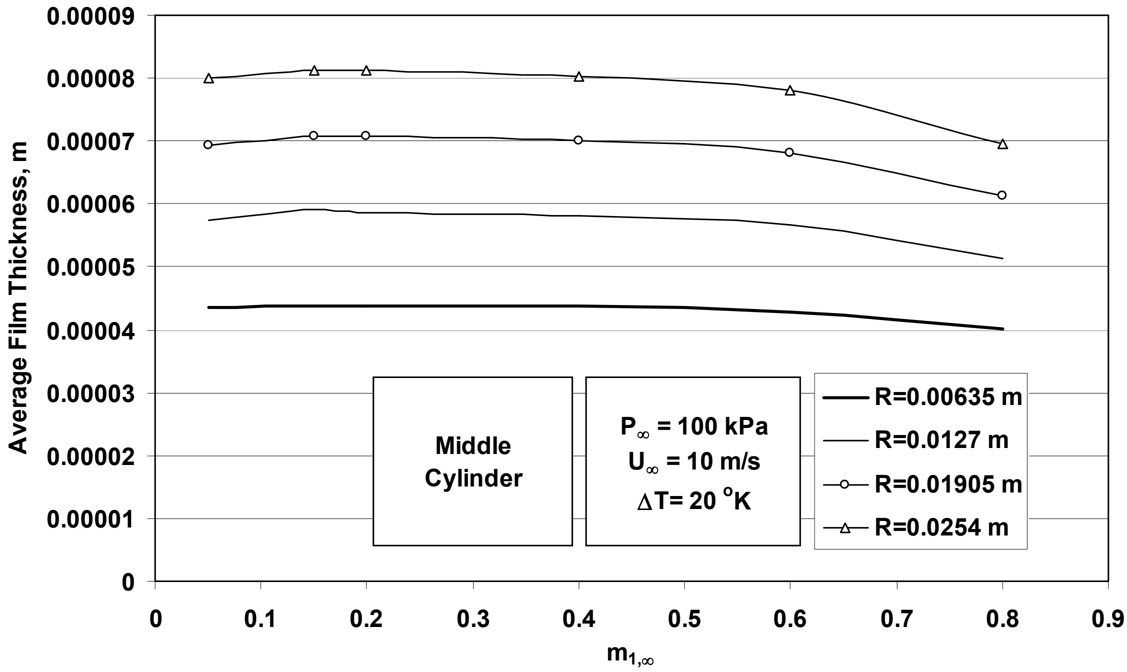


Figure 6.44b The effect of the cylinder diameter and the non-condensable gas concentrations on the average film thickness for the middle cylinder.

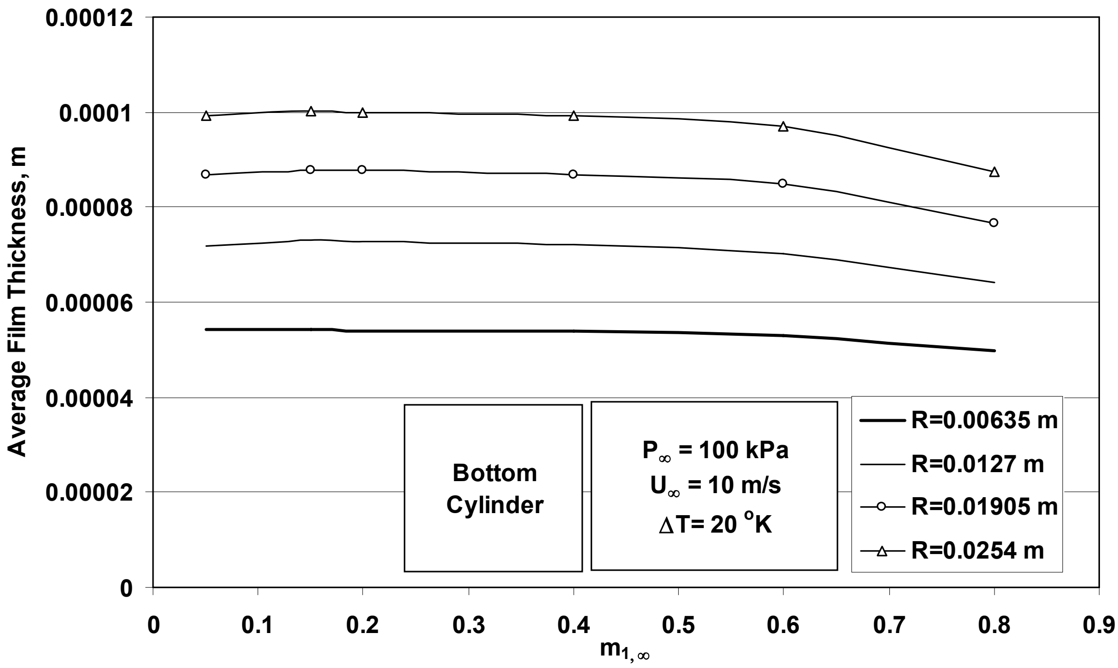


Figure 6.44c The effect of the cylinder diameter and the non-condensable gas concentrations on the average film thickness for the bottom cylinder.

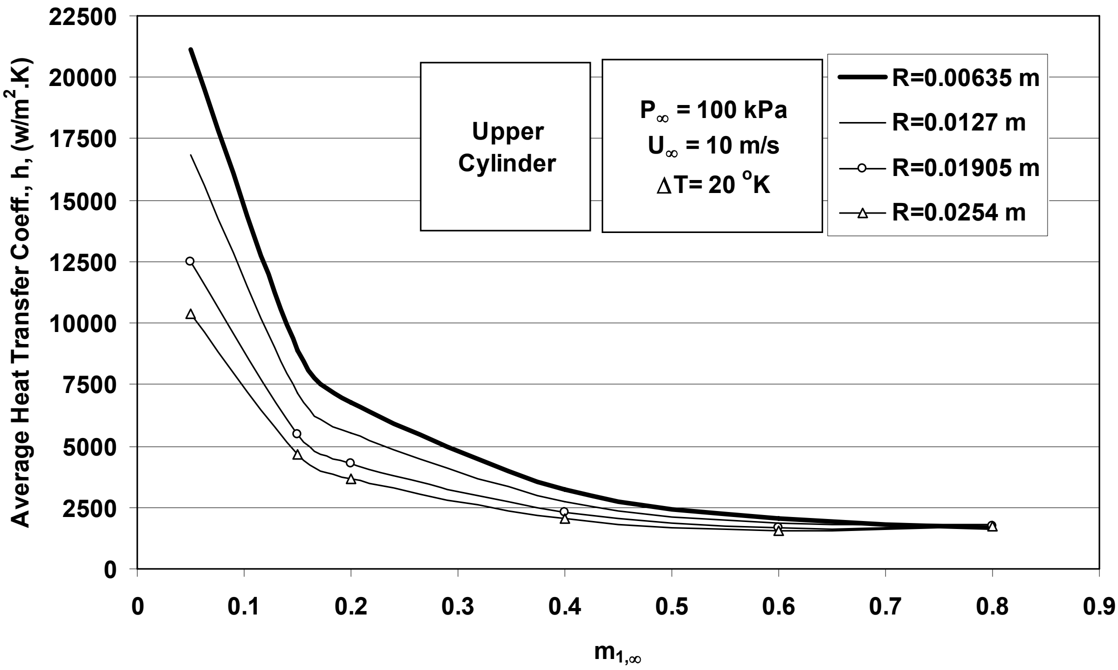


Figure 6.45a The effect of the cylinder diameter and the non-condensable gas concentrations on the average heat transfer coefficient for the upper cylinder.

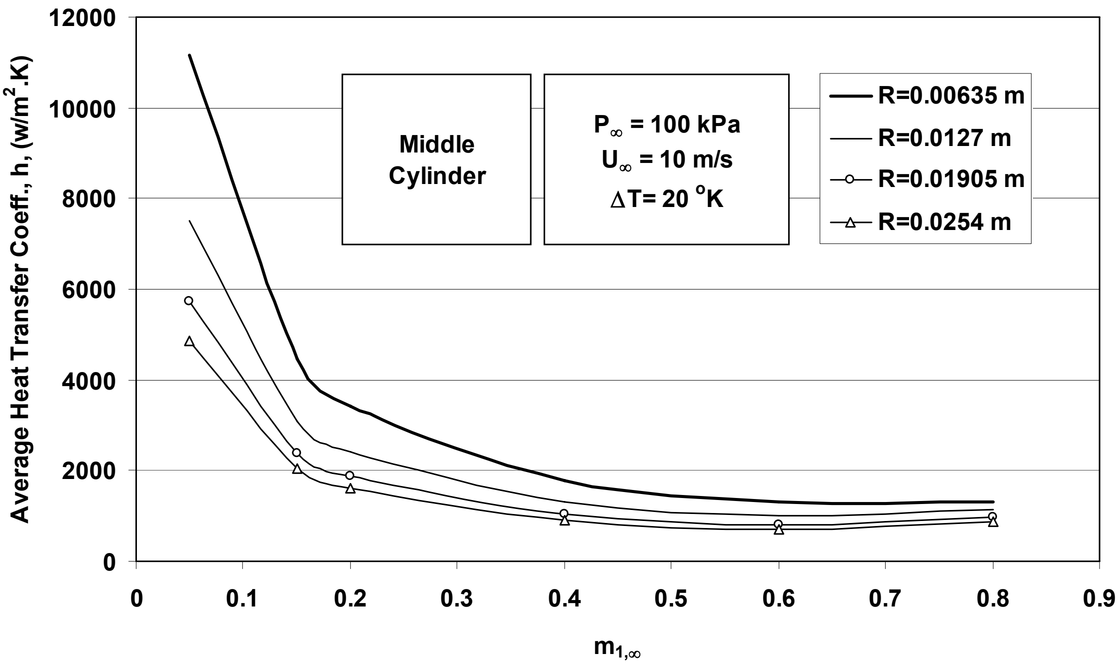


Figure 6.45b The effect of the cylinder diameter and the non-condensable gas concentrations on the average heat transfer coefficient for the middle cylinder.

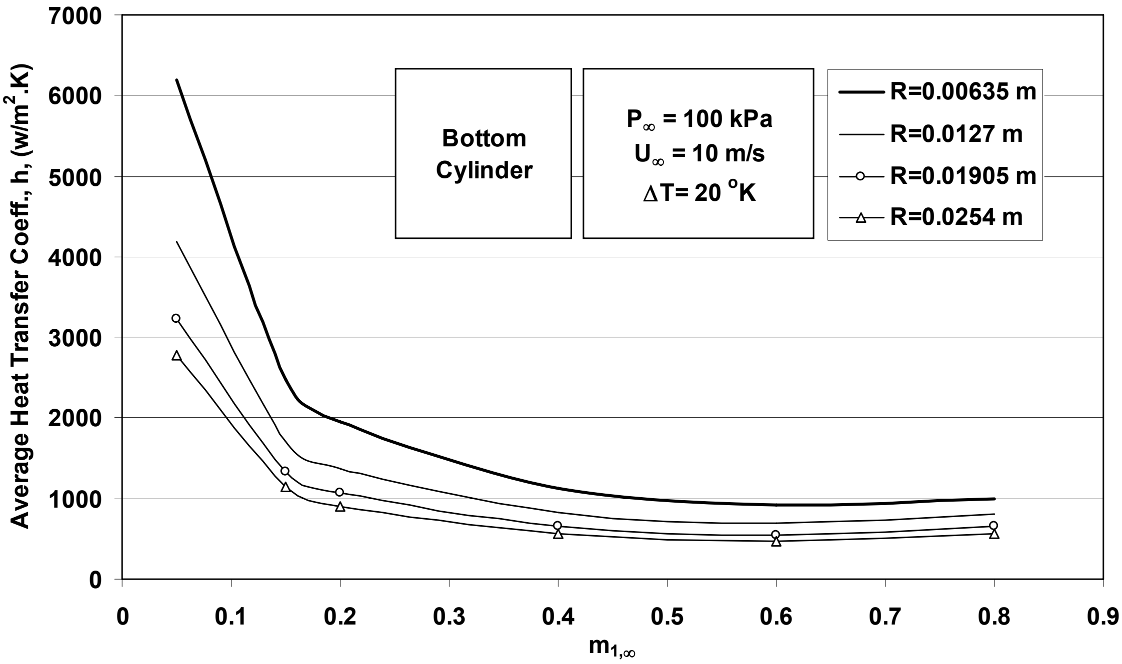


Figure 6.45c The effect of the cylinder diameter and the non-condensable gas concentrations on the average heat transfer coefficient for the bottom cylinder.

This is quite obvious since increasing the cylinder diameter results in a corresponding increase in the condensation surface area. This means more vapor will be condensate on the surface which in turn increases film thickness. As indicated before, the lower the cylinder is, the larger the film thickness becomes while the average heat transfer coefficient reversely related to film thickness.

## 6.4 Numerical results for vapor-air mixture on a tier of tubes, staggered arrangement

In order to study the effect of staggering of the cylinders on the heat transfer rates and to see how condensation is affected at the lower cylinders when condensate does not fall on to the center line of the cylinders, the whole setup is allowed to incline at different inclination angles. Numerical results are presented in this section to meet these requirements. Effects of the different stated parameters are analyzed and investigated.

### 6.4.1 The effect of angle of inclination

Figure 6.46 and Figure 6.47 show the effect of the angle of inclination on the local film thickness and the local heat transfer coefficient. For the middle and the bottom cylinders, film thickness gradually increases as for the upper cylinder until the point where the condensate falls from the upper cylinder on the middle cylinder which corresponding to the condensate fall angle ($\theta_o$). In this situation, a remarkable increase in the local film thickness is noticed. After this point, the local film thickness increases by the same manner as for the upper cylinder along the periphery of the cylinder. This effect

is similar for the bottom cylinder. This sudden increase in the film thickness at that point is attributed to the amount of the condensate that enters the control volume per unit time and the effect of momentum transfer. As angle of inclination increases, condensate fall angle increases too as indicated in Table 3.1.

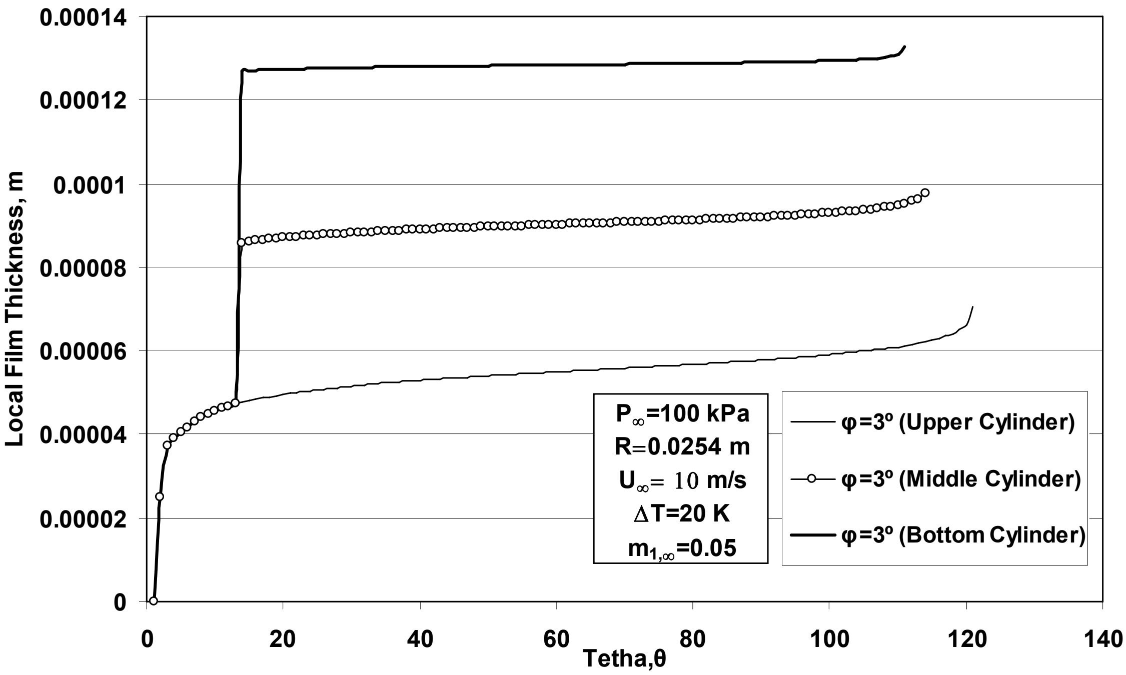


Figure 6.46a The effect of the angle of inclination on the local film thickness for upper, middle and bottom cylinders at ($\varphi=3^o$, $\theta_o=13^o$).

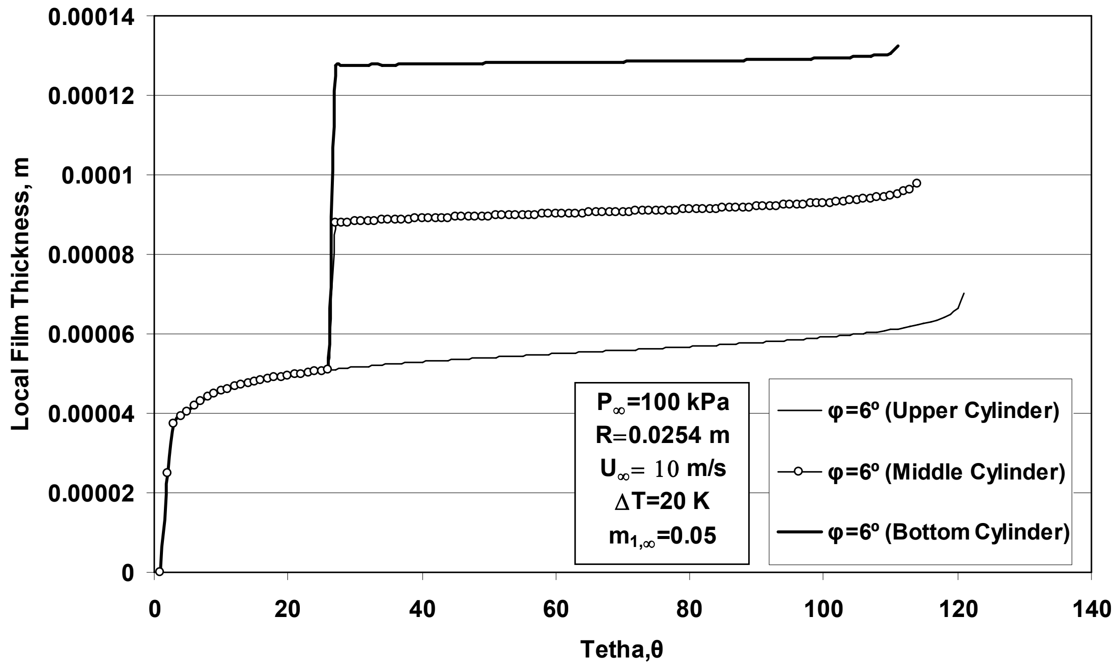


Figure 6.46b The effect of the angle of inclination on the local film thickness for upper, middle and bottom cylinders at ($\varphi=6^o$, $\theta_o=26^o$).

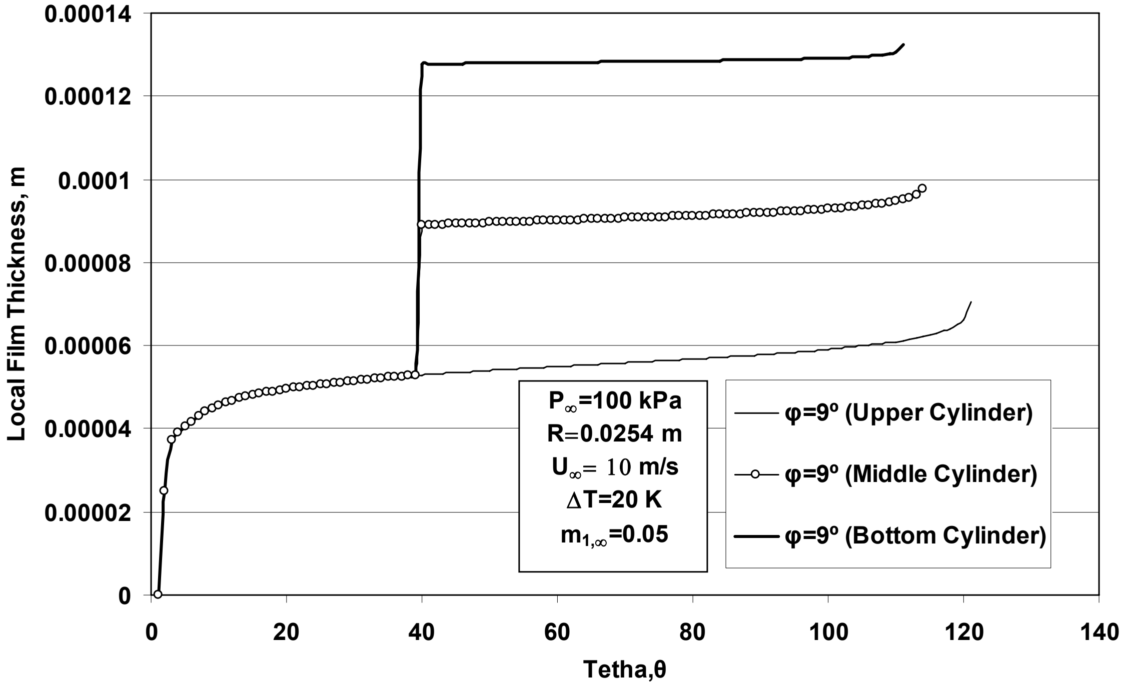


Figure 6.46c The effect of the angle of inclination on the local film thickness for upper, middle and bottom cylinders at ($\varphi=9^o$, $\theta_o=39^o$).

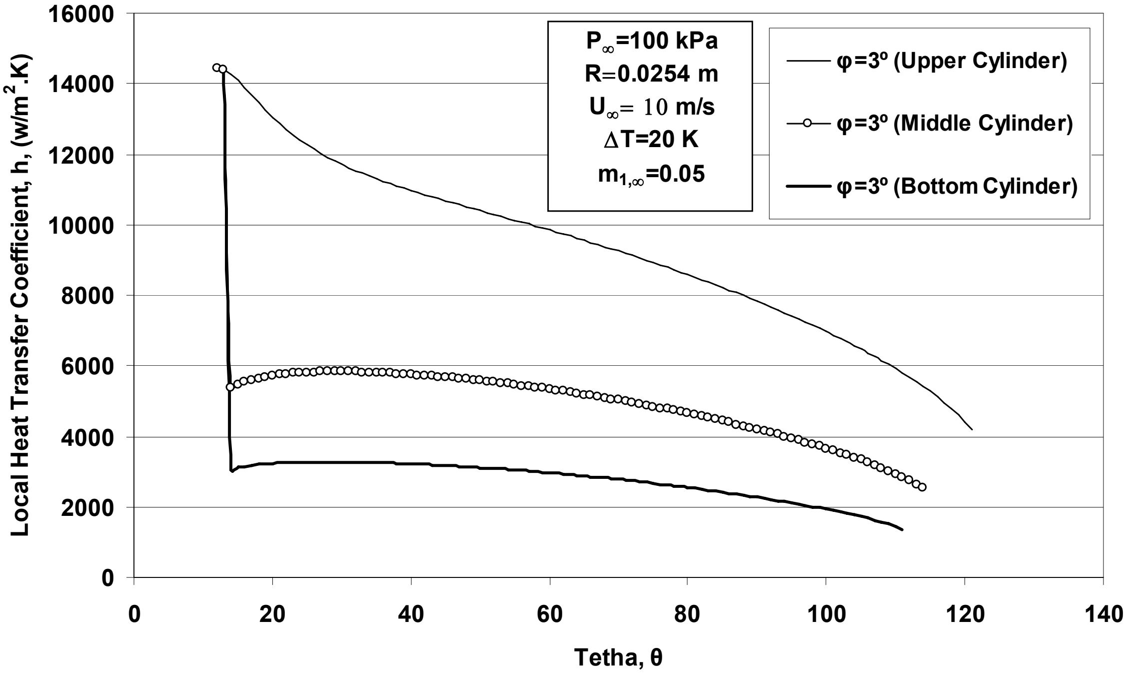


Figure 6.47a The effect of the angle of inclination on the local heat transfer coefficient for upper, middle and bottom cylinders at ($\varphi=3^o$, $\theta_o=13^o$).

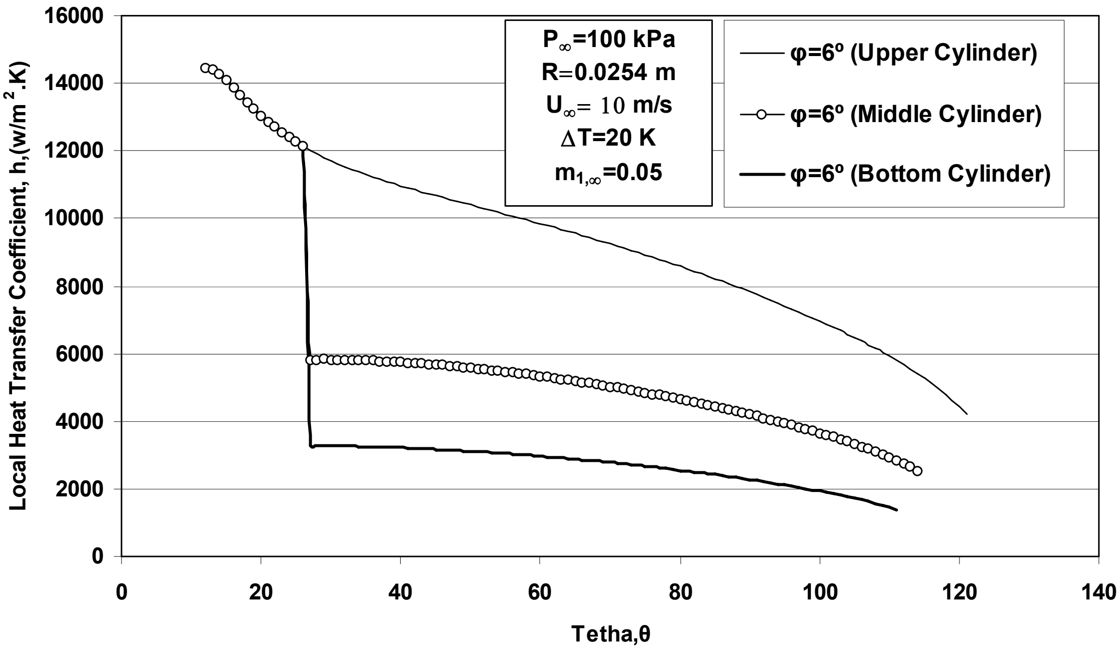


Figure 6.47b The effect of the angle of inclination on the local heat transfer coefficient for upper, middle and bottom cylinders at ($\varphi=6^o$, $\theta_o=26^o$).

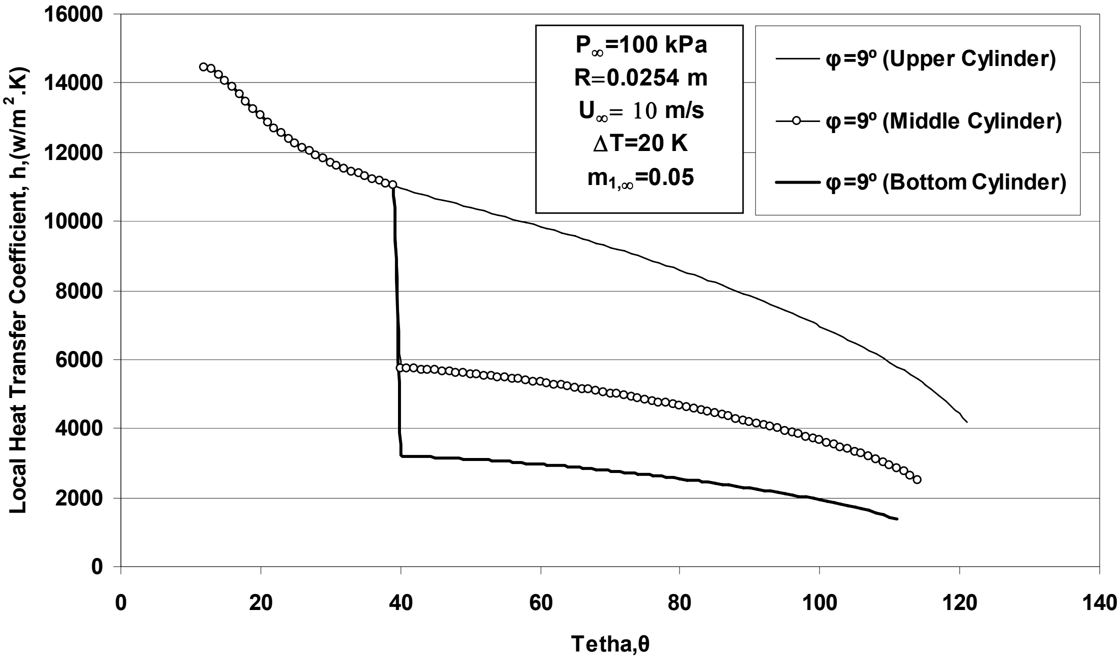


Figure 6.47c The effect of the angle of inclination on the local heat transfer coefficient for upper, middle and bottom cylinders at ($\varphi$=9$^o$, $\theta_o$=39$^o$).

This results in retarding the sudden film thickness increase. As a result, the average film thickness decreases as angle of inclination increases which in turn increases the average heat transfer coefficient also. In addition, the local heat transfer coefficient decreases for the middle and bottom cylinders when compared with that for the upper cylinder.

### 6.4.2 The effect of the non-condensable gas

Figure 6.48 indicates the effect of the non-condensable gas concentrations on the local heat transfer coefficient for the upper, the middle and the bottom cylinders at specified working conditions and at ($\varphi$=6$^o$ and $\theta_o$=26$^o$). As expected, when the non-condensable gas fractions increase, the local heat transfer coefficient decreases. For the middle and the bottom cylinders, local heat transfer coefficient gradually decreases until the point where the condensate falls on the lower cylinder at ($\theta_o$=26$^o$) from the upper cylinder. In that case, local heat transfer coefficient sharply decreases and then gradually decreases as for the upper cylinder.

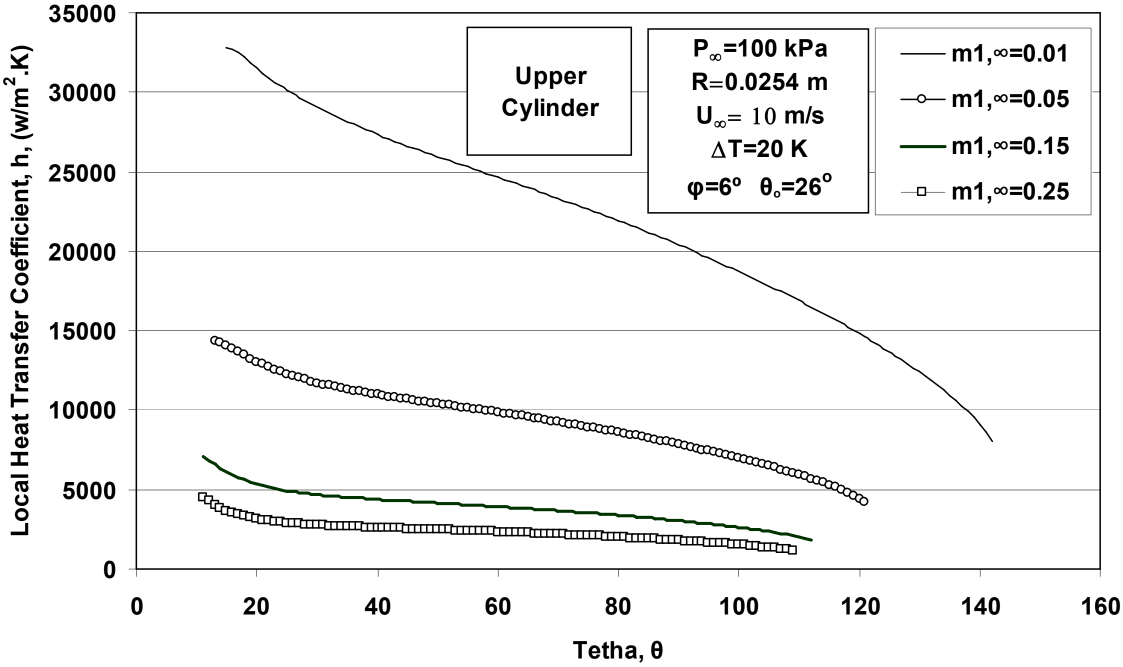


Figure 6.48a The effect of the non-condensable gas concentrations on the local heat transfer coefficient for the upper cylinder.

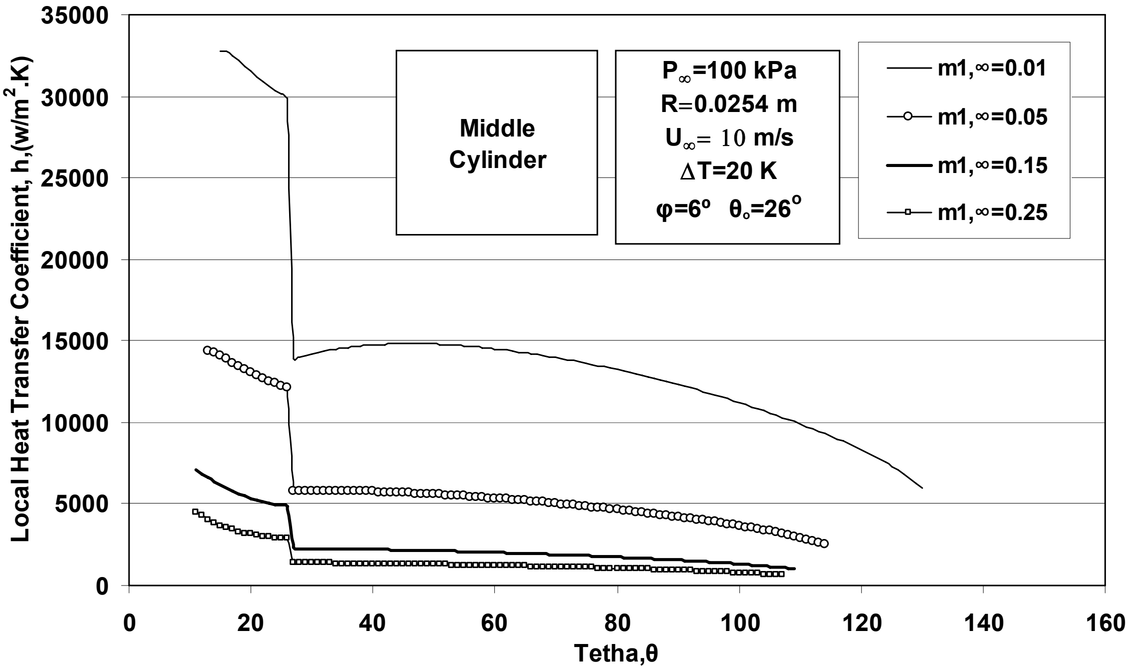


Figure 6.48b The effect of the non-condensable gas concentrations on the local heat transfer coefficient for the middle Cylinder.

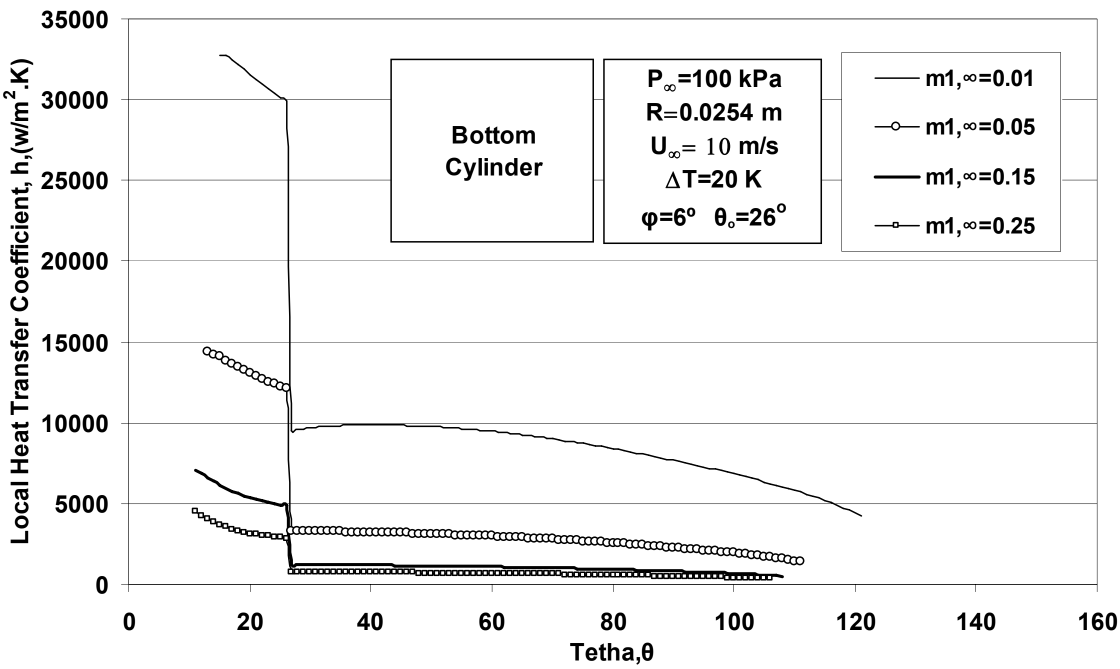


Figure 6.48c The effect of the non-condensable gas concentrations on the local heat transfer coefficient for the bottom cylinder.

This is attributed to the sharp increase of film thickness due to condensate fall at that point which increases the resistance to heat transfer. Moreover, the effect of the non-condensable gas accumulation at the liquid-vapor interface leads to a decrease in the vapor partial pressure at the interface which in turn reduces the interface temperature and consequently the heat transfer rate. Again, for the lower cylinders in the column, local heat transfer coefficient decreases when compared with the upper cylinder in the column.

### 6.4.3 The effect of the Reynolds number

The effect of Reynolds number on the local film thickness and local heat transfer coefficient is illustrated in Figure 6.49 and Figure 6.50. As Reynolds number increases, local film thickness decreases while local heat transfer coefficient increases. This is attributed to the effect of shear drag and viscous forces. Shear drag and viscous forces tend to decrease the thickness of the liquid boundary layer. It should be noted that; the results of the upper cylinder does not affected by the inclination.

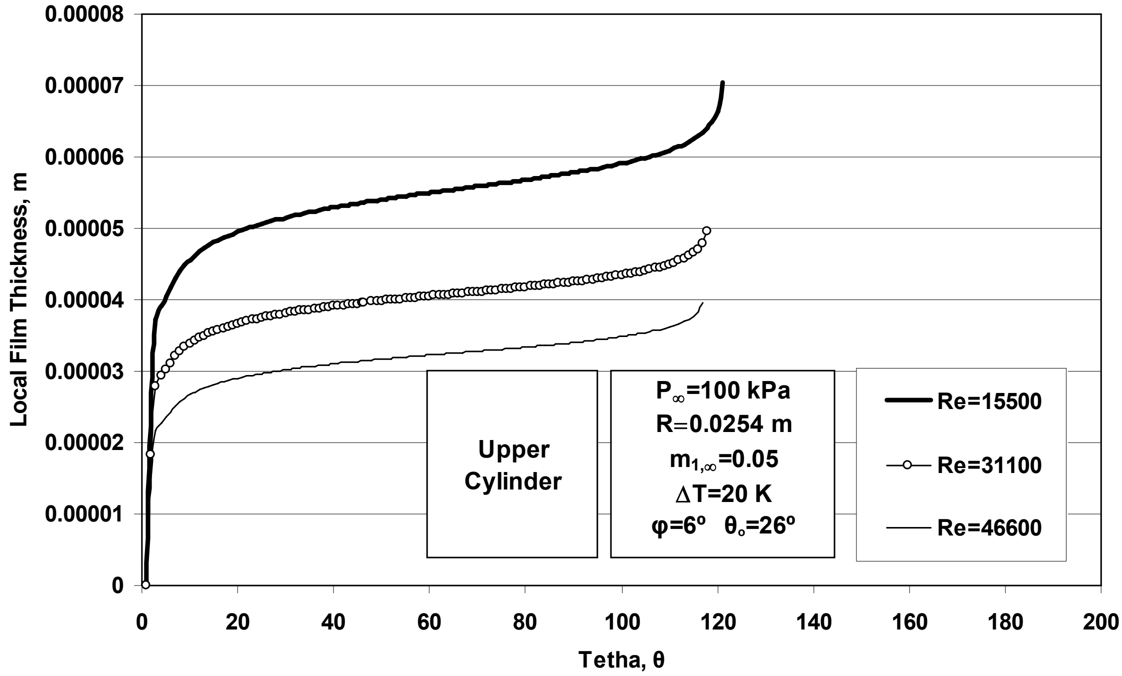


Figure 6.49a The effect of Reynolds number on the local film thickness for the upper cylinder.

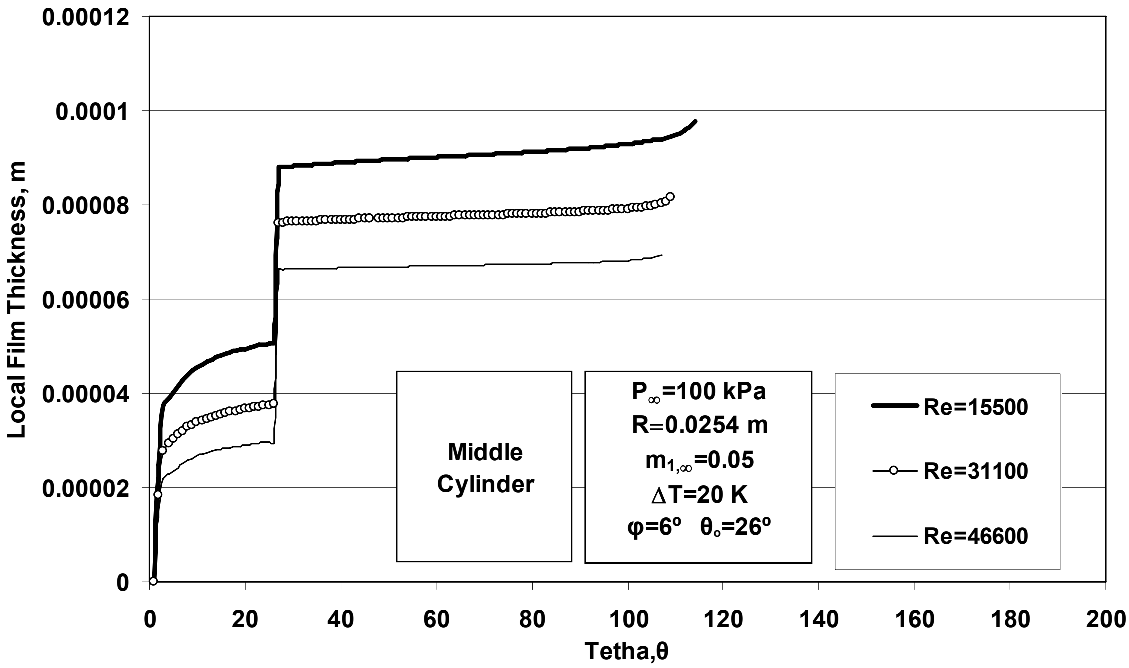


Figure 6.49 b The effect of Reynolds number on the local film thickness for the middle cylinder.

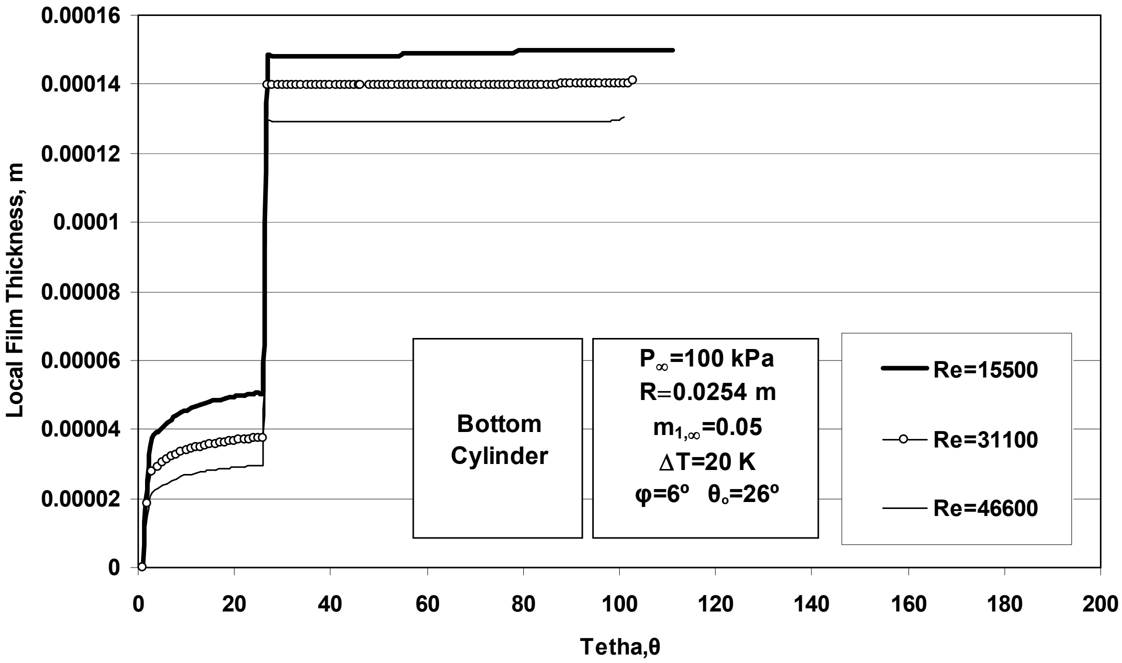


Figure 6.49c The effect of Reynolds number on the local film thickness for the bottom cylinder.

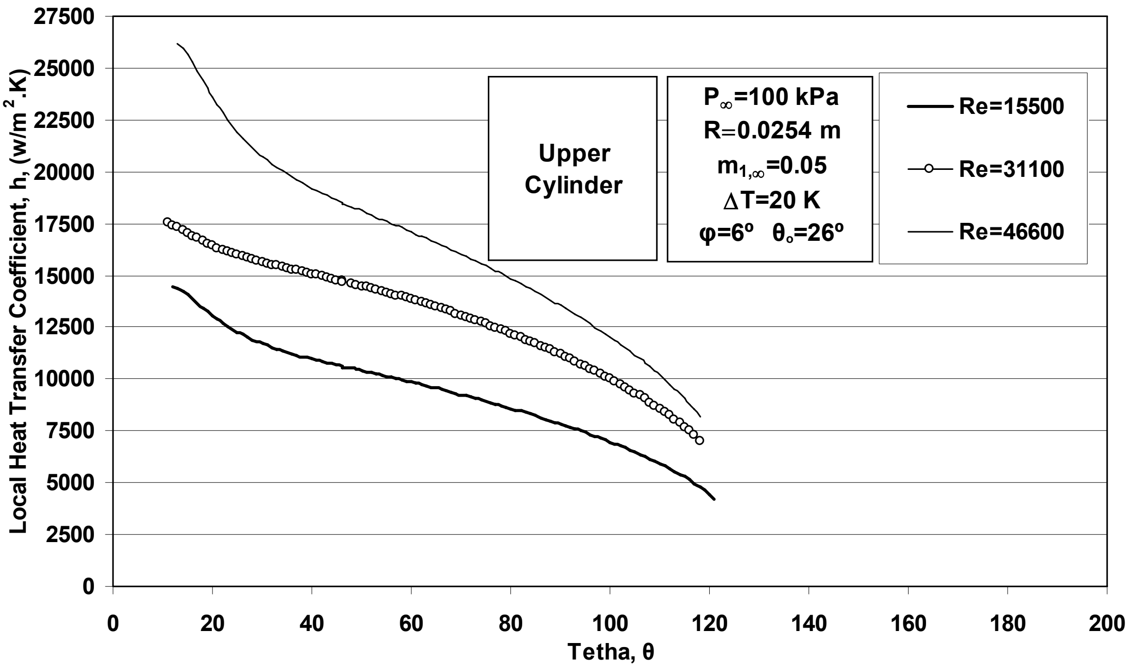


Figure 6.50a The effect of Reynolds number on the local heat transfer coefficient for the upper cylinder.

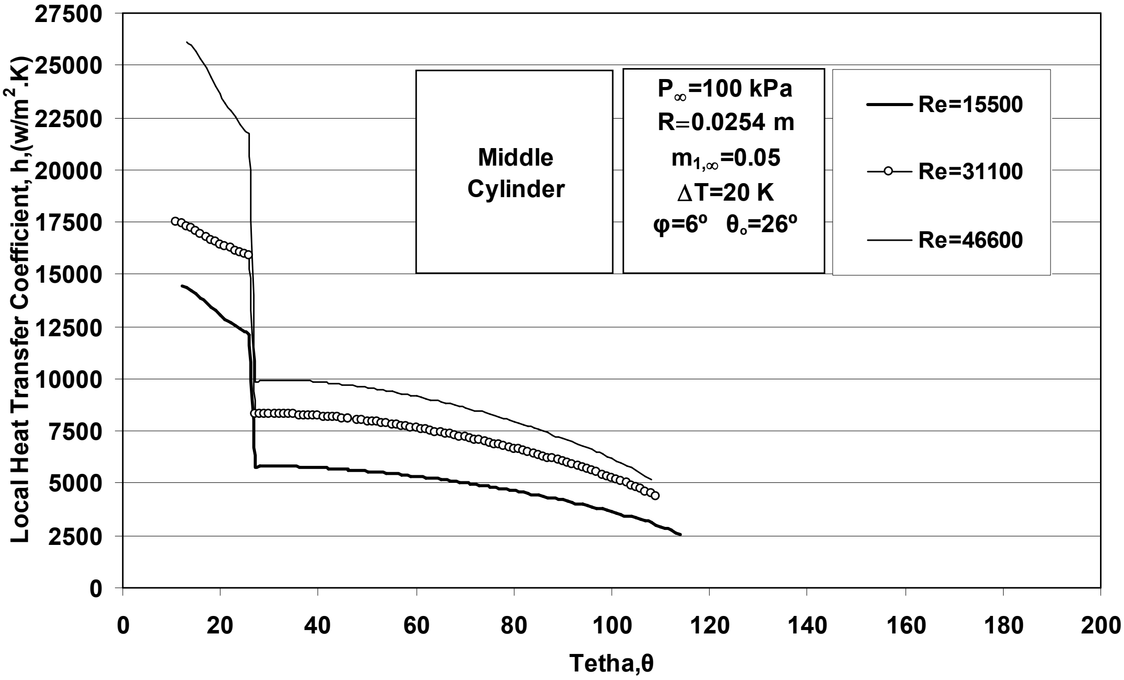


Figure 6.50b The effect of Reynolds number on the local heat transfer coefficient for the middle cylinder.

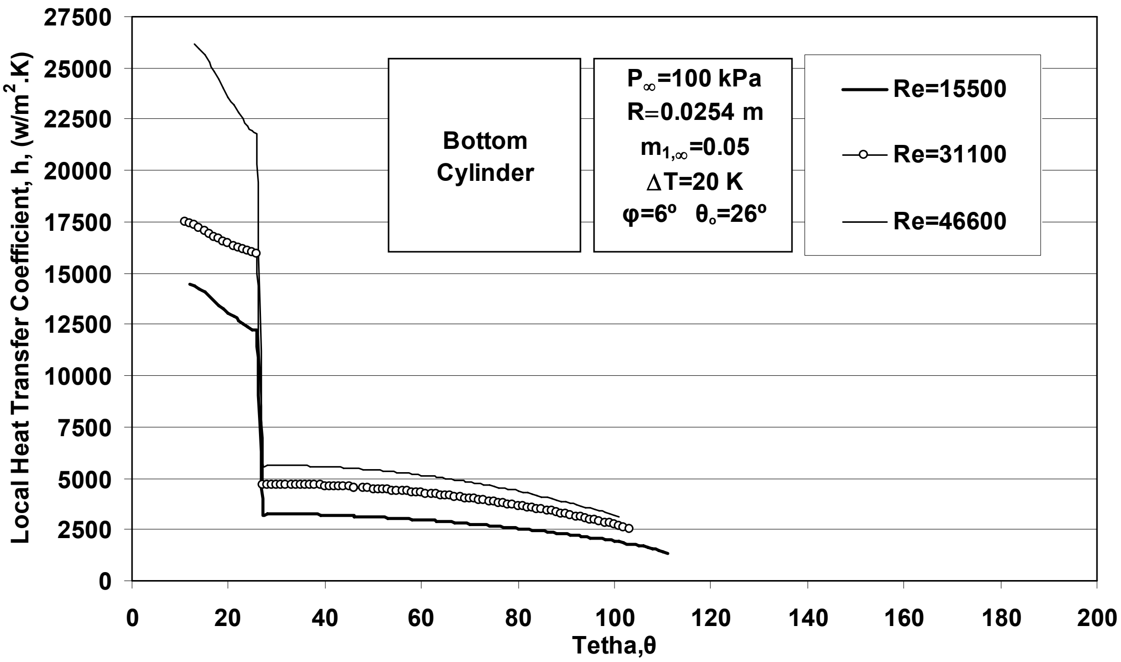


Figure 6.50c The effect of Reynolds number on the local heat transfer coefficient for the bottom cylinder.

### 6.4.4 The effect of the temperature difference

Figure 6.51 and Figure 6.52 show the effect of the temperature difference on the local film thickness and the local heat transfer coefficient under specified working conditions. Local film thickness increases as temperature difference increases. This is physically the case since the increase in the temperature difference leads vapor to liberate more latent heat energy which in turn increases the condensation rate and eventually the liquid film thickness. The effect of inclination angle on the local film thickness for middle and bottom cylinders is similar to previous cases. Sudden increase is noticed at the location that meets the condensate fall point. This corresponds to condensate fall angle ($\theta_o$=25.67$^o$). As expected, local heat transfer coefficient decreases as temperature difference increases. Sharp decrease is observed at the condensate fall point then gradual decrease in the local heat transfer coefficient with the angular position on the periphery of the cylinder is also noticed.

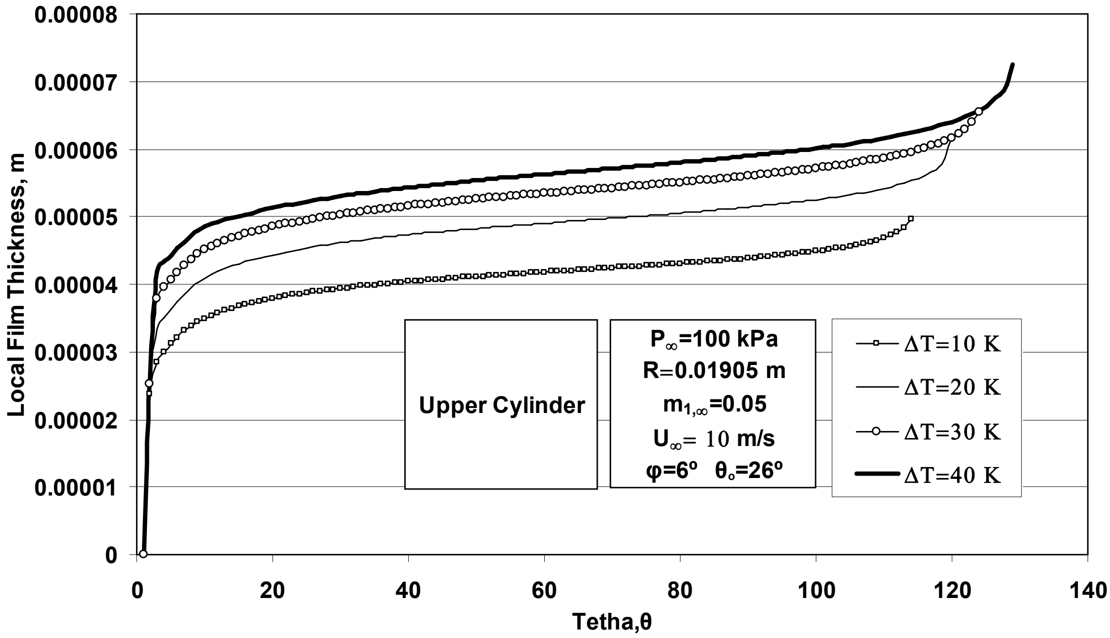


Figure 6.51a The effect of the temperature difference on the local film thickness for the upper cylinder.

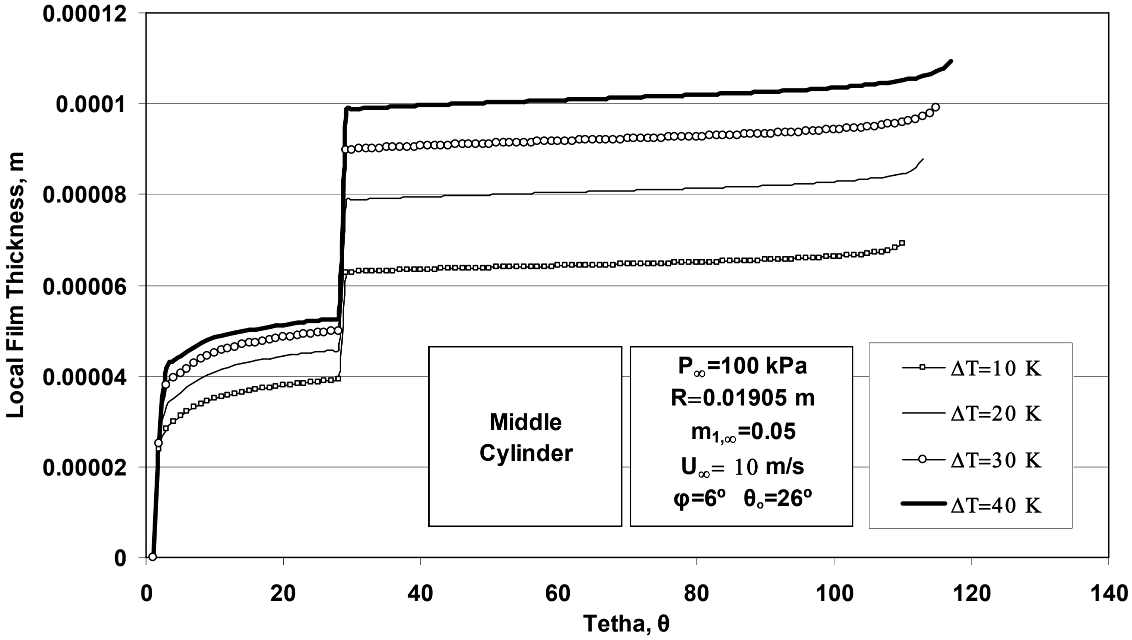


Figure 6.51b The effect of the temperature difference on the local film thickness for the middle cylinder.

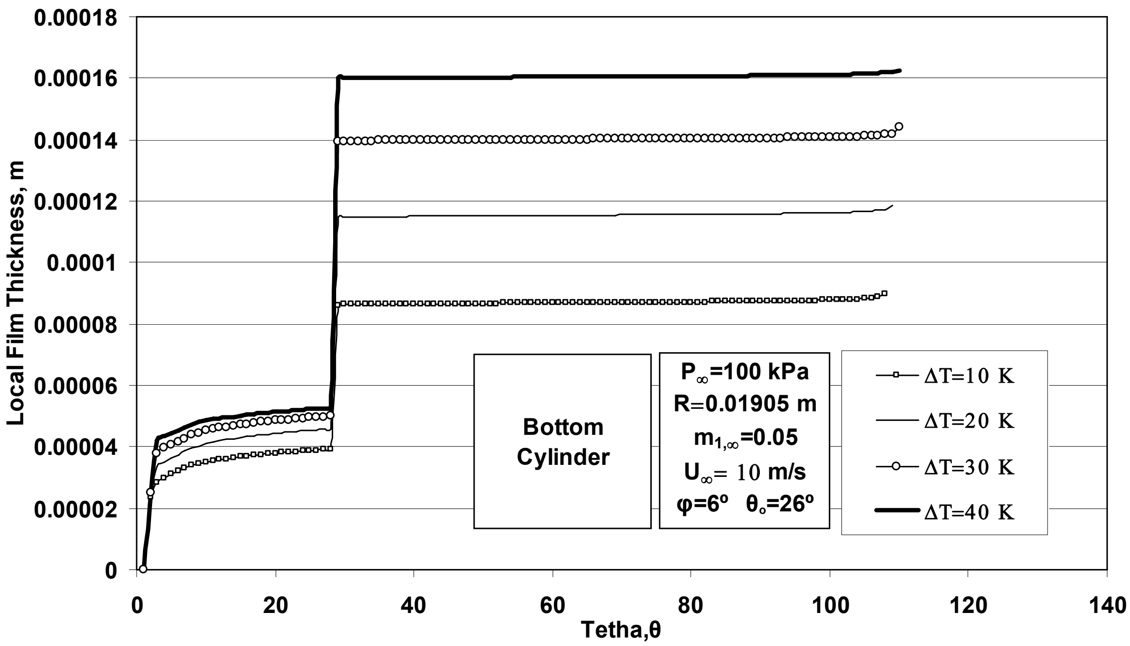


Figure 6.51c The effect of the temperature difference on the local film thickness for the bottom cylinder.

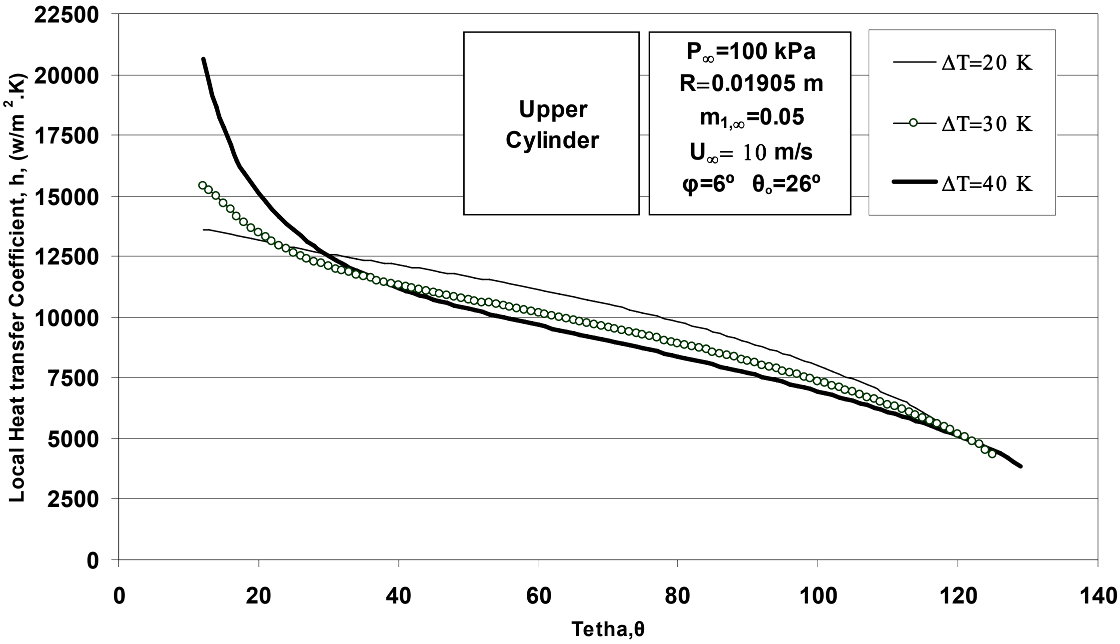


Figure 6.52a The effect of the temperature difference on the local heat transfer coefficient for the upper cylinder.

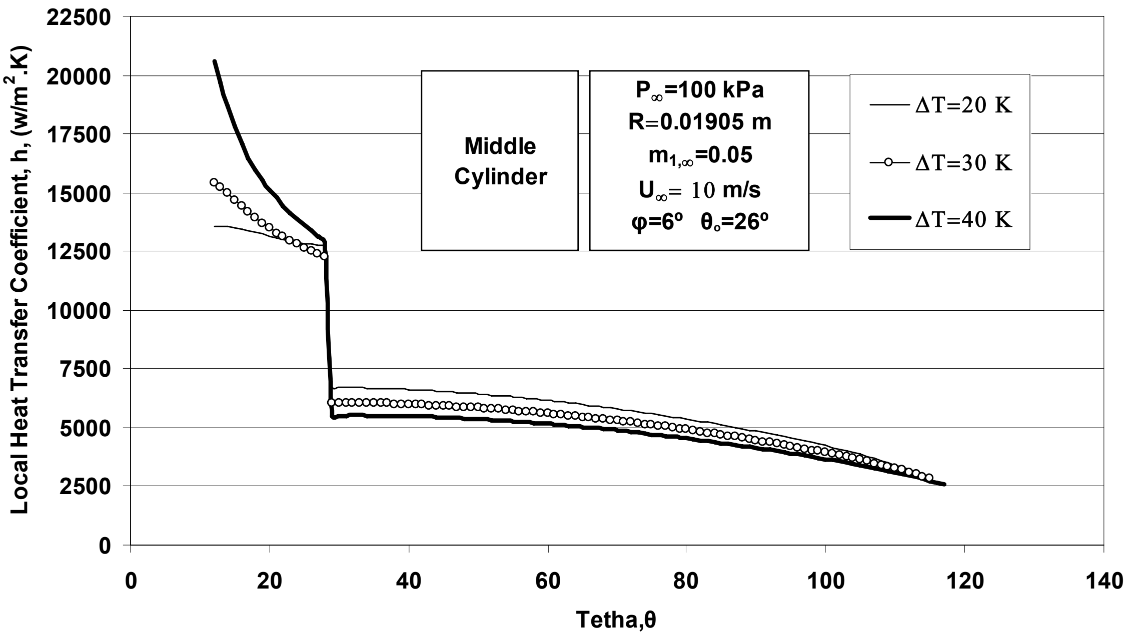


Figure 6.52b The effect of the temperature difference on the local heat transfer coefficient for the middle cylinder.

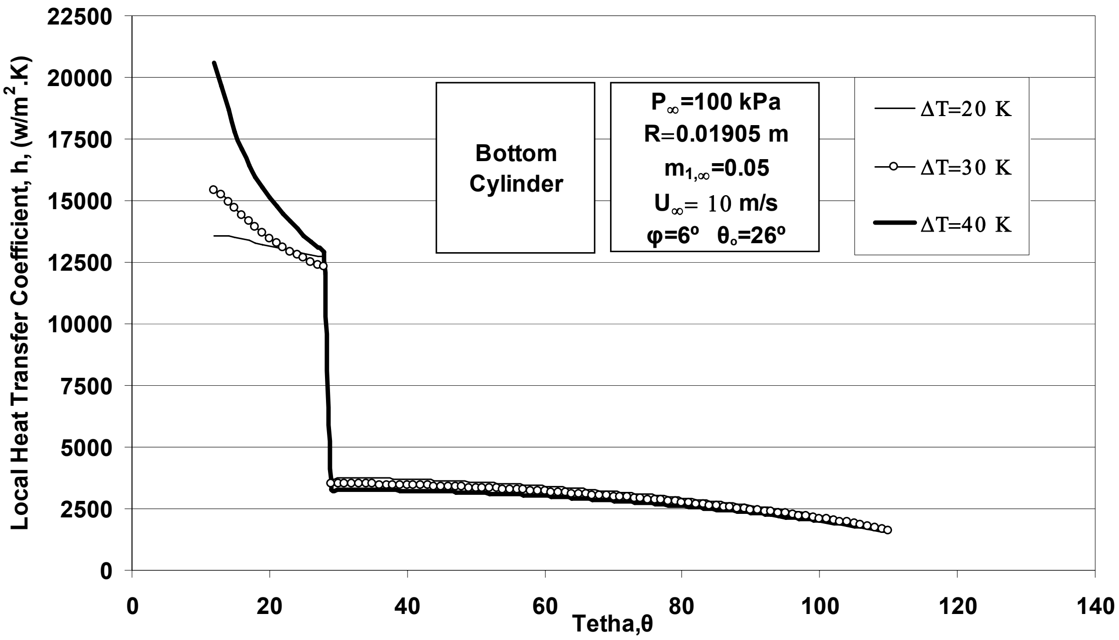


Figure 6.52c The effect of the temperature difference on the local heat transfer coefficient for the bottom cylinder.

### 6.4.5 The effect of the cylinder diameter

Figure 6.53 and Figure 6.54 show the effect of the cylinder diameter on the local film thickness and the local heat transfer coefficient. It is clearly shown that local film thickness increases as the cylinder diameter increases. This is attributed to the increase in the heat transfer surface area. As a result, more chance for vapor to condensate on the cylinder wall. On the other hand, local heat transfer coefficient decreases as cylinder diameter increases. It should be noted that as the cylinder diameter increases, condensate fall angle decreases, see Table 3.1. This is clearly shown in the figures.

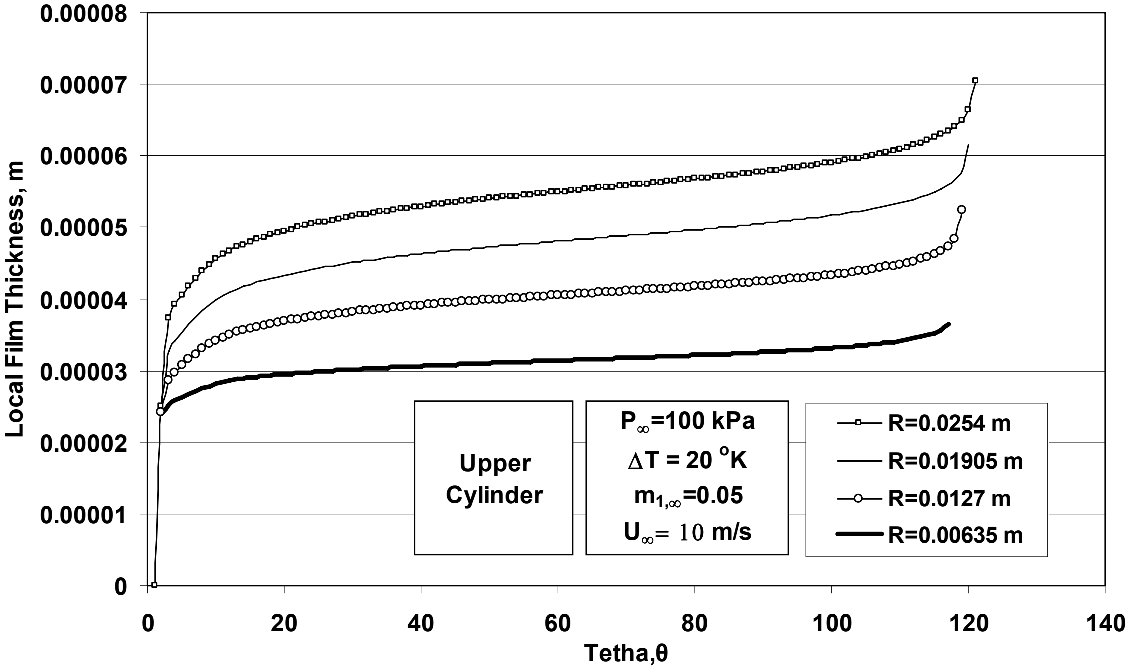


Figure 6.53a The effect of the cylinder diameter on the local film thickness for upper cylinder.

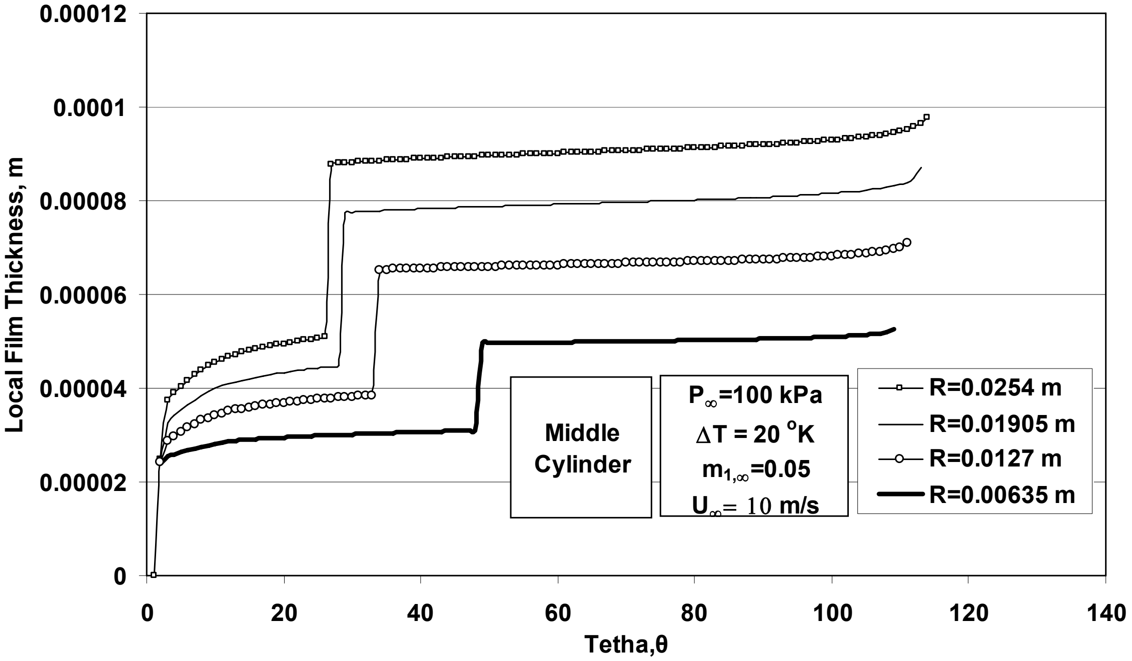


Figure 6.53b The effect of the cylinder diameter on the local film thickness for middle cylinder.

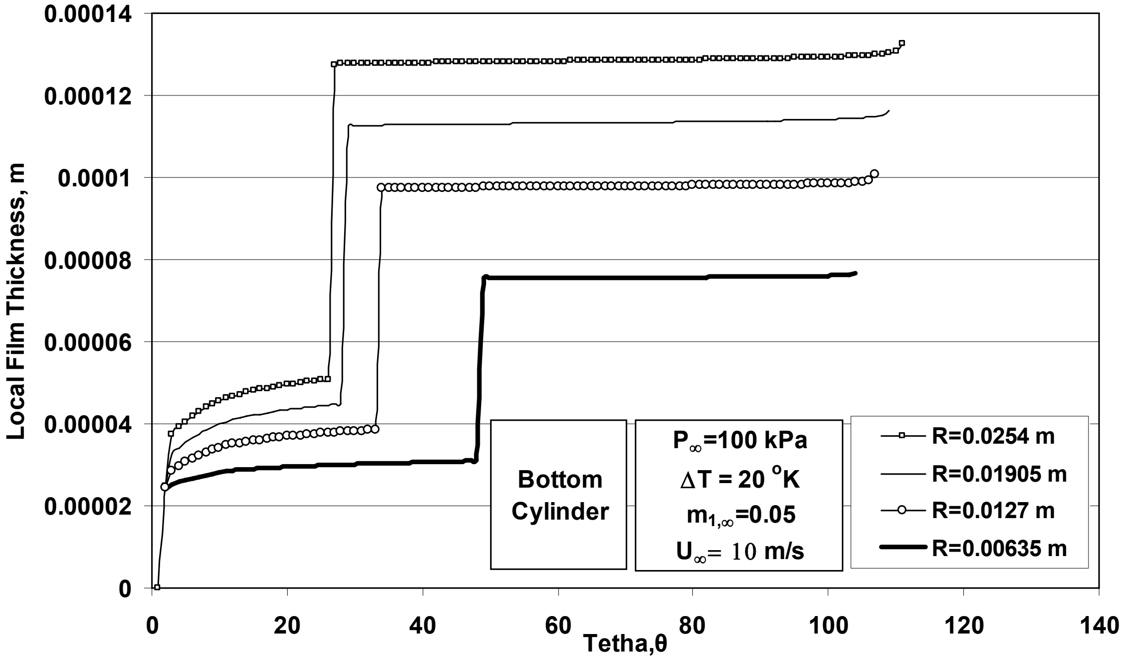


Figure 6.53c The effect of the cylinder diameter on the local film thickness for bottom cylinder.

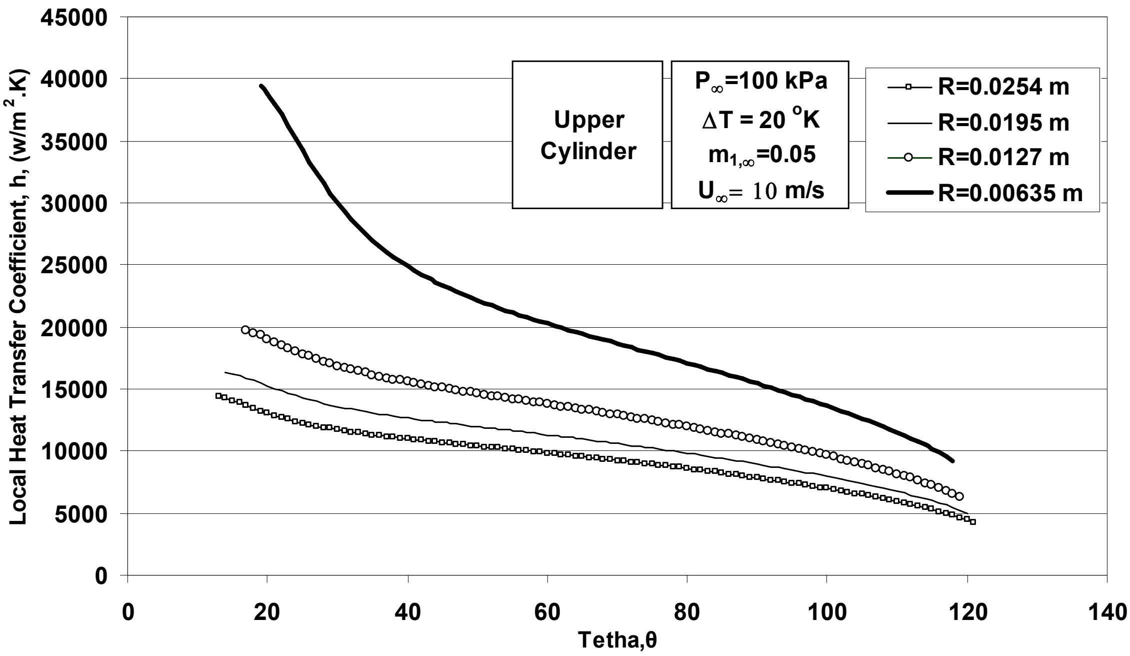


Figure 6.54a The effect of the cylinder diameter on the local heat transfer coefficient for upper cylinder.

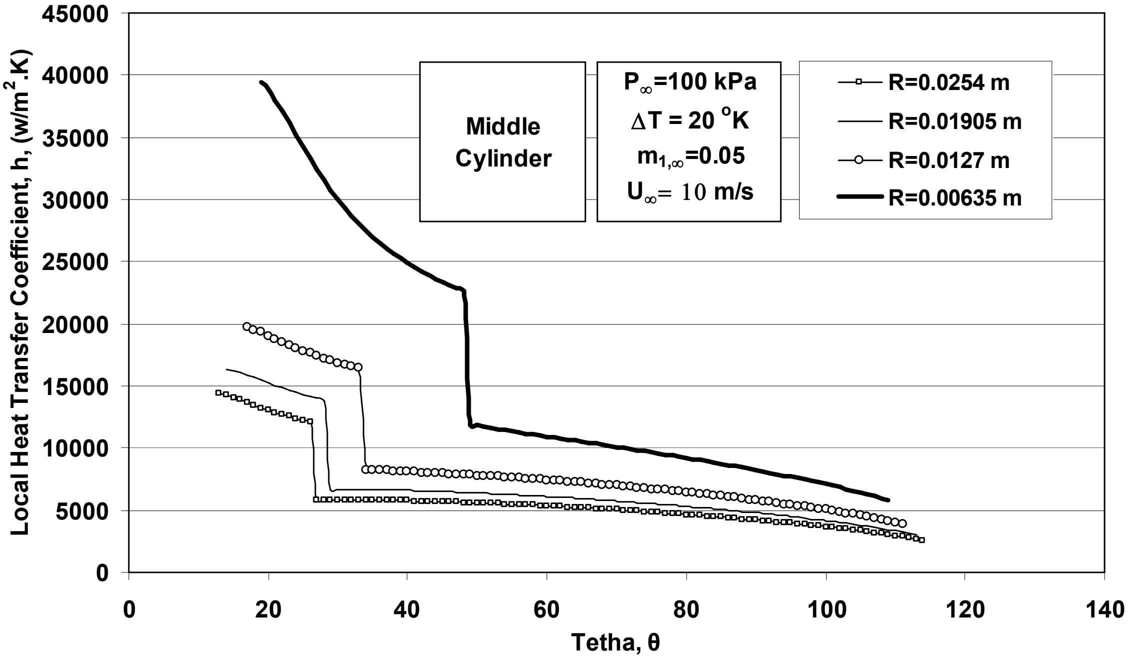


Figure 6.54b The effect of the cylinder diameter on the local heat transfer coefficient for middle cylinder.

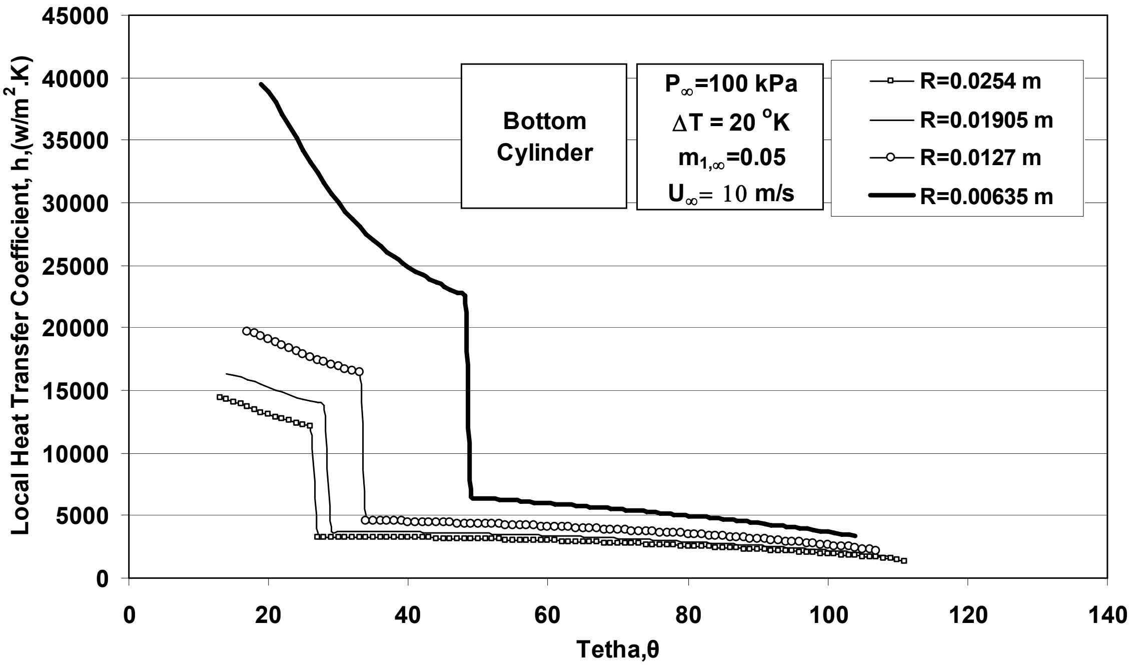


Figure 6.54c The effect of the cylinder diameter on the local heat transfer coefficient for bottom cylinder.

## 6.5 Experimental results for the present study

In this section, the experimental results for this study are presented to show the effect of various parameters on the condensation heat transfer down a bundle of tubes for both inline and staggered arrangements.

### 6.5.1 The effect of inclination angle

Figure 6.55 to Figure 6.59 are constructed to study the effect of inclination angle on the heat transfer rate and the heat transfer coefficient at different vapor or vapor-air mixture to wall temperature difference values down the bundle of tubes. The test section is inclined to predefined inclination angles of $0^o$, $3^o$, $6^o$, $9^o$ and $12^o$.

Results show that; heat transfer rates are increased with the increase in the temperature difference. Since more vapor will be condensed as the temperature difference increases. As a result, the highest heat transfer rate is observed at the lowest inlet cooling water temperature. In contrast, heat transfer coefficient is decreased with the increase in the temperature difference. This results from the high condensation rates at high temperature differences, which in turn lead to an increase in the condensate film thickness and heat resistance as well. As a result, the value heat transfer coefficient becomes lower.As expected, the values of both heat transfer rate and heat transfer coefficient are clearly decreased as the condensate falls down the tube rows. This agrees with the findings of the theoretical analysis.

Heat transfer rates for the middle and the bottom tubes are slightly increased by increasing the angle of inclination. This is attributed to the fact that condensate film falls on the lower tubes at a bigger condensate fall angle ($\Theta_o$) on the circumference of the cylinder. This leads to retard the sharp increase in the film thickness growth that caused by the condensate fall. As a result, average heat transfer coefficient gradually increased as inclination angle increases. However, the rate of heat transfer for the upper tubes does not change significantly with the change of inclination angle. When inclination angle is set to $12^o$, results for heat transfer rate and heat transfer coefficient are nearly the same for all tubes since none of the condensate falls on the lower tubes. This is expected since the value of $12^o$, is the value of the critical angle of inclination for this study. All of these findings coincide with those obtained from the theoretical results.

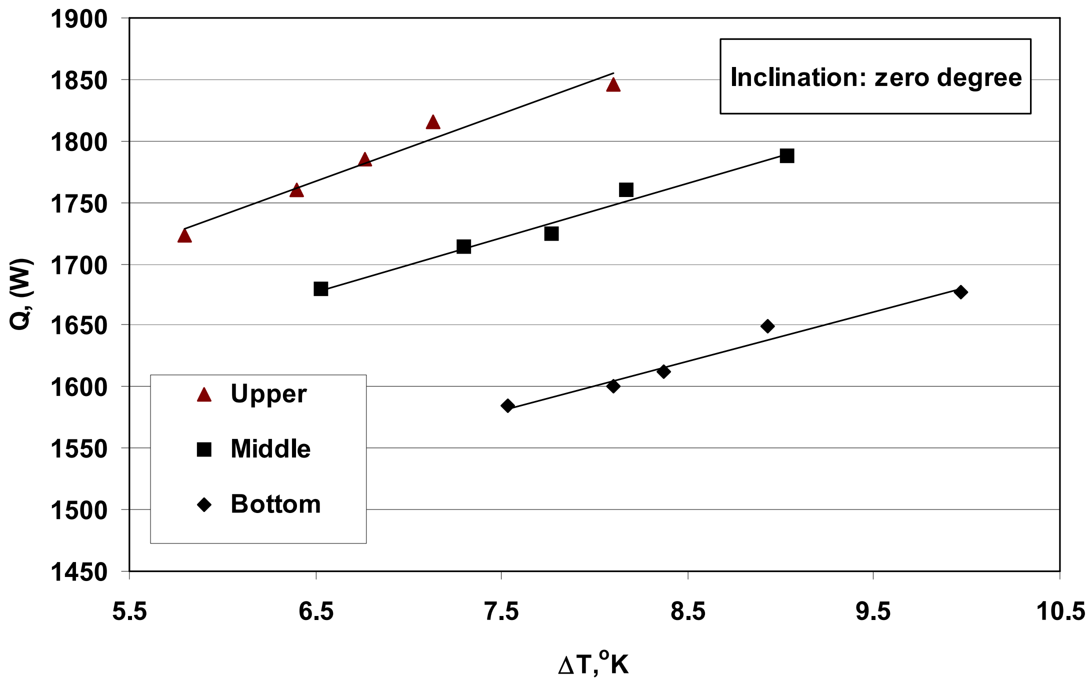


Figure 6.55 a Variation of heat transfer rates with temperature difference for 0° of inclination.

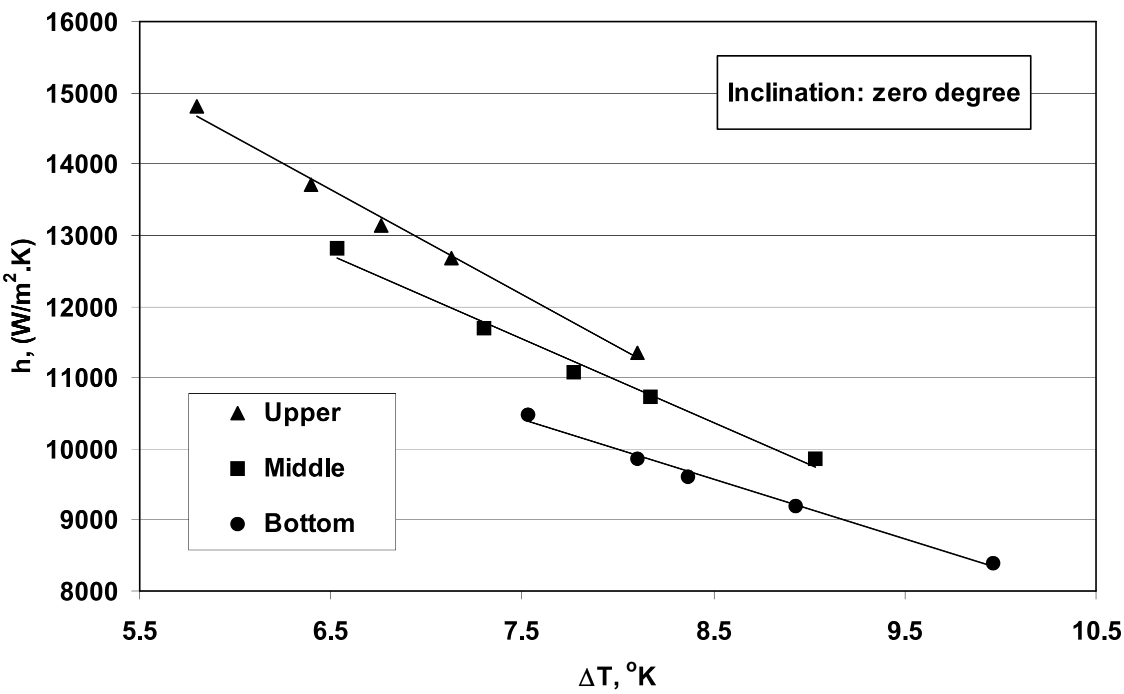


Figure 6.55 b Variation of heat transfer coefficients with temperature difference for 0° of inclination

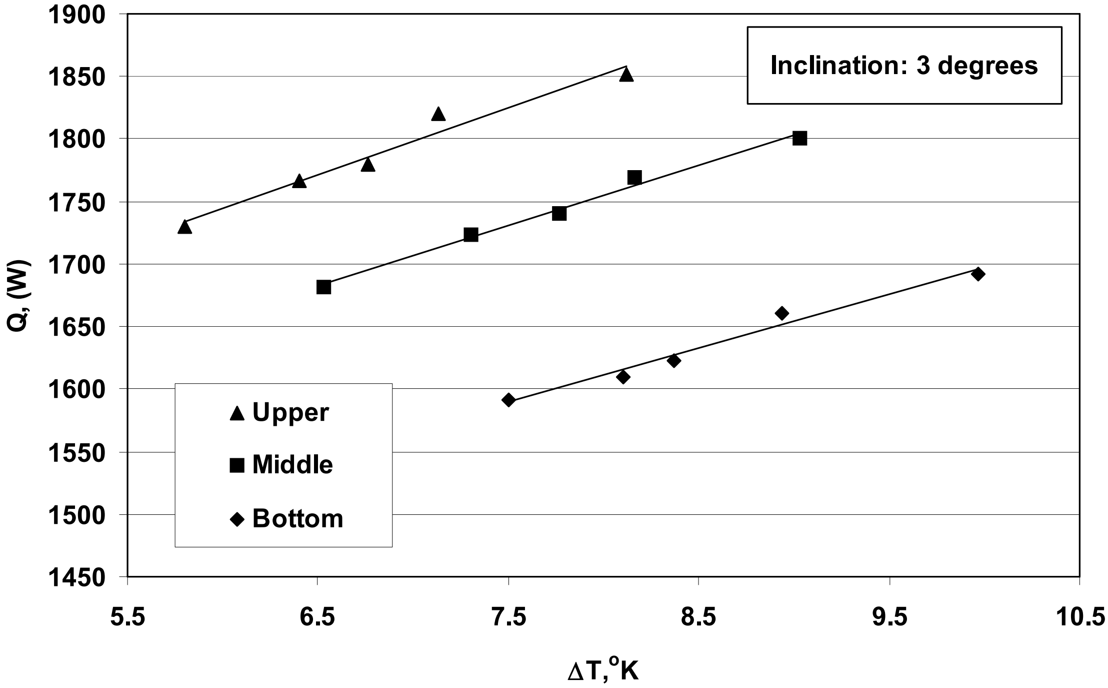


Figure 6.56a Variation of heat transfer rates with temperature difference for 3° of inclination.

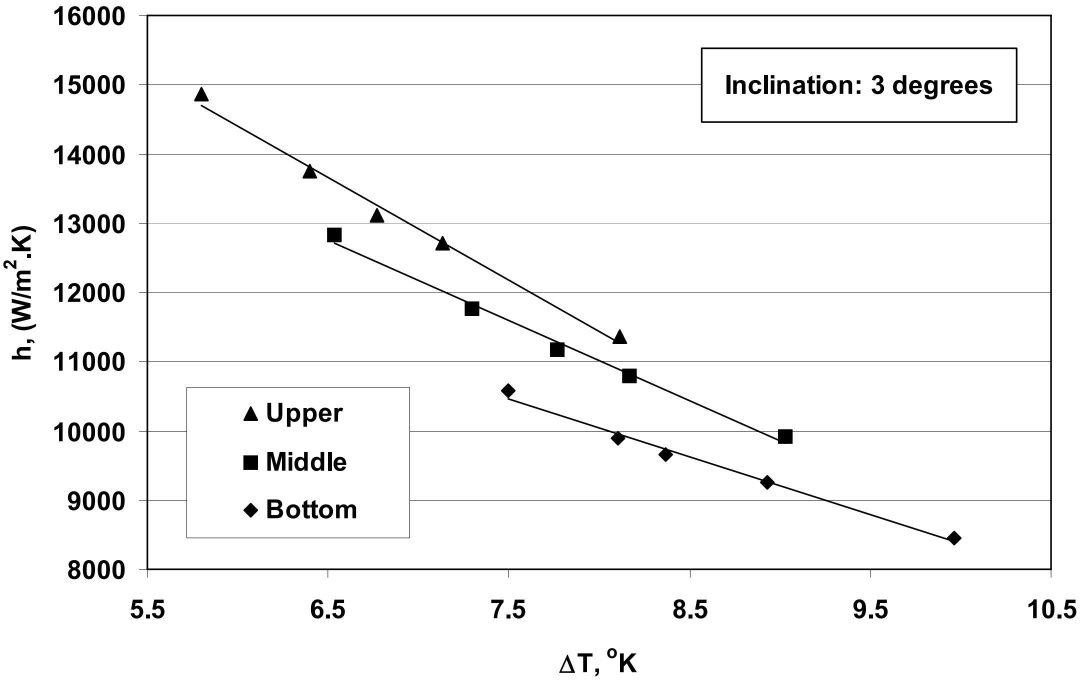


Figure 6.56b Variation of heat transfer coefficients with temperature difference for 3° of inclination.

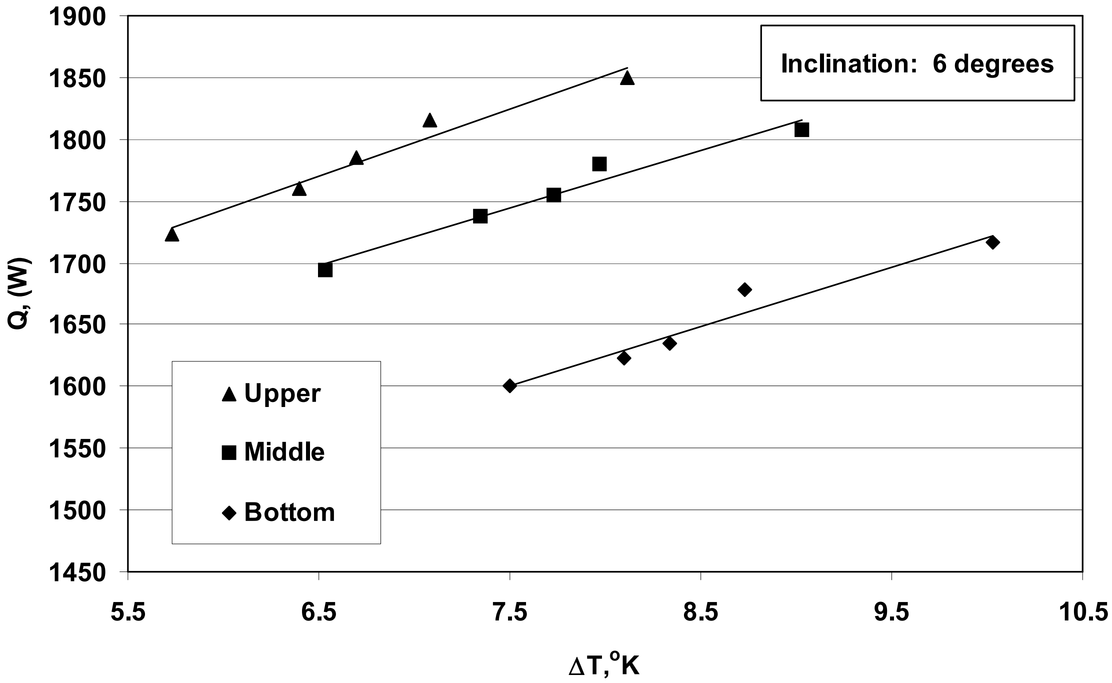


Figure 6.57a Variation of heat transfer rates with temperature difference for 6$^{o}$ of inclination

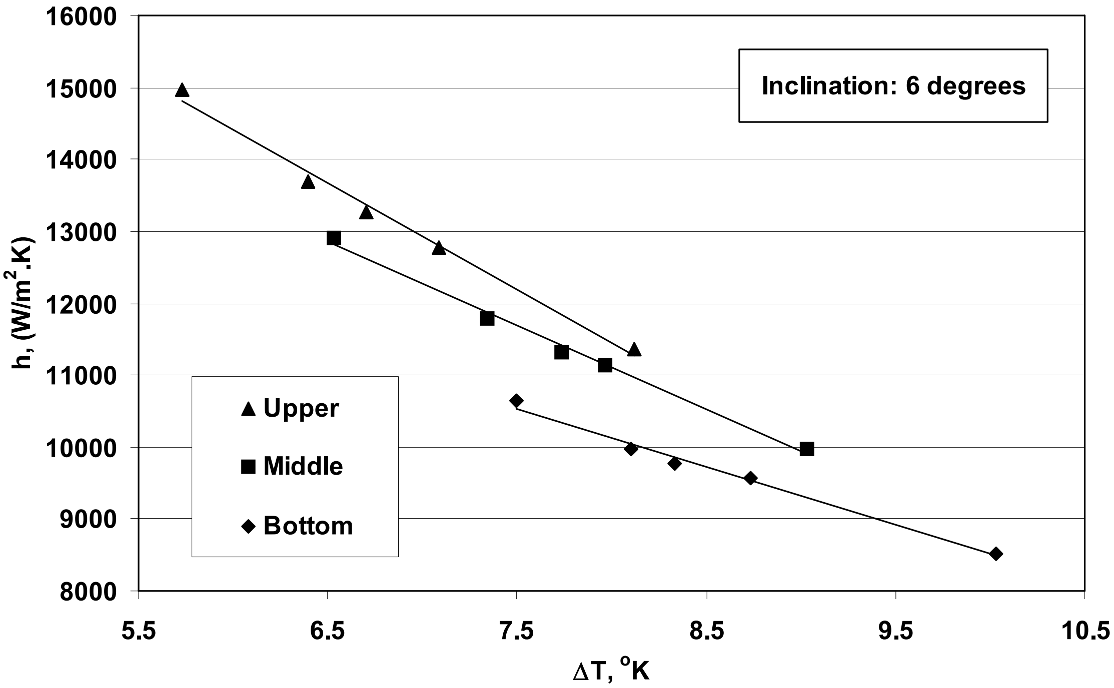


Figure 6.57b Variation of heat transfer coefficients with temperature difference for 6$^{o}$ of inclination.

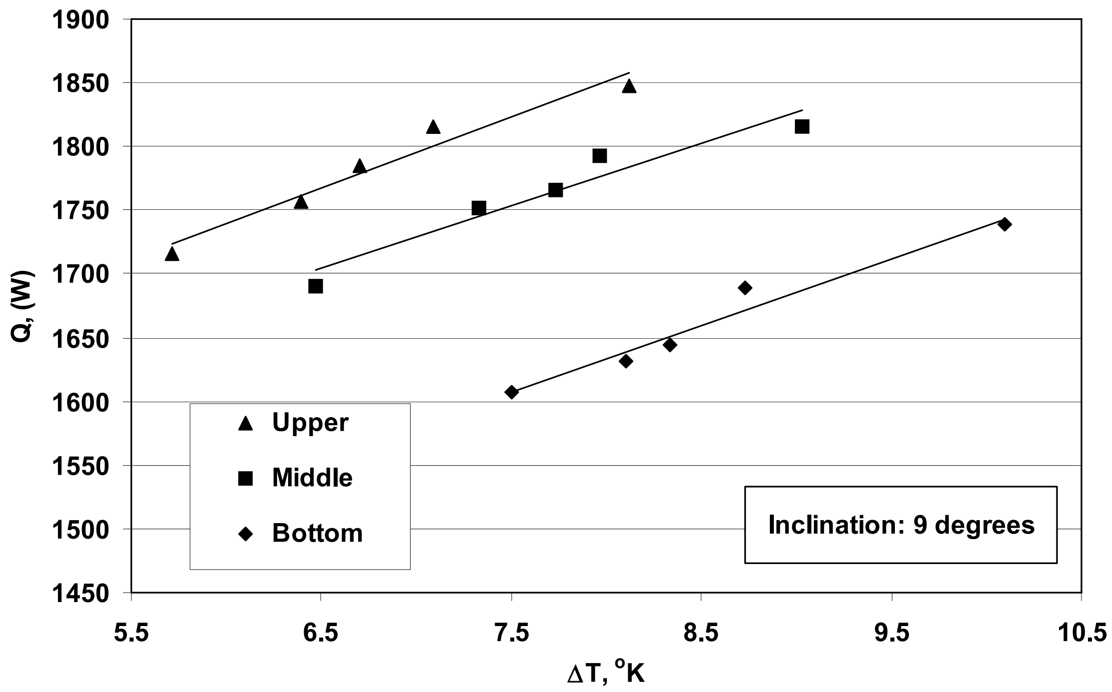


Figure 6.58a Variation of heat transfer rates with temperature difference for $9^o$ of inclination.

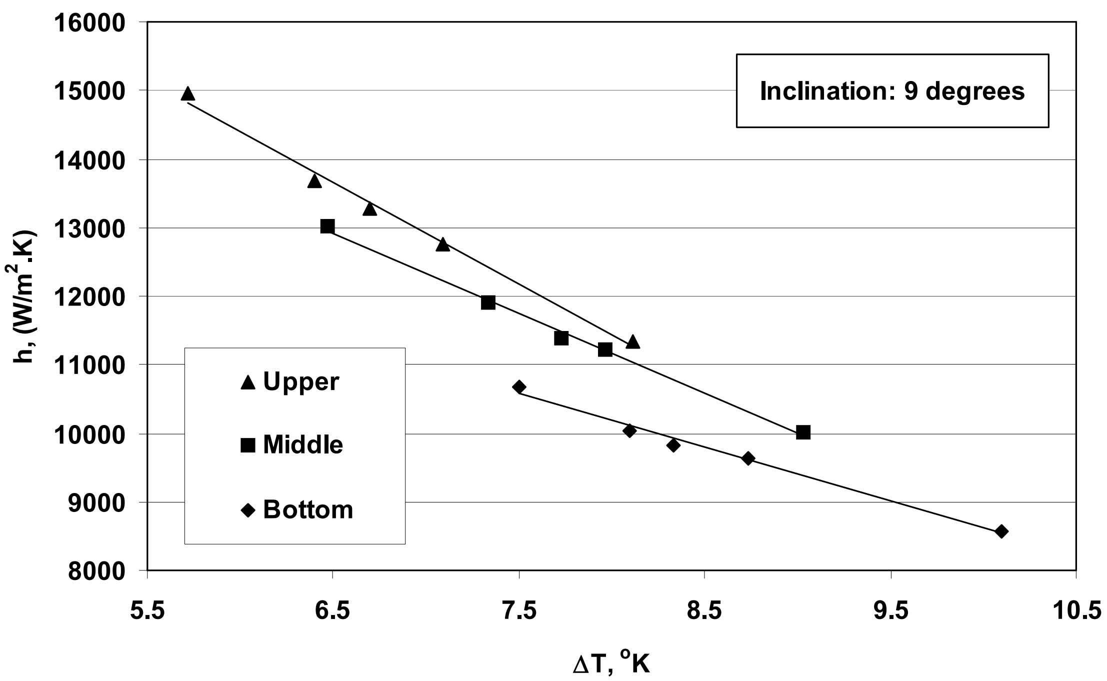


Figure 6.58b Variation of heat transfer coefficients with temperature difference for $9^o$ of inclination.

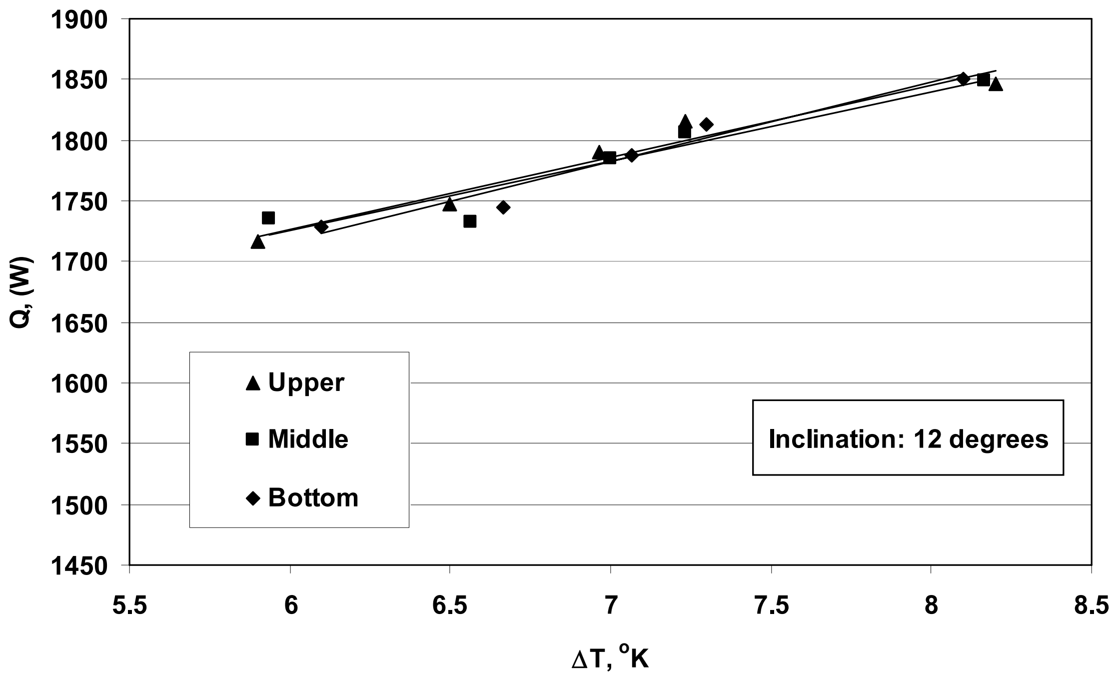


Figure 6.59a  Variation of  heat transfer rates with temperature difference for 12$^{o}$ of inclination.

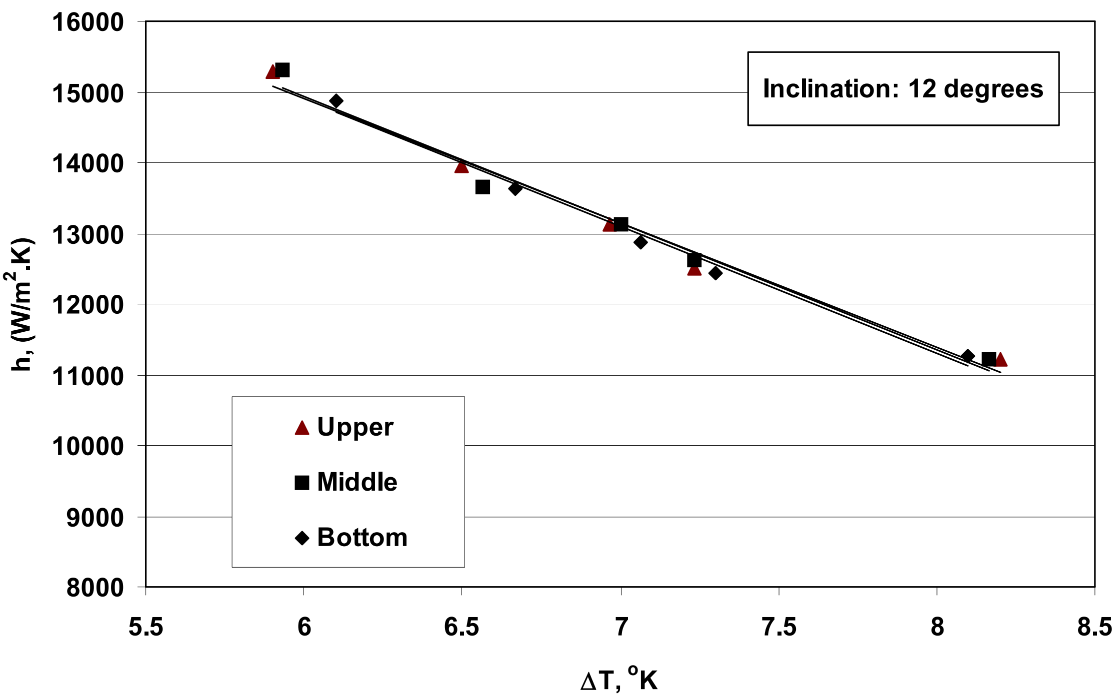


Figure 6.59b  Variation of heat transfer coefficients with temperature difference for 12$^{o}$ of inclination.

### 6.5.2 The effect of the non-condensable gas

Figure 6.60 shows the effect of the free stream air fractions on the heat transfer coefficient for upper, middle and bottom tube rows for two values, minimum value of ($m_{1,\infty}$ = 0.001) and maximum value of ($m_{1,\infty}$ = 0.021) at free stream velocity of ($U_\infty$ = 1.2 m/s). The switching between the minimum and the maximum values can be done experimentally by controlling the amount of supplied air via the adjustable switch for the small air compressor used in the experimental setup.

As expected, the increase in the non-condensable gas (air) fraction from ($m_{1,\infty}$ = 0.001) to ($m_{1,\infty}$ = 0.021) in the vapor-air mixture leads to a corresponding decrease in the heat transfer coefficient through the tube rows. Again, heat transfer coefficient decreases with the increase in the temperature difference and as condensate falls down the tube rows. This agrees with the findings of the theoretical results.

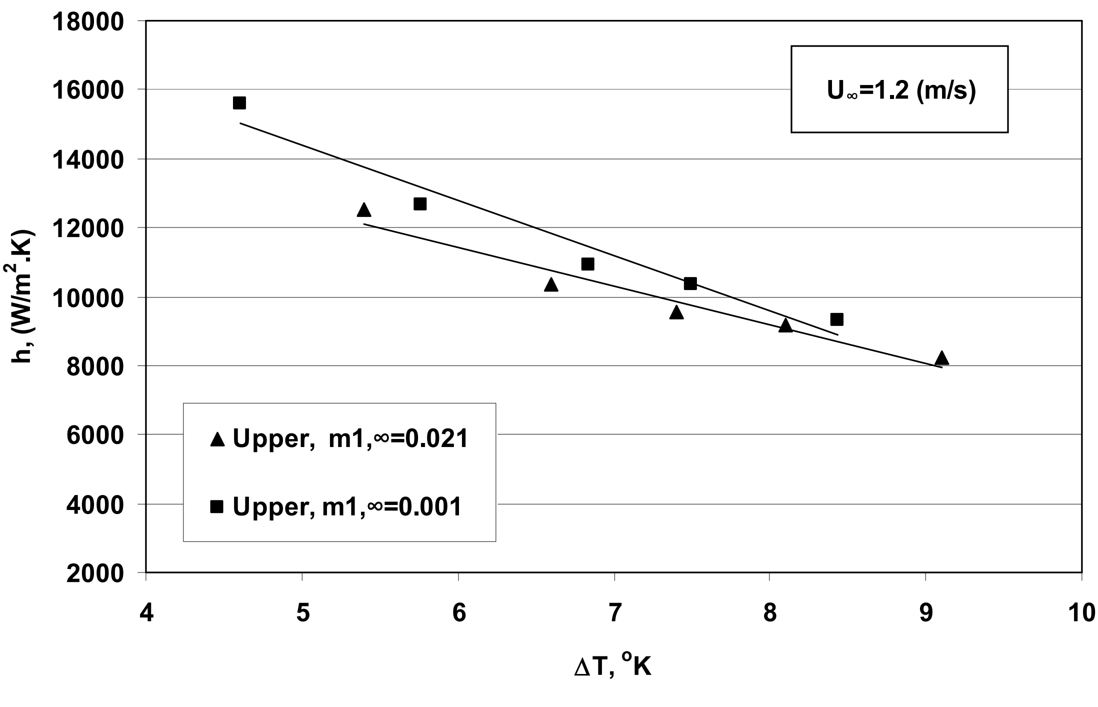


Figure 6.60a Variation of heat transfer coefficient with temperature difference at two values of air fractions for upper cylinder.

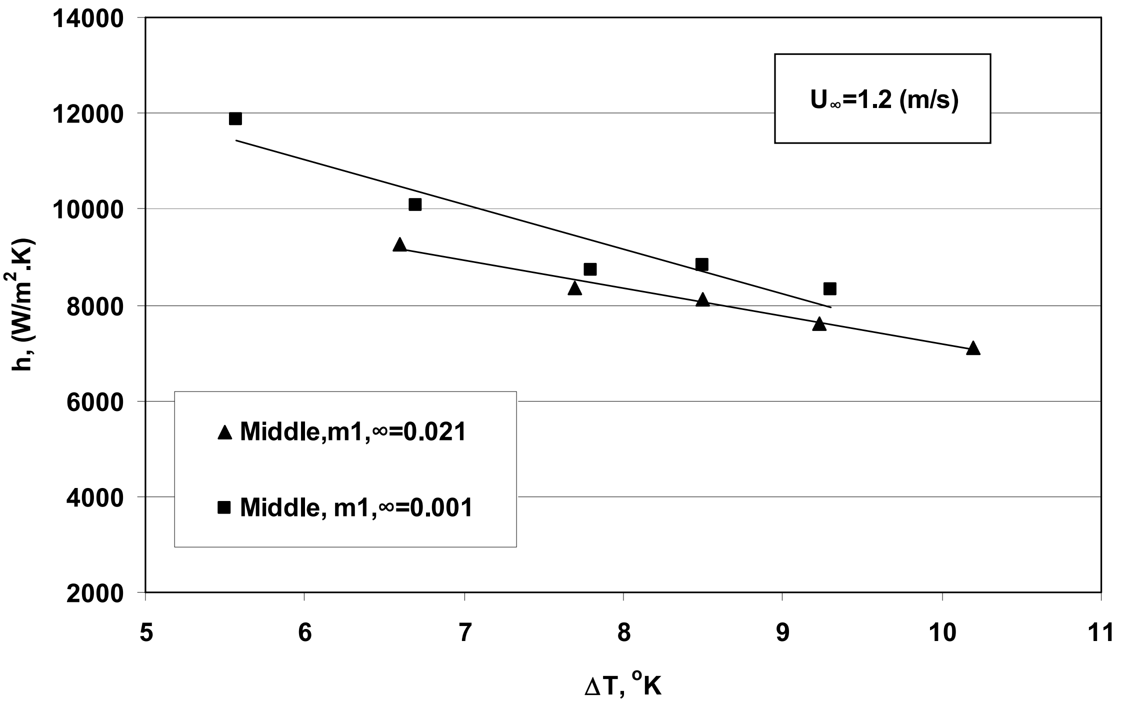


Figure 6.60b Variation of heat transfer coefficient with temperature difference at two values of air fractions for middle cylinder.

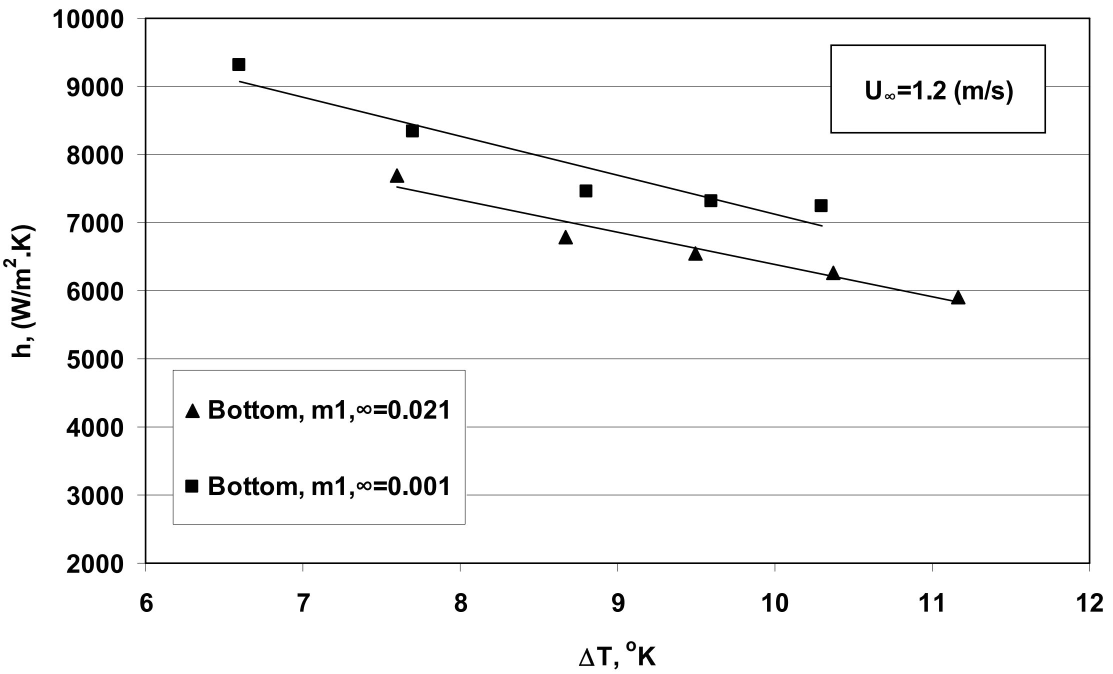


Figure 6.60c Variation of heat transfer coefficient with temperature difference at two values of air fractions for bottom cylinder.

### 6.5.3 The effect of the free stream velocity

The effect of the free stream velocity on the heat transfer coefficient for upper, middle and bottom tube rows at different temperature differences is presented in Figure 6.61. Two different values of free stream velocities are considered ($U_\infty$ = 0.012 m/s and $U_\infty$ = 1.2 m/s) at the same air fraction ($m_{1,\infty}$ =0.001).

As expected, experimental results for upper, middle and bottom tube rows revealed that; heat transfer coefficient increases as free stream velocity increases from its lower value of ($U_\infty$ = 0.012 m/s) to the upper one of ($U_\infty$ = 1.2 m/s). In addition, it decreases with the increase in temperature difference and as the condensate falls down on the lower tubes.

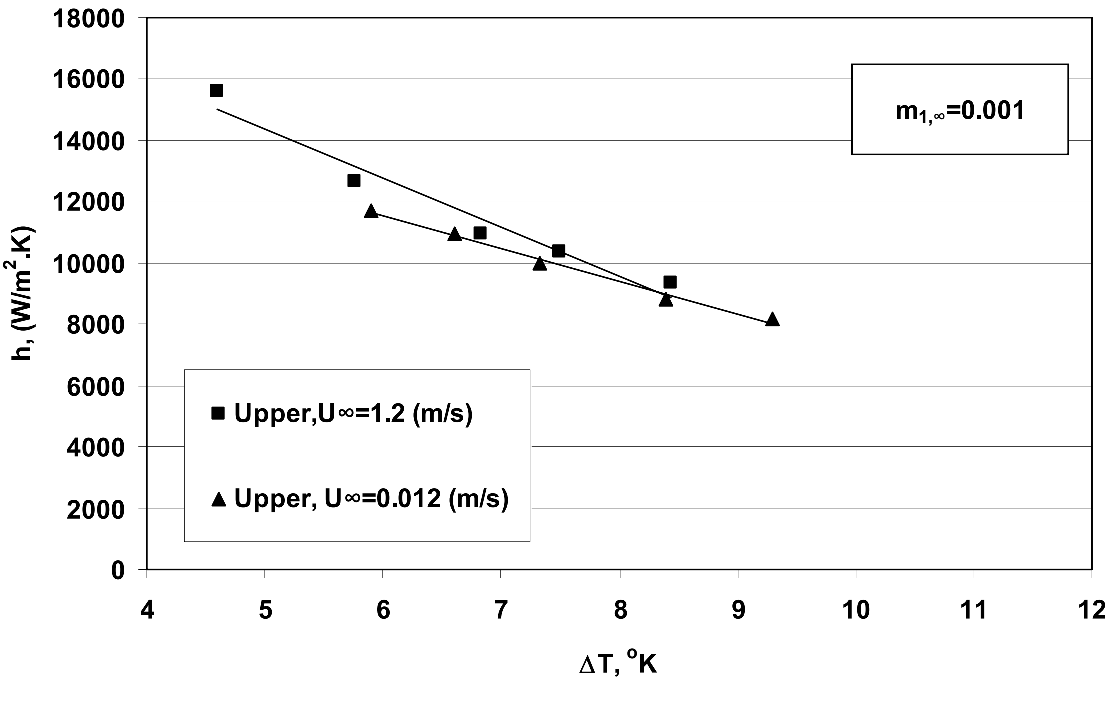


Figure 6.61a Variation of heat transfer coefficient with temperature difference at two values of free stream velocities for upper cylinder.

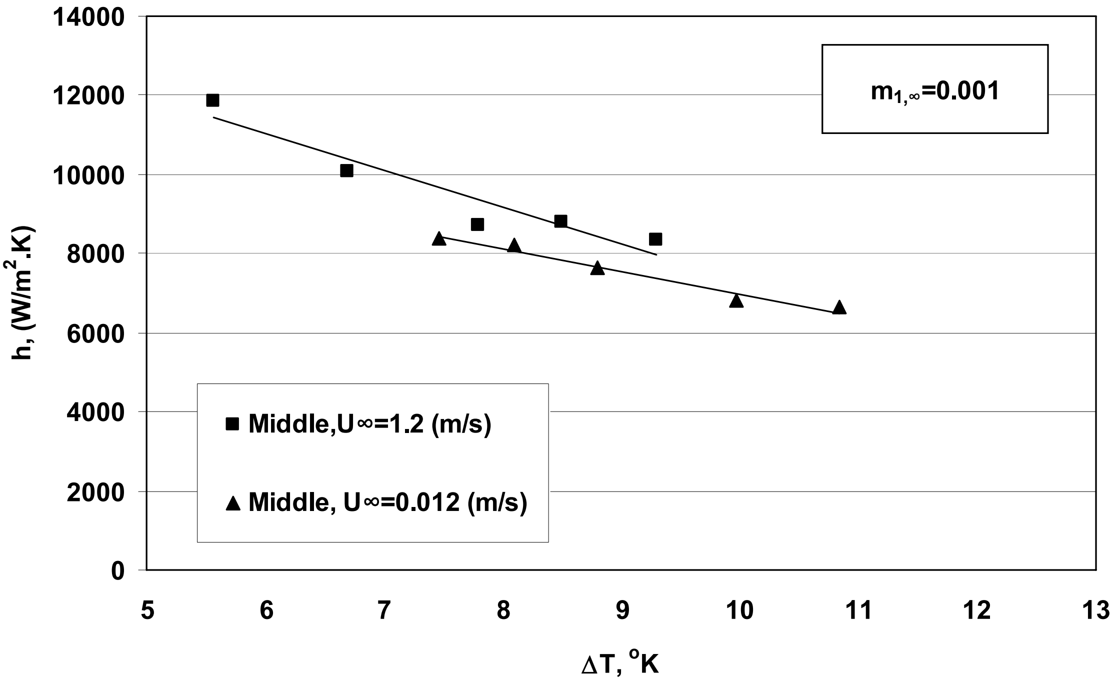


Figure 6.61b Variation of heat transfer coefficient with temperature difference at two values of free stream velocities for middle cylinder.

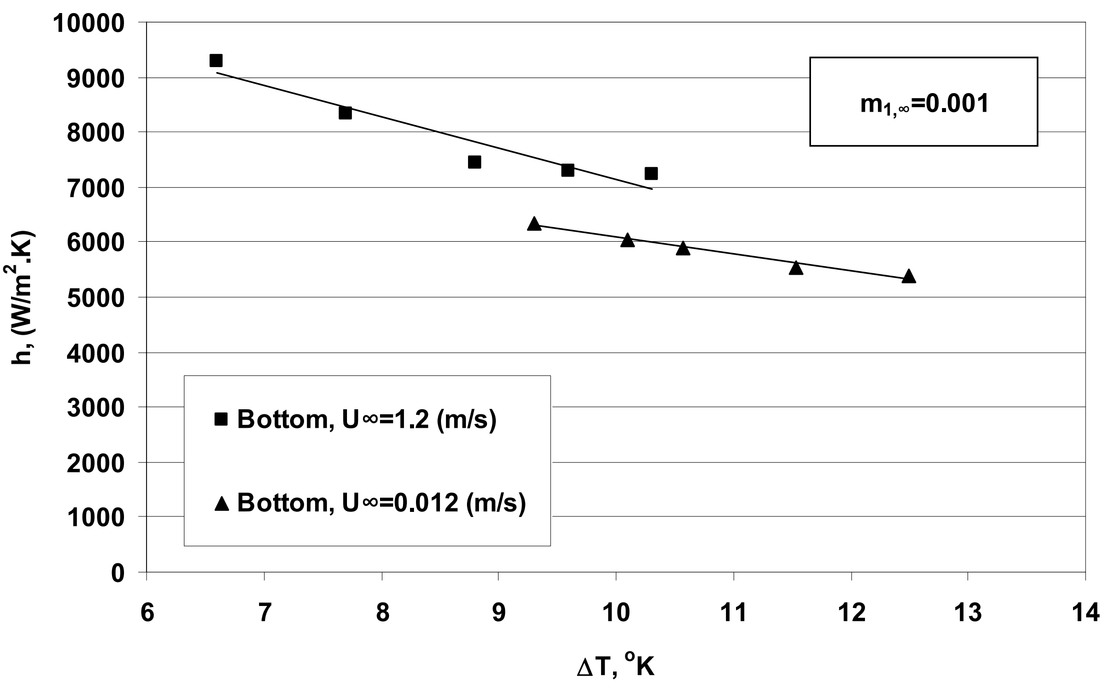


Figure 6.61c Variation of heat transfer coefficient with temperature difference at two values of free stream velocities for bottom cylinder.

### 6.6 Comparison of results

#### 6.6.1 Comparison between the theoretical and experimental results for the present study

Theoretical results for average heat transfer coefficient down the tube bundle are compared with those obtained from experimentation. Figure 6.62 illustrates the comparison between the average heat transfer coefficient for two different air fractions ($m_{1,\infty}$ = 0.001) and ($m_{1,\infty}$ = 0.021) at the free stream velocity of ($U_\infty$ = 1.2 m/s). As obtained from theoretical results, the higher the air fraction is, the lower the heat transfer coefficient becomes. In addition, average heat transfer coefficient decreases as the condensate falls down on the lower tubes. Some differences are noticed between the theoretical and experimental results. For the low air mass fraction, ($m_{1,\infty}$ = 0.001 ), the numerical results of the average heat transfer coefficient are higher than those for the experimental results by 30% for the upper cylinder, 25% for the middle cylinder and 18% for the bottom cylinder. However, for the higher air mass fraction ($m_{1,\infty}$ = 0.021), the numerical results are lower than those for the experimental results by 11% for the middle cylinder and 30% for the bottom cylinder. For the upper cylinder the numerical results are higher than those for the experimental results by 19%. These discrepancies may be resulted from the errors related to the numerical method used in solving the governing differential equations. These errors include truncation errors and round-off errors. Approximations in the initial profiles and boundary conditions, approximations in the numerical differentiation for interfacial fluxes at the vapor-liquid interface and constant properties assumption are also another possible source of these differences.

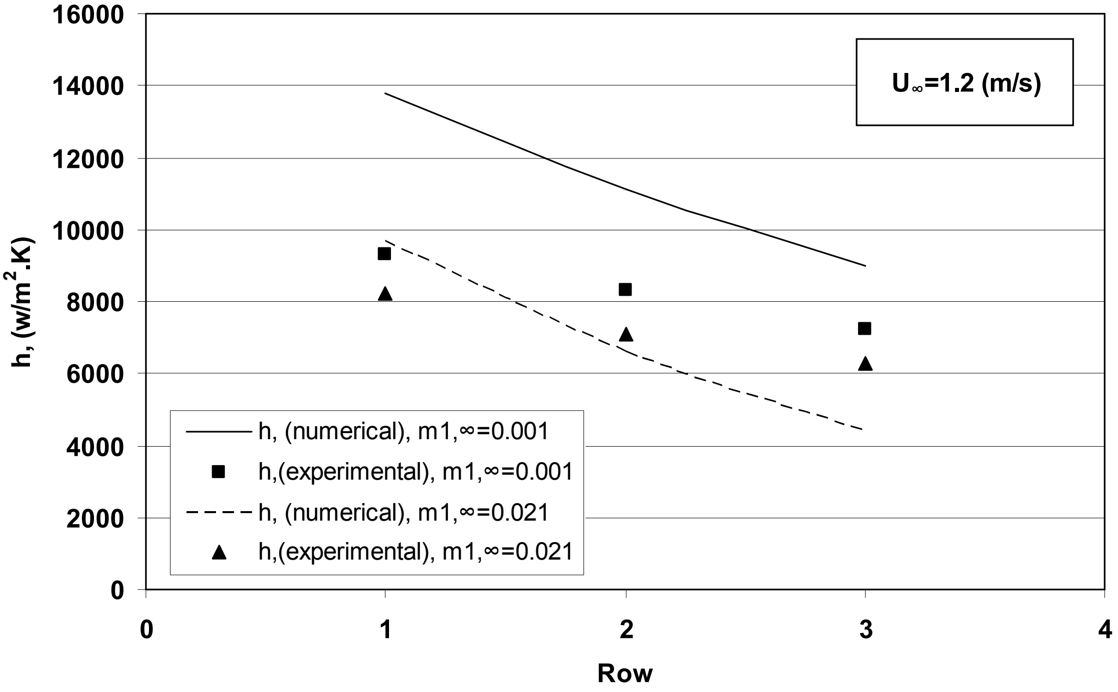


Figure 6.62 Comparison between heat transfer coefficients for the theoretical and experimental results of the present study at two values of air fractions.

Figure 6.63 shows another comparison between the theoretical and the experimental results for the heat transfer coefficient at two values of free stream velocity ($U_\infty$ = 0.012 m/s) and ($U_\infty$ = 1.2 m/s) and at the same air fraction ($m_{1,\infty}$ =0.001). Results show that; any increase in the free stream velocity leads to a corresponding increase in the heat transfer coefficient. As expected, heat transfer coefficient decreases as the condensate falls down the tube bundle. Again, there are many differences between the theoretical and experimental results. For the low free stream velocity, ($U_\infty$ = 0.012 m/s), the numerical results of the average heat transfer coefficient are higher than those for the experimental results by 27% for the upper cylinder, 17% for the middle cylinder and no difference was noticed for the bottom cylinder. Moreover, for the higher free stream velocity, ($U_\infty$ = 1.2 m/s), the numerical results are higher than those for the experimental results by 33% for the upper cylinder, 25% for the middle cylinder and 21% for the bottom cylinder. The differences between the results may be attributed to the same reasons that are mentioned above for Figure 6.62.

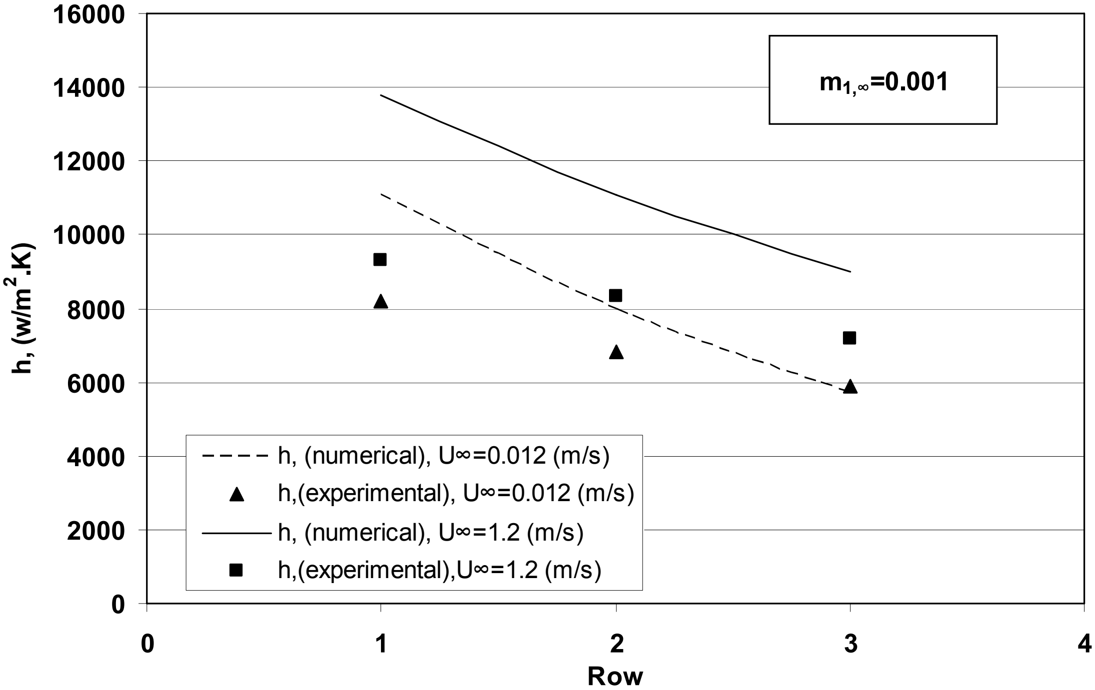


Figure 6.63 Comparison between heat transfer coefficients for the theoretical and experimental results of the present study at two values of free stream velocities.

### 6.6.2 Comparison between the present study results and the literature for pure vapor

In this section, the numerical results of this study are compared to those obtained by some researchers in the literature. Kumar et al. [28] performed an experimental investigation to find the heat transfer coefficient during condensation of steam over a plain tube, a circular integral-fin tube and a spine integral-fin tube. Their experiments, which were conducted on a plain copper tube, are of interest and the comparison between the upper tube of the present study and the study of Kumar et al. is given in Figure 6.64. The copper condensation tube has an outside diameter of 22.21 mm and an inside diameter of 18.42 mm. Kumar et al. stated that their experimental values of heat transfer coefficients are higher than those predicted by Nusselt's model in a range of 5 to 15 percent. Figure 6.64 reveals that; the numerical results for this study are also higher than those predicted by Nusselt's model by about 22% and those predicted by Kumar et al. [28] by about 15%. This is attributed to the errors related to the numerical method used in solving the governing differential equations. These errors include truncation errors, round-off errors. Approximations in the initial profiles and boundary conditions are also another possible source of these differences.

Experimental results of heat transfer coefficients for Makas [61] are slightly lower than those predicted by Nusselt Model by about 5% and about 10% for those obtained by Kumar et al. The differences between the experimental data of Makas [61] and the literature may result from the differences in test section dimensions, tube diameter and the experiment conditions and different parameters ranges. In addition, Air that may be present with steam is another reason for these discrepancies.

Table 6.1 shows a comparison between the experimental, Makas [61] and the present study numerical heat transfer rates for the present experimental study at different inclination angles. As expected, the rate of heat transfer for the upper tube does not significantly change in the experiments which were conducted at different angles. This result is also validated by the numerical results. However, it is seen that the heat transfer rates are slightly increased for the second and third tubes by increasing the inclination of the rows.

Table 6.1 Comparison between experimental, Makas [61] and the present study numerical heat transfer rates at different inclination angles for ($\Delta T=10\ ^{o}K$, d=19mm and L= 65 mm).

| Tube | Q(w) (num) | Q(w) (exp) |
|---|---|---|
| Upper Tube ($\varphi=0$) | 642 | 348 |
| Middle Tube ($\varphi=0$) | 489 | 343 |
| Bottom Tube ($\varphi=0$) | 444 | 337 |
| Middle Tube ($\varphi=3$) | 440 | 348 |
| Bottom Tube ($\varphi=3$) | 349 | 340 |
| Middle Tube ($\varphi=6$) | 470 | 351 |
| Bottom Tube ($\varphi=6$) | 392 | 340 |
| Middle Tube ($\varphi=10$) | 510 | 354 |
| Bottom Tube ($\varphi=10$) | 445 | 343 |
| Middle Tube ($\varphi=15$) | 641 | 350 |
| Bottom Tube ($\varphi=15$) | 640 | 349 |

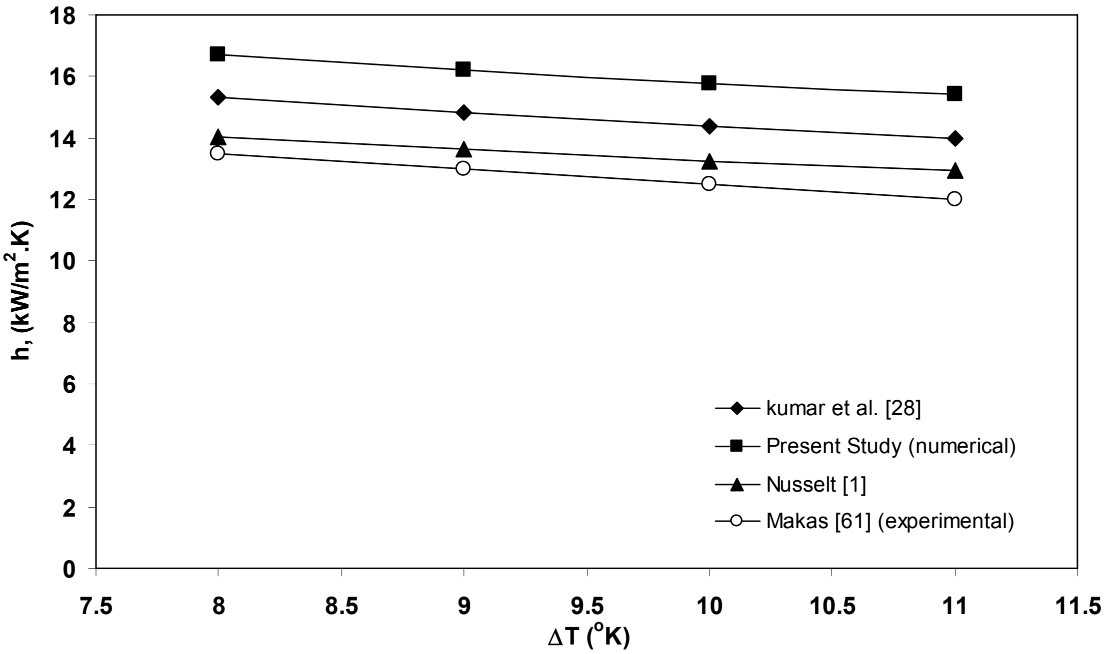


Figure 6.64 Comparison between heat transfer coefficients of the present study and those obtained from the literature.

When compared to heat transfer rates at vertical position ($\varphi = 0$), heat transfer rates are lower at ($\varphi = 3$) and start to increase as the inclination angle increases too. This is attributed to the increase in the film thickness which results in a corresponding increase in the resistance to heat transfer and consequently a decrease in the average heat flux as well. However, as the inclination angle increases, heat transfer rates increase too. This is attributed to the increase in the condensate fall angle ($\theta_o$) which makes the condensate from the upper cylinder falls at a bigger condensate fall angle ($\theta_o$) on the circumference of the cylinder. As a result, it retards the sharp increase in the film thickness grow caused by the condensate fall. Consequently, average heat transfer rates and average heat transfer coefficient are increased as inclination angle increases.

Results that obtained from the present study are also compared with that in the literature. The present results are compared with theory of Nusselt [1], Shekriladze and Gomelauri [8] and experimental data of Abdullah et al. [46], Lee and Rose [45], Michael et al. [24] and Briggs and Sabaratnam [47].

Nusselt [1] showed the effect of row number on the heat transfer due to inundation for pure vapor as;

$$\frac{h_n}{h_1} = n^{-m} \tag{6.3}$$

where ($h_n$) is the average heat transfer coefficient for a row of ($n$) tubes, ($h_1$) is the heat transfer coefficient for the top (single) tube and $m$ is a constant ($m = 0.25$).

The theoretical result of Shekriladze and Gomelauri [8] for forced convection condensation on a single tube for pure vapor is;

$$\frac{Nu}{\mathrm{Re}^{1/2}} = \frac{0.9 + 0.728F^{1/2}}{(1.0 + 3.44F^{1/2} + F)^{1/4}} \tag{6.4}$$

This approach ignores inundation and takes into account only of the decreasing vapor velocity down the bank.

Figure 6.65 shows a comparison of the present study data with the theory of Nusselt [1], Shekriladze and Gomelauri [8] and the experimental data of Abdullah et al. [46], Lee and Rose [45] and Briggs and Sabaratnam [47].

Although small differences are noticed, the present study data show a good agreement with the Nusselt theory. This is expected since the methodology used in this study is mainly based on Nusselt model and assumptions. Again, truncation and round-off errors beside the approximations in the initial profiles and boundary conditions may be the cause of such discrepancies between this study results and the theory. As expected, average heat transfer coefficient decreases down the bank of tubes. This results from the inundation from upper cylinder on the lower cylinder.

The present study numerical results are inline and in a satisfactory agreement with the theory and experiment. Although the present study numerical data are obtained at a very low vapor velocity, quiescent, the data from literature are obtained at higher vapor velocities as indicated in the figure below. The higher the vapor velocity is, the higher the heat transfer coefficient becomes. This explains the increase in the heat transfer coefficient of the literature data as compared to that of the present study data. The increase in the heat transfer coefficient results from the high shear drag forces that correspond to the increase in the vapor velocities. This leads to a significant decrease in the film thickness and lower the heat transfer resistance through the liquid boundary layer. As a result, heat transfer rates are increased and hence the heat transfer coefficients. It should be noted that the numerical results for this study were obtained based on the setup dimensions and the experimental working conditions for an earlier experimental study conducted by Makas [61] at the METU laboratory. A comparison reveals that there is a satisfactory agreement between the present study numerical results and the data obtained by Makas [61].

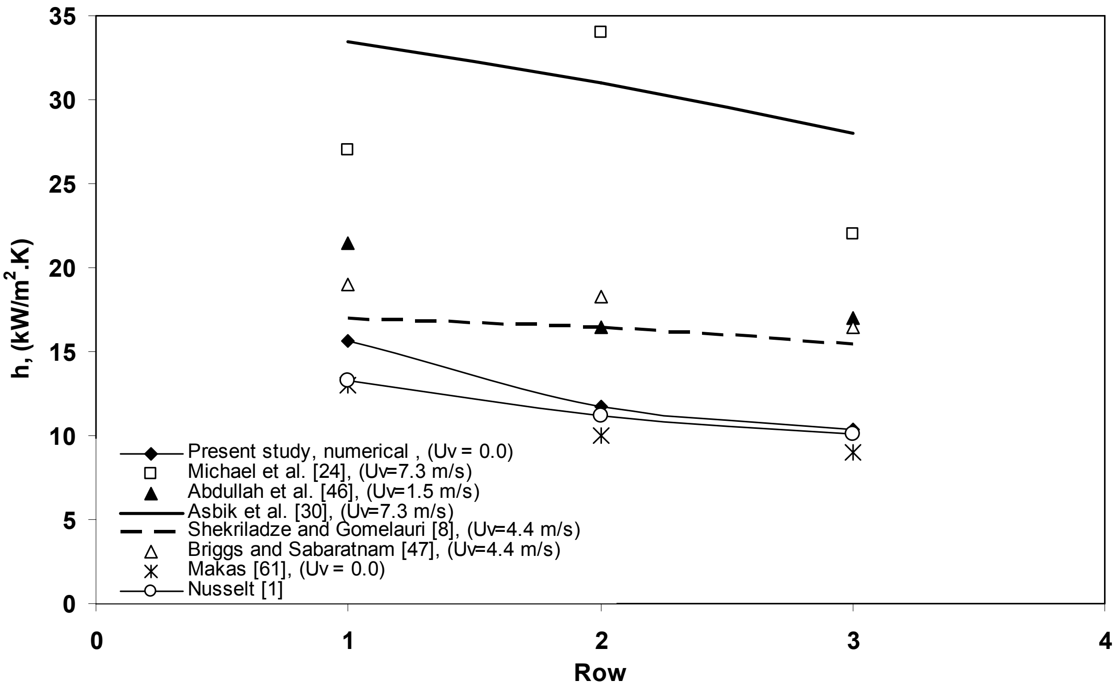


Figure 6.65 Comparison between the present study results with the theoretical and the experimental data in the literature.

### 6.6.3 Comparison between the present study results and the literature for vapor-air mixture

The comparison with the results obtained by Denny and SouthIII [39] is presented in Figure 6.66 and Figure 6.67. Denny and SouthIII studied the effects of noncondensables and temperature difference on the dimensionless heat flux for stagnation point heat transfer from saturated vapor mixtures undergoing forced flow over a horizontal cylinder. Comparison of the numerical results of this study with the literature show that; the dimensionless heat fluxes found by the present numerical study results are slightly higher than those found by Denny and SouthIII [39]. This deviation is more remarkable when the free stream velocity is increased to $U_\infty$=3.05 m/s, as shown in Figure 6.67. This is attributed to the effect of the shear drag at the vapor-liquid interface that tends to decrease the film thickness and consequently increases the dimensionless heat flux. In addition, it may be resulted from the assumptions made concerning the present study such as the constant properties assumption. On the other hand, the variable properties assumption is considered by Denny and SouthIII. Another source of the difference is the approximation errors resulted from the numerical approximations that used when treating the implicit finite difference scheme. These errors in the numerical approximations for this study may be resulted from truncation errors in the finite difference approximations for vapor side boundary layer equations, approximations in the numerical differentiation for interfacial fluxes and constant properties assumption and errors in initial conditions and profiles. Another possible source of these discrepancies is the difference between the numerical methods that were used in the solution of the problem. Similarity approach was used by Denny and SouthIII [39]. Whereas, an implicit finite difference method is used in this study.

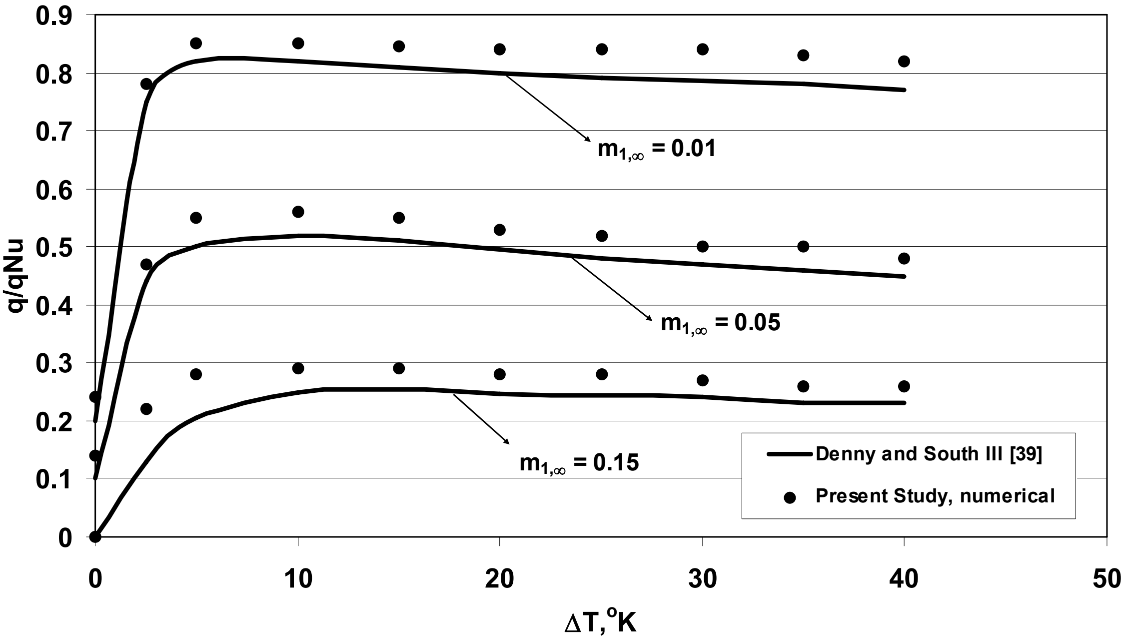


Figure 6.66 Effects of $T_\infty - T_w$ and $m_{1,\infty}$ on condensation heat transfer for steam-air;

($P_\infty = 100\,kPa, U_\infty = 0.305\,m/s\ and\ R = 0.01905m$).

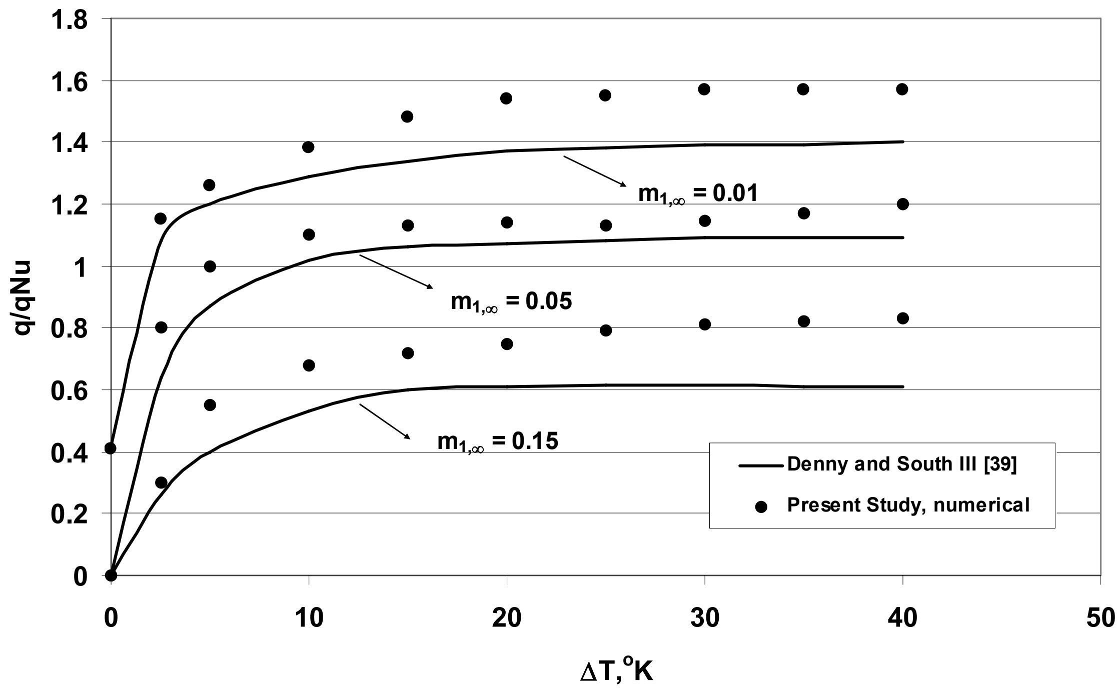


Figure 6.67 Effects of $T_\infty - T_w$ and $m_{1,\infty}$ on condensation heat transfer for steam-air;($P_\infty = 100\,kPa, U_\infty = 3.05\,m/s\ and\ R = 0.01905m$)

For the studies concerning the film condensation heat transfer of vapor or vapor-air mixture flowing downward tier of tubes, results obtained from the present study are compared with the experimental and the theoretical data presented in the literature. The steam-air results are compared with theory of Nusselt [1], Shekriladze and Gomelauri [8] and Rose [44]. Experimental data of Abdullah et al. [46], Lee and Rose [45] and Briggs and Sabaratnam [47] and [48] are also considered.

Nusselt [1] showed the effect of row number on the heat transfer due to inundation for pure vapor according to Equation (6.3).

The theoretical result of Shekriladze and Gomelauri [8] for forced convection condensation on a single tube for pure vapor is shown in Equation (6.4).

For vapor-air mixture, Rose [44] developed an approximate equation for forced convection condensation on a single horizontal tube in the presence of non-condensing gas. This equation is expressed as a relationship between the heat flux to the condensate film and the difference in air mass fractions between the free stream vapor and that at the liquid–vapor interface.

$$\frac{qd}{h_{fg}\rho D_{12}} = 0.5\,\mathrm{Re}^{1/2}\left[\left(1.0 + 2.28 Sc^{1/3}\,\frac{m_{1,i} - m_{1,\infty}}{m_{1,\infty}}\right)^{1/2} - 1.0\right] \tag{6.5}$$

The procedure of using Equation (6.4) and Equation (6.5) in comparison with the experimental results was stated by Abdullah et al. [46] by coupling both equations in order to determine heat flux or heat transfer coefficient. Starting with the measured wall temperature and the free stream vapor –air mixture temperature and a guessed interface temperature, the heat fluxes given by Equation (6.4) and Equation (6.5) were determined. The two measured heat fluxes were then compared, and if the difference was greater than 0.1%, an improved estimate of the interface temperature was made and the process was continued until convergence was achieved. It should be noted that Equation (6.4) is used to determine heat flux or heat transfer coefficient for liquid boundary layer and Equation (6.5) is used to determine those at vapor–gas side boundary layer.

Figure 6.68 shows a comparison of the present study data with the theory of Nusselt [1], Shekriladze and Gomelauri [8] and Rose [44] and the experimental data of Abdullah et al [46] for steam-air mixture free stream velocity of $U_\infty = 1.5$ *m/s*, different free stream air-mass fractions up to *10%* and different coolant velocities of $U_c=1.8$ *m/s* and $U_c=3.3$ *m/s* under atmospheric pressure conditions. Although small differences are noticed, Present numerical study results show a good agreement with the theory and experimentation. As expected, average heat transfer coefficient decreases down the bank of tubes. In addition, the effect of the free stream non-condensable gas (air) fractions is to reduce the average heat transfer coefficient as air–mass fractions increases. This agrees with the theory and the present study results. This is quite obvious when results are compared with Nusselt theory [1] for pure vapor.

Based on the graphs below, the differences in the results get smaller when free stream air-mass fractions are small. This agrees with the findings of Abdullah et al [46]. They mentioned that the applicability of single tube theory, coupled with the assumption of one dimensional flow, to banks of tubes can yield satisfactory results for high vapor velocities and low air concentrations for the first three rows at the top of the bank.

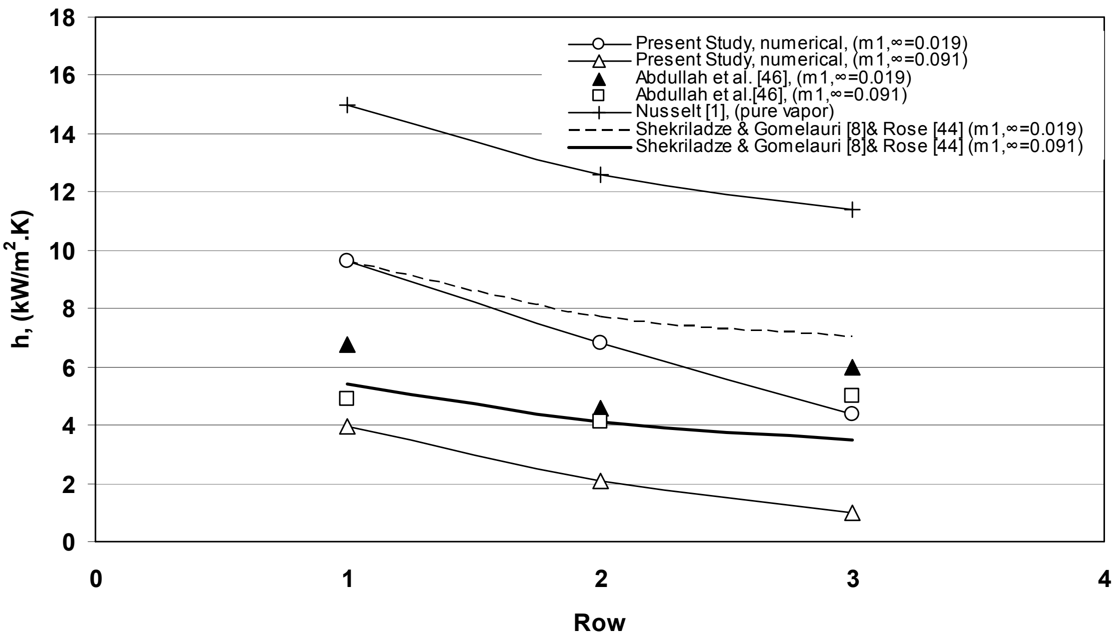


Figure 6.68a Comparison of theory and experiment for steam-air mixture ($U_c=1.8$ *m/s*).

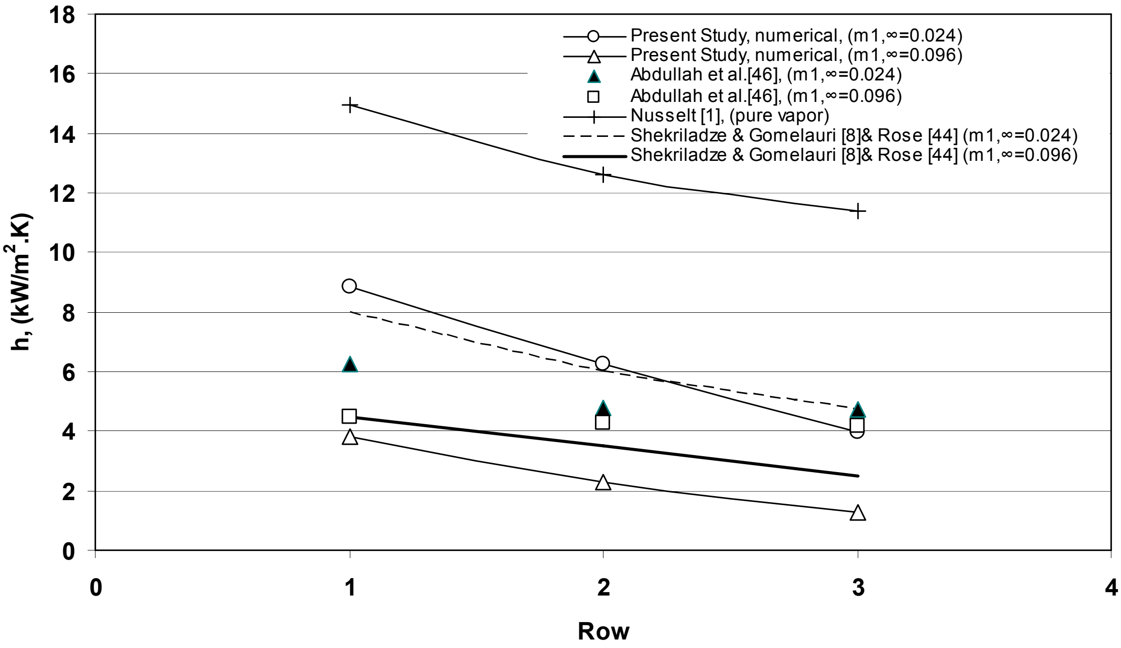


Figure 6.68b Comparison of theory and experiment for steam-air mixture ($U_c$=3.3 m/s)

In view of Equation (6.5), the present study results are compared with the theory of Rose [44] and the experimental data obtained by Abdullah et al [46], Lee and Rose [45] and Briggs and Sabaratnam [48] as shown in Figure 6.69. The present study numerical results are relatively higher than those obtained by Abdullah et al.[46] and Rose [44]. However, it shows good agreement with the data of Abdullah et al. [46] at tube rows down the bank, namely, at rows 7, 8 and 9, these data are corresponds to the range (1-2) for the ratio ($m_{1,i} / m_{1,\infty}$) as seen in Figure 6.69 below. When compared with the data of Lee and Rose [16], numerical results of the present study show a good agreement in the range (18-38) for the ratio ($m_{1,i} / m_{1,\infty}$) at x-axis of the figure below. Moreover, it shows a good agreement with the data of Briggs and Sabaratnam [48] in the range (3-10) for the ratio ($m_{1,i} / m_{1,\infty}$).

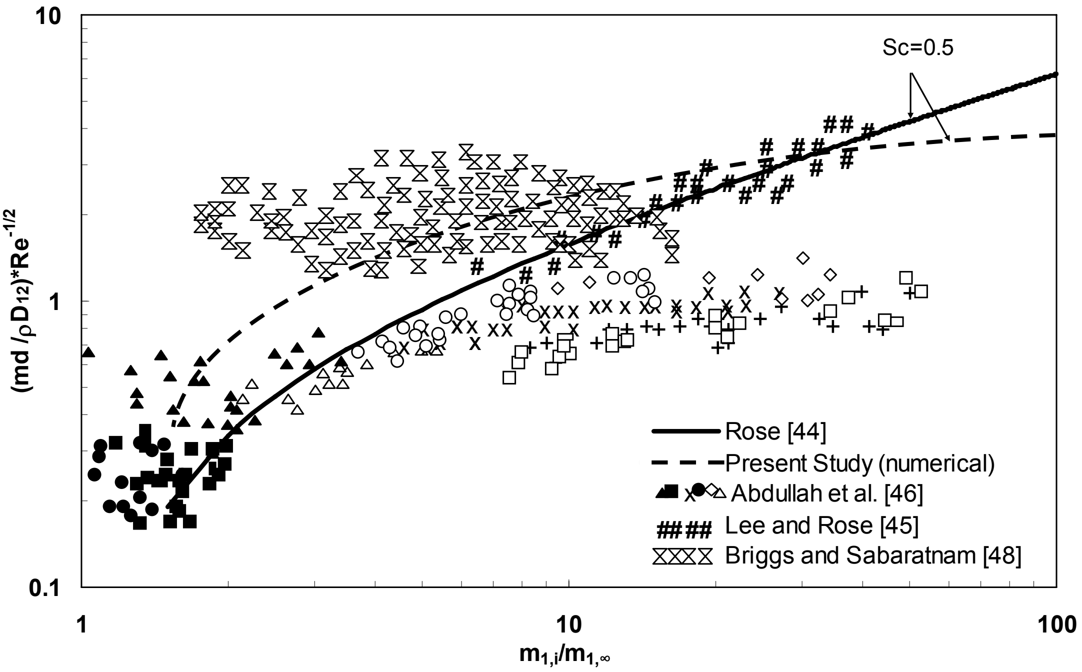


Figure 6.69 Comparison of steam-air mixture data with Equation (6.5).

Figure 6.70 and Figure 6.71 show a comparison of the present study results with the combined theory of Shekriladze and Gomelauri [8] and Rose [44] and with the experimental data of Briggs and Sabaratnam [47].

The variation of heat flux, $q$, with vapor-side temperature difference at free stream velocity of $U_{\infty} = 1.2\ m/s$ and a range of free stream air fractions of (6.2 – 29%) is illustrated in Figure 6.70a. A remarkable reduction in heat flux is observed as free stream air-mass fraction increases. The present results are in a reasonable agreement with the combined theory of Shekriladze and Gomelauri [8] and Rose [44], whereas, they are under predicting the experimental data by about 30% for a condensation on a single tube which presented by Briggs and Sabaratnam [47].

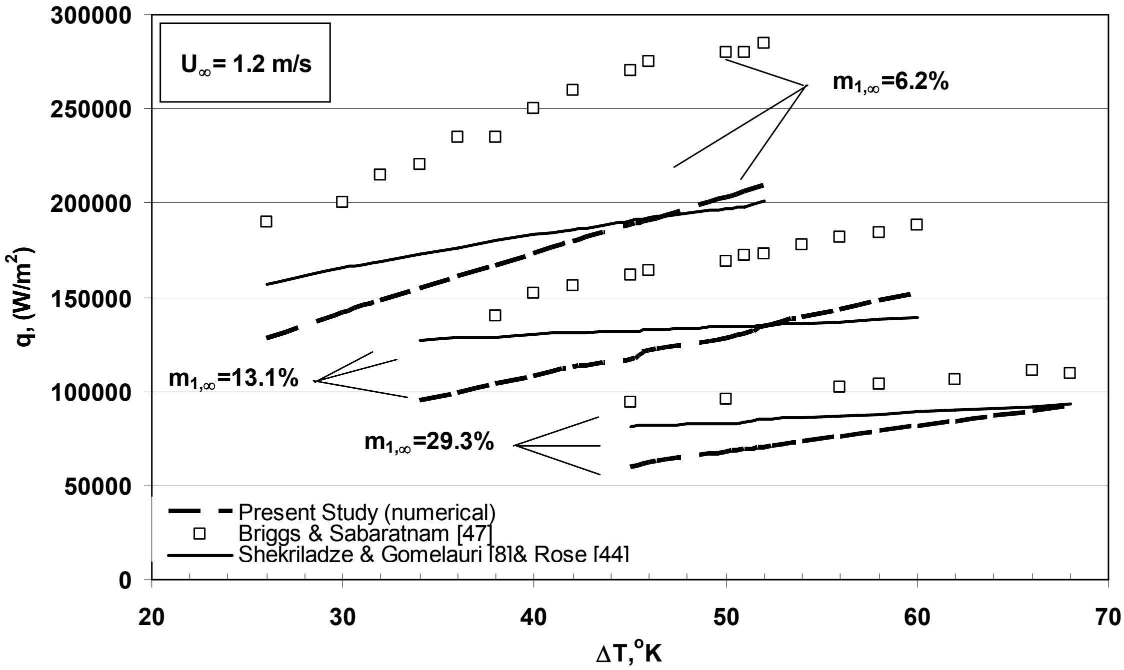


Figure 6.70a Effect of free stream air concentrations on condensation from steam-air mixtures-comparison with theory and experiment.

The effect of the free stream velocity on the condensation from steam-air mixtures is illustrated in Figure 6.70b. The free stream velocity is allowed to vary from ($U_\infty = 1.2$ *m/s* to $U_\infty = 3.6$ *m/s*) at free stream air-mass fraction of ($m_{1,\infty} = 6.1\%$). As expected, heat flux, $q$, increases as free stream velocity increases. In comparison with the combined theory of Shekriladze and Gomelauri [8] and Rose [44] and the data of Briggs and Sabaratnam [47], the present data show a good agreement with the combined theory at free stream velocity of ($U_\infty = 1.2$ *m/s*). In the other hand, they are under predicting the results of the combined theory by about 30% at higher stream velocity of ($U_\infty = 3.6$ *m/s*). When compared with the data of Briggs and Sabaratnam [47], the present results are under predicting their data by about 37% at ($U_\infty = 3.6$ *m/s*) and about 30% at ($U_\infty = 1.2$ *m/s*).

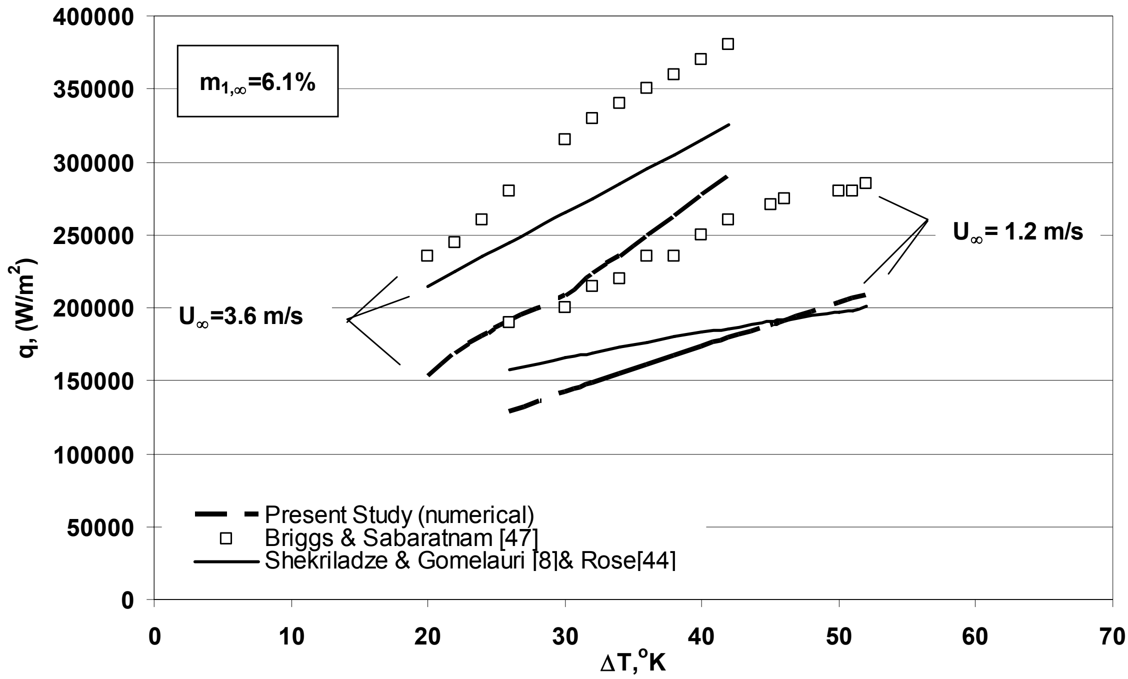


Figure 6.70b Effect of free stream vapor velocity on condensation from steam-air mixtures-comparison with theory and experiment.

Figure 6.71a and Figure 6.71b show the effect of free stream air-mass fraction on the heat transfer coefficient down tube bank. Free stream air–mass fractions are varied between ($m_{1,\infty}$ =1.2% to $m_{1,\infty}$ =15.2% ) for coolant velocity of ($U_c$ =3.2 m/s) and free stream velocities of ($U_\infty$ =4.4 m/s and $U_\infty$ =7.0 m/s). The present data are compared with the combined theory of Shekriladze and Gomelauri [8] and Rose [44] and the data of Briggs and Sabaratnam [47]. The present data are under predicting the experimental data of Briggs and Sabaratnam [47]. They are in reasonable agreement when compared with the combined theory of Shekriladze and Gomelauri [8] and Rose [44] at higher free stream air- mass fractions. However, the agreement is poor for lower free stream air-mass fractions.

This agrees with the findings of Briggs and Sabaratnam [47]. They concluded that; the agreement between the combined theory of Shekriladze and Gomelauri [8] and Rose [44] and their experimental data was very poor. The theoretical heat transfer coefficients up to 60% lower than those found experimentally. They attributed that to unclear reasons.

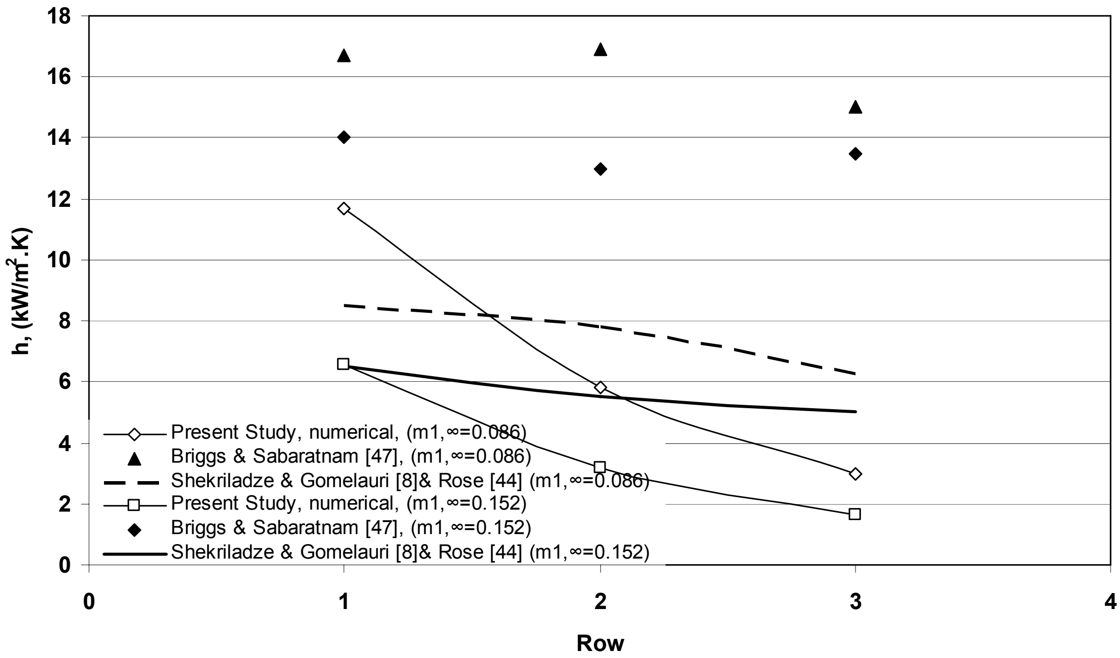


Figure 6.71a Effect of air fractions and free stream vapor velocity on condensation from steam-air mixtures, comparison with theory and experiment ($U_\infty$= *4.4 m/s*).

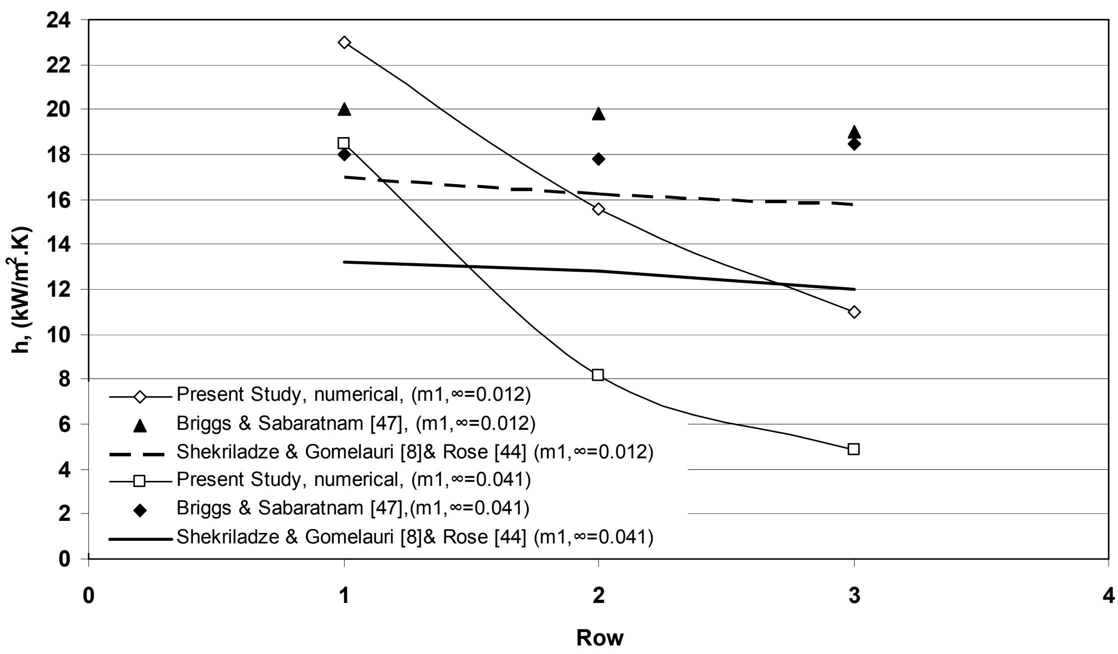


Figure 6.71b Effect of air fractions and free stream vapor velocity on condensation from steam-air mixtures, comparison with theory and experiment ($U_\infty$= *7.0 m/s*).

They thought that the increased mixing and re-circulation of the steam-air mixture down the bank may be act to enhance heat transfer compared to the situation of single tube. In addition, they stated that; results of Abdullah et al. [46] found better agreement with single tube theory for steam-air mixture on a bank of tubes but the vapor-gas velocities used in Abdullah et al [46] work were much lower than those used in their experimental work.

In summery, the present results show a good agreement with the combined theory of Shekriladze and Gomelauri [8] and Rose [44] and with the data of Abdullah et al. [46] and Briggs and Sabaratnam [48]. However, they show a poor agreement with the data of Briggs and Sabaratnam [47].

In the above figures, the small differences between the present results and the theoretical results of Shekriladze and Gomelauri [8] and Rose [44] and experimental data of Abdullah et al. [46] may be explained in view of the following facts;

The deviations in the present study results may be resulted from the approximations in the initial profiles and errors related to the implicit finite difference scheme used to solve the governing differential equations of the problem. These errors include truncation errors and round off errors.

The flow of pure vapor or vapor-air mixture down the tube banks is generally three dimensional and it involves complex interactions between vapor and condensate. As a result, simplifications and approximations were made in order to formulate the governing differential equations and supplementary equations that control the physical behavior of the condensation heat transfer. In addition, the combined effect of the increase in the air concentration, reduction in vapor velocity and inundation on the condensation heat transfer down the tube bank may result in such errors and deviations from the experimental data.

Increased mixing and recirculation of vapor-gas mixture down the tube bank may be act to enhance condensation heat transfer [47]. Down the bank, where air concentrations were higher and vapor velocities lower, discrepancies appeared between the theory and experiment may result from the buoyancy effects influencing the build up of air on the lower tubes [46].

# CHAPTER 7

# CONCLUSIONS AND RECOMMENDATIONS

## 7.1 Conclusions

Numerical and experimental results for laminar forced film condensation of pure vapor and vapor-air mixture on a bundle of tubes at different inclination angles are analyzed and discussed. Inline and staggered arrangements are considered. Suitable assumptions and approximations in the initial profiles, the boundary conditions, and the liquid–vapor interface flux equations are considered. The constant properties assumption is also taken into consideration. The main concluded points of this theoretical and experimental investigation can be summarized as;

1. Presence of non-condensable gas (air) in the vapor has a negative effect on the film condensation heat transfer phenomenon. Even for very small air mass fractions, a remarked reduction in the heat transfer rates and heat transfer coefficient is noticed.

2. The increase in the free stream velocity leads to a corresponding increase in the shear drag which in turn increases the heat transfer rate and heat transfer coefficient as well.

3. Down the bank, a rapid decrease in the vapor side heat transfer coefficient is remarked. It may be resulted from the combined effects of inundation, decrease in the vapor velocity and increase in the non-condensable gas (air). In addition, buoyancy effects may be dominant for vapor-air mixture at the bottom of the bank.

4. In order to study the effect of staggering of the cylinders on the heat transfer rates and to see how condensation is affected at the lower cylinders when condensate does not fall on to the center line of the cylinders, the whole setup is allowed to incline at different inclination angles.

5. As the cylinder diameter and the temperature difference increase, heat transfer coefficient and heat transfer rate decrease. Moreover, a remarked improvement in the heat transfer rate and the heat transfer coefficient is noticed at the middle and the bottom cylinders when the angle of inclination is increased. However, no significant change is observed for that of the upper cylinder.

6. Critical angle of inclination increases by increasing the diameter of the cylinder whereas the condensate fall angle decreases.

7. Liquid film thickness increases to about two times in the case of zero pressure gradients when compared to that when pressure gradient is considered.

8. For zero pressure gradients, results of the film condensation heat transfer are similar to that for flat plates. A remarked increase in the dimensionless heat flux, local heat transfer coefficient and local Nusselt number is noticed when pressure gradient is considered especially near the forward stagnation point of the cylinder.

9. For pure vapor, a good agreement with the Nusselt theory is remarked. In addition, the present study results are inline and in a reasonable agreement with the theory and the experiment in the literature. Referring to Figure 6.64, the numerical results for pure vapor are higher than those predicted by Nusselt's model by about 22% and those predicted by Kumar et al. [28] by about 15%, whereas, experimental results of heat transfer coefficients for this study are slightly lower than those predicted by Nusselt Model by about 5% and about 10% for those obtained by Kumar et al.

10. Comparison of the numerical results obtained by the implicit finite difference scheme for this study with the literature show that; the film condensation heat transfer results found by the present study are slightly higher than those found by the similarity solution of Denny and SouthIII [39]. This may be resulted from the assumptions made concerning the constant properties and the approximation errors from the implicit finite difference scheme used.

11. Although small differences are appeared, a good agreement is noticed for the present study numerical results when compared with the theory of Shekriladze and Gomelauri [8] and Rose [44] and experimental data of Abdullah et al [46] and Briggs and Sabaratnam [48].

12. When the present study numerical results are compared with Briggs and Sabaratnam [47], a poor agreement is noticed. Mixing and re-circulation in the steam-air mixture down the bank may be the reason for these discrepancies.

13. The differences between the numerical and the experimental results for this study and the literature may be resulted from the errors that related to the numerical method used in solving the governing differential equations. These errors include truncation and round off errors, approximations in the numerical differentiation for interfacial fluxes at the vapor-liquid interface, constant properties assumption and approximations in the initial profiles. In addition, unpredictable effects such as re-circulating and mixing in the vapor-air mixture down the tube bank, heat losses from the walls and fittings of the test section and the condensate dripping are also another possible source for these errors. Moreover, the differences between the experimental data of this study and the literature may result from the differences in the test sections dimensions, tubes diameters, tubes material and the experiment working conditions and parameters ranges.

## 7.2 Recommendations

1. Many different tube surface geometries are used to enhance the condensation heat transfer and to reduce the size of the heat exchangers. Finned tubes are a typical example of these geometries. For this purpose, beside the theoretical analysis, the present test section can be used to conduct the experimental work.

2. Constant fluid properties assumption is a common assumption in the analysis of condensation heat transfer phenomenon. Therefore, some errors are resulted. In order to avoid these deviations and discrepancies, variable fluid properties assumption can be considered.

3. For covering most of the engineering applications, different pure and binary vapors could be incorporated in the further studies. In addition, different non-condensable gases could be also tried.

4. The effect of thermal diffusion (Soret effect) and diffusion thermo (Dufour effect) on the condensation heat transfer phenomenon could be also studied and investigated under different conditions.

5. The effect of superheating of vapor-air mixture flowing downward a single cylinder or bank of tubes on the condensation process could be also studied.

6. Different flow pattern regimes are noticed in the liquid film when condensation heat transfer is considered. Namely, laminar, wavy- laminar and turbulent flow depending on the value of the Reynolds number at the liquid film. In further studies, wavy laminar and turbulent flow regimes could be also investigated.

## REFERENCES


[1] Nusselt, W., Die Oberflachen-Kondensation des Wasserdampfes, Zeitschrift des Vereines deutscher Ingenieure, **60**, 541-546, 569-575, 1916.

[2] Sparrow, E. M. and Gregg, J. L., A boundary layer treatment of laminar film condensation, Transactions of the ASME, Journal of Heat Transfer, **81C**, 13-18, February 1959.

[3] Sparrow, E. M. and Gregg, J. L., Laminar condensation heat transfer on a horizontal cylinder, Transactions of the ASME, Journal of Heat Transfer, **81C**, 291-296, November 1959.

[4] Dukler, A. E., Fluid mechanics and heat transfer in vertical falling-film systems, Chemical Engineering Progress Symposium Series No.30, **56**, 1-10, 1960.

[5] Koh, J. C. Y., Sparrow, E. M. and Hartnett, J. P., The two phase boundary layer in laminar film condensation, International Journal of Heat and Mass Transfer, **2**, 69-82, 1961.

[6] Chen, M. M., An analytical study of laminar film condensation: Part 2-Single and multiple horizontal tubes, Transactions of ASME, Journal of Heat Transfer, **83C**, 55-60, 1961.

[7] Koh, J. C. Y., Film condensation in a forced convection boundary layer flow, International Journal of Heat and Mass Transfer, **5**, 941-954, 1962.

[8] Shekriladze, I. G. and Gomelauri, V. I., Theoretical study of laminar film condensation of flowing vapor, International Journal of Heat and Mass Transfer, **9**, 581-591, 1966.

[9] Denny, V. E. and Mills, A. F., Non-similar solutions for laminar film condensation on a vertical surface, International Journal of Heat and Mass Transfer, **12**, 965-979, 1969.

[10] Denny, V. E. and Mills, A. F., Laminar film condensation of a flowing vapor on a horizontal cylinder at normal gravity, Transactions of ASME, Journal of Heat Transfer, **91C**, 495-501, November 1969.

[11] Fujii, T. and Uehara, H., Laminar film condensation on a vertical surface, International Journal of Heat and Mass Transfer, **15**, 217-233, 1972.

[12] Fujii, T. and Uehara, H. and Kurata, C., Laminar filmwise condensation of flowing vapor on a horizontal cylinder, International Journal of Heat and Mass Transfer, **15**, 235-246, 1972.

[13] Fujii, T., Uehara, H., Hirata, K. and Oda, K., Heat transfer and flow resistance in condensation of low pressure steam flowing through tube, International Journal of Heat and Mass Transfer, **15**, 247-260, 1972.

[14] Lee, C. Y. and Marschall, E., Laminar stability analysis of condensate film flow, Warme und Stoffubertragung, **7**, 14-21, 1974.

[15] Gaddis, E. S., Solution of the two phase boundary layer equations for laminar film condensation of vapor flowing perpendicular to a horizontal cylinder, International Journal of Heat and Mass Transfer, **22**, 371-382, 1979.

[16] Rose, J. W., Effect of pressure gradient in forced convection film condensation on a horizontal tube, International Journal of Heat and Mass Transfer, **27**, 39-47, 1984.

[17] Lee, W. C., Rahbar, S. and Rose, J. W., Film condensation of Refrigerant-113 and Ethanediol on a horizontal tube-effect of vapor velocity, Transactions of ASME, Journal of Heat Transfer, **106C**, 524-530, August 1984.

[18] Kutateladze, S. S. and Gogonin, I. I., Heat transfer in condensation of flowing vapor on a single horizontal cylinder, International Journal of Heat and Mass Transfer, **28**, 1019-1030, 1985.

[19] Kutateladze, S. S. and Gogonin, I. I., Investigation of heat transfer in film condensation of flowing vapor on horizontal tube banks, International Journal of Heat and Mass Transfer, **28**, 1831-1836, 1985.

[20] Kutateladze, S. S., Gogonin, I. I. and Sosunov, V. I., The influence of condensate flow rate on heat transfer in film condensation of stationary vapor on horizontal tube banks, International Journal of Heat and Mass Transfer, **28**, 1011-1018, 1985.

[21] Di Marzo, M. and Casarella, M. J., Film condensation over a horizontal cylinder for combined gravity and forced flow, Transactions of ASME, Journal of Heat Transfer, **107C**, 687-695, August 1985.

[22] Churchill, S. W., Laminar film condensation, International Journal of Heat and Mass Transfer, **29**, 1219-1226, 1986.

[23] Honda, H., Uchima, B., Nozu, S., Torigoe, E. and Imai, S., Film condensation of R-113 on staggered bundles of horizontal finned tubes, Transactions of ASME, Journal of Heat Transfer, **114C**, 442-449, May 1992.

[24] Michael, A. G., Lee, W. C. and Rose, J. W., Forced convection condensation of steam on a small bank of horizontal tubes, Transactions of ASME, Journal of Heat Transfer, **114C**, 708-713, August 1992.

[25] Memory, S. B., Lee, W. C. and Rose, J. W., Forced convection film condensation on a horizontal tube-effect of surface temperature variation, International Journal of Heat and Mass Transfer, **36**, 1671-1676, 1993.

[26] Memory, S. B. and Rose, J. W., Effect of variable viscosity in the presence of variable wall temperature on condensation on a horizontal tube, International Journal of Heat and Mass Transfer, **37**, 2321-2326, 1994.

[27] Memory, S. B., Adams, V. H. and Marto, P. J., Free and forced convection laminar film condensation on horizontal elliptical tubes, International Journal of Heat and Mass Transfer, **40**, 3395-3406, 1997.

[28] Kumar, R., Varma, H. K., Mohanty, B. and Agrawal, K. N., Augmentation of outside tube heat transfer coefficient during condensation of steam over horizontal copper tubes, International Communications in Heat and Mass Transfer, **25**, 81-91, 1998.

[29] Browne, M. W. and Bansal, P. K., An overview of condensation heat transfer on horizontal tube bundles, Applied Thermal Engineering, **19**, 565-594, 1999.

[30] Asbik, M., Daif, A., Pandy, P.K. and Khmou, A., Numerical study of laminar condensation of downward flowing vapor on a single horizontal cylinder or a bank of tubes, The Canadian journal of chemical engineering, **77,** 54-61, 1999.

[31] Mosaad, M., Combined free and forced convection laminar film condensation on an inclined circular tube with isothermal surface, International Journal of Heat and Mass Transfer, **42**, 4017-4025, 1999.

[32] Kumar, R., Varma, H. K., Mohanty, B. and Agrawal, K. N., Augmentation of heat transfer during filmwise condensation of steam and R-134a over single horizontal finned tubes, International Journal of Heat and Mass Transfer, **45**, 201-211, 2002.

[33] Cavallini, A., Censi, G., Del Col, D., Doretti, L., Longo, G. A., Rossetto, L. et al, Condensation inside and outside smooth and enhanced tubes-a review of recent research, International Journal of Refrigeration, **26**, 373-392, 2003.

[34] Minkowycz, W. J., Laminar film Condensation of water vapor on an isothermal vertical surface, Ph.D. dissertation, University of Minnesota, 1965.

[35] Minkowycz, W. J. and Sparrow, E. M., Condensation heat transfer in the presence of noncondensables, interfacial resistance, superheating, variable properties, and diffusion, International Journal of Heat and Mass Transfer, **9**, pp1125-1144, 1966.

[36] Sparrow, E. M., Minkowycz, W. J. and Saddy, M., Forced convection condensation in the presence of noncondensables and interfacial resistance, International Journal of Heat and Mass Transfer, **10**, pp1829-1845, 1967.

[37] Denny, V. E., Mills, A. F. and Jusionis, V. J., Laminar film condensation from a steam-air mixture undergoing forced flow down a vertical surface, Transactions of the ASME, Journal of Heat Transfer, **93**, pp 297-304, August 1971.

[38] Jusionis, V. J., Effects of noncondensables, forced flow and variable properties on film condensation of pure and binary vapors, Ph.D dissertation, University of California, Los Angeles, 1971.

[39] Denny, V. E. and South III, V. , Effects of forced flow, noncondensables and variable properties on film condensation of pure and binary vapors at the forward stagnation point of a horizontal cylinder, International Journal of Heat and Mass Transfer, **15**, pp 2133-2142, 1972.

[40] Al-diwany, H. K. and Rose, J. W., Free convection film condensation of steam in the presence of noncondensing gases, International Journal of Heat and Mass Transfer, **16**, pp 1359-1369, 1973.

[41] Saddy, M. and Del Pozo, F. V., Enhancement of condensation heat transfer in the presence of noncondensable by viscous dissipation, International Journal of Heat and Mass Transfer, **17**, pp 933-943, 1974.

[42] Srzic, V., Modeling of mixed-convection laminar film condensation from mixtures of a vapor and a lighter noncondensable gas, M.Sc. Thesis, University of Manitoba, Canada, 1997.

[43] Srzic, V., Soliman, H. M. and Ormiston, S. J., Analysis of laminar mixed-convection condensation on isothermal plates using the full boundary-layer equations: mixtures of a vapor and a lighter gas, International Journal of Heat and Mass Transfer, **42**, pp 685-695, 1999.

[44] Rose, J. W., Approximate equations for forced convection condensation in the presence of a noncondensing gas on a flat plate and horizontal tube, International Journal of Heat and Mass Transfer, **23**, pp 539-546, 1980.

[45] Lee, W. C. and Rose, J. W., Forced convection film condensation on a horizontal tube with and without non-condensing gases, International Journal of Heat and Mass Transfer, **27**, pp 519-528, 1984.

[46] Abdullah, R., Cooper, J. R., Briggs, A. and Rose, J. W., Condensation of Steam and R-113 on a Bank of Horizontal Tubes in the Presence of a noncondensing Gas, Experimental Thermal and Fluid Science, **10**, pp 298-306, 1995.

[47] Briggs, A., and Sabaratnam, S., Condensation of steam in the presence of air on a single tube and a tube bank, International Journal of Energy Research, **27**, pp 301-314, 2003.

[48] Briggs, A., and Sabaratnam, S., Condensation from pure steam and steam-air mixtures on Integral-Fin Tubes in a bank, Journal of Heat Transfer, **127**, pp 571-580, 2005.

[49] White, F. M., Viscous Fluid Flow, McGraw-Hill, 1980.

[50] Hirschfelder, J. O., Curtiss, C.F. and Bird, R.B., Molecular theory of gases and liquids, New York, Wiely, 1954.

[51] Holman, J. P., Heat transfer, McGraw-Hill, U.S.A., 1990.

[52] Incropera, F. P. and DeWitt, D. P., Fundamentals of heat and mass transfer, 3rd edition, Wiley, U.S.A., 1990.

[53] Kakaç, S. and Liu, H., Heat exchangers: selection, rating, and thermal design, CRC Press, Boca Raton, Fla, 1998.

[54] Arpacı, V., Lecture Notes, University of Michigan, 8.9-8.14.

[55] Kline, S. J. and McClintock, F. A., Describing Uncertainties in Single Sample Experiments, Mechanical Engineering, pp3-9, 1953.

[56] Moffat, R. J., Contributions to the theory of single sample uncertainty analysis, Transactions of the ASME, Journal of Fluids Engineering,**104**, pp 250-260, 1982.

[57] Yamalı, C., Dropwise Condensation Under High Gravity and At Large Subcooling, Ph.D. Dissertation, University of Michigan, 1983.

[58] Fox, R.W. and Mcdonald, A. T., Introduction to fluid mechanics, $2^{nd}$ edition, John Wiely and Sons, Inc., New York, 1978.

[59] Potter, M.C., Wiggert, D.C. and Hondzo, M., Mechanics of Fluids, $2^{nd}$ edition, Prentice-Hall, Inc.,1997.

[60] Herman Merte, JR.,Condensation heat transfer, Advances in heat transfer, **9**, pp 181-271, 1973.

[61] Makas, A., Condensation of steam on multiple horizontal tubes, M.Sc thesis, METU, April 2004.

[62] Dogus, E., Laminar filmwise condensation of flowing vapor on sphere, M.Sc thesis, METU, June 2004.

[63] Kaya, E., Effects of off-center angle on the heat transfer coefficient on vertical tier of multiple spherical surfaces, M.Sc thesis, METU, December 2004.

[64] Patankar, S.V., Numerical Heat Transfer and Fluid Flow, Hemisphere, Washington, DC, 1980.

[65] Lee, W. C., Filmwise condensation on a horizontal tube in the presence of forced convection and non-condensing gas, Ph.D thesis, University of London,1982.

[66] Irvine, T.F. Jr. and Liley, P.E., Steam and gas tables with computer equations, Academic press, London, 1984.

[67] Reid , R.C., Prausnitz, J. M. and Sherwood, T.K., The properties of gases and liquids, Third edition, McGraw-Hill, New York, 1977.

# APPENDIX A

## THERMODYNAMIC AND TRANSPORT PROPERTIES

In this section, the properties of steam and air are presented based on the correlations that were used by Srzic [42] in his study. These correlations, which were originally taken from Irvine and Liley [66] define steam saturation temperature and pressure, latent heat of vaporization of steam, liquid density and all the air properties. Moreover, the other properties like specific heat, thermal conductivity and viscosity of steam and liquid water were taken from steam tables provided by Incropera and Dewitt [52].

For steam-air mixture properties, the correlations provided by Hirschfelder et al [50] were followed. These properties include mixture density, mixture viscosity, mixture thermal conductivity and mixture specific heat. Whereas, diffusion coefficient was determined according to Reid et al [67] or according to Hirschfelder et al [50].

### A.1 Free stream pressure and partial pressure of vapor and gas

Under the assumption that the steam is at saturation state at the free stream, free stream pressure for a given $m_{1,\infty}$ and $T_\infty$ can be determined as follows;

$$P_\infty = P_{sat}(T_\infty)\left[\frac{M_g + m_{1,\infty}(M_v - M_g)}{M_g - m_{1,\infty}M_g}\right] \tag{A.1}$$

the partial pressure of gas and vapor can be calculated by assuming that the free stream pressure is the total system pressure and that it is constant across the mixture boundary layer.

$$P_g = P_\infty \left[ \frac{m_{1,\infty} M_v}{M_g + m_{1,\infty}(M_v - M_g)} \right] \tag{A.2}$$

and

$$P_v = P_\infty - P_g \tag{A.3}$$

## A.2 Water Properties

***Saturation pressure and temperature***

Used by Srzic [42]

Source: Irvine and Liley [66]

Saturation temperature as a function of saturation pressure is given by;

$$T_{sat} = A + \frac{B}{\ln(P_{sat}) + C} \tag{A.4}$$

where;

A, B and C are given for two pressure or temperature ranges;

| | |
|---|---|
| $0.611\,kPa \le P_{sat} \langle 12.33\times10^3\ kPa$ | $12.33\times10^3\ kPa \le P_{sat} \le 22.1\times10^3 kPa$ |
| $273.15K \le T_{sat} \langle\ 600.0\text{K}$ | $600.0K \le T_{sat} \langle\ 647.3\text{K}$ |
| $A = 0.426776\times10^2$ | $A = -0.387592\times10^3$ |
| $B = -0.38927\times10^4$ | $B = -0.125875\times10^5$ |
| $C = -0.948654\times10^1$ | $C = -0.152578\times10^2$ |

inverse of Equation (A.4) was used to calculate saturation pressure because it gives a unique pair of $P_{sat}$ and $T_{sat}$ [42].

$$P_{sat} = \exp\left( \frac{B}{T_{sat} - A} - C \right) \tag{A.5}$$

Constants A, B and C are the same as mentioned above.

***Latent heat of vaporization***

Used by Srzic [42]

Source: Irvine and Liley [66]

Temperature range; $273.15K \le T \langle 647.3K$

$$h_{fg} = 2.5009\times10^{3}\left[A + BT_c^{1/3} + CT_c^{5/6} + DT_c^{7/8} + \sum_{N=1}^{5} E(N)T_c^{N}\right] \quad \text{(A.6)}$$

where;

$$T_c = \frac{647.3 - T}{647.3}$$

$A = 0.0$
$B = 7.79221\times10^{-1}$
$C = 4.62668$
$D = -1.07931$
$E(1) = -3.87446$
$E(2) = 2.94553$
$E(3) = -8.06395$
$E(4) = 1.15633\times10^{1}$
$E(5) = -6.02884$

***Steam density***

Ideal gas equation of state can be used, since steam can be considered as an ideal gas

$$\rho_v = \frac{P_v M_v}{\overline{R}T_v} \quad \text{(A.7)}$$

where;

$P_v$ is the partial pressure of the vapor.
$\overline{R} = 8.1345 kJ / kmolK$ is universal gas constant

***Steam viscosity, thermal conductivity and specific heat***

Used by Srzic [42]

Source: Incropera and Dewitt [52]

See the thermo-physical properties of saturated water, Table A.6, page A22, in the source reference [52].

***Liquid water density***

Used by Srzic [42]

Source: Irvine and Liley [66]

Temperature range; $273.15K \le T_l \le 647.3K$

$$\rho_l = \frac{1}{3.155 \times 10^{-3}\left[A + BT_c^{1/3} + CT_c^{5/6} + DT_c^{7/8} + \sum_{N=1}^{5} E(N)T_c^N\right]} \tag{A.8}$$

where;

$$T_c = \frac{647.3 - T}{647.3}$$

$A = 1.0$
$B = -1.9153882$
$C = 1.2015186 \times 10^1$
$D = -7.84664025$
$E(1) = -3.888614$
$E(2) = 2.0582238$
$E(3) = -2.0829991$
$E(4) = 8.218 \times 10^{-1}$
$E(5) = 4.7549742 \times 10^{-1}$

***Liquid water viscosity, thermal conductivity and specific heat***

Used by Srzic [42]

Source: Irvine and Liley [66]

See the thermo-physical properties of saturated water, Table A.6, page A22, in the source reference [52].

## A.3 Air properties

***Air density***

Air is considered as an ideal gas, the air density can be determined as;

$$\rho_g = \frac{P_g M_g}{\bar{R} T_g} \tag{A.9}$$

where;

$P_g$ is partial pressure of the gas.

***Air viscosity***

Used by Srzic [42]

Source: Irvine and Liley [66]

Temperature range: $250K \le T \le 600K$

$$\mu_g = 10^{-6} \sum_{N=0}^{4} B(N) T^N \,, \tag{A.10}$$

where;

$B(0) = -9.8601 \times 10^{-1}$
$B(1) = 9.081025 \times 10^{-2}$
$B(2) = -1.17635575 \times 10^{-4}$
$B(3) = 1.2349703 \times 10^{-7}$
$B(4) = -5.7971299 \times 10^{-11}$

***Thermal conductivity***

Used by Srzic [42]

Source: Irvine and Liley [66]

Temperature range: $250K \le T \le 1050K$

$$k_g = 10^{-6} \sum_{N=0}^{5} C(N) T^N \,, \qquad \text{(A.11)}$$

where;

$C(0) = -2.27650 \times 10^{-3}$
$C(1) = 1.2598485 \times 10^{-4}$
$C(2) = -1.4815235 \times 10^{-7}$
$C(3) = 1.73550646 \times 10^{-10}$
$C(4) = -1.066657 \times 10^{-13}$
$C(5) = 2.47663035 \times 10^{-17}$

***Specific heat***

Used by Srzic [42]

Source: Irvine and Liley [66]

Temperature range: $250K \le T \le 2000K$

$$C_{p_g} = \sum_{N=0}^{4} A(N) T^N \,, \qquad \text{(A.12)}$$

$A(0) = 0.103409 \times 10^{1}$
$A(1) = -0.284887 \times 10^{-3}$
$A(2) = 0.7816818 \times 10^{-6}$
$A(3) = -0.4970786 \times 10^{-9}$
$A(4) = 0.1077024 \times 10^{-12}$

## A.4 Mixture properties

### *Diffusion coefficient*

Diffusion coefficient can be determined also according to Hirschfelder et al [50] as follows;

$$D_{12} = 0.0026280 \frac{\sqrt{T^3 (M_1 + M_2)/2M_1 M_2}}{P\sigma_{12}\Omega_{12}^{(1,1)*}(T_{12}^*)} \tag{A.13}$$

where;

$D_{12}$ =diffusion coefficient in cm$^2$/s,

$P$ =pressure in atmospheres,

$T$ = temperature in K,

$T_{12}^* = \dfrac{kT}{\varepsilon_{12}}$,

$M_1, M_2$ =molecular weights of species 1 and 2,

$\sigma_{12}, \varepsilon_{12}/k$ =molecular potential energy parameters characteristic of 1-2 interaction in $A$ and $K$, respectively.

$\Omega^{(1,1)}$ can be taken from tabulated functions for the Lennard-Jones(6-12) potential, Tables (I-M) and (I-N) in the Appendix, pages (1126-1129) at the same reference [50]. It can be evaluated also from the following correlation;

$$\Omega = \frac{A}{T^{*B}} + \frac{C}{\exp(DT^*)} + \frac{E}{\exp(FT^*)}$$

$A = 1.16145$
$B = 0.14874$
$C = 0.52487$
$D = 0.77320$
$E = 2.16178$
$F = 2.43787$

for steam-air mixture;

$\sigma_{vg} = 3.724 \ A$,

$\dfrac{\varepsilon}{k} = 50 \quad K$,

***Mixture density***

$$\rho = \rho_v + \rho_g \tag{A.14}$$

***Mixture viscosity***

Source: Hirschfelder et al [50]

$$\mu_{12} = 266.93\times10^{-7}\frac{\left[\frac{2TM_1M_2}{M_1+M_2}\right]^{1/2}}{\sigma_{12}^2\Omega^{(2,2)*}(T_{12}^*)} \tag{A.15}$$

where;

$T$ = temperature in K,

$T_{12}^* = \frac{kT}{\varepsilon_{12}}$ = reduced temperature,

$M_1, M_2$ =molecular weights of species 1 and 2,

$\sigma_{12}, \varepsilon_{12}/k$ =molecular potential energy parameters characteristic of 1-2 interaction in $A$ and $K$, respectively.

$\Omega^{(2,2)}$ can be taken from tabulated functions for the Lennard-Jones(6-12) potential, Tables (I-M) and (I-N) in the Appendix, pages (1126-1129) at the same reference [50].

or it can be evaluated from the following correlation;

$$\Omega = \frac{A}{T^{*B}} + \frac{C}{\exp(DT^*)} + \frac{E}{\exp(FT^*)}$$

$A = 1.16145$
$B = 0.14874$
$C = 0.52487$
$D = 0.77320$
$E = 2.16178$
$F = 2.43787$

### *Mixture thermal conductivity*

Source: Hirschfelder et al [50]

$$k_{12} = 1989.1\times 10^{-7}\frac{\left[\dfrac{T(M_1+M_2)}{2M_1M_2}\right]^{1/2}}{\sigma_{12}^2\Omega^{(2,2)*}(T_{12}^*)} \tag{A.16}$$

where;

$T$ = temperature in K,

$T_{12}^* = \dfrac{kT}{\varepsilon_{12}}$ = reduced temperature,

$M_1, M_2$ =molecular weights of species 1 and 2,

$\sigma_{12}, \varepsilon_{12}/k$ =molecular potential energy parameters characteristic of 1-2 interaction in $A$ and $K$ , respectively.

$\Omega^{(2,2)}$ can be taken from tabulated functions for the Lennard-Jones(6-12) potential, Tables (I-M) and (I-N) in the Appendix, pages (1126-1129) at the same reference [50]. It can be evaluated also from the following correlation;

$$\Omega = \frac{A}{T^{*B}} + \frac{C}{\exp(DT^*)} + \frac{E}{\exp(FT^*)}$$

$A = 1.16145$
$B = 0.14874$
$C = 0.52487$
$D = 0.77320$
$E = 2.16178$
$F = 2.43787$

### *Mixture specific heat*

$$C_p = m_{1,\infty}C_{p_g} + (1-m_{1,\infty})C_{p_v} \tag{A.17}$$

# APPENDIX B

## A SAMPLE OF THE EXPERIMENTAL DATA AND RESULTS

Table B.1 Experimental data and results for $0^{o}$ of inclination.

| Code | Different inlet cooling water temperature (°C) | | | | |
|---|---|---|---|---|---|
| | 1 | 2 | 3 | 4 | 5 |
| $T_{in1}$ | 15.1 | 25.3 | 34.8 | 45.1 | 55.3 |
| $T_{w1}$ | 90.0 | 91.2 | 92.3 | 93.4 | 94.1 |
| $T_{out1}$ | 35.0 | 45.0 | 54.2 | 64.0 | 74.0 |
| $T_{in2}$ | 15.0 | 24.9 | 35.0 | 45.1 | 55.8 |
| $T_{w2}$ | 89.7 | 91.3 | 92.4 | 93.5 | 94.0 |
| $T_{out2}$ | 35.1 | 44.5 | 54.1 | 64.1 | 74.3 |
| $T_{in3}$ | 15.0 | 25.0 | 34.6 | 44.9 | 55.9 |
| $T_{w3}$ | 90.0 | 91.0 | 92.0 | 93.3 | 94.2 |
| $T_{out3}$ | 34.8 | 44.5 | 53.9 | 64.0 | 74.5 |
| $T_{in4}$ | 15.0 | 25.0 | 35.4 | 45.5 | 56.2 |
| $T_{w4}$ | 89.0 | 90.0 | 91.0 | 92.5 | 93.4 |
| $T_{out4}$ | 34.0 | 43.9 | 54.0 | 63.9 | 74.1 |
| $T_{in5}$ | 15.0 | 25.0 | 35.4 | 45.4 | 55.8 |
| $T_{w5}$ | 88.9 | 90.3 | 91.3 | 92.6 | 93.2 |
| $T_{out5}$ | 34.4 | 44.0 | 54.1 | 64.0 | 74.0 |
| $T_{in6}$ | 15.0 | 25.0 | 35.6 | 45.2 | 56.3 |
| $T_{w6}$ | 89.0 | 90.1 | 91.4 | 92.4 | 93.5 |
| $T_{out6}$ | 34.5 | 44.1 | 54.2 | 63.7 | 74.6 |
| $T_{in7}$ | 15.0 | 25.2 | 35.0 | 45.7 | 56.0 |
| $T_{w7}$ | 88.0 | 89.3 | 90.8 | 91.8 | 92.5 |
| $T_{out7}$ | 33.2 | 43.0 | 52.5 | 63.1 | 73.1 |
| $T_{in8}$ | 15.0 | 25.1 | 35.0 | 45.7 | 56.2 |
| $T_{w8}$ | 88.3 | 89.5 | 90.6 | 91.6 | 92.4 |
| $T_{out8}$ | 33.0 | 42.8 | 52.4 | 62.9 | 73.2 |
| $T_{in9}$ | 15.0 | 25.0 | 35.0 | 45.7 | 55.7 |
| $T_{w9}$ | 87.8 | 89.3 | 90.5 | 91.7 | 92.2 |
| $T_{out9}$ | 33.1 | 42.9 | 52.3 | 62.9 | 72.9 |
| $T_{\infty}$ | 98.0 | 98.3 | 99.0 | 99.8 | 99.9 |
| | | | | | |
| $Q_1$ | 1843.3 | 1824.8 | 1797.0 | 1750.7 | 1732.2 |
| $Q_2$ | 1861.8 | 1815.5 | 1769.2 | 1759.9 | 1713.6 |
| $Q_3$ | 1834.1 | 1806.3 | 1787.7 | 1769.2 | 1722.9 |
| $Q_4$ | 1759.9 | 1750.7 | 1722.9 | 1704.4 | 1658.1 |
| $Q_5$ | 1797.0 | 1759.9 | 1732.2 | 1722.9 | 1685.8 |
| $Q_6$ | 1806.3 | 1769.2 | 1718.3 | 1713.6 | 1695.1 |
| $Q_7$ | 1685.8 | 1648.8 | 1621.0 | 1611.7 | 1584.0 |
| $Q_8$ | 1667.3 | 1639.5 | 1611.7 | 1593.2 | 1574.7 |
| $Q_9$ | 1676.6 | 1658.1 | 1602.5 | 1597.8 | 1593.2 |
| | | | | | |
| $h_1$ | 11477.8 | 12802.7 | 13360.5 | 13626.3 | 14876.8 |
| $h_2$ | 11174.1 | 12919.7 | 13353.2 | 13915.8 | 14468.2 |
| $h_3$ | 11420.1 | 12325.6 | 12722.0 | 13558.6 | 15056.8 |
| $h_4$ | 9741.1 | 10507.0 | 10728.0 | 11630.3 | 12706.8 |
| $h_5$ | 9836.8 | 10958.7 | 11205.9 | 11920.0 | 12534.1 |
| $h_6$ | 9997.4 | 10747.7 | 11262.3 | 11535.5 | 13193.7 |
| $h_7$ | 8397.8 | 9125.8 | 9847.4 | 10035.9 | 10662.5 |
| $h_8$ | 8562.4 | 9280.8 | 9558.0 | 9678.5 | 10458.8 |
| $h_9$ | 8187.9 | 9177.1 | 9391.2 | 9826.5 | 10307.0 |

Table B.2 Experimental data and results for 3$^{o}$ of inclination*.

| Code | Different inlet cooling water temperature (°C) | | | | |
|---|---|---|---|---|---|
| | 1 | 2 | 3 | 4 | 5 |
| $T_{in1}$ | 15.1 | 25.3 | 34.9 | 45.0 | 55.3 |
| $T_{w1}$ | 90.1 | 91.2 | 92.5 | 93.4 | 94.0 |
| $T_{out1}$ | 35.1 | 45.0 | 54.2 | 64.0 | 74.0 |
| $T_{in2}$ | 15.1 | 24.9 | 35.1 | 45.0 | 55.8 |
| $T_{w\,2}$ | 89.8 | 91.3 | 92.6 | 93.5 | 93.9 |
| $T_{out2}$ | 35.2 | 44.5 | 54.1 | 64.1 | 74.4 |
| $T_{in3}$ | 15.1 | 25.0 | 34.7 | 44.9 | 55.9 |
| $T_{w3}$ | 90.1 | 91.0 | 92.2 | 93.3 | 94.1 |
| $T_{out3}$ | 34.9 | 44.5 | 53.9 | 64.0 | 74.6 |
| $T_{in4}$ | 14.8 | 24.9 | 35.3 | 45.4 | 56.2 |
| $T_{w4}$ | 89.1 | 90.0 | 91.2 | 92.5 | 93.3 |
| $T_{out4}$ | 34.0 | 43.9 | 54.0 | 63.9 | 74.1 |
| $T_{in\,5}$ | 15.0 | 25.0 | 35.1 | 45.3 | 55.8 |
| $T_{w5}$ | 89.0 | 90.3 | 91.5 | 92.6 | 93.1 |
| $T_{out5}$ | 34.5 | 44.1 | 54.1 | 64.0 | 74.0 |
| $T_{in6}$ | 15.1 | 25.0 | 35.5 | 45.1 | 56.3 |
| $T_{w\,6}$ | 89.1 | 90.1 | 91.6 | 92.4 | 93.4 |
| $T_{out6}$ | 34.7 | 44.2 | 54.2 | 63.7 | 74.6 |
| $T_{in7}$ | 14.8 | 25.1 | 34.9 | 45.6 | 56.0 |
| $T_{w7}$ | 88.1 | 89.3 | 91.0 | 91.8 | 92.4 |
| $T_{out7}$ | 33.2 | 43.0 | 52.5 | 63.1 | 73.1 |
| $T_{in8}$ | 15.1 | 25.0 | 35.0 | 45.6 | 56.2 |
| $T_{w8}$ | 88.4 | 89.5 | 90.8 | 91.6 | 92.3 |
| $T_{out8}$ | 33.2 | 42.8 | 52.5 | 62.9 | 73.4 |
| $T_{in9}$ | 14.9 | 24.8 | 34.8 | 45.7 | 55.7 |
| $T_{w9}$ | 87.9 | 89.3 | 90.7 | 91.7 | 92.2 |
| $T_{out9}$ | 33.2 | 42.9 | 52.3 | 63.0 | 73.0 |
| $T_{\infty}$ | 98.1 | 98.3 | 99.2 | 99.8 | 99.8 |
| | | | | | |
| $Q_1$ | 1847.9 | 1829.4 | 1792.4 | 1759.9 | 1736.8 |
| $Q_2$ | 1866.5 | 1820.2 | 1764.6 | 1765.5 | 1721.0 |
| $Q_3$ | 1838.7 | 1810.9 | 1783.1 | 1773.8 | 1732.2 |
| $Q_4$ | 1778.5 | 1759.9 | 1732.2 | 1713.6 | 1662.7 |
| $Q_5$ | 1806.3 | 1769.2 | 1759.9 | 1732.2 | 1685.8 |
| $Q_6$ | 1815.5 | 1778.5 | 1727.5 | 1722.9 | 1695.1 |
| $Q_7$ | 1704.4 | 1658.1 | 1630.3 | 1621.0 | 1584.0 |
| $Q_8$ | 1676.6 | 1648.8 | 1616.4 | 1602.5 | 1593.2 |
| $Q_9$ | 1695.1 | 1676.6 | 1621.0 | 1607.1 | 1597.8 |
| | | | | | |
| $h_1$ | 11506.6 | 12835.2 | 13326.1 | 13698.4 | 14916.6 |
| $h_2$ | 11134.8 | 12952.7 | 13318.2 | 13959.8 | 14530.8 |
| $h_3$ | 11449.0 | 12357.2 | 12689.0 | 13594.1 | 15137.8 |
| $h_4$ | 9843.6 | 10562.6 | 10785.7 | 11693.5 | 12742.3 |
| $h_5$ | 9887.5 | 11016.4 | 11385.7 | 11984.1 | 12534.1 |
| $h_6$ | 10048.7 | 10804.0 | 11323.0 | 11597.8 | 13193.7 |
| $h_7$ | 8490.1 | 9177.1 | 9903.6 | 10093.5 | 10662.5 |
| $h_8$ | 8610.0 | 9333.2 | 9585.4 | 9734.8 | 10581.9 |
| $h_9$ | 8278.4 | 9279.6 | 9499.8 | 9883.5 | 10473.0 |

* it should be noted that the subscripts 1,2,3,……9 represent the tube numbers, see Figure 5.6.

Table B.3 Experimental data and results for $6^o$ of inclination.

| Code | Different inlet cooling water temperature ($^oC$) | | | | |
|---|---|---|---|---|---|
| | 1 | 2 | 3 | 4 | 5 |
| $T_{in1}$ | 15.1 | 25.3 | 34.8 | 45.1 | 55.3 |
| $T_{w1}$ | 90.2 | 91.1 | 92.7 | 93.5 | 94.3 |
| $T_{out1}$ | 35.0 | 45.0 | 54.2 | 64.0 | 74.0 |
| $T_{in2}$ | 14.9 | 24.9 | 35.0 | 45.1 | 55.8 |
| $T_{w\ 2}$ | 89.9 | 91.1 | 92.8 | 93.6 | 94.2 |
| $T_{out2}$ | 35.1 | 44.5 | 54.1 | 64.1 | 74.3 |
| $T_{in3}$ | 15.0 | 25.0 | 34.6 | 44.9 | 55.9 |
| $T_{w3}$ | 90.2 | 90.9 | 92.6 | 93.4 | 94.4 |
| $T_{out3}$ | 34.8 | 44.5 | 53.9 | 64.0 | 74.5 |
| $T_{in4}$ | 14.8 | 24.9 | 35.3 | 45.2 | 56.0 |
| $T_{w4}$ | 89.2 | 90.0 | 91.5 | 92.5 | 93.5 |
| $T_{out4}$ | 34.1 | 44.0 | 54.1 | 63.9 | 74.1 |
| $T_{in\ 5}$ | 15.0 | 24.8 | 35.1 | 45.1 | 55.7 |
| $T_{w5}$ | 89.1 | 90.3 | 91.8 | 92.6 | 93.3 |
| $T_{out5}$ | 34.6 | 44.1 | 54.2 | 64.0 | 74.0 |
| $T_{in6}$ | 15.0 | 24.9 | 35.2 | 45.0 | 56.2 |
| $T_{w\ 6}$ | 89.2 | 90.1 | 91.7 | 92.5 | 93.6 |
| $T_{out6}$ | 34.7 | 44.1 | 54.2 | 63.7 | 74.6 |
| $T_{in7}$ | 15.1 | 25.2 | 34.8 | 45.5 | 55.9 |
| $T_{w7}$ | 88.2 | 89.3 | 91.2 | 91.9 | 92.6 |
| $T_{out7}$ | 33.6 | 43.5 | 52.5 | 63.1 | 73.1 |
| $T_{in8}$ | 15.0 | 25.1 | 35.0 | 45.4 | 56.0 |
| $T_{w8}$ | 88.3 | 89.5 | 91.0 | 91.7 | 92.5 |
| $T_{out8}$ | 33.7 | 43.0 | 52.6 | 62.9 | 73.3 |
| $T_{in9}$ | 15.2 | 25.0 | 34.6 | 45.1 | 55.7 |
| $T_{w9}$ | 88.0 | 89.3 | 91.0 | 91.8 | 92.4 |
| $T_{out9}$ | 33.6 | 43.2 | 52.2 | 62.5 | 73.0 |
| $T_\infty$ | 98.2 | 98.1 | 99.4 | 99.9 | 100.0 |
| | | | | | |
| $Q_1$ | 1839.6 | 1824.8 | 1797.0 | 1750.7 | 1732.2 |
| $Q_2$ | 1871.1 | 1815.5 | 1769.2 | 1759.9 | 1713.6 |
| $Q_3$ | 1837.8 | 1806.3 | 1787.7 | 1769.2 | 1722.9 |
| $Q_4$ | 1787.7 | 1769.2 | 1741.4 | 1732.2 | 1676.6 |
| $Q_5$ | 1810.9 | 1787.7 | 1769.2 | 1750.7 | 1699.7 |
| $Q_6$ | 1824.8 | 1783.1 | 1755.3 | 1732.2 | 1704.4 |
| $Q_7$ | 1713.6 | 1695.1 | 1639.5 | 1630.3 | 1593.2 |
| $Q_8$ | 1732.2 | 1658.1 | 1630.3 | 1621.0 | 1602.5 |
| $Q_9$ | 1704.4 | 1681.2 | 1634.9 | 1616.4 | 1607.1 |
| | | | | | |
| $h_1$ | 11454.7 | 12893.5 | 13360.5 | 13626.3 | 15006.1 |
| $h_2$ | 11162.5 | 12919.7 | 13353.2 | 13915.8 | 14717.7 |
| $h_3$ | 11443.2 | 12496.8 | 13096.2 | 13558.6 | 15190.1 |
| $h_4$ | 9894.9 | 10880.4 | 10980.6 | 11707.6 | 12848.7 |
| $h_5$ | 9912.9 | 11417.2 | 11596.2 | 11995.6 | 12637.4 |
| $h_6$ | 10099.9 | 11102.9 | 11355.7 | 11660.2 | 13265.8 |
| $h_7$ | 8536.2 | 9595.4 | 9959.9 | 10151.2 | 10724.9 |
| $h_8$ | 8715.7 | 9603.9 | 9667.8 | 9847.4 | 10643.4 |
| $h_9$ | 8323.6 | 9516.8 | 9695.3 | 9940.4 | 10533.7 |

Table B.4 Experimental data and results for 9$^{o}$ of inclination.

| Code | Different inlet cooling water temperature (°C) | | | | |
|---|---|---|---|---|---|
| | 1 | 2 | 3 | 4 | 5 |
| $T_{in1}$ | 15.1 | 25.3 | 34.8 | 45.1 | 55.3 |
| $T_{w1}$ | 90.2 | 91.3 | 92.5 | 93.4 | 94.5 |
| $T_{out1}$ | 35.0 | 44.9 | 54.2 | 63.9 | 73.9 |
| $T_{in2}$ | 15.0 | 24.9 | 35.0 | 45.1 | 55.8 |
| $T_{w\ 2}$ | 89.9 | 91.3 | 92.6 | 93.5 | 94.4 |
| $T_{out2}$ | 35.1 | 44.5 | 54.1 | 64.0 | 74.3 |
| $T_{in3}$ | 15.0 | 24.9 | 34.5 | 44.8 | 55.9 |
| $T_{w3}$ | 90.2 | 91.1 | 92.4 | 93.3 | 94.6 |
| $T_{out3}$ | 34.9 | 44.5 | 53.9 | 64.0 | 74.4 |
| $T_{in4}$ | 15.0 | 24.8 | 35.0 | 45.4 | 56.0 |
| $T_{w4}$ | 89.2 | 90.2 | 91.3 | 92.5 | 93.7 |
| $T_{out4}$ | 34.4 | 44.0 | 54.0 | 64.2 | 74.2 |
| $T_{in\ 5}$ | 15.0 | 25.0 | 35.1 | 45.1 | 55.7 |
| $T_{w5}$ | 89.1 | 90.5 | 91.6 | 92.5 | 93.6 |
| $T_{out5}$ | 34.6 | 44.5 | 54.3 | 64.2 | 74.0 |
| $T_{in6}$ | 14.9 | 24.6 | 35.4 | 45.1 | 56.3 |
| $T_{w\ 6}$ | 89.2 | 90.3 | 91.5 | 92.4 | 93.9 |
| $T_{out6}$ | 34.7 | 44.0 | 54.5 | 64.0 | 74.6 |
| $T_{in7}$ | 14.8 | 25.0 | 35.0 | 45.3 | 55.8 |
| $T_{w7}$ | 88.2 | 89.5 | 91.0 | 91.8 | 92.8 |
| $T_{out7}$ | 33.4 | 43.4 | 52.8 | 63.1 | 73.1 |
| $T_{in8}$ | 14.6 | 25.1 | 34.9 | 45.3 | 56.0 |
| $T_{w8}$ | 88.3 | 89.7 | 90.8 | 91.6 | 92.7 |
| $T_{out8}$ | 33.5 | 43.1 | 52.6 | 62.9 | 73.4 |
| $T_{in9}$ | 14.8 | 24.9 | 34.8 | 45.5 | 55.4 |
| $T_{w9}$ | 87.8 | 89.5 | 90.8 | 91.7 | 92.6 |
| $T_{out9}$ | 33.6 | 43.2 | 52.5 | 63.0 | 72.8 |
| $T_{\infty}$ | 98.2 | 98.3 | 99.2 | 99.8 | 100.2 |
| | | | | | |
| $Q_1$ | 1847.9 | 1820.2 | 1792.4 | 1741.4 | 1722.9 |
| $Q_2$ | 1857.2 | 1810.9 | 1764.6 | 1750.7 | 1709.0 |
| $Q_3$ | 1838.7 | 1815.5 | 1797.0 | 1778.5 | 1717.3 |
| $Q_4$ | 1797.0 | 1778.5 | 1759.9 | 1741.4 | 1685.8 |
| $Q_5$ | 1815.5 | 1801.6 | 1773.8 | 1764.6 | 1695.1 |
| $Q_6$ | 1834.1 | 1797.0 | 1764.6 | 1750.7 | 1690.5 |
| $Q_7$ | 1722.9 | 1704.4 | 1648.8 | 1644.2 | 1602.5 |
| $Q_8$ | 1750.7 | 1667.3 | 1639.5 | 1630.3 | 1607.1 |
| $Q_9$ | 1741.4 | 1695.1 | 1644.2 | 1621.0 | 1611.7 |
| | | | | | |
| $h_1$ | 11435.2 | 12860.8 | 13326.1 | 13618.0 | 15056.8 |
| $h_2$ | 11146.3 | 12923.7 | 13318.2 | 13908.8 | 14677.9 |
| $h_3$ | 11449.0 | 12474.2 | 13164.0 | 13525.6 | 15141.1 |
| $h_4$ | 9946.1 | 10937.3 | 11097.4 | 11883.1 | 12919.7 |
| $h_5$ | 9938.3 | 11505.9 | 11626.5 | 12041.1 | 12793.9 |
| $h_6$ | 10151.2 | 11189.4 | 11415.6 | 11784.9 | 13366.5 |
| $h_7$ | 8582.4 | 9647.8 | 10016.2 | 10237.7 | 10787.2 |
| $h_8$ | 8808.9 | 9657.6 | 9722.8 | 9903.6 | 10674.2 |
| $h_9$ | 8341.0 | 9595.4 | 9750.2 | 9968.9 | 10564.1 |

Table B.5 Experimental data and results for 12$^{o}$ of inclination.

| Code | Different inlet cooling water temperature (°C) | | | | |
|---|---|---|---|---|---|
| | 1 | 2 | 3 | 4 | 5 |
| $T_{in1}$ | 15.1 | 25.3 | 34.8 | 45.1 | 55.0 |
| $T_{w1}$ | 90.0 | 91.2 | 92.3 | 93.4 | 94.1 |
| $T_{out1}$ | 35.0 | 45.0 | 54.3 | 64.0 | 74.0 |
| $T_{in2}$ | 15.0 | 24.9 | 35.0 | 45.1 | 55.4 |
| $T_{w\,2}$ | 89.7 | 91.3 | 92.4 | 93.5 | 94.0 |
| $T_{out2}$ | 35.1 | 44.5 | 54.0 | 63.7 | 73.7 |
| $T_{in3}$ | 15.0 | 25.0 | 34.6 | 44.9 | 55.1 |
| $T_{w3}$ | 90.0 | 91.0 | 92.0 | 93.3 | 94.2 |
| $T_{out3}$ | 34.8 | 44.5 | 54.1 | 64.0 | 73.4 |
| $T_{in4}$ | 15.0 | 25.0 | 34.6 | 45.5 | 55.2 |
| $T_{w4}$ | 90.0 | 91.3 | 92.2 | 93.3 | 94.0 |
| $T_{out4}$ | 35.0 | 44.4 | 54.0 | 64.1 | 73.5 |
| $T_{in\,5}$ | 15.0 | 25.0 | 34.6 | 45.4 | 55.1 |
| $T_{w5}$ | 89.8 | 91.2 | 92.4 | 93.4 | 94.0 |
| $T_{out5}$ | 35.1 | 44.5 | 54.1 | 63.8 | 74.0 |
| $T_{in6}$ | 15.0 | 25.0 | 34.7 | 45.2 | 55.2 |
| $T_{w\,6}$ | 90.0 | 91.0 | 92.0 | 93.3 | 94.2 |
| $T_{out6}$ | 34.8 | 44.6 | 53.6 | 64.3 | 74.2 |
| $T_{in7}$ | 15.0 | 25.2 | 35.0 | 45.2 | 55.2 |
| $T_{w7}$ | 90.1 | 91.2 | 92.1 | 93.2 | 94.0 |
| $T_{out7}$ | 35.1 | 44.9 | 54.4 | 64.0 | 74.0 |
| $T_{in8}$ | 15.0 | 25.1 | 35.0 | 45.1 | 55.3 |
| $T_{w8}$ | 89.9 | 91.1 | 92.3 | 93.3 | 93.9 |
| $T_{out8}$ | 34.9 | 44.7 | 54.3 | 64.1 | 73.8 |
| $T_{in9}$ | 15.0 | 25.0 | 35.0 | 45.1 | 55.0 |
| $T_{w9}$ | 90.0 | 91.0 | 92.0 | 93.2 | 93.8 |
| $T_{out9}$ | 35.0 | 44.4 | 54.2 | 63.8 | 73.7 |
| $T_{\infty}$ | 98.1 | 98.4 | 99.2 | 99.9 | 100.0 |
| | | | | | |
| $Q_1$ | 1843.3 | 1824.8 | 1806.3 | 1750.7 | 1759.9 |
| $Q_2$ | 1861.8 | 1815.5 | 1759.9 | 1722.9 | 1695.1 |
| $Q_3$ | 1834.1 | 1806.3 | 1806.3 | 1769.2 | 1695.1 |
| $Q_4$ | 1852.6 | 1797.0 | 1797.0 | 1722.9 | 1695.1 |
| $Q_5$ | 1861.8 | 1806.3 | 1806.3 | 1704.4 | 1750.7 |
| $Q_6$ | 1834.1 | 1815.5 | 1750.7 | 1769.2 | 1759.9 |
| $Q_7$ | 1861.8 | 1824.8 | 1797.0 | 1741.4 | 1741.4 |
| $Q_8$ | 1838.7 | 1815.5 | 1787.7 | 1759.9 | 1713.6 |
| $Q_9$ | 1852.6 | 1797.0 | 1778.5 | 1732.2 | 1732.2 |
| | | | | | |
| $h_1$ | 11336.1 | 12624.9 | 13040.1 | 13416.6 | 14859.3 |
| $h_2$ | 11041.1 | 12737.8 | 12892.6 | 13410.0 | 14073.3 |
| $h_3$ | 11279.1 | 12159.0 | 12496.8 | 13353.2 | 14558.6 |
| $h_4$ | 11393.1 | 12607.8 | 12787.9 | 13003.6 | 14073.3 |
| $h_5$ | 11174.1 | 12496.8 | 13231.9 | 13061.7 | 14534.7 |
| $h_6$ | 11279.1 | 12221.4 | 12112.2 | 13353.2 | 15115.4 |
| $h_7$ | 11593.1 | 12624.9 | 12607.8 | 12947.3 | 14457.8 |
| $h_8$ | 11169.7 | 12388.8 | 12906.4 | 13283.3 | 13993.8 |
| $h_9$ | 11393.1 | 12096.7 | 12304.5 | 12878.4 | 13917.0 |

## APPENDIX C

## UNCERTAINTY ANALYSIS

In this study, the constant odds method that proposed by Kline and Mc Clintock [55] is followed for calculating the uncertainties in single sample experiments. The suggested method can be summarized as follows;

- Describe the uncertainty in each variable as mean $\pm$ uncertainty interval. See Table C.1.
- Compute the uncertainty interval in each result as;

$$w_R = \left[ \left( \frac{\partial R}{\partial x_1} w_1 \right)^2 + \left( \frac{\partial R}{\partial x_2} w_2 \right)^2 + \cdots + \left( \frac{\partial R}{\partial x_n} w_n \right)^2 \right]^{1/2} \tag{C.1}$$

where $w_n$ denotes the uncertainty in the $n^{th}$ independent variable.

As Kline and McClintock [33] claimed, Equation C.1 gives the uncertainty in R with good accuracy for most functions of engineering importance. The rate of heat transfer and the heat transfer coefficient of the experiments are calculated with Equation (5.1). The uncertainties in the heat transfer rate and heat transfer coefficient will be determined for the results of the experiments conducted at METU labrotary. The values of the variables used in the equations and the uncertainties related to these variables are presented in Table C.1.

Table C.1 Uncertainties in the independent variables used in Equation (5.1).

| **Variable** | **Upper Tube** | **Middle Tube** | **Bottom Tube** |
|---|---|---|---|
| $\dot{m}$ $(g/s\}$ | 22.16 ± 1.0 | 22.16 ± 1.0 | 22.16 ± 1.0 |
| $C_p$ (J/kgK) | 4180 ± 2.0 | 4180 ± 2.0 | 4180 ± 2.0 |
| $T_{in}$ $(^oC)$ | 15 ± 0.1 | 15 ± 0.1 | 15 ± 0.1 |
| $T_{out}$ $(^oC)$ | 35.1 ± 0.1 | 34.3 ± 0.1 | 33.1 ± 0.1 |
| $R$ $(mm)$ | 10.65 ± 0.01 | 10.65 ± 0.01 | 10.65 ± 0.01 |
| $L$ $(mm)$ | 300.0 ± 1 | 300.0 ± 1 | 300.0 ± 1 |
| $T_{sat}$ $(^oC)$ | 98.0 ± 0.1 | 98.0 ± 0.1 | 98.0 ± 0.1 |
| $T_w$ $(^oC)$ | 89.8 ± 0.1 | 89.0 ± 0.1 | 88.0 ± 0.1 |

A sample of the uncertainty analysis for heat transfer rate, Equation (C.2) and heat transfer coefficient, Equation (C.15) for the upper tube is presented below;

$$Q = \dot{m} C_p \left(T_{out} - T_{in}\right) \tag{C.2}$$

$$\frac{\partial Q}{\partial \dot{m}} = C_p \left(T_{out} - T_{in}\right) \tag{C.3}$$

$$\frac{\partial Q}{\partial C_p} = \dot{m} \left(T_{out} - T_{in}\right) \tag{C.4}$$

$$\frac{\partial Q}{\partial T_{in}} = -\dot{m} C_p \tag{C.5}$$

$$\frac{\partial Q}{\partial T_{out}} = \dot{m} C_p \quad \text{(C.6)}$$

$$w_{\dot{m}} = \pm 1.0 \quad \text{(C.7)}$$

$$w_{C_p} = \pm 2 \quad \text{(C.8)}$$

$$w_{T_{in}} = \pm 0.1 \quad \text{(C.9)}$$

$$w_{T_{out}} = \pm 0.1 \quad \text{(C.10)}$$

Substituting these values into Equation C.1

$$w_Q = \left[ \left( \frac{\partial Q}{\partial \dot{m}} w_{\dot{m}} \right)^2 + \left( \frac{\partial Q}{\partial C_p} w_{C_p} \right)^2 + \left( \frac{\partial Q}{\partial T_{in}} w_{T_{in}} \right)^2 + \left( \frac{\partial Q}{\partial T_{out}} w_{T_{out}} \right)^2 \right]^{1/2} \quad \text{(C.11)}$$

$$w_Q = \left[ \left( C_p (T_{out} - T_{in})\, w_{\dot{m}} \right)^2 + \left( \dot{m} (T_{out} - T_{in})\, w_{C_p} \right)^2 + \left( -\dot{m} C_p w_{T_{in}} \right)^2 + \left( \dot{m} C_p w_{T_{out}} \right)^2 \right]^{1/2} \quad \text{(C.12)}$$

According to Cline and McClintock [55], Equation (C.12) is greatly simplified upon dividing by Equation (C.2) to non-dimensionless form as;

$$Uncertaint\,y = \frac{w_Q}{Q} = \left[ \left( \frac{w_{\dot{m}}}{\dot{m}} \right)^2 + \left( \frac{w_{C_p}}{C_p} \right)^2 + \left( \frac{-w_{T_{in}}}{(T_{out} - T_{in})} \right)^2 + \left( \frac{w_{T_{out}}}{(T_{out} - T_{in})} \right)^2 \right]^{1/2} \quad \text{(C.13)}$$

$$\text{Uncertainty } (\%) = \frac{w_Q}{Q} = 4.54\% \quad \text{(C.14)}$$

The same procedure can be applied to calculate the uncertainty in the heat transfer coefficient for the upper tube as follows;

$$h = \frac{Q}{2\pi RL\left(T_{sat} - T_w\right)} \tag{C.15}$$

$$\frac{\partial h}{\partial Q} = \frac{1}{2\pi RL\left(T_{sat} - T_w\right)} \tag{C.16}$$

$$\frac{\partial h}{\partial R} = \frac{-Q}{2\pi R^2 L\left(T_{sat} - T_w\right)} \tag{C.17}$$

$$\frac{\partial h}{\partial L} = \frac{-Q}{2\pi RL^2\left(T_{sat} - T_w\right)} \tag{C.18}$$

$$\frac{\partial h}{\partial T_{sat}} = \frac{-Q}{2\pi RL\left(T_{sat} - T_w\right)^2} \tag{C.19}$$

$$\frac{\partial h}{\partial T_w} = \frac{Q}{2\pi RL\left(T_{sat} - T_w\right)^2} \tag{C.20}$$

$$w_{T_w} = \pm 0.1 \tag{C.21}$$

$$w_{T_{sat}} = \pm 0.1 \tag{C.22}$$

$$w_R = \pm 0.01 \tag{C.23}$$

$$w_L = \pm 1 \tag{C.24}$$

Substituting these values into Equation (C.15)

$$w_h = \left[\left(\frac{\partial h}{\partial Q} w_Q\right)^2 + \left(\frac{\partial h}{\partial R} w_R\right)^2 + \left(\frac{\partial h}{\partial L} w_L\right)^2 + \left(\frac{\partial h}{\partial T_{sat}} w_{T_{sat}}\right)^2 + \left(\frac{\partial h}{\partial T_w} w_{T_w}\right)^2\right]^{1/2} \tag{C.25}$$

$$w_h = \left[ \left( \frac{w_Q}{2\pi RL(T_{sat} - T_w)} \right)^2 + \left( \frac{-Qw_R}{2\pi R^2 L(T_{sat} - T_w)} \right)^2 + \left( \frac{-Qw_L}{2\pi RL^2 (T_{sat} - T_w)} \right)^2 \right]^{1/2} +$$

$$\left[ \left( \frac{-Qw_{T_{sat}}}{2\pi RL(T_{sat} - T_w)^2} \right)^2 + \left( \frac{-Qw_{T_w}}{2\pi RL(T_{sat} - T_w)^2} \right)^2 \right]^{1/2} \tag{C.26}$$

The non-dimensionless form can be written as;

$$Uncertainty = \frac{w_h}{h} = \left[ \left( \frac{w_Q}{Q} \right)^2 + \left( \frac{-w_R}{R} \right)^2 + \left( \frac{-w_L}{L} \right)^2 + \left( \frac{-w_{T_{sat}}}{(T_{sat} - T_w)} \right)^2 + \left( \frac{w_{T_w}}{(T_{sat} - T_w)} \right)^2 \right]^{1/2} \tag{C.27}$$

$$\text{Uncertainty } (\%) = \frac{w_h}{h} = 4.86\,\% \tag{C.28}$$

If the same procedure is applied to Equation (C.2) and Equation (C.15) for all condensation tubes, the following results for the uncertainties in the experimental results are obtained and summarized in Table C.2.

Table C.2 Uncertainties in the experimental results.

| Item | Uncertainty in Q (%) | Uncertainty in h (%) |
|---|---|---|
| Upper Tube | 4.54 | 4.86 |
| Middle Tube | 4.57 | 4.84 |
| Bottom Tube | 4.58 | 4.81 |

Figure C.1 and Figure C.2 show samples of the experimental results for this study with error bars.

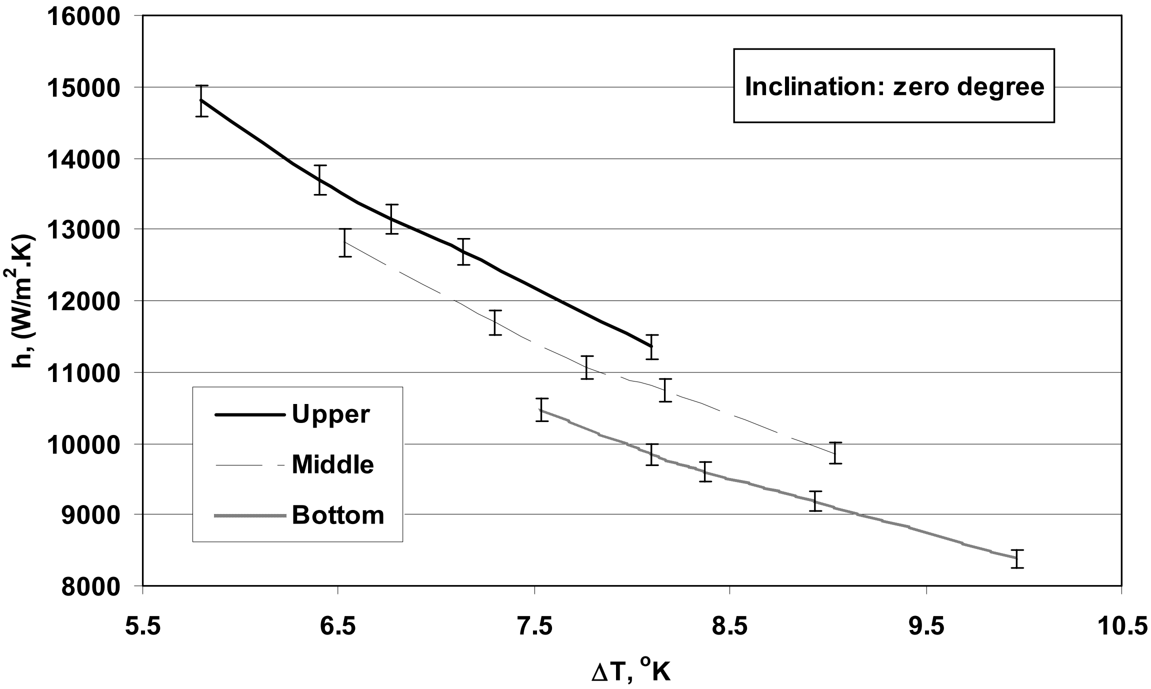


Figure C.1 Variation of heat transfer coefficients with temperature difference for $0^o$ of inclination (with error bars).

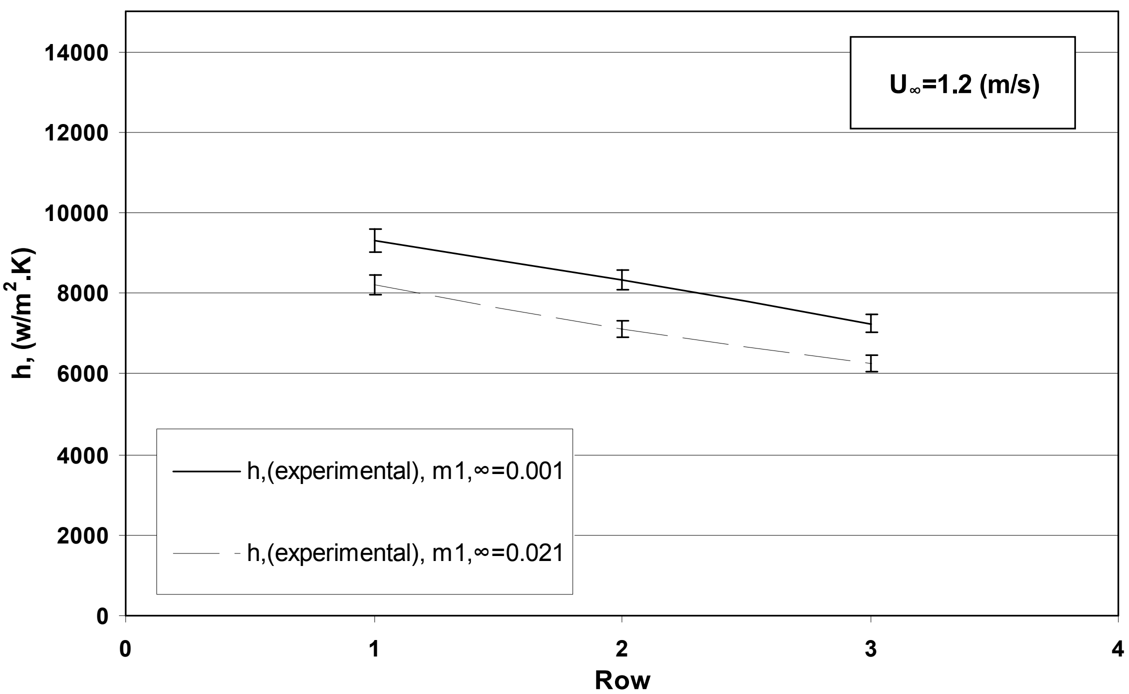


Figure C.2 Experimental heat transfer coefficients for different rows of the present study at two values of air fractions (with error bars).

# APPENDIX D

# COMPUTER CODES

## D.1 Program (CONDFG.FOR ) to solve the system of non-linear equations using Newton Raphson method for film condensation of pure vapor flowing downward horizontal cylinders for both inline and staggered arrangements.

```
$DEBUG


C****************************************************************
C                                                               *
C    PROGRAM (CONDFG.FOR) TO SOLVE A SYSTEM OF NON-LINEAR EQNS  *
C    USING (NEWTON RAPHSON METHOD)FOR A CONDENSATION ON HORI-   *
C    ZONTAL CYLINDERS(INLINE AND STAGGERED ARRAGEMENTS)         *
C                                                               *
C****************************************************************

      DIMENSION DEL(300),U(300),D(300),TETHA(300),DTETHA(300)

      DATA XPI,R,XNW,XMW,DT/3.14,0.01905,0.000000318,0.0003062,10.0/
      DATA G,XHFG,RHOF,XKF/9.81,2278000.0,963.0,0.613/
      DATA XHI,AXIS2,VHI/0.02,0.5,0.0/
C**********************************
C     START SOLUTION FOR FIRST CYLINDER
C **********************************

      NEQ=41
      DX=(XPI*R)/40.0
      XLOC=DX


C**************************************************
C CALCULATION OF CRITICAL ANGLE OF INCLINATION
C**************************************************
      WRITE(5,*)'ANGLE OF INCLINATION =',VHI

      VHI=VHI*(3.14/180.0)
      FF=(R/((2.0*R)+XHI))
      VHIC=ASIN(FF)
      VHIC=VHIC*(180.0/3.14)

      DY=R*SIN(VHI)
      ZETA=(XHI+R)*SIN(VHI)
```

```
      DV=DY+ZETA
      DF=(DV/R)

      TETHA0=ASIN(DF)
      TETHA0=TETHA0*(180.0/3.14)

      WRITE(5,*)'CRITICAL ANGLE OF INCLINATION=',VHIC
      WRITE(5,*)'TETHA0  =',TETHA0

C***************************************************************
C    INITIAL VELOCITY AND BOUNDARY LAYER THICKNESS DISTRIBUTION
C***************************************************************
      DTETHA(1)=ASIN(DX/R)
      DTETHA(1)=DTETHA(1)*(180.0/3.14)
      TETHA(1)=0.0
      WRITE(5,*)'     TETHA        FILM THICKNESS       VELOCITY'

      DO 10 I=1,NEQ
      A=(XNW*3.0*XKF*DT*XLOC)
      B=(G*RHOF*XHFG*SIN(X/R))

      DEL(I)=(A/B)**0.25
      U(I)=(G*RHOF*DEL(I)*DEL(I))/(2.0*XMW)

      WRITE(5,*)
c      WRITE(5,*)'FFFFFF'

      WRITE(5,*)TETHA(I),DEL(I),U(I)

      XLOC=XLOC+DX
      TETHA(I+1)=TETHA(I)+DTETHA(1)

  10  CONTINUE
      DELINC=DEL(NEQ)/1000.0
      UINC=U(NEQ)/1000.0
C      WRITE(5,*)'HHHHHH'
C      WRITE(5,*)DELINC,UINC

      DO 20 K=1,20
      C0=((5.0/8.0)*(DEL(1)*U(1)/DX)-((XKF*DT)/(RHOF*XHFG*DEL(1))))
      CA=((17.0/35.0)*RHOF*(DEL(1)*U(1)*U(1)/DX))
      CB=DEL(1)*RHOF*G*SIN(X/R)
      CC=(3.0/2.0)*XMW*U(1)/DEL(1)
      C1=CA-CB+CC

      PSI00A=((5.0/8.0)*((DEL(1)+DELINC)*U(1)/DX)
     + -((XKF*DT)/(RHOF*XHFG*(DEL(1)+DELINC))))
      PSI00B=((5.0/8.0)*(DEL(1)*U(1)/DX)-
     +((XKF*DT)/(RHOF*XHFG*DEL(1))))
      PSI00=(PSI00A-PSI00B)/DELINC

      PSI01A=((5.0/8.0)*(DEL(1)*(U(1)+UINC)/DX))
      PSI01B=((5.0/8.0)*(DEL(1)*U(1)/DX))
      PSI01=(PSI01A-PSI01B)/UINC

      PSI10A=((17.0/35.0)*RHOF*((DEL(1)+DELINC)*U(1)*U(1)/DX))
      PSI10B=(DEL(1)+DELINC)*RHOF*G*SIN(X/R)
      PSI10C=(3.0/2.0)*XMW*U(1)/(DEL(1)+DELINC)
      PSI10D=C1
      PSI10=((PSI10A-PSI10B+PSI10C)-PSI10D)/DELINC
```

```
      PSI11A=((17.0/35.0)*RHOF*(DEL(1)*(U(1)+UINC)*(U(1)+UINC)/DX))
      PSI11B=DEL(1)*RHOF*G*SIN(X/R)
      PSI11C=(3.0/2.0)*XMW*(U(1)+UINC)/DEL(1)
      PSI11=((PSI11A-PSI11B+PSI11C)-C1)/UINC

      XJ=((PSI00*PSI11)-(PSI01*PSI10))
      XH=((-C0*PSI11)+(C1*PSI01))/XJ
      XK=((-C1*PSI00)+(C0*PSI10))/XJ

      DEL(1)=DEL(1)+XH
      U(1)=U(1)+XK
C      WRITE(5,*)'KKKKKKK'
C      WRITE(5,*)K,DEL(1),U(1)
  20  CONTINUE
      WRITE(5,*)

      WRITE(5,*)'FIRST CYLINDER'
      WRITE(5,*)'     TETHA        FILM THICKNESS       VELOCITY'

      WRITE(5,*)TETHA(1),DEL(1),U(1)

      DO 30 M=2,NEQ
      DO 40 N=1,20
      C0=((5.0/8.0)*(((DEL(M)*U(M))-(DEL(M-1)*U(M-1)))/DX)
     + -((XKF*DT)/(RHOF*XHFG*DEL(M))))
      CA=((17.0/35.0)*RHOF
     + *((DEL(M)*U(M)*U(M))-(DEL(M-1)*U(M-1)*U(M-1)))/DX)
      CB=DEL(M)*RHOF*G*SIN(X/R)
      CC=(3.0/2.0)*XMW*U(M)/DEL(M)
      C1=CA-CB+CC

      PSI00A=((5.0/8.0)*(((DEL(M)+DELINC)*U(M)-(DEL(M-1)*U(M-1)))/DX)
     + -((XKF*DT)/(RHOF*XHFG*(DEL(M)+DELINC))))
      PSI00B=((5.0/8.0)*((DEL(M)*U(M))-(DEL(M-1)*U(M-1)))/DX)
     + -((XKF*DT)/(RHOF*XHFG*DEL(M)))
      PSI00=(PSI00A-PSI00B)/DELINC

      PSI01A=((5.0/8.0)*((DEL(M)*(U(M)+UINC))-(DEL(M-1)*U(M-1)))/DX)
      PSI01B=((5.0/8.0)*((DEL(M)*U(M))-(DEL(M-1)*U(M-1)))/DX)
      PSI01=(PSI01A-PSI01B)/UINC

      PSI10A=((17.0/35.0)
     +*RHOF*((((DEL(M)+DELINC)*U(M)*U(M))-(DEL(M-1)*U(M-1)*U(M-
     +1)))/DX))
      PSI10B=(DEL(M)+DELINC)*RHOF*G*SIN(X/R)
      PSI10C=(3.0/2.0)*XMW*U(M)/(DEL(M)+DELINC)
      PSI10D=C1
      PSI10=((PSI10A-PSI10B+PSI10C)-PSI10D)/DELINC

      PSI11A=((17.0/35.0)*RHOF
     + *((DEL(M)*(U(M)+UINC)*(U(M)+UINC))-(DEL(M-1)*U(M-1)*U(M-
     +1)))/DX)
      PSI11B=DEL(M)*RHOF*G*SIN(X/R)
      PSI11C=(3.0/2.0)*XMW*(U(M)+UINC)/DEL(M)
      PSI11=((PSI11A-PSI11B+PSI11C)-C1)/UINC

      XJ=((PSI00*PSI11)-(PSI01*PSI10))
      XH=((-C0*PSI11)+(C1*PSI01))/XJ
      XK=((-C1*PSI00)+(C0*PSI10))/XJ
```

```
      DEL(M)=DEL(M)+XH
      U(M)=U(M)+XK
C       WRITE(5,*)
C       WRITE(5,*)M,DEL(M),U(M)


 40   CONTINUE
C       WRITE(5,*)'MMMMMMMM'


      WRITE(5,*)TETHA(M),DEL(M),U(M)
 30   CONTINUE

C*****************************************************************
C     START SOLUTION FOR THE SECOND CYLINDER
C*****************************************************************

      UM=U(NEQ)
      V1=UM
      DEL1=DEL(NEQ)
      V2=(((V1*V1)+2.0*G*XHI))**0.5
      DEL2=(DEL1*V1/V2)
      U(1)=V2
      D(1)=(DEL2*AXIS2)+del(neq-37)
      WRITE(5,*)'DDDD D',Del1,v1,v2,del2,del(neq-37),d(1)
      XHI=R*(1.0-COS(DX/R))
      U(1)=(((V2*V2)+2.0*G*XHI))**0.5
      D(1)=((V2)*D(1))/U(1)
      WRITE(5,*)'GGGGG D',DEL(1)


      DO 50 I=1,20
      CAA=((5.0/8.0)*(DEL(1)*U(1))/DX)
      CBB=((XKF*DT)/(RHOF*XHFG*(DEL(1)+D(1))))
      CCC=((D(1)*U(1))-(((DEL2*AXIS2)+DEL(NEQ-37))*(V2)))/DX
      C0=CAA-CBB+CCC

      CA=((17.0/35.0)*RHOF*(DEL(1)*U(1)*U(1)/DX))
      CB=DEL(1)*RHOF*G*SIN(X/R)*COS(VHI)
      CC=(3.0/2.0)*XMW*U(1)/DEL(1)
      CD=RHOF*(((D(1)*U(1)*U(1))-((DEL2*AXIS2+DEL(NEQ-
     *37))*(V2*V2)))/DX)
      C1=CA-CB+CC+CD

      PSI00AA=((5.0/8.0)*((DEL(1)+DELINC)*U(1))/DX)
      PSI00BB=((XKF*DT)/(RHOF*XHFG*(DEL(1)+DELINC+D(1))))
      PSI00CC=(D(1)*U(1)/DX)
      PSI00A=PSI00AA-PSI00BB+PSI00CC

      PSI00DD=((5.0/8.0)*DEL(1)*U(1))/DX
      PSI00EE=((XKF*DT)/(RHOF*XHFG*(DEL(1)+D(1))))
      PSI00FF=(D(1)*U(1)/DX)
      PSI00B=PSI00DD-PSI00EE+PSI00FF
      PSI00=(PSI00A-PSI00B)/DELINC

      PSI01A=((5.0/8.0)*(DEL(1)*(U(1)+UINC)/DX))
      PSI01B=((5.0/8.0)*(DEL(1)*U(1)/DX))
      PSI01=(PSI01A-PSI01B)/UINC
```

```
      PSI10A=((17.0/35.0)*RHOF*((DEL(1)+DELINC)*U(1)*U(1)/DX))
      PSI10B=(DEL(1)+DELINC)*RHOF*G*SIN(X/R)*COS(VHI)
      PSI10C=(3.0/2.0)*XMW*U(1)/(DEL(1)+DELINC)
      CA=((17.0/35.0)*RHOF*(DEL(1)*U(1)*U(1)/DX))
      CB=DEL(1)*RHOF*G*SIN(X/R)*COS(VHI)
      CC=(3.0/2.0)*XMW*U(1)/DEL(1)
      PSI10D=(CA-CB+CC)
      PSI10=((PSI10A-PSI10B+PSI10C)-PSI10D)/DELINC

      PSI11A=((17.0/35.0)*RHOF*(DEL(1)*(U(1)+UINC)*(U(1)+UINC)/DX))
      PSI11B=DEL(1)*RHOF*G*SIN(X/R)*COS(VHI)
      PSI11C=(3.0/2.0)*XMW*(U(1)+UINC)/DEL(1)

      PSI11=((PSI11A-PSI11B+PSI11C)-PSI10D)/UINC

      XJ=((PSI00*PSI11)-(PSI01*PSI10))
      XH=((-C0*PSI11)+(C1*PSI01))/XJ
      XK=((-C1*PSI00)+(C0*PSI10))/XJ

      DEL(1)=DEL(1)+XH
      U(1)=U(1)+XK
C      WRITE(5,*)'HKHKHKHKLL'

50    CONTINUE

      WRITE(5,*)'**************************************'

C      WRITE(5,*)U(1),DEL(1)
      WRITE(5,*)'SECOND CYLINDER'
      WRITE(5,*)'     TETHA        FILM THICKNESS       VELOCITY'

      WRITE(5,*)TETHA(1),DEL(1),U(1)


      DO 60 MM=2,NEQ

      U(MM)=((U(MM-1)*U(MM-1))+(2.0*G*XHI))**0.5

      D(MM)=(U(MM-1)*D(MM-1))/U(MM)
      XHI=R*(1.0-COS(DX/R))

      DO 70 J=1,20
      C0=((5.0/8.0)*(((DEL(MM)*U(MM))-(DEL(MM-1)*U(MM-1)))/DX)
     + -((XKF*DT)/(RHOF*XHFG*(DEL(MM)+D(MM))))
     + +(D(MM)*U(MM)-D(MM-1)*U(MM-1))/DX)

      CA=((17.0/35.0)*RHOF
     + *((DEL(MM)*U(MM)*U(MM))-(DEL(MM-1)*U(MM-1)*U(MM-1)))/DX)
      CB=DEL(MM)*RHOF*G*SIN(X/R)*COS(VHI)
      CC=(3.0/2.0)*XMW*U(MM)/DEL(MM)
      CD=(RHOF*((D(MM)*U(MM)*U(MM))-(D(MM-1)*U(MM-1)*U(MM-1)))/DX)
      C1=CA-CB+CC+CD

      PSI00A=((5.0/8.0)*(((DEL(MM)+DELINC)*U(MM)
     + -(DEL(MM-1)*U(MM-1)))/DX)
     + -((XKF*DT)/(RHOF*XHFG*(DEL(MM)+DELINC+D(MM)))))
      PSI00B=((5.0/8.0)*((DEL(MM)*U(MM))-(DEL(MM-1)*U(MM-1)))/DX)
     + -((XKF*DT)/(RHOF*XHFG*(DEL(MM)+D(MM))))
      PSI00=(PSI00A-PSI00B)/DELINC
```

```
      PSI01A=((5.0/8.0)*((DEL(MM)*(U(MM)+UINC))-(DEL(MM-1)*U(MM-
     *1)))/DX)
      PSI01B=((5.0/8.0)*((DEL(MM)*U(MM))-(DEL(MM-1)*U(MM-1)))/DX)
      PSI01=(PSI01A-PSI01B)/UINC

      PSI10A=((17.0/35.0)
     +*RHOF*((((DEL(MM)+DELINC)*U(MM)*U(MM))
     +-(DEL(MM-1)*U(MM-1)*U(MM-1)))/DX))
      PSI10B=(DEL(MM)+DELINC)*RHOF*G*SIN(X/R)*COS(VHI)
      PSI10C=(3.0/2.0)*XMW*U(MM)/(DEL(MM)+DELINC)
      PSI10D=(CA-CB+CC)
      PSI10=((PSI10A-PSI10B+PSI10C)-PSI10D)/DELINC

      PSI11A=((17.0/35.0)*RHOF
     + *((DEL(MM)*(U(MM)+UINC)*(U(MM)+UINC))
     + -(DEL(MM-1)*U(MM-1)*U(MM-1)))/DX)
      PSI11B=DEL(MM)*RHOF*G*SIN(X/R)*COS(VHI)
      PSI11C=(3.0/2.0)*XMW*(U(MM)+UINC)/DEL(MM)
      PSI11=((PSI11A-PSI11B+PSI11C)-PSI10D)/UINC

      XJ=((PSI00*PSI11)-(PSI01*PSI10))
c      WRITE(5,*)PSI00,PSI11,PSI01,PSI10,XJ
      XH=((-C0*PSI11)+(C1*PSI01))/XJ
      XK=((-C1*PSI00)+(C0*PSI10))/XJ

      WRITE(5,*)PSI00,PSI11,PSI01,PSI10,XJ

      DEL(MM)=DEL(MM)+XH
      U(MM)=U(MM)+XK

 70   CONTINUE
      WRITE(5,*)TETHA(MM),DEL(MM),U(MM)

      DEL(MM)=DEL(MM)+D(MM)
  60  CONTINUE

C*************************************************
C     START SOLUTION FOR THE THIRD CYLINDER
C**************************************************

      UM=U(NEQ)
      V1=UM
      DEL1=DEL(NEQ)
      XHI=0.02
      V2=(((V1*V1)+2.0*G*XHI))**0.5
      DEL2=(DEL1*V1/V2)
      U(1)=V2
      D(1)=(DEL2*AXIS2)+del(neq-30)
C      WRITE(5,*)'SSSSSD',D(1),DEL(11)
      XHI=R*(1.0-COS(DX/R))
      U(1)=(((V2*V2)+2.0*G*XHI))**0.5
      D(1)=(V2*D(1)/U(1))
C      WRITE(5,*)'EEEEEE',D(1)
C      WRITE(5,*)U(1),DEL(1),D(1)

      DO 90 I=1,20
      CAA=((5.0/8.0)*(DEL(1)*U(1))/DX)
      CBB=((XKF*DT)/(RHOF*XHFG*(DEL(1)+D(1))))
      CCC=(((D(1)*U(1))-(DEL2*AXIS2*V2))/DX)
      C0=CAA-CBB+CCC
```

```
      CA=((17.0/35.0)*RHOF*(DEL(1)*U(1)*U(1)/DX))
      CB=DEL(1)*RHOF*G*SIN(X/R)*COS(VHI)
      CC=(3.0/2.0)*XMW*U(1)/DEL(1)
      CD=RHOF*(((D(1)*U(1)*U(1))-(DEL2*AXIS2*V2*V2))/DX)
      C1=CA-CB+CC+CD

      PSI00AA=((5.0/8.0)*((DEL(1)+DELINC)*U(1))/DX)
      PSI00BB=((XKF*DT)/(RHOF*XHFG*(DEL(1)+DELINC+D(1))))
      PSI00CC=(D(1)*U(1)/DX)
      PSI00A=PSI00AA-PSI00BB+PSI00CC

      PSI00DD=((5.0/8.0)*DEL(1)*U(1))/DX
      PSI00EE=((XKF*DT)/(RHOF*XHFG*(DEL(1)+D(1))))
      PSI00FF=(D(1)*U(1)/DX)
      PSI00B=PSI00DD-PSI00EE+PSI00FF
      PSI00=(PSI00A-PSI00B)/DELINC

      PSI01A=((5.0/8.0)*(DEL(1)*(U(1)+UINC)/DX))
      PSI01B=((5.0/8.0)*(DEL(1)*U(1)/DX))
      PSI01=(PSI01A-PSI01B)/UINC

      PSI10A=((17.0/35.0)*RHOF*((DEL(1)+DELINC)*U(1)*U(1)/DX))
      PSI10B=(DEL(1)+DELINC)*RHOF*G*SIN(X/R)*COS(VHI)
      PSI10C=(3.0/2.0)*XMW*U(1)/(DEL(1)+DELINC)
      CA=((17.0/35.0)*RHOF*(DEL(1)*U(1)*U(1)/DX))
      CB=DEL(1)*RHOF*G*SIN(X/R)*COS(VHI)
      CC=(3.0/2.0)*XMW*U(1)/DEL(1)
      PSI10D=(CA-CB+CC)
      PSI10=((PSI10A-PSI10B+PSI10C)-PSI10D)/DELINC

      PSI11A=((17.0/35.0)*RHOF*(DEL(1)*(U(1)+UINC)*(U(1)+UINC)/DX))
      PSI11B=DEL(1)*RHOF*G*SIN(X/R)*COS(VHI)
      PSI11C=(3.0/2.0)*XMW*(U(1)+UINC)/DEL(1)
      PSI11=((PSI11A-PSI11B+PSI11C)-PSI10D)/UINC

      XJ=((PSI00*PSI11)-(PSI01*PSI10))
      XH=((-C0*PSI11)+(C1*PSI01))/XJ
      XK=((-C1*PSI00)+(C0*PSI10))/XJ

      DEL(1)=DEL(1)+XH
      U(1)=U(1)+XK


 90   CONTINUE

      WRITE(5,*)'**********************************************'
      WRITE(5,*)'THIRD CYLINDER'
      WRITE(5,*)'     TETHA        FILM THICKNESS       VELOCITY'

      WRITE(5,*)TETHA(1),DEL(1),U(1)
      D(1)=D(1)+DEL(NEQ-30)

      DO 100 MM=2,NEQ

      U(MM)=((U(MM-1)*U(MM-1))+(2.0*G*XHI))**0.5

      D(MM)=(U(MM-1)*D(MM-1))/U(MM)
      XHI=R*(1.0-COS(DX/R))
```

```
      DO 110 J=1,20
      C0=((5.0/8.0)*(((DEL(MM)*U(MM))-(DEL(MM-1)*U(MM-1)))/DX)
     + -((XKF*DT)/(RHOF*XHFG*(DEL(MM)+D(MM))))
     + +(D(MM)*U(MM)-D(MM-1)*U(MM-1))/DX)

      CA=((17.0/35.0)*RHOF
     + *((DEL(MM)*U(MM)*U(MM))-(DEL(MM-1)*U(MM-1)*U(MM-1)))/DX)
      CB=DEL(MM)*RHOF*G*SIN(X/R)*COS(VHI)
      CC=(3.0/2.0)*XMW*U(MM)/DEL(MM)
      CD=(RHOF*((D(MM)*U(MM)*U(MM))-(D(MM-1)*U(MM-1)*U(MM-1)))/DX)
      C1=CA-CB+CC+CD

      PSI00A=((5.0/8.0)*(((DEL(MM)+DELINC)*U(MM)
     + -(DEL(MM-1)*U(MM-1)))/DX)
     + -((XKF*DT)/(RHOF*XHFG*(DEL(MM)+DELINC+D(MM)))))
      PSI00B=((5.0/8.0)*((DEL(MM)*U(MM))-(DEL(MM-1)*U(MM-1)))/DX)
     + -((XKF*DT)/(RHOF*XHFG*(DEL(MM)+D(MM))))
      PSI00=(PSI00A-PSI00B)/DELINC

      PSI01A=((5.0/8.0)*((DEL(MM)*(U(MM)+UINC))-(DEL(MM-1)*U(MM-
     *1)))/DX)
      PSI01B=((5.0/8.0)*((DEL(MM)*U(MM))-(DEL(MM-1)*U(MM-1)))/DX)

      PSI01=(PSI01A-PSI01B)/UINC

      PSI10A=((17.0/35.0)
     +*RHOF*((((DEL(MM)+DELINC)*U(MM)*U(MM))
     +-(DEL(MM-1)*U(MM-1)*U(MM-1)))/DX))
      PSI10B=(DEL(MM)+DELINC)*RHOF*G*SIN(X/R)*COS(VHI)
      PSI10C=(3.0/2.0)*XMW*U(MM)/(DEL(MM)+DELINC)
      PSI10D=(CA-CB+CC)
      PSI10=((PSI10A-PSI10B+PSI10C)-PSI10D)/DELINC

      PSI11A=((17.0/35.0)*RHOF
     + *((DEL(MM)*(U(MM)+UINC)*(U(MM)+UINC))
     + -(DEL(MM-1)*U(MM-1)*U(MM-1)))/DX)
      PSI11B=DEL(MM)*RHOF*G*SIN(X/R)*COS(VHI)
      PSI11C=(3.0/2.0)*XMW*(U(MM)+UINC)/DEL(MM)
      PSI11=((PSI11A-PSI11B+PSI11C)-PSI10D)/UINC

      XJ=((PSI00*PSI11)-(PSI01*PSI10))
C      WRITE(5,*)PSI00,PSI11,PSI01,PSI10,XJ
      XH=((-C0*PSI11)+(C1*PSI01))/XJ
      XK=((-C1*PSI00)+(C0*PSI10))/XJ

      DEL(MM)=DEL(MM)+XH
      U(MM)=U(MM)+XK

 110  CONTINUE
C      WRITE(5,*)MM,DEL(MM),U(MM)

      WRITE(5,*)TETHA(MM),DEL(MM),U(MM)

      DEL(MM)=DEL(MM)+D(MM)
 100  CONTINUE

      STOP
      END
```

### D.2 Program (FASTM10.FOR) to solve the system of governing partial differential equations for the investigation of forced film condensation of vapor–air mixture flowing downward bundle of horizontal cylinders for both inline and staggered arrangements

```
$DEBUG


C*****************************************************************
C     PROGRAM (FASTM10.FOR) TO SOLVE THE PDE'S SYSTEM OF EQNS FOR*
C     INVESTIGATION OF FORCED FILM CONDENSATION OF VAPOR-AIR     *
C     MIXTURE FLOWING DOWNWARD BUNDLE OF HORIZONTAL CYLINDERS    *
C     FOR BOTH INLINE AND STAGGERED CYLINDERS                    *
C                                                                *
C*****************************************************************

C     OPEN ARRAYS DIMENSIONS AND INPUT DATA
C     **************************************

      DIMENSION  UL(300,300),VL(350),TL(350),UV(350),UVP(250),UVN(250)
      DIMENSION VV(250),TV(250),XMV(250),UVE(540),XXQ(250)
      DIMENSION FN(250),FR(250),ALPHA(250),CN(250)


      DIMENSION DEL(250),XP(250),XQ(250),XPM(250),XQM(250),DELL(250)

      DIMENSION BETA(250),GAMA(250),XPG(250),XQG(250),GN(250)
      DIMENSION TAUI(250)
      DIMENSION XNU(250),TI(250),DELNU(250),QNU(250),DELTA(250)

      DIMENSION SC(250),XQ1(250),Q(250),QS(250),XH(250)


      DATA G,TW,TE,UE,VHI/9.81,353.15,373.15,1.0,0.0/
      DATA XME,CPL,CPV,SC(1)/0.019,4214.0,2029.0,0.5/
      DATA BMUL,PR/0.000289,0.7/
      DATA R,XKL,XKV/0.0254,0.680,0.0248/
      DATA XM1,XM2,XPI,RR/28.97,18.015,3.14,8.3145/
      DATA A,B,C,EPS,H/42.6776,-3892.70,-9.48654,0.000001,0.02/

C     START WITH CALCULATION OF FROUD NO., INTERFACIAL TEMP.,
C     FREE PRESURE,CP FOR MIXTURE AND SATURATION PRESSURE
C*******************************************************************
      WRITE(5,*)'RADIUS',R

      CPA=SPECA(TE)
      WRITE(5,*)' CPA',CPA

      BMUV=VISCV(TE)
      WRITE(5,*)' BMUV',BMUV

      XKA=CONDA(TE)
      WRITE(5,*)' XKA',XKA

      TR=TW+0.33*(TE-TW)
```

```
      CPE=((XME*CPA)+((1.0-XME)*CPV))
C      FR=(G*R/(4.0*UE*UE))

      TI(1)=TW+0.9*(TE-TW)
      HFG=LATENT(TI(1))
      WRITE(5,*)' HFG',TR,HFG

C      TII=TI(1)
      RHOL=RHOO(TR)
      WRITE(5,*)'RHOL',RHOL
      WRITE(5,*)'UE ',UE
      BNUL=BMUL/RHOL

      XMM=XME
      PS=EXP((B/(TE-A))-C)
      PE=(PS*((XM1+XMM*(XM2-XM1))/(XM1-XMM*XM1)))
      PG=PE*((XME*XM2)/(XM1+XME*(XM2-XM1)))
      PV=PE-PG



      RHOG=((PG*1000.0*XM1)/(RR*TI(1)))
      RHOV=((PV*1000.0*XM2)/(RR*TI(1)))
      RHOE=RHOG+RHOV

      PSAI=EXP((B/(TI(1)-A))-C)

      XMV(1)=((PE-PSAI)/(PE-(1.0-(XM2/XM1))*PSAI))
C      XMV(1)=0.0

      BNUV=BMUV/RHOV


      BMUE=VISCE(TE,XM1,XM2)
      XKE=CONDE(TE,XM1,XM2)
      BNUE=BMUE/RHOE

      SCE=SCCE(TE,PE,XM1,XM2,BNUV)
C      PR=(CPV*BMUV)/XKV

      WRITE(5,*)'XME ',XME
      WRITE(5,*)'SCE ',SCE
      WRITE(5,*)'PE ',PE
      WRITE(5,*)'PS ',PS
      WRITE(5,*)'TE ',TE
      WRITE(5,*)'TR ',TR
      WRITE(5,*)'TW ',TW
      WRITE(5,*)'TI(1) ',TI(1)
      WRITE(5,*)'RHOE ',RHOE
      WRITE(5,*)'RHOG ',RHOG
      WRITE(5,*)'RHOV ',RHOV
      WRITE(5,*)'XKE ',XKE
      WRITE(5,*)'XKV ',XKV
      WRITE(5,*)'XKL ',XKL
      WRITE(5,*)'XMV(1) ',XMV(1)

C***************************************************
C CALCULATION OF CRITICAL ANGLE OF INCLINATION
C****************************************************
```

```
      WRITE(5,*)
      WRITE(5,*)
      WRITE(5,*)'ANGLE OF INCLINATION =',VHI

      VHI=VHI*(3.14/180.0)
      FF=(R/((2.0*R)+H))
      VHIC=ASIN(FF)
      VHIC=VHIC*(180.0/3.14)

      TETHA0=VHI*90.0/VHIC
      TETHA0=TETHA0*(180.0/3.14)
C      WRITE(5,*)
      WRITE(5,*)'CRITICAL ANGLE OF INCLINATION=',VHIC
      WRITE(5,*)'TETHA0  =',TETHA0
      WRITE(5,*)
      WRITE(5,*)


C    CALCULATION OF INITIAL VALUES OF FILM THICKNESS AND INTEFACIAL
C    SHEAR
C*******************************************************************
      WRITE(5,*)'AAAAAAAA',DEL(1)

C FOR UE=0.305 M/S
C      DY=0.0000042
C      XLX=DY*250.0
C      L=XLX/DY

C FOR UE=1.0 M/S
C      DY=0.0000029
C      XLX=DY*250.0
C      L=XLX/DY

C FOR UE=1.0 M/S
C      DY=0.0000033
C      XLX=DY*250.0
C      L=XLX/DY


C FOR UE=1.0 M/S, R=0.00955
C      DY=0.0000020
C      XLX=DY*250.0
C      L=XLX/DY

C FOR UE=2.7 M/S, R=0.00955
C      DY=0.0000016
C      XLX=DY*250.0
C      L=XLX/DY


C FOR UE=3.05 M/S, XME=0.01
C      DY= 0.00000440
C      XLX=DY*250.0
C      L=XLX/DY

C FOR UE=20.0 M/S, XME=0.01
C      DY= 0.0000018
C      XLX=DY*250.0
C      L=XLX/DY
```

```
C FOR UE=3.05 M/S
c       DY= 0.0000020
c       XLX=DY*250.0
c       L=XLX/DY



C FOR UE=3.05 M/S
      DY= 0.0000024
      XLX=DY*250.0
      L=XLX/DY

C FOR UE=10 M/S  R=0.00635
C       DY= 0.0000016
C       XLX=DY*250.0
C       L=XLX/DY


C FOR UE=10 M/S  R=0.0127
c       DY= 0.0000020
C       XLX=DY*250.0
C       L=XLX/DY

C FOR UE=10 M/S  R=0.01905 DT=40
C       DY= 0.0000020
C       XLX=DY*250.0
C       L=XLX/DY

C FOR UE=10 M/S  R=0.01905
C       DY= 0.0000020
C       XLX=DY*250.0
C       L=XLX/DY

C FOR UE=10 M/S R=0.0254
C       DY= 0.0000025
C       XLX=DY*250.0
C       L=XLX/DY

C FOR UE=10 M/S,XME=0.01
C       DY= 0.0000027
C       XLX=DY*250.0
C       L=XLX/DY

C FOR UE=20.0 M/S
C       DY= 0.0000015
C       XLX=DY*250.0
C       L=XLX/DY

C FOR UE=30.0 M/S
C       DY= 0.0000015
C       XLX=DY*250.0
C       L=XLX/DY


      DX=XPI*R/180.0

      DETA=0.004
      N=1.0/DETA

      M=XPI*R/DX
```

```
      WRITE(5,*)'N,L,M,DX,DY,XLX',N,L,M,DX,DY,XLX

      X=0.005
      R1=(XKL*(TI(1)-TW)/(BMUL*HFG))
      F1=(1.0/(1.0+R1))
      F2=(4.0+R1)*(1.0+R1)/4.0
      GG=G*(1.0-(RHOE/RHOL))
      FS=(UE*UE+(16.0*GG*X/R1)*F2)**0.5
      FT=(UE+FS)/8.0
      FE=((F1/(BNUL*X))*FT)**0.5
      DEL(1)=(1.0/FE)


      XM=(XKL*(TI(1)-TW)/(HFG*DEL(1)))

      US=XM*UE
      UL(1,N)=F1*((G*(RHOL-RHOE)*DEL(1)*DEL(1)/(2.0*BMUL))+US)

      TAUI(1)=XM*(UE-UL(1,N))
      TAUI(1)=ABS(TAUI(1))

      WRITE(5,*)'TAUI,DEL1,XM,ULN',TAUI(1),DEL(1),XM,UL(1,N)
      DT=TE-TW
      DELNU(1)=((BNUL*3.0*XKL*DT*X)/(G*RHOL*HFG*SIN(X/R)))**0.25
      Q(1)=XKL*DT/DEL(1)
      QNU(1)=XKL*DT/DELNU(1)

C     INCREMENTS AND INITIAL AND BOUNDARY CONDITIONS
C***************************************************

      DO 10 I=1,M
      X=I*DX
      UL(I,1)=0.0
      VL(1)=0.0
      TL(1)=TW

      XMV(L)=XME
      TV(L)=TE
      SSIN=SIN(X/R)
      UVE(I)=2.0*UE*SSIN
      FR(I)=(G*R/(4.0*UVE(I)*UVE(I)))
C      WRITE(5,*)I,DX,X,R,SSIN,UVE(I)
 10   CONTINUE

      WRITE(5,*)'AAAAAAAA',DEL(1)

C     START CALCULATIONS FOR FIRST PROFILES AT STAGNATION POINT
C *************************************************************

      DO 20 J=2,N
      ETA=J*DETA
      UL(1,J)=((G*DEL(1)*DEL(1)*DX)/(BNUL*R))*(ETA-(ETA*ETA/2.0))
      VL(J)=((G*DEL(1)*DEL(1)*DEL(1))/(BNUL*R))*((ETA*ETA*ETA/6.0)
     * -(ETA*ETA/2.0))-(UL(1,J)*DEL(1)*ETA/DX)
C      WRITE (5,*)'ASSASS',BNUL,DEL(1),UL(1,J)
C      XML(1,J)=1.0
  20  CONTINUE
      WRITE(5,*)'AAAAAAAA',DEL(1)

      DO 30 J=2,N
```

```
      ETA=J*DETA
      TL(J)=((TI(1)-TW)*ETA+TW)
  30  CONTINUE


      DO 40 K=1,L-1
      UV(K)=UL(1,N)
      UVP(K)=UL(1,N)
      XMV(K)=XMV(1)
      TV(K)=TL(N)
  40  CONTINUE

      DO 50 K=1,L
      VV(K)=VL(N)
  50  CONTINUE

      QS(1)=XKV*((-TV(3)+(4.0*TV(2))-(3.0*TV(1)))/(2.0*DY))

C     START CALCULATION FOR THE COMPLETE NUMERICAL SCHEME
C***************************************************
C*************************************************
C********************************************
      DO 60 I=2,M
C      DO 65 ITER=1,100
      X=I*DX
C      WRITE(5,*)'LIQUID BOUNDARY LAYER RESULTS'
C

C     START SOLUTION FOR LIQUID BOUNDARY LAYER
C********************************************

      DO 70 J=2,N
      ETA=J*DETA
      ZA=((-DEL(I-1)*DEL(I-1)*G*SIN(X/R))/BMUL)*RHOL*COS(VHI)
C      DP=0.0
      DP=((RHOE-(RHOE/FR(I))*COS(X/R))*G*SIN(X/R))
      ZB=((DEL(I-1)*DEL(I-1))*DP)/BMUL
      ZC=(TAUI(I-1)*DEL(I-1)*ETA/BMUL)
      UL(I,J)=((ZA+ZB)*((ETA*ETA/2.0)-ETA))+ZC

      ZAA=((((RHOL*COS(VHI))-RHOE)*DEL(I-1)*DEL(I-1)*DEL(I-1))*G*X*
     + COS(X/R))/BMUL
      ZBB=RHOE*DEL(I-1)*DEL(I-1)*DEL(I-1)*G*X/BMUL
      ZCC=(COS(X/R)*COS(X/R))-(SIN(X/R)*SIN(X/R))
      VL(J)=(ZAA+(ZBB*ZCC))*((ETA*ETA*ETA/6.0)-(ETA*ETA/2.0))
C      WRITE(5,*)ETA,UL(I,J),VL(J)
  70  CONTINUE

      DO 80 J=2,N
      ETA=J*DETA
      TL(J)=(TI(I-1)-TW)*ETA+TW
  80  CONTINUE

C      WRITE(5,*)'FR,TAUI,DEL,DX',FR(I),TAUI(I-1),DEL(I-
     +1),DX,ETA,DETA

      DO 85 J=1,N
      ETA=J*DETA
C      WRITE(5,*)J,UL(I,J),TL(J)
  85  CONTINUE
```

```
      XD=((XKL*DX*(TL(2)-TW))/(DEL(I-1)*DETA*RHOL*HFG))
      XC=((XKV*DX*(TV(2)-TV(1)))/(DY*RHOL*HFG))
      CC11=((G*SIN(X/R)/BMUL)*((RHOL-RHOE)+(RHOE/FR(I))*COS(X/R)))
      CC22=CC11*DEL(I-1)*DEL(I-1)
      CC33=(CC22+(TAUI(I-1)*DEL(I-1)/BMUL))

      DEL(I)=((XD+XC+(CC33*DEL(I-1)))/CC33)



C     START SOLUTION FOR VAPOR BOUNDARY LAYER
C*******************************************
C     START SOLUTION FOR VAPOR VELOCITY BOUNDARY LAYER
C****************************************************

      DO 90 K=2,L-1
      ALPHA(K)=(BNUV*DX/(UV(K)*DY*DY))
      AF=((VV(K)*DX)/(2.0*UV(K)*DY))
      BF=(UV(K+1)-UV(K-1))
C      CF=0.0
      CF=((UVE(I)*UVE(I)-UVE(I-1)*UVE(I-1))/(2.0*UV(K)))
      DF=(G*SIN(X/R)*COS(VHI)*DX)/UV(K)
      CN(K)=UV(K)-(AF*BF)+CF+DF
      UVP(K)=UV(K)
      UV(L)=UVE(I)
 90   CONTINUE


      XP(2)=(ALPHA(2)/(1.0+(2.0*ALPHA(2))))
      XQ(2)=((ALPHA(2)*UL(I,N)+CN(2))/(1.0+2.0*ALPHA(2)))

      DO 100 K=3,L-1
      XP(K)=(ALPHA(K)/(1.0+2.0*ALPHA(K)-ALPHA(K)*XP(K-1)))
      XQ(K)=(ALPHA(K)*XQ(K-1)+CN(K))/(1.0+2.0*ALPHA(K)-
     *ALPHA(K)*XP(K-1))
 100  CONTINUE
C      WRITE(5,*)' DISTRIBUTION  AT VAPOR BOUNDARY LAYER'

      DO 110 K=2,L-1
      KK=L-(K-1)
      UV(KK)=((XP(KK)*UV(KK+1))+XQ(KK))
      UVN(KK)=UV(KK)
 110  CONTINUE

C      XAX=(2.0*TAUI(I-1)*DY/(3.0*BMUV))
C      UV(1)=((-UV(3)/3.0)+(4.0*UV(2)/3.0)-XAX)
      UV(1)=UL(I,N)

C     START SOLUTION FOR VAPOR CONCENTRATION BOUNDARY LAYER
C*******************************************************

      DO 120 K=2,L-1
      BETA(K)=(BNUV*DX/(SC(I-1)*UV(K)*DY*DY))
      FN(K)=XMV(K)-((((VV(K)*DX)/(2.0*UV(K)*DY))*(XMV(K+1)-XMV(K-1)))
 120  CONTINUE

      XPM(2)=(BETA(2)/(1.0+2.0*BETA(2)))
      XQM(2)=(BETA(2)*XMV(1)+FN(2))/(1.0+2.0*BETA(2))
```

```
      DO 130 K=3,L-1
      XPM(K)=(BETA(K)/(1.0+2.0*BETA(K)-BETA(K)*XPM(K-1)))
      XQM(K)=(BETA(K)*XQM(K-1)+FN(K))/(1.0+2.0*BETA(K)-
     *BETA(K)*XPM(K-1))
  130 CONTINUE

      DO 140 K=2,L-1
      KK=L-(K-1)
      XMV(KK)=XPM(KK)*XMV(KK+1)+XQM(KK)
C      WRITE(5,*)KK,UV(KK),XMV(KK),XMV(L)
 140  CONTINUE
      XAAX=((2.0*XM*SC(I-1)*DY/BMUV)-3.0)
      XMV(1)=((-4.0*XMV(2))+XMV(3))/XAAX

C     START SOLUTION FOR VAPOR TEMPERATURE DISTRIBUTION
C*******************************************************

      DO 150 K=2,L-1
      GAMA(K)=(BNUV*DX/(PR*UV(K)*DY*DY))
      GA=((VV(K)*DX)/(2.0*UV(K)*DY))
      GB=(TV(K+1)-TV(K-1))
      GC=((BNUV*DX*((CPA-CPV)/CPE))/(4.0*SC(I-1)*UV(K)*DY*DY))
      GD=(XMV(K+1)-XMV(K-1))
      GN(K)=TV(K)-(GA*GB)+(GC*GB*GD)
 150  CONTINUE

      XPG(2)=(GAMA(2)/(1.0+2.0*GAMA(2)))
      XQG(2)=(GAMA(2)*TL(N)+GN(2))/(1.0+2.0*GAMA(2))

      DO 160 K=3,L-1
      XPG(K)=(GAMA(K)/(1.0+2.0*GAMA(K)-GAMA(K)*XPG(K-1)))
      XQG(K)=(GAMA(K)*XQG(K-1)+GN(K))/(1.0+2.0*GAMA(K)-
     *GAMA(K)*XPG(K-1))
  160 CONTINUE

      DO 170 K=2,L-1
      KK=L-(K-1)
      TV(KK)=XPG(KK)*TV(KK+1)+XQG(KK)
 170  CONTINUE
C      XAAAX=(2.0*QS(I-1)*DY/(3.0*XKV))
C      TV(1)=((-TV(3)/3.0)+(4.0*TV(2)/3.0)-XAAAX)
      TV(1)=TL(N)
C     START CALCULATION OF LIQUID FILM THICKNESS
C ***********************************************
      DO 171 K=1,L
C      WRITE(5,*)K,UV(K),TV(K),XMV(K)
 171  CONTINUE

C START CALCULATION FOR VERTICAL COMPONENT OF LIQUID AND VAPOR
C     VELOCITY
C *************************************************************

      VV(1)=((UV(1)*((DEL(I)-DEL(I-1))/DX))-(XM/RHOV))

      UVN(L)=UVE(I)
      UVP(L)=UVE(I)
      DO 182 K=2,L
      VV(K)=VV(K-1)-((DY/(2.0*DX))*(UVN(K)-UVP(K)+UVN(K-1)-UVP(K-1)))
C      VV(K)=-VV(K)
```

```
C       WRITE(5,*)'DDDDVV,VV(K)',K ,VV(1),VV(K),UVN(K),UVP(K)
 182  CONTINUE


C START CALCULATION FOR INTERFACIAL SHEAR, LOCAL HEAT TRANSFER COEFF.
C AND LOCAL NUSSELT NUMBER
C*********************************************************************

      TAUI(I)=BMUV*((-UV(3)+(4.0*UV(2))-(3.0*UV(1)))/DY)
C       TAUU=BMUL*((UL(I,N)-UL(I,N-1))/(DEL(I)*DETA))

      QS(I)=XKV*((-TV(3)+(4.0*TV(2))-(3.0*TV(1)))/(2.0*DY))

C       WRITE(5,*) 'NEW SHEAR',I,TAUI(I),XMV(1)

CC       XH(I)=(XKL*(TL(2)-TL(1))/(DETA*DEL(I)*(TI(I-1)-TW)))
CC       XNU(I)=(2.0*R*XH(I)/XKL)

      IF(UL(I,2).LE.0) GOTO 188

CC       WRITE(5,*)'XHI,XNU',XH(I),XNU(I)
CC       WRITE(5,*)XH(I),XNU(I)

C CALCULATION OF MASS FLOW RATE, AIR CONCENTRATION, VAPOR          C
CONCENTRATION,
C     PRESSURE AND INTERFACIAL TEMPERATURE TI AT INTERFACE
C*********************************************************************


      PVI=(PE*(1.0-XMV(1))/(1.0-(XMV(1)*(1.0-(XM2/XM1)))))

      TI(I)=(A+(B/(ALOG(PVI)+C)))

      TG=TI(I)

      SC(I)=SCC(PVI,TG,XM1,XM2,BNUV)
      AX=(BMUV/(SC(I)*DY))
      XM4=AX*((XMV(2)-XMV(1))/XMV(1))
      XM=-XM4
C       WRITE(5,*)'XM,XMV(1),TAUI,TI',XM,XMV(1),TAUI(I),TI(I)
C  65  CONTINUE

C---------------------------------------------

C  START TO CALCULATE HEAT ENERGY FOR PRESENT STUDY AND NUSSELT
C  SOLUTION



      DT=TI(I)-TW
      DELNU(I)=((BNUL*3.0*XKL*DT*X)/(G*(RHOL-
     *RHOE)*HFG*SIN(X/R)))**0.25
C       WRITE(5,*)'DELNU',DT,DELNU(I)


      QNU(I)=XKL*(TI(I)-TW)/DELNU(I)
      XHNU=QNU(I)/DT

C       DEL(I)=(XKL*(TI(I)-TW)/(XM*HFG))
```

```
C       XM=(XKL*DT)/(DEL(I)*HFG)
      XQ(I)=XM*HFG
      XXQ(I)=XKL*DT/DEL(I)

      RATIO=XQ(I)/QNU(I)
      RATTIO=XXQ(I)/QNU(I)
      XH(I)=XQ(I)/(TI(I)-TW)
      XNU(I)=XH(I)*2.0*R/XKL

      DO 186 J=1,N
C       WRITE(5,*)J,UL(I,J),TL(J)
 186  CONTINUE
      DO 187 K=1,L
C       WRITE(5,*)K,UV(K),TV(K),XMV(K)
 187  CONTINUE
C       WRITE(5,*)'============================'
C       WRITE(5,*)I,UL(I-1,N),DEL(I),TI(I),RATIO

      WRITE(5,1)I,DEL(I),RATIO,XH(I),XNU(I)
 1    FORMAT (I4,2X,F20.10,2X,F15.5,2X,F15.5,2X,F15.5)
C     WRITE(5,*)'**************************************************'
      UUL=UL(I-2,N)
      XMVV=XMV(1)
      DELL(I)=DEL(I)
 60   CONTINUE

C*****************************************************************
C*****************************************************************
C START CALCULATION FOR THE SECOND CYLINDER
C*****************************************************************
C*****************************************************************
C     SET BOUNDARY CONDITIONS BETWEEN FIRST CYLINDER
C     AND SECOND CYLINDER (CONTINUITY AND BERNOULLI EQUATIONS
C**********************************************************

  188 UY=UUL
      U1=UY
C       U2=UY
      DELONE=DEL(I-2)
C       DEL(1)=DELONE
      UUR=((U1*U1)+(2.0*G*H))
      U2=(UUR)**0.5
      DELTWO=DELONE*U1/U2
      JJJ=TETHA0
C       DELTA(1)=(DELTWO)+DELL(JJJ)

       DELTA(1)=DELTWO

CC       DELTA(1)=(0.5*DELTWO)+DELL(JJJ)
C       DELTA(1)=DELTWO+DELL(JJJ)

      WRITE(5,*)'G,H,U1,U2,DELTA,DEL(JJJ),JJJ',G,H,U1,U2,DELTA(1),
     + DEL(JJJ),JJJ

C       DELTA(1)=DELONE
C       XMV(1)=((PE-PSAI)/(PE-(1.0-(XM2/XM1))*PSAI))

      XMV(1)=(XMVV+XME)/2.0
```

```
      WRITE(5,*)'SECOND CYLINDER*************************'

WRITE(5,*)'U1,DELONE,U2,G,H,DELTWO,DELTA,XMV',I,U1,DELONE,U2,G,H,
     * DEL(2),DELTA(1),XMV(1)
      WRITE(5,*)'N,L,M,DX,DY,XLX',N,L,M,DX,DY,XLX

C    CALCULATION OF INITIAL VALUES OF INTEREFACIAL LIQUID VELOCITY
C    AND SHEAR
C    FILM THICKNESS AND HEAT
C*******************************************************************

      DEL(1)=DELONE+DELTA(1)

C      DEL(1)=DELTA(1)
      WRITE(5,*)'I,DEL1',I,DEL(1)

      XM=(XKL*(TI(1)-TW)/(HFG*DEL(1)))

C      US=XM*UE
C      UL(1,N)=F1*((G*(RHOL-RHOE)*DEL(1)*DEL(1)/(2.0*BMUL))+US)
      UL(1,N)=U2

C      TAUI(1)=0.23
      TAUI(1)=XM*(UE-UL(1,N))
      TAUI(1)=ABS(TAUI(1))
      WRITE(5,*)'I,TAUI,DEL1,XM,ULN',I,TAUI(1),DEL(1),XM,UL(1,N)

C      DT=TE-TW
C      DELNU(1)=((BNUL*3.0*XKL*DT*X)/(G*RHOL*HFG*SIN(X/R)))**0.25
C      Q(1)=XKL*DT/DEL(1)
C      QNU(1)=XKL*DT/DELNU(1)



      WRITE(5,*)'I,DEL1,DELTA',I,DEL(1),DELTA(1)
C    INCREMENTS AND INITIAL AND BOUNDARY CONDITIONS
C***************************************************


      DO 190 I=1,M
      X=I*DX
      UL(1,1)=0.0
      VL(1)=0.0
      TL(1)=TW

      XMV(L)=XME
      TV(L)=TE
      SSIN=SIN(X/R)
      UVE(I)=2.0*UE*SSIN
      FR(I)=(G*R/(4.0*UVE(I)*UVE(I)))
C      WRITE(5,*)I,DX,X,R,SSIN,UVE(I)
 190  CONTINUE


C     START CALCULATIONS FOR FIRST PROFILES AT STAGNATION POINT
C *************************************************************

      DO 200 J=2,N
      ETA=J*DETA
      UL(1,J)=((G*DEL(1)*DEL(1)*DX)/(BNUL*R))*
```

```
     * (ETA-(ETA*ETA/2.0))
      VL(J)=((G*DEL(1)*DEL(1)*DEL(1))/(BNUL*R))*
     * ((ETA*ETA*ETA/6.0)-(ETA*ETA/2.0))-(UL(1,J)*DEL(1)*ETA/DX)

 200  CONTINUE

      WRITE(5,*)'DEL(1),UL(1,N)',DEL(1),UL(1,N)
      DO 210 J=2,N
      ETA=J*DETA
      TL(J)=((TI(1)-TW)*ETA+TW)
 210  CONTINUE

      DO 220 K=1,L-1
      UV(K)=UL(1,N)
      UVP(K)=UL(1,N)
      XMV(K)=XMV(1)

C      XMV(K)=XMVV
      TV(K)=TL(N)
 220  CONTINUE

      DO 230 K=1,L
      VV(K)=VL(N)
 230  CONTINUE

      QS(1)=XKV*((-TV(3)+(4.0*TV(2))-(3.0*TV(1)))/(2.0*DY))

C     START CALCULATION FOR THE COMPLETE NUMERICAL SCHEME
C*********************************************************
C*****************************************************
C**********************************************
      DO 240 I=2,M
C      DO 65 ITER=1,100
      X=I*DX
C      WRITE(5,*)'LIQUID BOUNDARY LAYER RESULTS'
C

C     START SOLUTION FOR LIQUID BOUNDARY LAYER
C**********************************************

      DO 250 J=2,N
      ETA=J*DETA
      ZA=((-DEL(I-1)*DEL(I-1)*G*SIN(X/R))/BMUL)*RHOL*COS(VHI)
C      DP=0.0
      DP=((RHOE-(RHOE/FR(I))*COS(X/R))*G*SIN(X/R))
      ZB=((DEL(I-1)*DEL(I-1))*DP)/BMUL
      ZC=(TAUI(I-1)*DEL(I-1)*ETA/BMUL)
      UL(I,J)=((ZA+ZB)*((ETA*ETA/2.0)-ETA))+ZC

      ZAA=((((RHOL*COS(VHI))-RHOE)*DEL(I-1)*DEL(I-1)*DEL(I-1))*G*X*
     + COS(X/R))/BMUL
      ZBB=RHOE*DEL(I-1)*DEL(I-1)*DEL(I-1)*G*X/BMUL
      ZCC=(COS(X/R)*COS(X/R))-(SIN(X/R)*SIN(X/R))
      VL(J)=(ZAA+(ZBB*ZCC))*((ETA*ETA*ETA/6.0)-(ETA*ETA/2.0))
C      WRITE(5,*)ETA,UL(I,J),VL(J)
 250  CONTINUE

      DO 260 J=2,N
      ETA=J*DETA
      TL(J)=(TI(I-1)-TW)*ETA+TW
```

```
 260  CONTINUE

C       WRITE(5,*)'FR,TAUI,DEL,DX',FR(I),TAUI(I-1),DEL(I-
1),DX,ETA,DETA

      DO 270 J=1,N
      ETA=J*DETA
C       WRITE(5,*)J,UL(I,J),TL(J)
 270  CONTINUE

      XD=((XKL*DX*(TL(2)-TW))/(DEL(I-1)*DETA*RHOL*HFG))
      XC=((XKV*DX*(TV(2)-TV(1)))/(DY*RHOL*HFG))
      CC11=((G*SIN(X/R)/BMUL)*((RHOL-RHOE)+(RHOE/FR(I))*COS(X/R)))
      CC22=CC11*DEL(I-1)*DEL(I-1)
      CC33=(CC22+(TAUI(I-1)*DEL(I-1)/BMUL))

      DEL(I)=((XD+XC+(CC33*DEL(I-1)))/CC33)

      DELTA(I)=(UL(I-1,N)*DELTA(I-1))/UL(I,N)
      DEL(I)=DEL(I)+DELTA(I)

C     START SOLUTION FOR VAPOR BOUNDARY LAYER
C*******************************************
C     START SOLUTION FOR VAPOR VELOCITY BOUNDARY LAYER
C****************************************************

      DO 280 K=2,L-1
      ALPHA(K)=(BNUV*DX/(UV(K)*DY*DY))
      AF=((VV(K)*DX)/(2.0*UV(K)*DY))
      BF=(UV(K+1)-UV(K-1))
C       CF=0.0
      CF=((UVE(I)*UVE(I)-UVE(I-1)*UVE(I-1))/(2.0*UV(K)))
      DF=(G*SIN(X/R)*COS(VHI)*DX)/UV(K)
      CN(K)=UV(K)-(AF*BF)+CF+DF
      UVP(K)=UV(K)
      UV(L)=UVE(I)
 280  CONTINUE


      XP(2)=(ALPHA(2)/(1.0+(2.0*ALPHA(2))))
      XQ(2)=((ALPHA(2)*UL(I,N)+CN(2))/(1.0+2.0*ALPHA(2)))

      DO 290 K=3,L-1
      XP(K)=(ALPHA(K)/(1.0+2.0*ALPHA(K)-ALPHA(K)*XP(K-1)))
      XQ(K)=(ALPHA(K)*XQ(K-1)+CN(K))/(1.0+2.0*ALPHA(K)-
     *ALPHA(K)*XP(K-1))
 290  CONTINUE
C       WRITE(5,*)' DISTRIBUTION  AT VAPOR BOUNDARY LAYER'

      DO 300 K=2,L-1
      KK=L-(K-1)
      UV(KK)=((XP(KK)*UV(KK+1))+XQ(KK))
      UVN(KK)=UV(KK)
 300  CONTINUE

C       XAX=(2.0*TAUI(I-1)*DY/(3.0*BMUV))
C       UV(1)=((-UV(3)/3.0)+(4.0*UV(2)/3.0)-XAX)
      UV(1)=UL(I,N)

C     START SOLUTION FOR VAPOR CONCENTRATION BOUNDARY LAYER
```

```
C*********************************************************

      DO 310 K=2,L-1
      BETA(K)=(BNUV*DX/(SC(I-1)*UV(K)*DY*DY))
      FN(K)=XMV(K)-(((VV(K)*DX)/(2.0*UV(K)*DY))*(XMV(K+1)-XMV(K-1)))
 310  CONTINUE

      XPM(2)=(BETA(2)/(1.0+2.0*BETA(2)))
      XQM(2)=(BETA(2)*XMV(1)+FN(2))/(1.0+2.0*BETA(2))

      DO 320 K=3,L-1
      XPM(K)=(BETA(K)/(1.0+2.0*BETA(K)-BETA(K)*XPM(K-1)))
      XQM(K)=(BETA(K)*XQM(K-1)+FN(K))/(1.0+2.0*BETA(K)-
     *BETA(K)*XPM(K-1))
 320  CONTINUE

      DO 330 K=2,L-1
      KK=L-(K-1)
      XMV(KK)=XPM(KK)*XMV(KK+1)+XQM(KK)
C       WRITE(5,*)KK,UV(KK),XMV(KK),XMV(L)
 330  CONTINUE
      XAAX=((2.0*XM*SC(I-1)*DY/BMUV)-3.0)
      XMV(1)=((-4.0*XMV(2))+XMV(3))/XAAX

C     START SOLUTION FOR VAPOR TEMPERATURE DISTRIBUTION
C*****************************************************

      DO 340 K=2,L-1
      GAMA(K)=(BNUV*DX/(PR*UV(K)*DY*DY))
      GA=((VV(K)*DX)/(2.0*UV(K)*DY))
      GB=(TV(K+1)-TV(K-1))
      GC=((BNUV*DX*((CPA-CPV)/CPE))/(4.0*SC(I-1)*UV(K)*DY*DY))
      GD=(XMV(K+1)-XMV(K-1))
      GN(K)=TV(K)-(GA*GB)+(GC*GB*GD)
 340  CONTINUE

      XPG(2)=(GAMA(2)/(1.0+2.0*GAMA(2)))
      XQG(2)=(GAMA(2)*TL(N)+GN(2))/(1.0+2.0*GAMA(2))

      DO 350 K=3,L-1
      XPG(K)=(GAMA(K)/(1.0+2.0*GAMA(K)-GAMA(K)*XPG(K-1)))
      XQG(K)=(GAMA(K)*XQG(K-1)+GN(K))/(1.0+2.0*GAMA(K)-
     *GAMA(K)*XPG(K-1))
 350  CONTINUE

      DO 360 K=2,L-1
      KK=L-(K-1)
      TV(KK)=XPG(KK)*TV(KK+1)+XQG(KK)
 360  CONTINUE
C       XAAAX=(2.0*QS(I-1)*DY/(3.0*XKV))
C       TV(1)=((-TV(3)/3.0)+(4.0*TV(2)/3.0)-XAAAX)
      TV(1)=TL(N)
C     START CALCULATION OF LIQUID FILM THICKNESS
C ***********************************************
      DO 370 K=1,L
C       WRITE(5,*)K,UV(K),TV(K),XMV(K)
 370  CONTINUE

C     START CALCULATION FOR VERTICAL COMPONENT OF LIQUID AND VAPOR
C     VELOCITY
```

```
C ******************************************************************

      VV(1)=((UV(1)*((DEL(I)-DEL(I-1))/DX))-(XM/RHOV))

      UVN(L)=UVE(I)
      UVP(L)=UVE(I)
      DO 380 K=2,L
      VV(K)=VV(K-1)-((DY/(2.0*DX))*(UVN(K)-UVP(K)+UVN(K-1)-UVP(K-1)))
C      VV(K)=-VV(K)
C      WRITE(5,*)'DDDDVV,VV(K)',K ,VV(1),VV(K),UVN(K),UVP(K)
 380  CONTINUE


C     START CALCULATION FOR INTERFACIAL SHEAR, LOCAL HEAT TRANSFER
C     COEFF.
C     AND LOCAL NUSSELT NUMBER
C*******************************************************************

      TAUI(I)=BMUV*((-UV(3)+(4.0*UV(2))-(3.0*UV(1)))/DY)
C      TAUU=BMUL*((UL(I,N)-UL(I,N-1))/(DEL(I)*DETA))

      QS(I)=XKV*((-TV(3)+(4.0*TV(2))-(3.0*TV(1)))/(2.0*DY))

C      WRITE(5,*) 'NEW SHEAR',I,TAUI(I),XMV(1)

CC      XH(I)=(XKL*(TL(2)-TL(1))/(DETA*DEL(I)*(TI(I-1)-TW)))
CC      XNU(I)=(2.0*R*XH(I)/XKL)

      IF(UL(I,2).LE.0) GOTO 450

CC      WRITE(5,*)'XHI,XNU',XH(I),XNU(I)
CC      WRITE(5,*)XH(I),XNU(I)

C     CALCULATION OF MASS FLOW RATE, AIR CONCENTRATION, VAPOR
CONCENTRATION,
C     PRESSURE AND INTERFACIAL TEMPERATURE TI AT INTERFACE
C*******************************************************************
********


      PVI=(PE*(1.0-XMV(1))/(1.0-(XMV(1)*(1.0-(XM2/XM1)))))

      TI(I)=(A+(B/(ALOG(PVI)+C)))

      TG=TI(I)

      SC(I)=SCC(PVI,TG,XM1,XM2,BNUV)
      AX=(BMUV/(SC(I)*DY))
      XM4=AX*((XMV(2)-XMV(1))/XMV(1))
      XM=-XM4
C      WRITE(5,*)'XM,XMV(1),TAUI,TI',XM,XMV(1),TAUI(I),TI(I)
C  65  CONTINUE

C---------------------------------------------

C     START TO CALCULATE HEAT ENERGY FOR PRESENT STUDY AND NUSSELT
C     SOLUTION
C*****************************************************************
```

```
      DT=TI(I)-TW
      DELNU(I)=((BNUL*3.0*XKL*DT*X)/(G*(RHOL-
     *RHOE)*HFG*SIN(X/R)))**0.25
C      WRITE(5,*)'DELNU',DT,DELNU(I)


      QNU(I)=XKL*(TI(I)-TW)/DELNU(I)

C      XM=(XKL*DT)/(DEL(I)*HFG)

C      DEL(I)=(XKL*(TI(I)-TW)/(XM*HFG))

      XQ(I)=XM*HFG
      XXQ(I)=XKL*DT/DEL(I)


      RATIO=XQ(I)/QNU(I)
      RATTIO=XXQ(I)/QNU(I)

      XH(I)=XQ(I)/(TI(I)-TW)
      XNU(I)=XH(I)*2.0*R/XKL

      DO 390 J=1,N
C      WRITE(5,*)J,UL(I,J),TL(J)
 390  CONTINUE
      DO 400 K=1,L
C      WRITE(5,*)K,UV(K),TV(K),XMV(K)
 400  CONTINUE
C      WRITE(5,*)'============================='
C      WRITE(5,*)I,XM,XMV(1),TI(I),RATIO

      WRITE(5,2)I,DEL(I),RATIO,XH(I),XNU(I)
 2    FORMAT (I4,2X,F20.10,2X,F15.5,2X,F15.5,2X,F15.5)

C      WRITE(5,*)'============================='

C
WRITE(5,*)'*****************************************************'
      UUL=UL(I-2,N)
      XMVV=XMV(1)

 240  CONTINUE


CC*****************************************************************
C******************************************************************
C START CALCULATION FOR THE THIRD CYLINDER
C******************************************************************
C******************************************************************
C     SET BOUNDARY CONDITIONS BETWEEN SECOND CYLINDER
C     AND THIRD CYLINDER (CONTINUITY AND BERNOULLI EQUATIONS
C***********************************************************

  450 UY=UUL
      U1=UY
C      U2=UY
      DELONE=DEL(I-2)
C      DEL(1)=DELONE
      UUR=((U1*U1)+(2.0*G*H))
      U2=(UUR)**0.5
```

```
      DELTWO=DELONE*U1/U2

      JJJ=TETHA0
C      DELTA(1)=(DELTWO)+DELL(JJJ)
      DELTA(1)=DELTWO

CC      DELTA(1)=0.5*DELTWO+DELL(JJJ)
C      DELTA(1)=DELTWO+DELL(JJJ)

      WRITE(5,*)'G,H,U1,U2,DELTA,DELL(JJJ),JJJ',G,H,U1,U2,DELTA(1),
     + DELL(JJJ),JJJ

C      DELTA(1)=DELONE
C      XMV(1)=((PE-PSAI)/(PE-(1.0-(XM2/XM1))*PSAI))

      XMV(1)=(XMVV+XME)/2.0

      WRITE(5,*)'THIRD CYLINDER***************************'

      WRITE(5,*)'U1,DELONE,U2,G,H,DELTWO,DELTA,XMVV',U1,DELONE,U2,G,
      H,DEL(2),DELTA(1),XMVV



C    CALCULATION OF INITIAL VALUES OF INTEREFACIAL LIQUID VELOCITY
C    AND SHEAR
C    FILM THICKNESS AND HEAT
C*******************************************************************

      DEL(1)=DELONE+DELTA(1)
C      DEL(1)=DELTA(1)
      WRITE(5,*)'I,DEL1',I,DEL(1)

      XM=(XKL*(TI(1)-TW)/(HFG*DEL(1)))

C      US=XM*UE
C      UL(1,N)=F1*((G*(RHOL-RHOE)*DEL(1)*DEL(1)/(2.0*BMUL))+US)

      UL(1,N)=U2
C      TAUI(1)=0.23
      TAUI(1)=XM*(UE-UL(1,N))
      TAUI(1)=ABS(TAUI(1))
      WRITE(5,*)'TAUI,DEL1,XM,ULN',TAUI(1),DEL(1),XM,UL(1,N)

C      DT=TE-TW
C      DELNU(1)=((BNUL*3.0*XKL*DT*X)/(G*RHOL*HFG*SIN(X/R)))**0.25
C      Q(1)=XKL*DT/DEL(1)
C      QNU(1)=XKL*DT/DELNU(1)



      WRITE(5,*)'DEL1,DELTA',DEL(1),DELTA(1)

C     INCREMENTS AND INITIAL AND BOUNDARY CONDITIONS
C***************************************************

      DO 460 I=1,M
      X=I*DX
      UL(1,1)=0.0
      VL(1)=0.0
```

```
      TL(1)=TW

      XMV(L)=XME
      TV(L)=TE
      SSIN=SIN(X/R)
      UVE(I)=2.0*UE*SSIN
      FR(I)=(G*R/(4.0*UVE(I)*UVE(I)))
C      WRITE(5,*)I,DX,X,R,SSIN,UVE(I)
 460  CONTINUE

      WRITE(5,*)'AAAAAAAA',DEL(1)

C     START CALCULATIONS FOR FIRST PROFILES AT STAGNATION POINT
C *************************************************************

      DO 470 J=2,N
      ETA=J*DETA
      ETA=J*DETA
      UL(1,J)=((G*DEL(1)*DEL(1)*DX)/(BNUL*R))*
     * (ETA-(ETA*ETA/2.0))
      VL(J)=((G*DEL(1)*DEL(1)*DEL(1))/(BNUL*R))*
     * ((ETA*ETA*ETA/6.0)-(ETA*ETA/2.0))-(UL(1,J)*DEL(1)*ETA/DX)
 470  CONTINUE
      WRITE(5,*)'AAAAAAAA',DEL(1)

      DO 480 J=2,N
      ETA=J*DETA
      TL(J)=((TI(1)-TW)*ETA+TW)
 480  CONTINUE

      DO 490 K=1,L-1
      UV(K)=UL(1,N)
      UVP(K)=UL(1,N)
      XMV(K)=XMV(1)
C      XMV(K)=XME

      TV(K)=TL(N)
 490  CONTINUE

      DO 500 K=1,L
      VV(K)=VL(N)
 500  CONTINUE

      QS(1)=XKV*((-TV(3)+(4.0*TV(2))-(3.0*TV(1)))/(2.0*DY))


C     START CALCULATION FOR THE COMPLETE NUMERICAL SCHEME
C*****************************************************
C*************************************************
C******************************************
      DO 510 I=2,M
C      DO 65 ITER=1,100
      X=I*DX
C      WRITE(5,*)'LIQUID BOUNDARY LAYER RESULTS'
C

C     START SOLUTION FOR LIQUID BOUNDARY LAYER
C******************************************

      DO 520 J=2,N
```

```
      ETA=J*DETA
      ZA=((-DEL(I-1)*DEL(I-1)*G*SIN(X/R))/BMUL)*RHOL*COS(VHI)
C      DP=0.0
      DP=((RHOE-(RHOE/FR(I))*COS(X/R))*G*SIN(X/R))
      ZB=((DEL(I-1)*DEL(I-1))*DP)/BMUL
      ZC=(TAUI(I-1)*DEL(I-1)*ETA/BMUL)
      UL(I,J)=((ZA+ZB)*((ETA*ETA/2.0)-ETA))+ZC

      ZAA=((((RHOL*COS(VHI))-RHOE)*DEL(I-1)*DEL(I-1)*DEL(I-1))*G*X*
     + COS(X/R))/BMUL
      ZBB=RHOE*DEL(I-1)*DEL(I-1)*DEL(I-1)*G*X/BMUL
      ZCC=(COS(X/R)*COS(X/R))-(SIN(X/R)*SIN(X/R))
      VL(J)=(ZAA+(ZBB*ZCC))*((ETA*ETA*ETA/6.0)-(ETA*ETA/2.0))
C      WRITE(5,*)ETA,UL(I,J),VL(J)
 520  CONTINUE

      DO 530 J=2,N
      ETA=J*DETA
      TL(J)=(TI(I-1)-TW)*ETA+TW
 530  CONTINUE

C      WRITE(5,*)'FR,TAUI,DEL,DX',FR(I),TAUI(I-1),DEL(I-
1),DX,ETA,DETA

      DO 540 J=1,N
      ETA=J*DETA
C      WRITE(5,*)J,UL(I,J),TL(J)
 540  CONTINUE

      XD=((XKL*DX*(TL(2)-TW))/(DEL(I-1)*DETA*RHOL*HFG))
      XC=((XKV*DX*(TV(2)-TV(1)))/(DY*RHOL*HFG))
      CC11=((G*SIN(X/R)/BMUL)*((RHOL-RHOE)+(RHOE/FR(I))*COS(X/R)))
      CC22=CC11*DEL(I-1)*DEL(I-1)
      CC33=(CC22+(TAUI(I-1)*DEL(I-1)/BMUL))

      DEL(I)=((XD+XC+(CC33*DEL(I-1)))/CC33)

C      DELTA(I)=(UL(I-1,N)*DELTA(I-1))/UL(I,N)
C      DEL(I)=DEL(I)+DELTA(I)




C     START SOLUTION FOR VAPOR BOUNDARY LAYER
C*********************************************
C     START SOLUTION FOR VAPOR VELOCITY BOUNDARY LAYER
C******************************************************

      DO 550 K=2,L-1
      ALPHA(K)=(BNUV*DX/(UV(K)*DY*DY))
      AF=((VV(K)*DX)/(2.0*UV(K)*DY))
      BF=(UV(K+1)-UV(K-1))
C      CF=0.0
      CF=((UVE(I)*UVE(I)-UVE(I-1)*UVE(I-1))/(2.0*UV(K)))
      DF=(G*SIN(X/R)*COS(VHI)*DX)/UV(K)
      CN(K)=UV(K)-(AF*BF)+CF+DF
      UVP(K)=UV(K)
      UV(L)=UVE(I)
 550  CONTINUE
```

```
      XP(2)=(ALPHA(2)/(1.0+(2.0*ALPHA(2))))
      XQ(2)=((ALPHA(2)*UL(I,N)+CN(2))/(1.0+2.0*ALPHA(2)))

      DO 560 K=3,L-1
      XP(K)=(ALPHA(K)/(1.0+2.0*ALPHA(K)-ALPHA(K)*XP(K-1)))
      XQ(K)=(ALPHA(K)*XQ(K-1)+CN(K))/(1.0+2.0*ALPHA(K)-
     *ALPHA(K)*XP(K-1))
 560  CONTINUE
C      WRITE(5,*)' DISTRIBUTION  AT VAPOR BOUNDARY LAYER'

      DO 570 K=2,L-1
      KK=L-(K-1)
      UV(KK)=((XP(KK)*UV(KK+1))+XQ(KK))
      UVN(KK)=UV(KK)
 570  CONTINUE

C      XAX=(2.0*TAUI(I-1)*DY/(3.0*BMUV))
C      UV(1)=((-UV(3)/3.0)+(4.0*UV(2)/3.0)-XAX)
      UV(1)=UL(I,N)

C     START SOLUTION FOR VAPOR CONCENTRATION BOUNDARY LAYER
C*********************************************************

      DO 580 K=2,L-1
      BETA(K)=(BNUV*DX/(SC(I-1)*UV(K)*DY*DY))
      FN(K)=XMV(K)-(((VV(K)*DX)/(2.0*UV(K)*DY))*(XMV(K+1)-XMV(K-1)))
 580  CONTINUE

      XPM(2)=(BETA(2)/(1.0+2.0*BETA(2)))
      XQM(2)=(BETA(2)*XMV(1)+FN(2))/(1.0+2.0*BETA(2))

      DO 590 K=3,L-1
      XPM(K)=(BETA(K)/(1.0+2.0*BETA(K)-BETA(K)*XPM(K-1)))
      XQM(K)=(BETA(K)*XQM(K-1)+FN(K))/(1.0+2.0*BETA(K)-
     *BETA(K)*XPM(K-1))
 590  CONTINUE

      DO 600 K=2,L-1
      KK=L-(K-1)
      XMV(KK)=XPM(KK)*XMV(KK+1)+XQM(KK)
C      WRITE(5,*)KK,UV(KK),XMV(KK),XMV(L)
 600  CONTINUE
      XAAX=((2.0*XM*SC(I-1)*DY/BMUV)-3.0)
      XMV(1)=((-4.0*XMV(2))+XMV(3))/XAAX

C     START SOLUTION FOR VAPOR TEMPERATURE DISTRIBUTION
C*****************************************************

      DO 610 K=2,L-1
      GAMA(K)=(BNUV*DX/(PR*UV(K)*DY*DY))
      GA=((VV(K)*DX)/(2.0*UV(K)*DY))
      GB=(TV(K+1)-TV(K-1))
      GC=((BNUV*DX*((CPA-CPV)/CPE))/(4.0*SC(I-1)*UV(K)*DY*DY))
      GD=(XMV(K+1)-XMV(K-1))
      GN(K)=TV(K)-(GA*GB)+(GC*GB*GD)
 610  CONTINUE

      XPG(2)=(GAMA(2)/(1.0+2.0*GAMA(2)))
      XQG(2)=(GAMA(2)*TL(N)+GN(2))/(1.0+2.0*GAMA(2))
```

```
      DO 620 K=3,L-1
      XPG(K)=(GAMA(K)/(1.0+2.0*GAMA(K)-GAMA(K)*XPG(K-1)))
      XQG(K)=(GAMA(K)*XQG(K-1)+GN(K))/(1.0+2.0*GAMA(K)-
     *GAMA(K)*XPG(K-1))
 620  CONTINUE

      DO 630 K=2,L-1
      KK=L-(K-1)
      TV(KK)=XPG(KK)*TV(KK+1)+XQG(KK)
 630  CONTINUE
C      XAAAX=(2.0*QS(I-1)*DY/(3.0*XKV))
C      TV(1)=((-TV(3)/3.0)+(4.0*TV(2)/3.0)-XAAAX)
      TV(1)=TL(N)
C     START CALCULATION OF LIQUID FILM THICKNESS
C ***********************************************
      DO 640 K=1,L
C      WRITE(5,*)K,UV(K),TV(K),XMV(K)
 640  CONTINUE

C     START CALCULATION FOR VERTICAL COMPONENT OF LIQUID AND VAPOR
VELOCITY
C *****************************************************************

      VV(1)=((UV(1)*((DEL(I)-DEL(I-1))/DX))-(XM/RHOV))

      UVN(L)=UVE(I)
      UVP(L)=UVE(I)
      DO 650 K=2,L
      VV(K)=VV(K-1)-((DY/(2.0*DX))*(UVN(K)-UVP(K)+UVN(K-1)-UVP(K-1)))
C      VV(K)=-VV(K)
C      WRITE(5,*)'DDDDVV,VV(K)',K ,VV(1),VV(K),UVN(K),UVP(K)
 650  CONTINUE


C     START CALCULATION FOR INTERFACIAL SHEAR, LOCAL HEAT TRANSFER
C     COEFF.AND LOCAL NUSSELT NUMBER
C*****************************************************************

      TAUI(I)=BMUV*((-UV(3)+(4.0*UV(2))-(3.0*UV(1)))/DY)
C      TAUU=BMUL*((UL(I,N)-UL(I,N-1))/(DEL(I)*DETA))

      QS(I)=XKV*((-TV(3)+(4.0*TV(2))-(3.0*TV(1)))/(2.0*DY))

C      WRITE(5,*) 'NEW SHEAR',I,TAUI(I),XMV(1)

CC      XH(I)=(XKL*(TL(2)-TL(1))/(DETA*DEL(I)*(TI(I-1)-TW)))
CC      XNU(I)=(2.0*R*XH(I)/XKL)

      IF(UL(I,2).LE.0) GOTO 680

CC      WRITE(5,*)'XHI,XNU',XH(I),XNU(I)
CC      WRITE(5,*)XH(I),XNU(I)

C     CALCULATION OF MASS FLOW RATE, AIR CONCENTRATION, VAPOR
C     CONCENTRATION,PRESSURE AND INTERFACIAL TEMPERATURE TI AT
C     INTERFACE
C****************************************************************
```

```
      PVI=(PE*(1.0-XMV(1))/(1.0-(XMV(1)*(1.0-(XM2/XM1)))))

      TI(I)=(A+(B/(ALOG(PVI)+C)))

      TG=TI(I)

      SC(I)=SCC(PVI,TG,XM1,XM2,BNUV)
      AX=(BMUV/(SC(I)*DY))
      XM4=AX*((XMV(2)-XMV(1))/XMV(1))
      XM=-XM4
C      WRITE(5,*)'XM,XMV(1),TAUI,TI',XM,XMV(1),TAUI(I),TI(I)
C  65  CONTINUE

C---------------------------------------------

C     START TO CALCULATE HEAT ENERGY FOR PRESENT STUDY AND NUSSELT
C     SOLUTION
C*******************************************************************


      DT=TI(I)-TW
      DELNU(I)=((BNUL*3.0*XKL*DT*X)/(G*(RHOL-
     *RHOE)*HFG*SIN(X/R)))**0.25
C      WRITE(5,*)'DELNU',DT,DELNU(I)


      QNU(I)=XKL*(TI(I)-TW)/DELNU(I)

C      XM=(XKL*DT)/(DEL(I)*HFG)

C      DEL(I)=(XKL*(TI(I)-TW)/(XM*HFG))

      XQ(I)=XM*HFG
      XXQ(I)=XKL*DT/DEL(I)

      RATIO=XQ(I)/QNU(I)
      RATTIO=XXQ(I)/QNU(I)

      XH(I)=XQ(I)/(TI(I)-TW)
      XNU(I)=XH(I)*2.0*R/XKL

      DO 660 J=1,N
C      WRITE(5,*)J,UL(I,J),TL(J)
 660  CONTINUE
      DO 670 K=1,L
C      WRITE(5,*)K,UV(K),TV(K),XMV(K)
 670  CONTINUE
C      WRITE(5,*)'============================'
C      WRITE(5,*)I,XM,XMV(1),TI(I),RATIO
C      WRITE(5,*)I,UL(I-1,N),DEL(I),TI(I),XQ(I)
      WRITE(5,3)I,DEL(I),RATIO,XH(I),XNU(I)
 3    FORMAT (I4,2X,F20.10,2X,F15.5,2X,F15.5,2X,F15.5)

C      WRITE(5,*)'*************************************************'
 510  CONTINUE

 680  STOP
      END
```

```
      FUNCTION RHOO(TR)

      TC=(647.3-TR)/647.3

      A=1.0
      B=-1.9153882
      C=1.2015186E+01
      D=-7.84664025
      E=-3.888614
      F=2.0582238
      G=-2.0829991
      H=8.218E-01
      R=4.7549742E-01

      RHOLL=(3.155E-03*(A+(B*(TC)**0.3333)+(C*(TC)**0.8333)+
     * (D*(TC)**0.875)+(E*TC)+(F*TC*TC)+(G*TC*TC*TC)+
     * (H*TC*TC*TC*TC)+(R*TC*TC*TC*TC*TC)))
      RHOL= (1.0/RHOLL)
      RHOO=RHOL
      RETURN
      END


      FUNCTION VISCE(TE,XM1,XM2)


      SEG=3.724
      A11=1.16145
      B12=0.14874
      C13=0.52487
      D14=0.77320
      E15=2.16178
      F16=2.43787

      TSTAR=TE/50.0
      TST=TSTAR**B12
      WRITE(5,*)'BMUA', BMUG
      OMEGA=((A11/TST)+(C13/EXP(D14*TSTAR))+(E15/EXP(F16*TSTAR)))

      XY=((2.0*XM1*XM2)/(XM1+XM2))**0.5
      YY=SEG*SEG*OMEGA
      TT=(TE)**0.5

      BMUE=(266.93E-08*TT*XY)/(YY)
      WRITE(5,*)'BMUE',BMUE

      VISCE=BMUE
      RETURN
      END

      FUNCTION CONDE(TE,XM1,XM2)

      SEG=3.724
      A11=1.16145
      B12=0.14874
      C13=0.52487
      D14=0.77320
      E15=2.16178
```

```
      F16=2.43787

      TSTAR=TE/50.0
      TST=TSTAR**B12
C      WRITE(5,*)'TSTAR', TE
      OMEGA=((A11/TST)+(C13/EXP(D14*TSTAR))+(E15/EXP(F16*TSTAR)))

      XY=((XM1+XM2)/(2.0*XM1*XM2))**0.5
      YY=SEG*SEG*OMEGA
      TT=(TE)**0.5

C      WRITE(5,*)'OMEGA',OMEGA
      XKE=((1989.1E-07*TT*XY)/(YY))*418.4

      CONDE=XKE
      RETURN
      END



      FUNCTION VISCV(TE)

      BMUV=4.0E-09*(TE)**1.353
      VISCV=BMUV
      RETURN
      END



      FUNCTION SPECA(TE)
      AO=0.103409E+01
      A1=-0.284887E-03
      A2=0.7816818E-06
      A3=-0.4970786E-09
      A4=0.1077024E-12

      CPA=(AO+(A1*TE)+(A2*TE*TE)+(A3*TE*TE*TE)
     * +(A4*TE*TE*TE*TE))

      SPECA=CPA*1000.0
      RETURN
      END

      FUNCTION CONDA(TE)
      CO=-2.27650E-03
      C1=1.259845E-04
      C2=-1.4815235E-07
      C3=1.73550646E-10
      C4=-1.066657E-13
      C5=2.47663035E-17

      XKA=(CO+(C1*TE)+(C2*TE*TE)+(C3*TE*TE*TE)
     * +(C4*TE*TE*TE*TE)+(C5*TE*TE*TE*TE*TE))

      CONDA=XKA
      RETURN
      END

      FUNCTION LATENT(TR)
      TC=(647.3-TR)/647.3
```

```
      DO=0.0
      D1=7.79221E-01
      D2=4.62668
      D3=-1.07931
      D4=-3.87446
      D5=2.94553
      D6=-8.06395
      D7=1.15633E+01
      D8=-6.02884
      HFG=(2.5009E+03*(DO+(D1*(TC)**0.3333)+(D2*(TC)**0.8333)+
     * (D3*(TC)**0.875)+(D4*TC)+(D5*TC*TC)+(D6*TC*TC*TC)+
     * (D7*TC*TC*TC*TC)+(D8*TC*TC*TC*TC*TC)))

      LATENT=HFG*1000.0
      RETURN
      END

      FUNCTION SCC(PVI,TG,XM1,XM2,BNUV)
      TX=TG
C      WRITE(5,*)'TX,PVI',TX,PVI

      SEG=3.724
      A11=1.06036
      B12=0.15610
      C13=0.19300
      D14=0.47635
      E15=1.03587
      F16=1.52996
      G17=1.76474
      H18=3.89411

      TSTAR=TX/50.0
      TST=TSTAR**B12
C      WRITE(5,*)'TSTAR', TI
      OMEGA=((A11/TST)+(C13/EXP(D14*TSTAR))+(E15/EXP(F16*TSTAR))+
     + (G17/(EXP(H18*TSTAR))))

      XYY=((XM1+XM2)/(2.0*(XM1*XM2)))**0.5
      XXP=(PE)
      YYX=SEG*SEG*OMEGA
      TTS=(TE)**1.5

      D12=(0.002628*TTS*XYY)/(XXP*YYX)

      SCC=BNUV/D12

C      WRITE(5,*)'SCC',TX,PVI,XP,YY

      RETURN
      END

      FUNCTION SCCE(TE,PE,XM1,XM2,BNUV)
      TI=TE
      SEG=3.724
      A11=1.06036
      B12=0.15610
      C13=0.19300
      D14=0.47635
      E15=1.03587
```

```
      F16=1.52996
      G17=1.76474
      H18=3.89411

      TSTAR=TE/50.0
      TST=TSTAR**B12
C      WRITE(5,*)'TSTAR', TE
      OMEGA=((A11/TST)+(C13/EXP(D14*TSTAR))+(E15/EXP(F16*TSTAR))+
     + (G17/(EXP(H18*TSTAR))))

      XYY=((XM1+XM2)/(2.0*(XM1*XM2)))**0.5
      XXP=(PE)
      YYX=SEG*SEG*OMEGA
      TTS=(TE)**1.5

      D12=(0.002628*TTS*XYY)/(XXP*YYX)

      SCCE=BNUV/D12

C      WRITE(5,*)'SCCE',PVI,SCCE

      RETURN
      END
```

## CURRICULUM VITAE

### PERSONAL INFORMATION

Surname, Name: Ramadan, Abdul-ghani
Nationality: Libyan
Date and Place of Birth: 1965, Libya
Marital Status: Married
Phone:+90 555 377 16 72
email: abdulghanir@yahoo.com

### EDUCATION

| **Degree** | **Institution** | **Year of Graduation** |
|---|---|---|
| MS | Al-Fateh University, Tripoli-Libya | 1999 |
| BS | Garyounis University, Benghazi-Libya | 1986 |
| High School | 7th of April High School, Gharian-Libya | 1982 |

### WORK EXPERIENCE

| **Year** | **PLace** | **Enrollment** |
|---|---|---|
| 2001-present | Ph.D student at METU, Ankara-Turkey | Ph.D Student |
| 1994-2001 | 7th of April University, Zawia-Libya | Research Assistant |
| 1986-1993 | Mechanical Complex, Gharian-Libya | Maintenance Engineer |

### FOREIGN LANGUAGES

English

### PUBLICATIONS

1- Agha K., Abughres S.M. and Ramadan A.M.," Design Methodology for a Salt Gradient Solar Pond coupled with an Evaporation Pond", Solar Energy, 72, 447-454 (2002).
2- Agha K.R., Abughres S.M. and Ramadan A.M." Maintenance Strategy for a Salt Gradient Solar Pond coupled with an Evaporation Pond", Solar Energy, 77, 95-104 (2004).

### HOBBIES

Reading, Computer Technologies, Classic Music